

System Level Monitoring for Time-Varying Conditions with Application to
Ground Engaging Equipment

by

Nima Yousefi

A thesis submitted in partial fulfilment of the requirements for the degree of

Doctor of Philosophy

Department of Mechanical Engineering

University of Alberta

© Nima Yousefi, 2015

Abstract

Condition monitoring is an effective tool for protecting equipment against unplanned and costly downtime. Conventionally, condition monitoring is only focused on the state of equipment's health and tracks the internal changes. However, more recent studies pointed out that an effective monitoring system not only should track the changes occurring at the equipment level, but it should also take the variability in the equipment operational environment into account. In this approach, environmental variability, along with the load and speed changes are considered as operational variations. These external changes, similar to the internal ones, trigger a non-stationary operating envelope, and therefore need to be monitored at a system level. Shovels and wind turbines are primary examples of systems exposed to such conditions.

In this context, the present work aims to advance the body of knowledge in the area of system level monitoring for earthmoving equipment, such as ground engaging equipment. System level monitoring presented in this study entails assessment of environmental properties as well as equipment condition, and it is addressed in two steps. An algorithm is developed for monitoring and detection of the environmental/external variation. It takes machine-ground interaction force as input, and estimates characteristic features of the ground. The detection of the internal changes (i.e. structural damages) is accomplished through a novel acceleration-based monitoring method. It tracks the changes in the kinetic energy of the system caused by developing structural defect. By performing the internal and external monitoring,

it is possible to identify the root cause of the change in the system level.

To evaluate these methods, a simplified shovel test rig is designed and fabricated. Using an off-set crank-slider mechanism, the rig can generate a time-varying motion and simulate the tool-ground interaction of a real shovel. The design of the test rig allows for it to be used as a platform to study the behavior of a system that is under speed and load variations. The test rig can perform cutting and pushing through a variety of granular material, in a controlled manner which facilitates the study of the environmental variation. Measuring the soil-tool interaction force and using a tool-ground interaction model the mechanical properties of the medium can be estimated. The test rig is designed such that it enables the replication of various structural damages. Acceleration signal of the slider, that is a representation of the kinetic energy of the system, is recorded and used for the assessment of the condition of the test rig. In order to extract fault signatures from the signal, a variety of signal processing methods in time, frequency and time-frequency domains are used. Analyzing these features, it is found that the acceleration signal carries fault signatures, and all faulty conditions can be distinguished from the healthy ones. Application of advanced signal processing methods such as STFT and HHT, support the proposed approach and suggest that it can be successfully used for both detection and identification of the considered faults.

Methods developed for external and internal monitoring provide a platform for equipment situational awareness that can be adopted in other areas such as earthwork planning, excavation automation and equipment health monitoring.

I dedicate my dissertation work to my family for their unconditional love, endless support, and encouragement throughout my life.

Acknowledgement

I wish to thank my supervisory committee members for their insight and generosity with their time. I would like to thank my supervisor Dr. Michael Lipsett for his support, encouragement and patience throughout the entire process. Acknowledgements are extended to Dr. Ming Zuo, Dr. Robert Hall and Dr. Bob Koch for their thorough examination of my work and their invaluable feedbacks. My examiners Dr. Laeeque Daneshmend and Dr. Martin Barczyk were cognizant of my work and its core concepts. I am grateful for their time and constructive suggestions. The list will be incomplete, without including Dr. John Doucette who guided and supported me during the final phase of my study. I would like to acknowledge the contribution of my colleagues in the Oil Sands Integrated Reliability Lab: James Hendry, Pavel Pineda and Amanda Kotchon. They each assisted me with an aspect of the design, fabrication or lab testing.

Over the past five years I have been privileged to work whilst undertaking my doctoral studies and have met a handful of amazing people who contributed to my success. Amongst which are Ellen Schoeck and Heather Hogg from Graduate Students' Association who have always supported me with their words and advice during and even after my tenure as a vice-president there. I also would like to thank my colleagues from CoSyn Technology and Syncrude Research and Development: David Childs, Mike Foote, Dan Bulbuc and Gary Anthieren. I have learnt a great deal from them. Without their continuous support and encouragement I would not have been able to invest the much needed time into completion of my studies.

Finally I would like to express my gratitude to my colleagues and friends: Ayat, Saeed, Ramin, Maryam, Saina and Beeta. They have been a source of inspiration, and encouragement throughout my studies and occasionally reminded me that the light at the end of the tunnel is not an incoming train! Thank you all for being there for me.

Contents

Table of Contents	ix
List of Tables	x
List of Figures	xv
Abbreviations	xviii
1 Introduction	1
1.1 Motivation	3
1.2 Background and Challenges	5
1.3 Scope of Work	14
1.4 Thesis Outline	17
2 Literature Review	20
2.1 System Modeling	22
2.1.1 Ground-Tool Interaction Models	24
2.1.1.1 Fundamental Earthmoving Equation (FEE)	29
2.1.1.2 Mohr-Coulomb Soil Model	32
2.1.2 Medium Property Estimation	34
2.1.2.1 Estimation based on the FEE	36
2.1.2.2 Estimation Based on Coulomb Earth Pressure Model	37
2.2 Maintenance & Condition Monitoring	39

2.2.1	Condition-Based Maintenance	41
2.2.2	Vibration Analysis	43
2.2.2.1	Vibration Signature and Failure Modes	51
2.2.2.2	Signal Processing	60
2.3	State of the Art in Earthmoving Equipment Monitoring	66
3	Methodology	72
3.1	Experimental Platform Design	77
3.2	Environment Monitoring	77
3.3	Equipment Monitoring	78
4	Experimental Platform	81
4.1	Design Requirements	81
4.1.1	System Dynamic and Time-Varying Behavior	82
4.1.2	Task-Specific Requirements	84
4.2	Structure and Subsystems	86
4.2.1	Structure & Implement Assembly	87
4.2.2	Power & Transmission	89
4.3	Failure Modes of Experimental Apparatus	89
4.4	Data Acquisition and Sensors	94
5	Soil Parameter Estimation	98
5.1	Machine-Ground Interaction	99
5.2	Modified Newton-Raphson Method (MNRM)	101
5.2.1	Proposed Estimation Scheme	103
5.3	Experiments & Results	104
5.3.1	Shearbox Measurement of Soil Properties	105
5.3.2	Cutting Force	106
5.4	Discussion and Chapter Summary	111

6 Monitoring and Fault Detection	115
6.1 Non-Stationary Behavior	117
6.2 Fault Diagnostic	119
6.2.1 Time-Domain Analysis	119
6.2.1.1 Dimension Reduction and Classification	124
6.2.2 Frequency and Time-Frequency Domain	126
6.2.2.1 Hilbert-Huang Transform (HHT)	130
6.3 Chapter Summary	145
7 Conclusions and Recommendations for Future Work	148
7.1 Conclusions	150
7.2 Recommendations for Future Work	152
References	154
A Mohr-Coulomb Failure Criterion	182
B Numerical Study of the Crack Fault	184
C VI Program for Data Collection	187
D Newton-Raphson Method	189
E Interactive Period Monitoring	192
E.1 Short-time Fourier Transform	193
E.2 Hilbert-Huang Transform	195

List of Tables

2.1	Time-Domain Features Extracted Based on Statistical Method	61
4.1	Properties of the Crank-Slider System	88
4.2	Gear Numbers in the Parallel Shaft Gearbox	90
4.3	Description of the Failure Modes Under Study	94
4.4	Shovel Rig Sensors	96
5.1	Measured Density and Friction Angles for Soil Samples	106
5.2	Reported Density and Friction Angles of Soil Samples	106
5.3	Cutting Force Measurement for Glass Beads & Play Sand	109
5.4	Averaged Oil Sand Cutting Force at 60°, 70°, and 80°.	110
5.5	Property Estimation Result for Cohesive and Non-Cohesive Soils . .	112
6.1	Typical Statistical Features Extracted from the Acceleration Signal	123

List of Figures

1.1	Autonomous Digger Capability Plan to 2025	6
1.2	System Level Monitoring: Equipment & Environment Conditions	8
1.3	System Level Monitoring vs. Classical Condition Monitoring	15
2.1	Machine and Environmental Factors Contributing to the Production	21
2.2	Division of Factors Influencing Vibration Signals	22
2.3	Modeling of Equipment and the Interaction for Earthmovers	23
2.4	Mass/Spring/Damper Model Representation of Soil-Tool Interaction	26
2.5	Shovel's Bucket Interacting with the Environment	27
2.6	Rheological Modeling of the Bucket-Ground Interaction	28
2.7	Interaction Force Cycles Due to Progressive Soil Failure	28
2.8	Cutting Soil with a Blade Modeled with FEE	30
2.9	Calculation of the Cutting Force Based on FEE	31
2.10	Static Equilibrium for the reformulated soil-tool interaction	32
2.11	Static Equilibrium Analysis for Coulomb's Earth Pressure Model	33
2.12	Medium property Estimation and Interaction Force Prediction	35
2.13	Soil Property Estimation Algorithm Using the FEE Model	36
2.14	Robotic Arms Used for Soil Parameter Estimation	38
2.15	Soil Property Estimation Scheme Based on NRM	38
2.16	Estimation Based on Modified Newton-Raphson Method and the Hybrid Soil Model	40
2.17	Taxonomy of Maintenance Philosophies	41

2.18	Condition Monitoring Allows Early Detection of Potential Failures	42
2.19	Examples of Single Degree of Freedom (SDOF) System	44
2.20	Mechanical Vibration As A Process	45
2.21	Energy Flows in Two Coupled Subsystems	46
2.22	Vibration Response to Forcing Function and Transfer Path	48
2.23	Main Signal Categories	49
2.24	Typical Signals in the Time and Frequency Domains	51
2.25	Some of the Machinery Defects Detected using Vibration Analysis.	52
2.26	Representation of a Revolute Joint with Clearance	53
2.27	Effect of Revolute Joint Clearance on Acceleration Signal	55
2.28	Slider-Crank Mechanism with a Cracked Con-Rod	56
2.29	Factors Influencing the Transverse Amplitude of a Breathing Crack	57
2.30	Components of a Multi-Stage Gearbox System and Their Interaction	58
2.31	Gearbox common Failure Modes and Their FFT Spectrum	59
3.1	Environmental Changes and External Load Variabilities Affects Equipments Operation	73
3.2	Internal and External Changes can Affect the Operating Envelope	74
3.3	Research Road Map: Preliminary Study, Experimental set-up and Design of Experiment, Experiments and Data Collection, Implementation of Monitoring Methods, System Level Monitoring: Environment Characterization and Fault Detection	75
4.1	Offset Crank-Slider Mechanism	83
4.2	Shovel Assembly Driven by the Slider-Crank	85
4.3	Full Cycle of the Crank-Slider Motion	86
4.4	Shovel Assembly with the Blade at an Attack Angle of $\alpha = 70^\circ$	87
4.5	Commissioned Shovel Test Rig and Data Acquisition System	90
4.6	Characteristic of Intermittent vs. Abrupt faults	91

4.7	Select Structural Fault Locations	92
4.8	FEM Analysis of a Defective (Cracked) Connecting Rod	93
4.9	Sensing and Data Acquisition Element	95
5.1	Planar Failure Surface According to Coulomb Theory	100
5.2	Attack Angles (α) and the Depth of Penetration H	100
5.3	Proposed Material Property Estimation Scheme	103
5.4	Principles of Direct Shear Testing	105
5.5	Interaction Force from Play Sand Cutting at 70°	107
5.6	Interaction Force from Play Sand Cutting at 80°	107
5.7	Interaction Force from Glass Beads Cutting at 70°	108
5.8	Interaction Force from Glass Beads Cutting at 80°	108
5.9	Interaction Force from Oil Sand Cutting at 60°	110
5.10	Interaction Force from Oil Sand Cutting at 70°	111
6.1	x_s , A_s , $\dot{\phi}$, and Shaking Force F_N^{SH} for Normal Condition	118
6.2	x_s , A_s , $\dot{\phi}$, and Shaking Force F_{FA}^{SH} for Fault A Condition	120
6.3	x_s , A_s , $\dot{\phi}$, and Shaking Force F_{FB}^{SH} for Fault B Condition	121
6.4	x_s , A_s , $\dot{\phi}$, and Shaking Force F_{FC}^{SH} for Fault C Condition	122
6.5	Feature Extraction and PCA Applied on Acceleration Signal	125
6.6	Classifying All Four Health Classes Using Linear Classifier	125
6.7	FFT Spectrum of the Acceleration Signal for All Health Conditions	127
6.8	Spectrogram (stft) of the Acceleration Signal For All Conditions .	129
6.9	Acceleration Signal Decomposed into its IMFs for Normal Condition	131
6.10	Hilbert spectrum and Marginal Spectrum of the Acceleration Signal for Normal Condition	132
6.11	Acceleration Signal Decomposed into its IMFs for Fault A Condition	134
6.12	Hilbert spectrum and Marginal Spectrum of the Acceleration Signal for Fault A Condition	135

6.13 Acceleration Signal Decomposed into its IMFs for Fault B Condition	137
6.14 Hilbert spectrum and Marginal Spectrum of the Acceleration Signal for Fault B Condition	138
6.15 Acceleration Signal Decomposed into its IMFs for Fault C Condition	140
6.16 Hilbert spectrum and Marginal Spectrum of the Acceleration Signal for Fault C Condition	141
6.17 Marginal Hilbert Spectrum for the IMFs 1 to 3 for the Acceleration signal for Normal case.	142
6.18 Marginal Hilbert Spectrum for the IMFs 1 to 4 for the Acceleration signal for Fault A case.	143
6.19 Marginal Hilbert Spectrum for the IMFs 1 to 3 for the Acceleration signal for Fault B case.	143
6.20 Marginal Hilbert Spectrum for the IMFs 1 to 4 for the Acceleration signal for Fault C case.	144
7.1 Implementation of the System Level Monitoring	149
A.1 Mohr Diagram and Failure Envelopes	183
B.1 Original CAD Model Built in SOLIDWORKS	185
B.2 Numerical Analysis using CAD Translation and SimMechanics . . .	186
B.3 Impact of the Crack Fault on the Residue Signal	186
C.1 LabView VI Program for Data Collection	188
D.1 Newton-Raphson and Modified Newton-Raphson Methods	190
E.1 STFT of the Acceleration During the Soil-Tool Interaction for Normal Condition	193
E.2 STFT of the Acceleration During the Soil-Tool Interaction for Fault A Condition	194

E.3	STFT of the Acceleration During the Soil-Tool Interaction for Fault B Condition	194
E.4	STFT of the Acceleration During the Soil-Tool Interaction for Fault C Condition	195
E.5	IMF of the Acceleration During the Soil-Tool Interaction for Normal Condition	196
E.6	HHT of the Acceleration During the Soil-Tool Interaction for Normal Condition	196
E.7	IMF of the Acceleration During the Soil-Tool Interaction for Fault A Condition	197
E.8	HHT of the Acceleration During the Soil-Tool Interaction for Fault A Condition	197
E.9	IMF of the Acceleration During the Soil-Tool Interaction for Fault B Condition	198
E.10	HHT of the Acceleration During the Soil-Tool Interaction for Fault B Condition	198
E.11	IMF of the Acceleration During the Soil-Tool Interaction for Fault C Condition	199
E.12	HHT of the Acceleration During the Soil-Tool Interaction for Fault C Condition	199

Abbreviations

α	Blade's Angle with Respect to Horizontal Axis
β	The Angle of Soil Surface
\ddot{x}_s	Second Time Derivative of the Slider's Displacement
δ	Soil-Tool Interface Friction Angle
$\dot{\xi}$	Mass Velocity in the Direction of the Force
\dot{x}_s	First Time Derivative of the Slider's Displacement
γ	Soil Density
ϕ	Soil-Soil Internal Friction Angle
φ	Crank's Angular Displacement
ξ	Mass Displacement
A_s	Slider's Acceleration
C	Coriolis and Centripetal Matrix
c	Soil Cohesion
c_a	Adhesion Between the Soil and Blade
F	Total Resistive Force
F^{SH}	Shaking Force
F_s	Cutting Force
F_{int}	Soil-Tool Interaction Force
G	Gravity Matrix
H	Height of the Blade

h	Depth of Penetration
J	Jacobian Matrix
K_A	Active Earth Pressure Coefficient
K_P	Passive Earth Pressure Coefficient
L_f	Length of the Failure Surface
L_t	Length of the Tool
M	Inertia Matrix
Q	Surcharge Pressure
q	Tool Depth Below Soil
R	Force Resisting Movement of Wedge
W	Weight of the Moving Soil Wedge
w	Width of the Blade
x_s	Slider's Displacement
DOF	Degree of Freedom
EMD	Empirical Mode Decomposition
FDI	Fault Detection and Identification
FEE	Fundamental Earthmoving Equation
FFT	Fast Fourier Transform
FRF	Frequency Response Function
HHT	Hilbert-Huang Transform
HT	Hilbert Transform
IMF	Intrinsic Mode Function
IRF	Impulse Response Function
IRF	Impulse response Function
MHS	Marginal Hilbert Spectrum

OA	Order Analysis
PCA	Principal Component Analysis
PDF	Probability Density Function
RMS	Root Mean Square
ROT	Revolution Order Transform
STFT	Short Time Fourier Transform
TF	Time-Frequency

Chapter 1

Introduction

Among many different types of loading units used in surface mining, shovels and excavators are the primary equipment for removing the overburden and collecting the ore material [Paes and Throckmorton, 2008, Tatum et al., 2006a,b]. The basic operating cycle of a shovel consists of a digging pass through the face (ground engaging tool interacting with the environment), swinging and carrying to the dump position, dumping into a truck, swinging empty back to the digging face, and repositioning the bucket at the face [Rodriguez et al., 2004]. Fragmenting and loading rock and soil during the excavation requires a high amount of interaction between the machine and the environment [Flores, 2007, Frimpong and Li, 2007, Ho and Hodkiewicz, 2013]. Repetitive and often variable interaction loads (due to variability in the terrain) can damage structural components and elements of the power transmission, if the reaction load on the machine exceed a certain level [Allen and Sundermeyer, 2005, Yin et al., 2007, Raza and Frimpong, 2013]. Other factors such as soft ground conditions, and recurring excessive pay load can also contribute to fatigue failure in equipment elements [Joseph, 2003, Frimpong et al., 2008a, Raza and Frimpong, 2013]. Repetitive overloading of key asset, with a developing structural fault, can originate or worsen a fault condition, and potentially propagate it to other components. A component failure may then lead to consequential damage

to other parts of the machine, long and costly shutdowns, reduced availability, and potentially high cost of lost production [Majumdar, 1995, Dhillon, 2008, Edwards et al., 2002, Hall and Daneshmend, 2003].

The presence of a fault in a piece of machinery will not only degrade the reliability of the equipment but also hinder effective use of models developed for those systems. Dynamic model of the equipment, and the equipment-environment interaction model, are developed based on an ideal representation - fault free condition - of the equipment [Martin and Kinkead, 1983]. For example, a progressive failure mode can impact the structure of the machine in a way that it will affect the fidelity of the dynamical models [Khoshzaban-Zavarehi, 1997, Lipsett and Yousefi, 2011], and lead to miscalculate the internal forces acting on machine elements. Hence the force calculated for the end-effector will differ from what the actual force the machine is sensing, or estimated through the machine-ground interaction model [Karmakar and Kushwaha, 2006, Luengo et al., 1998, Hemami, 1992]. There are methods for dealing with the small variabilities in a system model due to presence of fault, i.e., sliding-mode, model predictive control, observer-based and adaptive control approaches [Shekhar and Maciejowski, 2010, Tafazoli et al., 2002, Lever, 2001, Lever and Wang, 1995, Araya and Kagoshima, 2001]. Another strategy is to deploy a control system that has a dynamic response independent from the characteristics of the environment [Richardson-Little and Damaren, 2005]. There are two major downsides to these methods. First, the degree of the inaccuracy that a controller can compensate for is limited [Maeda, 2013]. Hence, as the fault condition worsens, the corrective actions get more limited. Second, these approaches can correct the system response while masking the mechanical faults [Dabrowski and Madej, 2012]. If repetitive overloading of machine parts and consequential damage propagation goes unnoticed (because of the way the algorithm ignores the variability), it will only aggravate the faulty condition and may accelerate machine level failure and costly shutdowns [Majumdar, 1995, Dhillon, 2008, Edwards et al., 2002, Hall and

Daneshmend, 2003].

For the above reasons, high availability is preferred to be achieved by on-line monitoring and early maintenance, and not by replacement of the key assets at the end of each operation [Elevli et al., 2008]. Monitoring the condition of the system (equipment health and the environment) can be a primary tool to ensure the system model being used is still valid [Ho and Hodkiewicz, 2013].

While the reliability of the earthmoving equipment depends on the environment [Raza and Frimpong, 2013, Lever, 2011], many studies have considered it from an ‘equipment only’ standpoint [Frimpong and Li, 2007, Frimpong et al., 2005, Raza and Frimpong, 2013, Ho and Hodkiewicz, 2013, Gao et al., 2013]. Only a few works have acknowledged the importance [Frimpong et al., 2008a, Raza and Frimpong, 2013] or recommended to explore this territory - accounting for the environment - from a high level point of view [Lever, 2011]. In the context of autonomous excavation, the present work reviews the reliability and condition monitoring literature in the area of the mining equipment, and introduces alternative approaches for monitoring environmental and structural variations.

1.1 Motivation

Shovels and excavators are complex dynamic systems, and their operating conditions are non-stationary, randomly changing, and severe in terms of the interaction loads and the power requirement. Access to machine is often very limited, and downtime of equipment due to unexpected maintenance interventions (breakdown, failures) is extremely costly. Therefore, reducing the downtime through the use advanced maintenance techniques is a critical motivation.

The presence of a fault in a piece of machinery, can change the behavior of a system such that the system can no longer deliver the required level of performance. This will not only affect the machine reliability and integrity, but may also lower its

acceptable loading threshold. Progressive failure modes can affect the dynamics of the machine, which in turn affects the structure of the dynamical model [Khoshzaban-Zavarehi, 1997, Lipsett and Yousefi, 2011]. The repetitive and often variable interaction loads (due to variability in the terrain) can damage structural components and elements of the power transmission, if the interaction loading exceed the equipment's force capacity [Tan et al., 2003, Ha and Rye, 2004, Hemami, 1995, Allen and Sundermeyer, 2005, Yin et al., 2007, Frimpong et al., 2008a]. Many studies reported strong correlation between the method and magnitude of loading and the equipment structural damage [Yin et al., 2007, Allen and Sundermeyer, 2005, Raza and Frimpong, 2013, Hall, 2002, Frimpong and Li, 2007, Frimpong and Hu, 2004]. The behavior of an item of mechanical equipment can be regarded as being dictated by a number of interactive systems with associated structural elements constituting a load chain [Martin, 1980]. In this context, each element of the equipment may be regarded as operating within different environment [Martin and Kinkead, 1983]. Hence it can be suggested that any equipment has internal and external environments where the failure can occur.

The objective of this work is to develop tools capable of systematically monitoring the environmental properties and health of the equipment such as shovels that operate under non-stationary and severe conditions in real-time. This will be done by defining and studying the two major modes of variabilities: internal changes, which represent the physical changes in the equipment structure, and external changes, which represent the changes in the environmental properties of the ground (i.e. ore body). If the external variabilities (change in the environmental properties) could be successfully detected and isolated, then variability in the emitted energy can be contributed to the internal variabilities (i.e. structural fault). Therefore, it is critical to understand whether the machinery's integrity is compromised or not and; how the medium characteristics is changing over time.

To study the external variabilities, machine-environment interaction will be

reviewed and a medium property estimation algorithm will be developed that accounts for the impact of the environmental variability.

For the study of the internal variability in the system, non-interactive phase of the operation is investigated using a novel approach. Advanced signal processing techniques will be used for monitoring the changes in the components of the kinetic energy of the system and to detect presence of fault.

1.2 Background and Challenges

Forecasting the future of the equipment automation, particularly needed for shovels, Lever identified three areas where technology gaps need to be addressed [Lever, 2011], with a clear emphasis on the machine and load area situational awareness as demonstrated in fig. 1.1:

- Machine situational awareness,
- Shovel automation,
- Load area situational awareness capabilities

Equipment integrity and structural health fall under developing and future development categories related to situational awareness. Terrain information collection e.g. medium characterization lends itself to dig assisting, dig energy and optimal dig planning and relates to both shovel automation and load area situational awareness capabilities, depicted in fig. 1.1. These areas are among the developing or future development efforts. Accordingly, autonomous excavators require advanced status monitoring capabilities to identify situations associated with the machine and the environment. This includes monitoring structural and health trends for early prognostication of events and failures; and on-line information gathering e.g terrain information for planning every next step [Lever, 2011]. Lever's study suggested that such interactive machines should have accurate models with high fidelity.

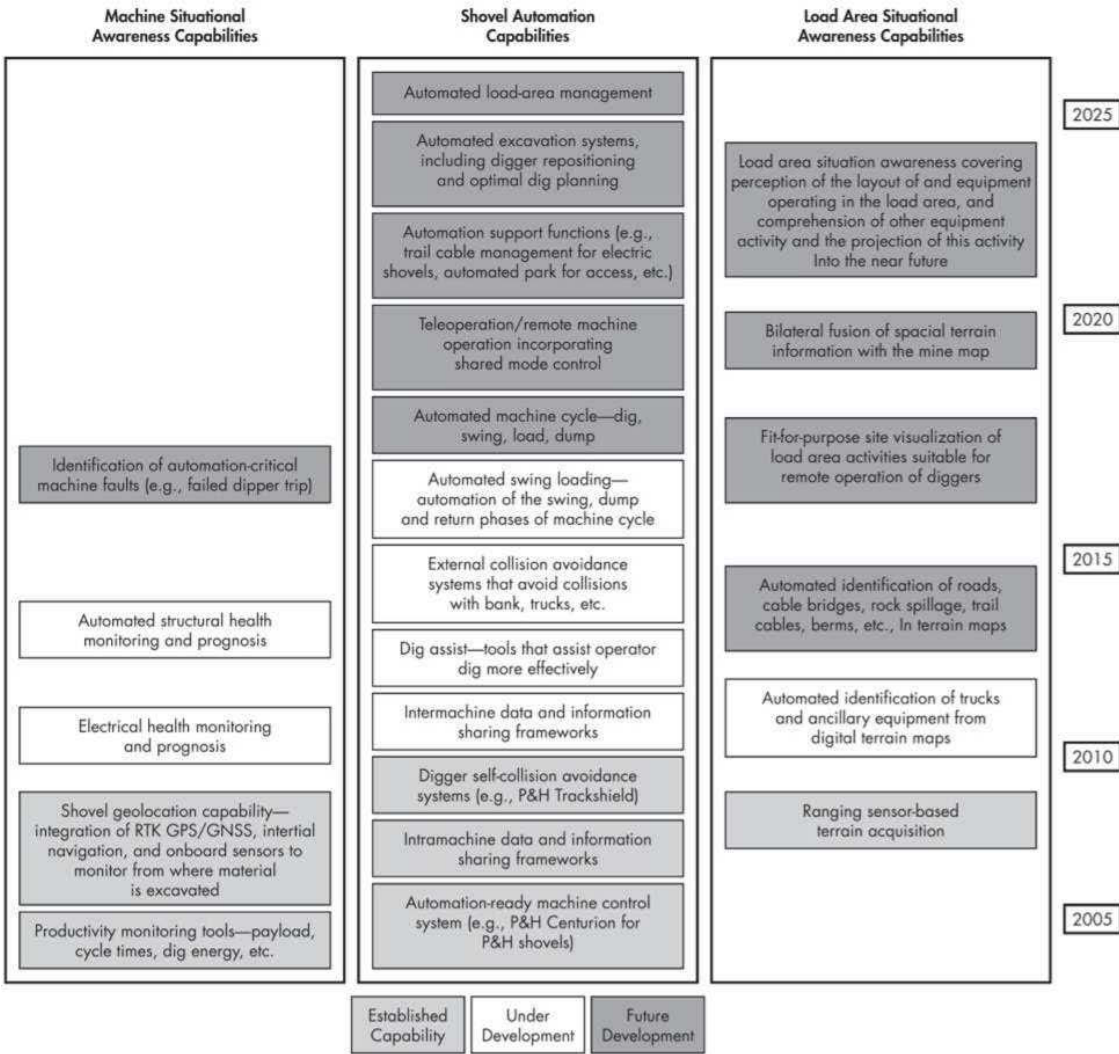


Figure 1.1: Autonomous Digger Capability Plan to 2025 after [Lever, 2011]

Some other pioneering studies in automatic excavation have also commented on the parallel importance of the environmental properties and the equipment integrity. In a review of the fundamentals of excavation automation, Hemami categorized the earthmoving equipment based on a number of factors that affect their operations [Hemami, 1995]. Accordingly, he proposed that the two detrimental factors highlighted in autonomous earthmoving machinery are the ‘mechanical properties’ and ‘power requirement’ of the excavation - which are affected by “the

variation in the properties of the material to be excavated” - and “the structure of the machine carrying the tool”.

In a more recent group of studies, Frimpong *et al.* investigated the energy requirements for the excavation activity, and noted how the change in the property of the material can result in varying mechanical energy input to the machine, and deteriorate shovel’s health and longevity [Frimpong et al., 2008a, Frimpong and Li, 2007]. Hence, the power requirement of the earthmoving equipment in general terms can be defined as a function of the medium property and the ground interaction force. Knowing that the power is the energy consumed per unit time, one can use the conservation of energy to explain the Power in/Power out relation:

$$\text{Energy in} \approx \text{Energy out} + \text{Dissipated Energy.}$$

Internal variabilities representing faults (e.g. misalignment and unbalance) may be reflected in vibration in rotating machinery [Toth and Ganeriwala, 2014, Ramesh Kumar et al., 2011], and presence of these faults can lead into increased vibration, thereby increasing the energy and power requirements above the normal condition. Hence, structural integrity, interaction force and power consumption are closely linked.

Using the ground-tool interaction model and the dynamic model of the equipment, it is assumed that the environment properties are known and time-invariable [Dechao and Yusu, 1992, Zhang and Kushwaha, 1995, Cannon, 1999, Xia, 2008, Mak et al., 2012]. This assumptions might be valid in well-controlled environment, but it is rarely the case in the field: A variety of medium properties can be found in a given work site. It means that, even though the machine might be digging the same material, internal properties of the medium can be different. Variability in internal properties of the medium will vary the required interaction forces [Bernold, 1993]. Assuming the invariability of the medium characteristics significantly increases the prediction error probability [Tan et al., 2003, 2005a,b, Vahed et al., 2007, 2008], which will make the system control unstable.

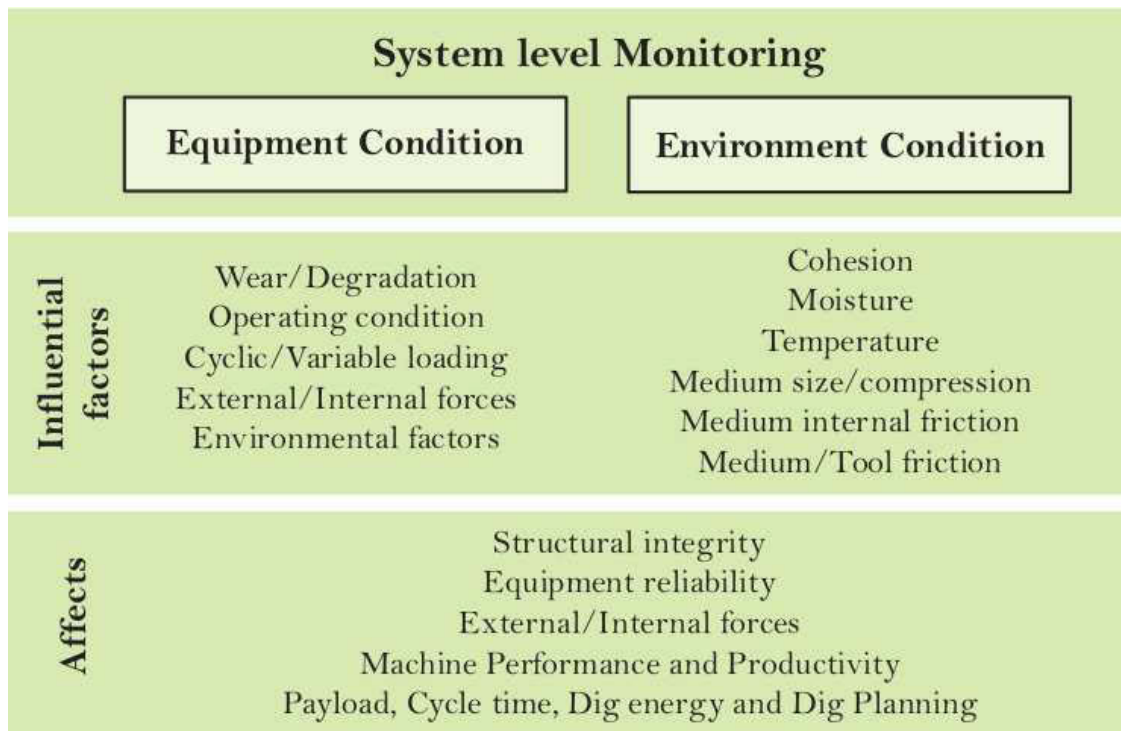


Figure 1.2: System Level Monitoring: Equipment & Environment Conditions

Although the earlier studies in automated excavation pointed out the need to consider both environmental and structural variabilities, there is still a number of challenges associated with each of the two subjects. Figure 1.2 summarizes the equipment and environmental factors, and their effect on the overall equipment.

A. Machine-Ground Interaction Models and Property Estimation

Over the past few decades many have studied the Machine-Ground interaction models to predict the interaction force. A significant body of work has contributed to robotic excavation, with a focus on planning and optimizing a dig, or simple control scheme developments to avoid collision. While they are primarily focused on predicting the interaction force only, a few of them have attempted to solve the more challenging problem of estimating the properties of the soil. This is a critical step for proper assessment of the ground condition, and to identify the environmental

variabilities. Among the few studies that have tackled this problem, none have been able to develop a universal property estimation scheme that is capable of handling both cohesive ($c > 0$) and non-cohesive ($c = 0$) materials effectively. This thesis is intended to fill a gap in the existing body of research and present an enhanced methodology for property estimation that can be applied to larger selection of mediums and used for assessment of the ground condition in earthmoving activity.

A variety of models are developed based on classical soil mechanics, plasticity theory, fluid dynamics and finite element approaches [Gill and Berg, 1967, Godwin and Spoor, 1977, McKyes and Ali, 1977, Alekseeva et al., 1985, Swick and Perumpral, 1988, Hemami et al., 1994, Karmakar et al., 2009]. These models have been used for machine-ground interaction control [Hong, 2001, Shekhar and Maciejowski, 2010, DiMaio, 1998, Richardson-Little and Damaren, 2005, Zweiri et al., 2003, Maeda, 2013], autonomous excavation [Singh, 1991, Bernold, 1993, Malaguti, 1994, Cannon and Singh, 2000, Singh, 2002, Awuah-Offei, 2005], and for predicting the resistive force [Vaha et al., 1991, Hemami et al., 1994, Zhang and Kushwaha, 1995, Singh, 1995, Shiao et al., 2008, Awuah-Offei and Frimpong, 2006, Godwin and O'Dogherty, 2007, Frimpong and Hu, 2004]. There are two main streams for approaching the interaction modeling problem:

The first approach is based on the Fundamental Equation of Earthmoving (FEE) developed by Reece [Reece, 1964]. An improved form of this equation was developed by McKyes [McKyes and Ali, 1977] is among the most studied models for predicting the forces acting on a soil cutting blade. In an effort to predict the interaction force for automated excavation, Luengo, Singh, and Cannon [Luengo et al., 1998] developed a reformulated model of the Fundamental Earth-moving Equation (FEE) for interaction force prediction. They also presented an online method to estimate the inherent soil properties from measured force data.

The second approach to interaction modeling was developed to overcome the shortcomings of methods based on FEE model. In his review of the existing methods,

Hong argued that the properties estimated based on FEE model in [Luengo et al., 1998] are not unique [Hong, 2001]. Also, in addition to the interaction forces, other prior information is also required to make the estimation work. Among a few other interaction models, Hong examined Coulomb's earth pressure model, earlier introduced by Terzaghi [Terzaghi et al., 1995], for parameter estimation and control of robot-soil interaction. The test apparatus used in Hong's study had to obey a certain loading requirements, ruled by a control system. The inherent parameters of this model were similar to the (FEE) model. Despite the improvement made by Hong, this method was limited by the number of parameters it could estimate and the estimation time [Tan et al., 2003].

Following this work, other researchers proposed different methods for soil property estimation. Tan *et al.* used a combination of Coulomb's earth pressure model and Chen and Liu Upper Bound (CLUB) models for failure force prediction and the experimental results presented in [Hong, 2001]. They applied the Newton-Raphson Method (NRM), instead of the parameter space intersection method (PSIM), to minimize the failure force prediction error, and estimated two parameters of (soil-soil friction) and (density) for some low-cohesion soil samples [Tan et al., 2003, 2005b,a].

In an attempt to expand the number of parameters they can estimate, Althoefer *et al.* used a robotic manipulator and developed a modified version of their estimation method (MNRM) which would estimate two parameters from two separate force reading, and then use the two estimated parameters and two additional cutting force readings to estimate the remaining two parameters [Althoefer et al., 2009]. For cohesionless ($c = 0$) materials, which is a much simpler problem, their algorithm showed an error of up to 22.1% for estimation of the three remaining parameters. They also applied their algorithm to moderately cohesive material (moist soil sample). In order for their method to converge, they used a prior knowledge of approximate soil parameters to make initial estimates that were sufficiently close or the same as the actual values. Under these conditions, the relative error in their estimated

parameters could go as high as 9%. Recognizing the error in estimation is yet based on a very close initial guess, the algorithm would have very little practical value.

B. Integrity and Structural Health Monitoring

Any device or equipment can fail as a result of degradation processes resulting from the combined effects of the loading and environmental conditions [Martin and Kinkead, 1983]. Loading applied on mechanical components has a more pronounced effect, once it is random or variable. As the variability and randomness gets greater, it would be more difficult to determine and predict the strength degradation [Gao et al., 2013]. However, the failure mechanism of mechanical equipment would involve a failure event initiating a sequence of ‘consequential’ failure events that may lead into the catastrophic failure of the equipment [Martin and Kinkead, 1983]. Equipment level mechanical failure is often the end product of a series of failures that are triggered by one of the three basic modes of physical degradation: Cracking, Deformation and Wear [Martin and Kinkead, 1983]. These degradation processes are often slow enough to allow for a fault signatures to surface.

With predictive maintenance methods such as *condition monitoring* potential failure could be forecasted early enough to take action and avoid system break down. Over the last decade the science and practice of the condition monitoring has advanced, and a variety of techniques are now available. The most commonly used method for rotating machinery, among these methods, is vibration monitoring. Vibration monitoring or vibration analysis entails measurement of the vibration of the casing in one or more locations, and processing these signals in order to identify the presence of abnormalities or defects in elements of the rotating equipment, e.g. bearings, gears, and shafts [Randall, 2011, John M. Vance, 2010, Girdhar, 2004].

The use of vibration analysis methods for condition monitoring can be classified into time domain and frequency domain methods. Time domain methods are often based on statistical analysis techniques, that apply statistical operation such as

standard deviation and kurtosis on the actual time series of the vibration signal. Features based on these operations will be defined and used to detect parametric or pattern changes as the anomaly occurs. Frequency domain methods such as the Fast Fourier Transform (FFT) on the other hand transform the signals from the time domain into their corresponding frequency domain. After conditioning the signal, and similar to time domain analysis, specific operations can be applied on the transformed signals in order to define appropriate features. These features can then be used to monitor development and progression of potential failures [Randall, 2011, John M. Vance, 2010].

Mining equipment such as shovels and trucks have a variety of rolling elements and therefore vibration monitoring techniques have been historically used for fault detection. A number of studies investigated the application of time-domain analysis for monitoring the shovel condition [Brown and Jorgensen, 1988, Burrows, 1996, Ramirez, 2009, 2010]. Effective condition monitoring using these methods often require extensive prior knowledge about the normal operating condition of the equipment, and also how each of the failure modes will affect the vibration signature. Development of the database of normal operating conditions, particularly for machines with transient operating modes has been the subject of many studies [Timusk et al., 2008, 2009b, McBain and Timusk, 2009].

When it comes to the application of the frequency based methods, there lies a fundamental challenge. Vibration monitoring for machines that operate under conditions of constant speed and load could be accomplished through conventional signal processing techniques e.g. Fourier transform. However, such methods are not suitable tools for monitoring of equipment that operate under transient and non-stationary conditions, i.e. in presence of variable load or rotational speed. Earthmovers and shovels are examples of such systems. Some researchers attempted to apply the conventional frequency-domain techniques to a period when machine is not in a transient or non-stationary operating mode [Brown and Jorgensen, 1988,

Burrows, 1996, Nower, 2013]. Some others have applied modern and improved signal processing techniques such as order tracking to overcome this challenge. For example, Saavedra *et al.* suggested to normalize the machinery vibration data with order spectrum analysis to relax speed change effects [Saavedra and Molina Vicuna, 2007].

Others signal processing techniques such as Time-Frequency transformations have also provided more powerful tools for vibration analysis investigation. These methods will be further discussed in chapter 2. Although these method have shown promising results, they only have been used for a limited number of applications, and are still at an early stages of development.

Limited capability of the processing techniques, is not the only challenge. In most applications of the vibration-based monitoring effective detection of an anomaly relies on the appearance of particular fault-related frequencies in the vibration signal emitted from the equipment. A known downfalls of this approach is when the equipment is operating in the presence of external vibrations that can interfere with the fault signature. Additionally, the physical distance of the faulty component from the vibration probe location can also weaken the visibility of the signatures furthermore.

For machines operating in transient and non-stationary condition, such as in earthmoving activity, it is desired to use indicators that are sensitive to the condition of the equipment and not to the condition of operation. Variability of the operating condition may come from variability in the speed or load [Timusk et al., 2009b]. For interactive systems (systems that interact with their environment) such as shovels, an additional source of variability is the change in the environment.

Some earlier studies have suggested the use of novelty detection [Timusk et al., 2009b,a] to identify the operating mode of the equipment for improved condition monitoring. However, this approach will not suffice to deal with the complexity of interactive systems, where the load variability is not sufficiently an indicator of a

different operating condition. However, if the load variability can be contributed to environmental variabilities, then a new operating condition can be concluded.

Classical novelty detection is based on the identification of new or unknown data, that may represent a faulty condition. Some modern novelty detection algorithms, as stated earlier, can benefit from classification algorithms to detect operating modes [Timusk et al., 2009b,a].

Unlike the classical novelty detection methods that are sensitive to changes in the operating condition, system level monitoring allows multiple states of normal operating condition, by accounting for environmental variabilities. Change in the system level needs to be tested for environmental variability first. Once external variabilities are detected and isolated, then the change can be contributed to internal variability (a physical change in the system), as shown in fig. 1.3. It should be noted that (internal/external) monitoring can be done concurrently, or in two separate steps as is the case in this investigation.

1.3 Scope of Work

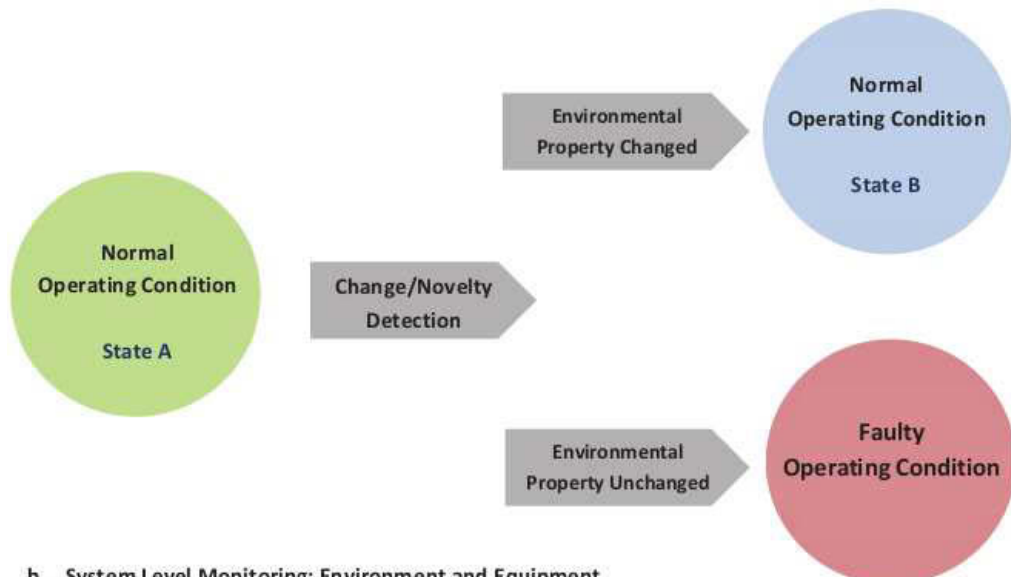
This work aims to advance the body of knowledge needed for system level monitoring of earthmoving equipment, such as shovels. Considering the equipment and its surrounding environment as a system, system level monitoring entails assessment of the environmental properties, as well as the equipment condition.

This is done in two steps: First, by developing a soil property estimation algorithm for detection of (external) environmental variability, and then by investigating the changes in the acceleration signal for detection of the internal variabilities (faults).

A new methodology for environmental property estimation is developed and validated based on data collected from a custom-designed, laboratory-scale shovel test rig. The shovel test rig performed dirt-pushing operation during a time-varying



a. Classical Condition Monitoring: Equipment



b. System Level Monitoring: Environment and Equipment

Figure 1.3: Proposed System Level Monitoring vs. Classical Condition Monitoring

condition of load/speed, and for different attack angles and on a variety of mediums. Interaction force and other controlled parameters of the shovel rig were monitored in a laboratory setting and as such is not entirely reflective of the true shovel operations. Environmental variability was introduced by changing the medium to be dug entirely, which also discounts the level of complexity an actual shovel might face during its operation.

The approach used in this work for fault detection is based on monitoring change in the acceleration signal of the end-effector during the non-interactive period of

operation. Unlike the conventional methods, the vibration signal of the machine casing is not used. There were two reasons for this. First, to eliminate the effect of distance of fault from the vibration probe, and second, to be able to observe the impact of the fault on the dynamics of the system. The acceleration signal (measured at the end effector), is more resistant to external excitation, which is a plus compared to the vibration measurement on the frame. It is hypothesized that a mechanical fault in key elements of the equipment must dissipate a fraction of the input energy. With properly defined failure modes, this would change the dynamic response of the equipment and might become observable (e.g. through acceleration, speed, or angular velocity).

Consequently, the scope of effort in the investigation of the proposed system level monitoring is limited to the following:

1. Design, development and fabrication of a shovel test rig with an inherent time-varying behavior. The shovel test rig will perform a dirt-pushing action at multiple rake angles which is essential for generating the interaction force between the machine and environment. It also will provide a platform to introduce controlled mechanical faults at multiple locations. Such design will allow investigating both internal and external variabilities.
2. Development and validation of a method for online assessment of the environmental variability and estimation of the medium property based on experimental data generated from the dirt-pushing action. It is desired to be able to handle both cohesive and non-cohesive material.
3. Assess the observability of the internal variabilities (presence of fault) through the use of the acceleration signal, under non-interactive phase of the operation. This will be done by developing a baseline for healthy condition, and monitoring the change in the signal in presence of internal variabilities (i.e. three types of structural defects). Signal processing techniques in Time and Frequency

domain will be applied for fault detection.

1.4 Thesis Outline

To better understand the concept of the system level monitoring, **Chapter 2** is divided into two sections and offers the necessary background and trends for external (Environment) and internal (Equipment) monitoring. Predicting the interaction force has been the primary focus of the studies in the area of automated excavation, and is regarded as a subsection of equipment modeling. Pioneering studies in this area come from geomechanics and civil engineering disciplines. System modeling is broken down in section [2.1](#). First, an overview of the fundamental of the interaction modeling is presented in section [2.1.1](#). Different approaches to modeling and important factor for setting up a model, that includes properties of the medium that undergoes the earthwork in some models, will be reviewed. It is then followed by the review of the literature on property estimation in section [2.1.2](#). Medium property estimation uses the inverses model of the interaction and the measured interaction force, in addition to some auxiliary assumption in order to predict the properties of the medium that is being excavated.

The second part of the review is dedicated to the review of equipment condition monitoring, and its methods and applications in section [2.2](#). It will offer an overview of the maintenance paradigm, its relation to equipment reliability and life, equipment monitoring in earthmoving, and commercial monitoring systems. This chapter pays particular attention to the reviews of condition monitoring, and provides an introduction to the types and root causes of the vibration in equipment, especially rotating equipment. Vibration analysis tools and techniques (in time, frequency, and time frequency) will be discussed with a particular focus on the methods that are appropriate for systems under time-varying condition. This chapter will be concluded with a high level review of the state of the art condition monitoring

methods for earthmoving equipment.

A high level summary of the remaining challenges toward the development of a system level monitoring is presented in **chapter 3**, followed by the description of the methodology used in this investigation. Sections 3.1 to 3.3 outline the procedures used in design of the test rig and data collection, and explains the techniques used for analyzing the data for environmental and equipment monitoring.

The experimental platform designed and fabricated for this investigation is presented in **chapter 4**. Description of the apparatus design and its time-varying behavior and subsystems are reviewed in section 4.2. It is followed by the details of the data collection system. The remainder of the chapter gives an overview of the specifications of the shovel assembly, and potential failure modes and their possible behaviors.

The next two chapters investigate the proposed environmental (external) and equipment (internal) monitoring: The proposed property estimation algorithm is presented in **chapter 5**. This chapter presents the method and formulation developed for property estimation, underlying assumptions and the steps taken to validate the estimation method. Experiment details and the results from the application of the property estimation algorithm are discussed in section 5.3.

Vibration analysis techniques are adopted to monitor the structural integrity of the equipment through the dynamic parameters of the system in **chapter 6**. Experimental procedure for development of the baseline condition (fault free) and the three faulty conditions is presented. First, a time-domain analysis based on the statistical features of the signals is used for detection of faulty conditions and presented in section 6.2.1. Using Principal Component Analysis (PCA) and the healthy data, a linear transformation was developed that would map the signal from time domain to a new coordinate system based on principle components. A linear classifier is then used to separate all four classes of health condition. Upon successful fault detection and identification (FDI) in time-domain, application of Frequency

and Time-Frequency domains analysis is discussed in this chapter. Time-Frequency signal processing techniques such as STFT and HTT are applied on the signals, and their effectiveness in fault detection is compared.

Chapter 7 summarizes the main results of the work and discusses the limitations of the proposed methods and directions for future work.

Chapter 2

Literature Review

Earthwork and excavation entails physical treatment or moving of the earth's surface. The task is often done using a piece of earthmoving machinery and requires interaction with a medium of some sort (soil, gravel or unformed rock).

Application and development of the earthmoving equipment (earthmovers) and their systems is discussed extensively in a number of references [[Rutherford, 1971](#), [Haycraft, 2002](#), [Tatum et al., 2006a,b](#)]. Earthmovers act like a simple machine in the sense that they transform the input force applied by the machine (through the *Power train*) into the force that the machine exerts on the environment (through elements of *Implement*). These two systems, along with the *Structure*, *Control & information* and the *Traction system* are the five key systems that determine the capability of a piece of equipment to operate under varying operating condition and production rates [[Tatum et al., 2006a](#)], are shown in fig. 2.1.

Control and information system is the latest addition to the earthmoving systems. Hence, there's a lot of development needed in the areas of communication, control, automation, performance monitoring and health monitoring [[Tatum et al., 2006a](#), [Lever, 2001](#)]. There are already a number of onboard information system that monitor a set of key parameters associated with each of the systems (e.g. engine temperature, oil level). Monitoring these parameters will allow users to detect



Figure 2.1: Machine and Environmental Factors Contributing to the Production, after [Tatum et al., 2006a]

anomaly or faulty conditions and trigger a maintenance procedure. However, the progress made to date in this area has been very slow and capabilities developed toward the autonomous digger plan is much behind the forecasted objectives [Lever, 2001].

The concept of the system level monitoring proposed in the present study, suggest that for systems that interact with their environment, critical environmental and equipment parameters must be monitored. This is particularly important for systems that operate under variable or non-stationary conditions, e.g mining machinery, wind turbines, aerospace. This way the variability in the operating condition due to an environmental factor can be identified and separated from a degradation process [Bartelmus, 2012].

In this context two streams of research are of particular interest to the present work. Under the first stream studies that included the external loading in the model constructed for the equipment will be reviewed. Special attention will be paid to the ones that accounted for the machine/environment interaction. Also, previous studies that investigated methods for modeling the interaction force, and applied inverse models to estimate environmental properties will be reviewed.

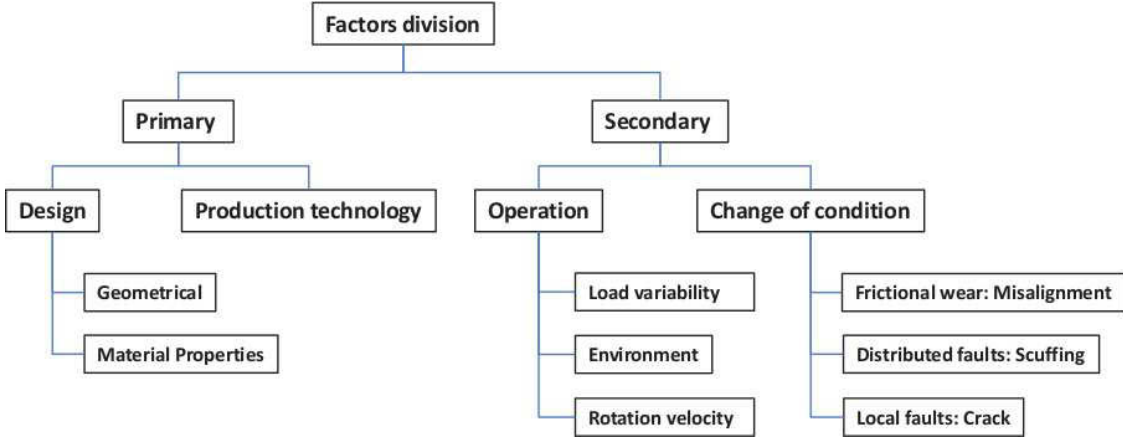


Figure 2.2: Division of Factors Influencing Vibration Signals [Bartelmus, 2012]

Equipment condition monitoring draws on a broad range of topics. Hence, the literature reviewed for the second stream of studies would have a wider variety. The review would start with equipment reliability, maintenance paradigms, and condition monitoring methods particularly the ones applied to rotating equipment. Then it will explore methods and applications of vibration analysis, and will delve further into signal processing and statistical approaches for interpreting the vibration data for systems including non-stationary ones. The review will be concluded by an overview of the state of the art studies and products in earthmovers condition monitoring.

2.1 System Modeling

Automated excavation has been a very attractive research area for more than a quarter century, with a variety of applications from mining in remote and hazardous area, to space explorations [Seward et al., 1988, Hemami, 1993, Vaha and Skibniewski, 1993, Baiden et al., 1996, Bradley and Seward, 1998, Cannon, 1999, Cannon and Singh, 2000, Marshal, 2001, Singh, 2002, Huntsberger et al., 2005, Zeng et al., 2007, Marshall et al., 2008, Shao et al., 2008, Bonchis et al., 2011, Lever, 2011]. Each of

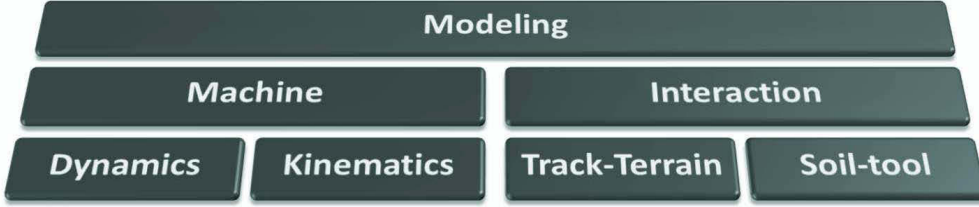


Figure 2.3: Modeling of Equipment and the Interaction for Earthmovers

these studies contributed to several areas of excavators control and automation, but one way or another all had to adopt a system model to work with.

While some of the earlier shovel models were mere kinematics or multi-body dynamic models developed for trajectory planning [Koivo, 1994, Bradley and Seward, 1998], later studies began to develop more detailed models to address complex problems such as position control [Bernold, 1993, Richardson-Little and Damaren, 2005], load control [Frimpong et al., 2008b, DiMaio, 1998, Salcudean et al., 1997, Quang, 2000, Richardson-Little and Damaren, 2005], and dig planning [Singh and Cannon, 1998, Cannon and Singh, 2000, Shao et al., 2008]. These models started to deploy the machine-ground interaction, accounting for track-terrain and the tool-ground interaction [DiMaio, 1998, Singh, 1997, Wang et al., 2008], as shown in fig. 2.3.

Soil-Tool interactions contribute to the external interaction force exerted to the equipment, and needs to be considered in the dynamic model of the system. Shovels can be represented as a multi-body mechanism consisting of a series of connected elements, and actuators at each joint [Koivo et al., 1996]. Hence, benefiting from the robotic terminology [Spong et al., 2005] the standard equation of motion can represent the dynamic model of this system as shown in eq. (2.1):

$$M(\theta)\ddot{\theta} + C(\theta, \dot{\theta})\dot{\theta} + G(\theta) = \tau - J^T(\theta) F_{Int} \quad (2.1)$$

where θ is the joint position vector, $\dot{\theta}$ joint velocity vector, $M(\theta)$ is the equipment inertia matrix, $C(\theta, \dot{\theta})$ is the manipulator coriolis and centripetal matrix, $G(\theta)$ is

the gravity matrix, τ is joint torque vector, J manipulator jacobian matrix, F_{Int} is the interaction force vector representing the end-effector contact forces [Luengo et al., 1998, Richardson-Little and Damaren, 2005]. It is often assumed that the acceleration and velocity terms are negligible during digging [Luengo et al., 1998], hence the system model can be reduced to eq. (2.2):

$$F = J^T(\tau - G) \quad (2.2)$$

Therefore, accurate soil parameter identification is essential for precise traction and cutting force prediction, and machine control. This in return requires the knowledge of mechanics of the medium e.g. soil, for earthmoving activities and soil manipulation operations [Selig, 1966]. Although the track-terrain interaction contributes to the full model of the excavator, by assuming a rigid contact between the carriage and the ground, the effect of the ground condition on the track-terrain interaction could be discounted.

2.1.1 Ground-Tool Interaction Models

As describe in previous section for automation and control purposes, a ground interaction model is a necessary part of the equipment model. Early investigations and experimental work on the excavation force components have been conducted by Zelenin *et al.* [Zelenin et al., 1985], and Alekseeva *et al.* [Alekseeva et al., 1985]. These studies developed the earliest empirical methods for calculating the soil-cutting force based on characteristics of the soil and geometrical parameters of the bucket. Many other studies in the area of the ground-tool interaction focused on developing analytical models for *cutting force* prediction. Cutting force is defined as the maximum resistive force of a medium on a tool during a general excavation task before the medium fails. Soil cutting models can be defined and used to describe the motion of the tool in the medium for both cutting and excavation actions, using a wide blade or a bucket [McKyes, 1985]. Ideally it is represented

by a number of parameters of the medium (generally soil), the tool, and the tool motion [Hemami et al., 1994]. Based on classical soil mechanics Terzaghi [Terzaghi, 1943] developed a method to predict the interaction load between the ground and an object. In this approach *Coulomb's Earth Pressure* theory was used to predict the magnitude of the total pressure ground and an object (with a relative motion) could apply on each other. Active pressure (F_A : pressure applied to the back of the object) and passive pressure (F_P : pressure required to fail the soil in front of the object) could be calculated and used to predict the total amount of the interaction force ($F = F_P - F_A$). A number of studies have adopted this model for soil-tool interaction [Hong, 2001, Tan et al., 2003, 2005b]. Reece also developed the *Fundamental Equations for Earthmoving* mechanics based on soil mechanics [Reece, 1964]. Reece et al. later on presented an additive equation for calculation of the forces required to produce any kind of two-dimensional soil failure [Hettiaratchi et al., 1966]. This model got improved and further developed by McKyes [McKyes and Ali, 1977], which became one of the most used models for predicting the forces acting on a soil cutting blade. In addition to the studies mentioned above, many have developed and improved a variety of methods for 2-D and 3-D soil failure [Gill and Berg, 1967, Godwin and Spoor, 1977, Swick and Perumpral, 1988], and also models based on Computational Fluid Dynamics principals Karmakar et al. [2009], Karmakar and Kushwaha [2006], Finite Element Shiau et al. [2008], and Discrete element method Franco [2005], Asaf [2006], Franco et al. [2007], Shmulevich et al. [2007], Shmulevich [2010], Mak et al. [2012], Obermayr et al. [2011], Obermayr M. [2013], Obermayr et al. [2013].

Hemami et al. expanded this research in a series of studies, added more details and established a mathematical basis for interaction modeling [Hemami et al., 1994, Hemami, 1995, Hemami and Hassani, 2007].

Hemami broke the ground-tool activities into (cutting, digging and scooping) and explained how these activities may involve one or more of the following key forces

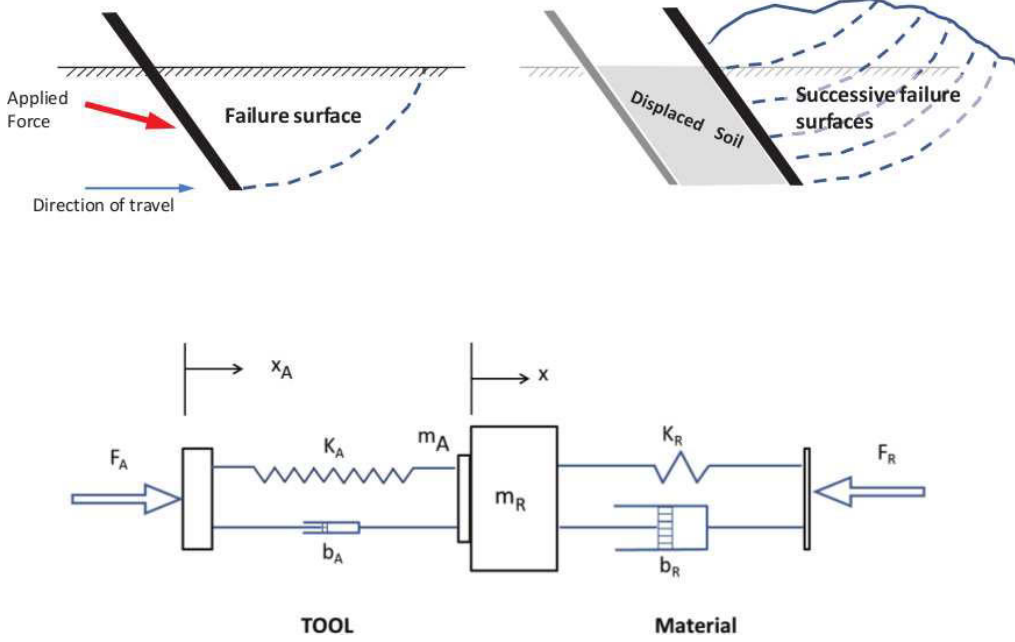


Figure 2.4: A Simple Mass/Spring/Damper Model to Describe a System of the Cutting Tool and Excavation Medium

[Hemami and Hassani, 2007]: The weight of the soil accumulated in the bucket, the compacting resistance of the soil in front of the bucket blade, the friction force between the soil and the bucket walls, and the cutting force required to shear the soil. He discussed the case of a one-dimensional excavator, where single blade (tool) is connected to a hydraulic cylinder and is inserted into a heap of soil [Hemami, 1995]. The tool assembly (actuator and blade), and the material can be modeled as two systems of mass-spring-damper system, as shown in fig. 2.4. Material, as seen in the model, has a larger stiffness (K_R), mass (m_R) and damping factor (b_R). Applying active force F_A to the tool, and in presence of the resistive force F_R , the equation of motion can be defined as:

$$F_A - K_A(x_A - x) - b_A(\dot{x}_A - \dot{x}) - (m_A - m_R)\ddot{x} - k_Rx - b_R\dot{x} - F_R = 0 \quad (2.3)$$

where, x_A and x are the displacements of the actuator and the material respectively. Bucket's motion through the medium, shown in fig. 2.5, is very similar to

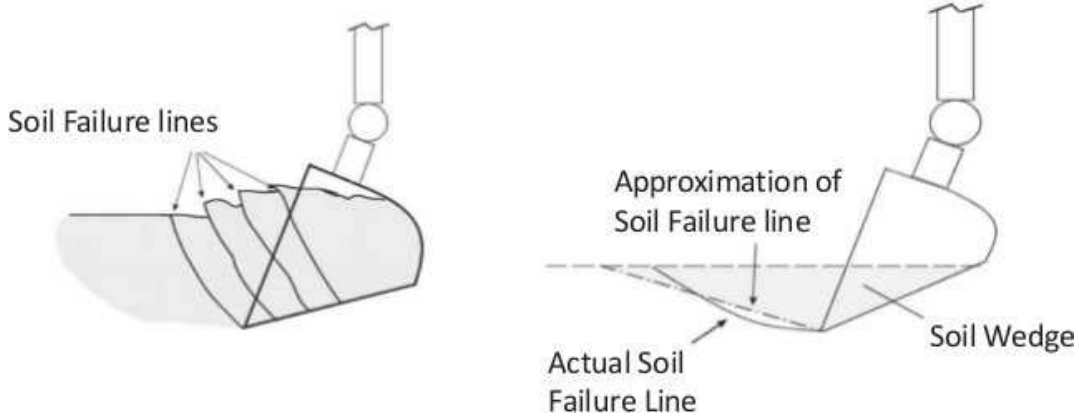


Figure 2.5: Shovel's Bucket Interacting with the Environment (adapted from [Richardson-Little and Damaren, 2005])

the motion of the blade, and this approach can be applied. Equation (2.4) presents a simple rheological model for the interaction force between the bucket and the ground. This way the interaction force can be modeled as a passive resistance to motion (in vertical and horizontal directions).

$$M_t \ddot{\rho} + B_t \dot{\rho} + K_t(\rho - \rho_{env}) = F_{Int} \quad (2.4)$$

where, $\rho = [x \ y]^T$, and $\rho_{env} = [x_{env} \ y_{env}]^T$.

Penetration represent a vertical insertion of the tool in the medium, motion in y direction, while cutting is a lateral motion, in x direction, into a medium. The tool is a solid, blade-like body, which is inclined (attack angle α) and usually maintained at a constant depth (h) and with respect to the surface of the medium, as shown in fig. 2.6. Soil progressively fails at a regular interval as the tool moves forward through it. This forms a sawtooth force profile that represent the built up force at the blade interface. Once the built up force is enough to shear soil, it will shear along a new rupture surface. The phenomena is shown in fig. 2.5, with an example of the resultant force shown in fig. 2.7. Recalling eq. (2.4), the stiffness parameter of the environment (K_t), relates to the depth of penetration, and resets to zero every time soil fails. Damping coefficient (B_t), represent the soil-tool friction, and

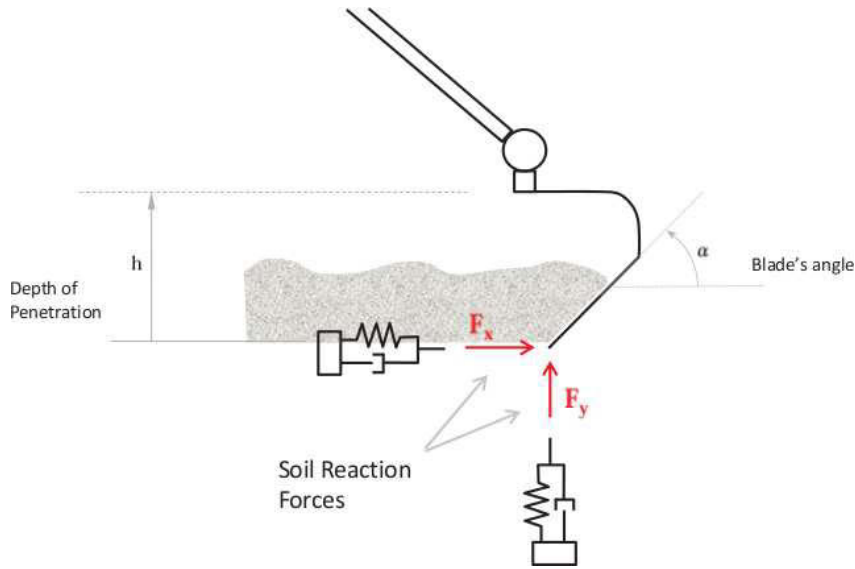


Figure 2.6: Rheological Modeling of the Bucket-Ground Interaction Using Spring-Damper: Bucket Is Moving Left and Down.

only produces the frictional component of the interaction force when the tool moves forward. Lastly, mass parameter (M_t) relates to the soil accumulated in front of the tool. The medium under excavation deforms plastically, whereas the spring term represent elastic deformation. Variability in soil parameters (e.g. density, texture and moisture) is a major challenge in modeling the interaction force and hence an obstacle for control and automation [DiMaio, 1998], whereas varying the stiffness parameter has a limited effect on the model.

Many of the studies in the area of ground-tool interaction are based on the

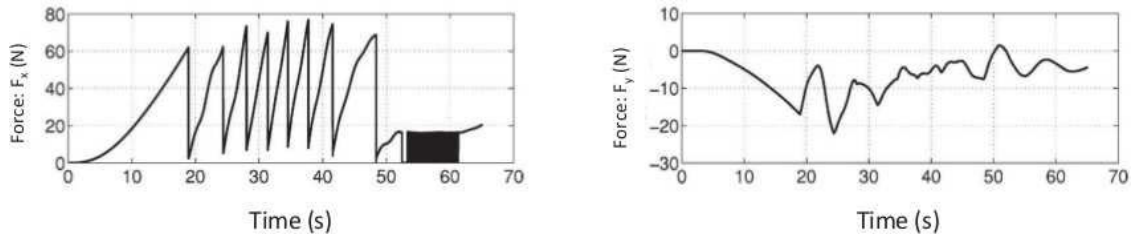


Figure 2.7: Example of the Interaction Force Cycles Due to Progressive Soil Failure (adapted from [Richardson-Little and Damaren, 2005])

pioneering work of Reece, Hettiaratchi and McKyes in 70s. Due to the importance of these studies, two of these approaches will be reviewed. In one approach the Fundamental Earthmoving Equation (FEE) is used for interaction force prediction [Reece, 1964, McKyes and Ali, 1977, Hettiaratchi et al., 1966]. This model is well-known and many researchers have developed different variations of it [Luengo et al., 1998]. The other important approach to the interaction modeling problem applies the Coulomb's earth pressure model introduced by Terzaghi [Terzaghi, 1943] for prediction of the interaction force [Liang et al., 1985].

2.1.1.1 Fundamental Earthmoving Equation (FEE)

By the time Reece tackled the soil cutting problem, it was already known that the force required for a cutting blade in earthmoving can be expressed as a function of soil and tool properties shown in fig. 2.8:

$$\frac{F}{\gamma d^2} = f\left(\frac{c}{\gamma d}, \phi, \delta, \frac{c_a}{\gamma d}, \frac{q}{\gamma d}, \theta\right) \quad (2.5)$$

This was based on the idea that the mechanics of earthmoving are similar to the bearing capacity of shallow foundations on soil, where soil weight, cohesion and surcharge pressure can be added to produce the maximum bearing pressure. Equation (2.5) represents a dimensionless relationship between the draught force, cohesion, internal friction, soil-metal friction, soil-metal adhesion, and surcharge force due to gravity [Reece, 1964]. In this equation, θ represented the shape of the engaging tool, which can be described by the rake angle for the case of an inclined plate. Velocity did not show up in the equation, as it is widely accepted that the rate of shearing does not appreciably affect the shear strength of soil for earthmoving machinery.

Reece developed the fundamental earthmoving equation (FEE) in [Reece, 1964] which was later adopted and improved by McKyes [McKyes and Ali, 1977, McKyes,

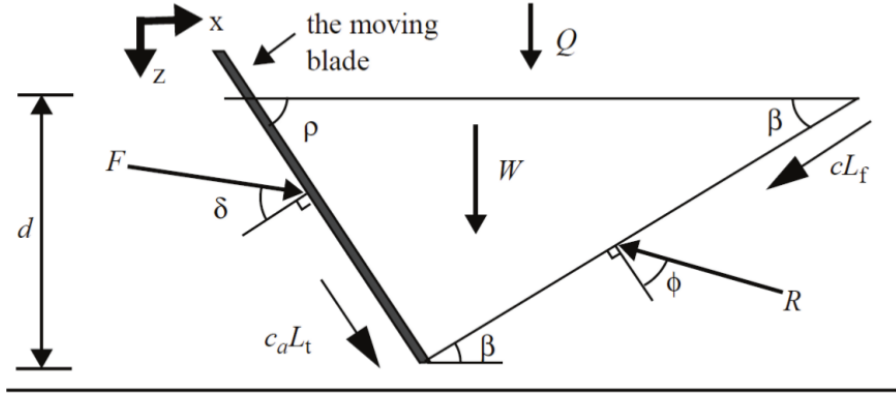


Figure 2.8: Cutting Soil with a Blade Can Be Modeled with FEE (after [Luengo et al., 1998]): F Is the Total Tool Force, W Is the Weight of the Moving Soil in Front of the Blade, Q Is the Surcharge Pressure Vertically Acting on the Soil Surface, R is the Force Resisting Movement of Wedge

1985] into the following form:

$$F = (\gamma g d^2 N_\gamma + c d N_c + q d N_q) w \quad (2.6)$$

where γ is the total soil density, g is the acceleration due to gravity, d is the tool working depth below the soil surface, c is the soil cohesion strength, q is the surcharge pressure vertically acting on the soil surface and w is the tool width. N_γ , N_c , and N_q are factors which depend not only on the soil frictional strength, but also on the tool geometry and tool to soil strength properties [McKyes, 1985, Luengo et al., 1998] presented in eq. (2.7).

$$N_\gamma = \frac{\cot \rho + \cot \beta}{2 [\cos(\rho + \delta) + \sin(\rho + \delta) \cot(\beta + \phi)]} \quad (2.7)$$

$$N_c = \frac{1 + \cot \beta \cot(\beta + \phi)}{\cos(\rho + \delta) + \sin(\rho + \delta) \cot(\beta + \phi)} \quad (2.7)$$

$$N_q = \frac{\cot \rho + \cot \beta}{\cos(\rho + \delta) + \sin(\rho + \delta) \cot(\beta + \phi)} \quad (2.7)$$

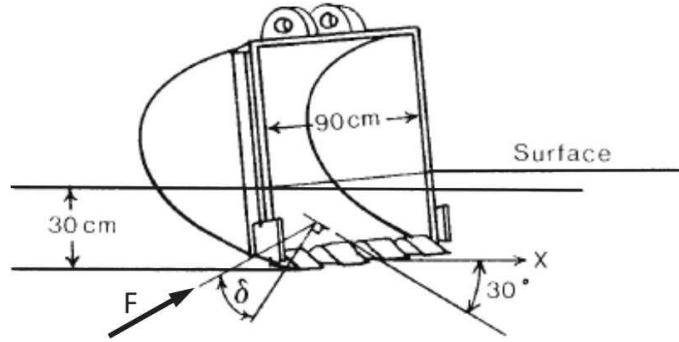


Figure 2.9: For a Soil-Tool system with Known $\gamma = 1.3t/m^3$, $\phi = 35^\circ$, $c = 30 kPa$, $\delta = 25^\circ$, $\alpha = 30^\circ$, $w=90$ cm and $d=30$ cm, N_γ and N_c Can Be Found to Be 1.8 and 1.86. This Allows to Calculate the Cutting Force of the Excavator Bucket $F=16.9$ kN (Example after [McKyes, 1985])

Luengo et al. reformulated the soil-tool model to account for inclined surface and surcharge accumulation, and decomposed the total force into the following three forces [Luengo et al., 1998]:

$$\begin{aligned} F_s &= d^2 w \gamma g N_\gamma + c w d N_c + V_s \gamma g (N_q - 1) \\ F_g &= V_s \gamma g \\ F_r &= V_r \gamma g d \end{aligned} \quad (2.8)$$

Where F_s is the cutting force experienced at a blade, F_g is the gravity force, F_r is the remolding force (in case bucket is used). Note that in eq. (2.8) the gravitational

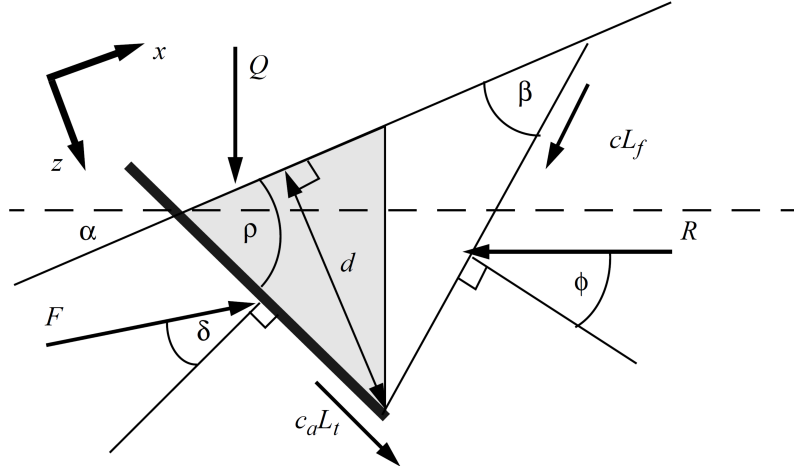


Figure 2.10: Static Equilibrium Analysis for the reformulated soil-tool interaction after [Luengo et al., 1998]

force (F_g) has been subtracted from the cutting force equation (F_s) so that it is not accounted for twice.

The update parameters of N_γ , N_c , and N_q can be described as:

$$N_\gamma = \frac{(\cot \beta - \tan \alpha)(\cos \alpha + \sin \alpha \cot(\beta + \phi))}{2 [\cos(\rho + \delta) + \sin(\rho + \delta) \cot(\beta + \phi)]}$$

$$N_c = \frac{1 + \cot \beta \cot(\beta + \phi)}{\cos(\rho + \delta) + \sin(\rho + \delta) \cot(\beta + \phi)} \quad (2.9)$$

$$N_q = \frac{\cos \alpha + \sin \alpha \cot(\beta + \phi)}{\cos(\rho + \delta) + \sin(\rho + \delta) \cot(\beta + \phi)}$$

2.1.1.2 Mohr-Coulomb Soil Model

Terzaghi described the interaction of a cohesive material and frictional object with a relative motion in [Terzaghi, 1943, Terzaghi et al., 1995, McKyes, 1985]. He adopted the Coulomb's theory of earth pressure - a *Limit Equilibrium Method* - to calculate the active and passive pressures, and to predict the soil failure force when

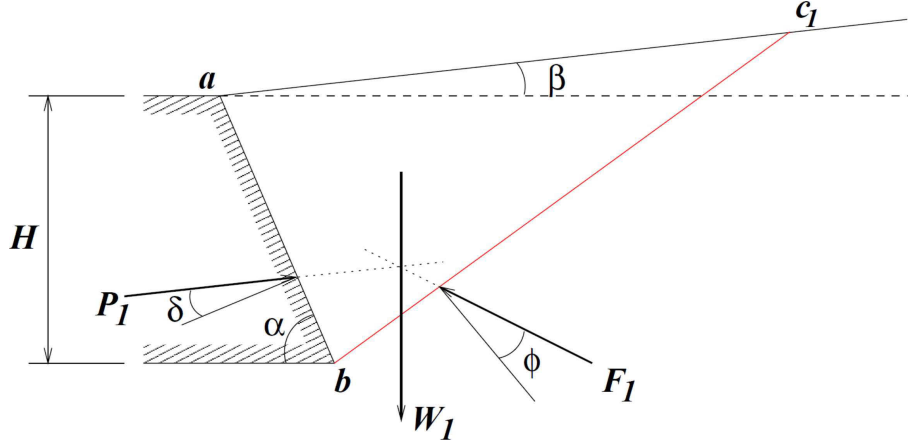


Figure 2.11: Coulomb's Earth Pressure Model after [Hong, 2001]

cutting the soil with wide blades (a large width to depth ratio, near 5:1 or greater). Limit equilibrium methods investigate the equilibrium of the soil mass tending to slide down under the influence of gravity. These models, which pre-assume a failure surface and compute a force equilibrium based upon this failure surface, are commonly referred to as limit equilibrium methods. Mohr-Coulomb failure criterion is presented in appendix A. One limitation to the theory proposed by Coulomb is that for soil-tool interfaces that exhibit friction, the larger the friction angle is, the greater the prediction error will be[Hong, 2001]

Hong [Hong, 2001] reformulated the equation to account for the sloped surfaces and inclined tools as shown in fig. 2.11. To calculate the failure force, the required soil parameters are: soil density γ , soil-tool interface (external) friction angle δ , soil-soil internal friction angle ϕ , and soil cohesion c . Required geometric properties of the tool include: height of the blade H , the rake angle of the blade with respect to horizontal axis α , and angle of soil surface β .

The net force on the plate at failure for cohesive material can then be expressed as [Terzaghi et al., 1995]:

$$\begin{aligned} F(\alpha, \beta, \phi, \delta, c, \gamma,) &= F_P - F_A \\ &= \frac{1}{2}\gamma H^2 \left(\left[K_P + \frac{4c}{\gamma H} \sqrt{K_P} \right] - \left[K_A - \frac{4c}{\gamma H} \sqrt{K_A} \right] \right) \end{aligned} \quad (2.10)$$

Where F_P is the passive force and F_A is the active force for cohesive material, and passive and active pressure coefficients can be described as [Hong, 2001]:

$$K_P(\alpha, \beta, \phi, \delta) = \frac{\sin^2(\alpha - \phi) \cos \delta}{\sin \alpha \sin(\alpha + \delta) \left[1 - \sqrt{\frac{\sin(\phi + \delta) \sin(\phi + \beta)}{\sin(\alpha + \delta) \sin(\alpha + \beta)}} \right]^2} \quad (2.11)$$

$$K_A(\alpha, \beta, \phi, \delta) = \frac{\sin^2(\alpha_A + \phi) \cos \delta}{\sin \alpha_A \sin(\alpha_A - \delta) \left[1 + \sqrt{\frac{\sin(\phi + \delta) \sin(\phi - \beta_A)}{\sin(\alpha_A - \delta) \sin(\alpha_A + \beta_A)}} \right]^2}$$

In active pressure coefficient, $\alpha_A = \pi - \alpha$ and $\beta_A = -\beta$.

2.1.2 Medium Property Estimation

Priory knowledge of the mechanical properties of the medium (e.g. density ρ , internal friction angle ϕ , cohesion c) and soil-tool properties (e.g. soil-tool friction angle δ) is the key to accurate prediction of the interaction force. These parameters can be measured directly with basic equipment available in a soil mechanics lab [Terzaghi et al., 1995, Anochie-Botaeng, 2007, Stafford and Tanner, 1983a,b]. However, direct measurement of these parameters require multiple steps, and are often very time consuming.

Since the soil under excavation is not always homogenous, its mechanical properties can vary dramatically from one location to another. Hence using the lab data for prediction of the interaction force is not an effective choice in such a dynamic environment. This has motivated development of an on-line estimation algorithms for medium property, which can give in-situ information as the machine continues its operating.

Figure 2.12 demonstrates the basic idea behind the use of property estimation for real-time interaction force prediction. In theory, property estimation algorithms employs the inverse model of the tool-ground interaction and the external force measurements, to provide an estimate for the mechanical properties of the medium.



Figure 2.12: On-line Medium Property Estimation and its Implication for Interaction Force Prediction

An effective estimation algorithm will account for the critical mechanical properties and specific properties of the tool-ground, while minimizing the error between the measured and predicted force. Obviously, the estimated properties can be compared to the directly measured values for validation.

Pioneering work on soil property estimation has been conducted for surface sampling in space explorations. Viking 1 and 2 landers (1976-1978), and the Pathfinder lander (1997), conducted studies of soil properties on Mars [Hong, 2001]. In the former mission, investigators measured the force applied by a robotic arm, and estimated the cohesion (c), and internal friction angle (ϕ) using the model developed by McKyes [McKyes and Ali, 1977], presented in section 2.1.1.

There are two major streams of studies in parameter estimation: the first group of studies were carried out by Singh et. al. [Luengo et al., 1998, Cannon, 1999, Cannon and Singh, 2000] that applies the FEE soil-tool model. The other group of studies started with the extensive study carried out by Hong [Hong, 2001] on property estimation for cohesionless material. Inspired by this work, Tan *et al.* conducted a series of theoretical work on cohesionless material applying the Mohr-Coulomb soil model. Their work eventually evolved into experimental work that tackled property estimation for cohesive material [Tan et al., 2003, 2005b,a].

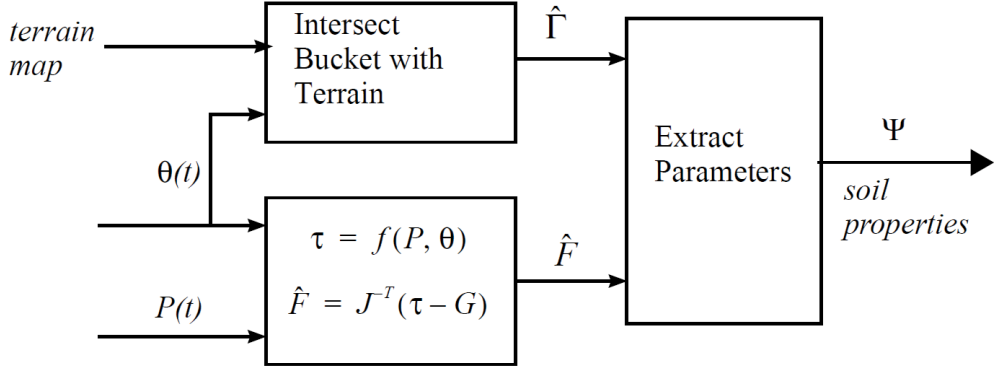


Figure 2.13: Soil Property Estimation Algorithm Using the FEE Model [Cannon and Singh, 2000]

2.1.2.1 Estimation based on the Fundamental Earthmoving Equation

Defining Γ as a function of the geometry of the Tool/Terrain intersection, and Ψ as a function of the inherent properties of the soil

$$\begin{aligned}\Gamma &= f(d, \alpha, \rho, V_s) \\ \Psi &= g(\delta, \phi, \beta, \gamma, c)\end{aligned}\tag{2.12}$$

the resistive force F (force acting on the tool) can be presented as:

$$F = f(\Gamma, \Psi)\tag{2.13}$$

Assuming, $\hat{F} = \hat{\Gamma}\Psi$ where \hat{F} and $\hat{\Gamma}$ are the actual measured values, then Ψ can be estimated by forming the pseudo-inverse of the geometry matrix:

$$\Psi = (\hat{\Gamma}^T \hat{\Gamma})^{-1} \hat{\Gamma}^T \hat{F}\tag{2.14}$$

Due to the difficulties arising from the non-linearity of the FEE interaction model presented in eqs. (2.8) and (2.9), the equation is not invertible [Luengo et al., 1998, Cannon, 1999, Cannon and Singh, 2000]. Therefore, finding the soil parameters (vector Ψ) requires solving an optimization problem, as shown in fig. 2.13: finding Ψ that minimizes the difference between the predicted and measured forces.

Exhaustive search was one of the methods used by Cannon *et al.* and the results were considered to form a baseline. They applied two other optimization methods, efficient gradient descent and the stochastic search, on 20 digs to extract soil parameters. Best estimation was possible using the exhaustive search (after almost 20 hours). While the stochastic search estimates the properties in as quickly as 4 minutes, but convergence was non-uniform. Cannon *et al.* reported a force prediction accuracy roughly within 10-60%, but they did not assess the error of their soil property estimation method.

2.1.2.2 Estimation Based on the Coulomb Earth Pressure Model

Hong applied limit equilibrium techniques (including Mohr-Coulomb, Ohde, and Caquot & Kerisel) introduced in [Terzaghi et al., 1995], and Limit analysis methods (Chen & Liu CLUB model, Numerical FE model) for interaction force prediction [Hong, 2001].

In this approach a flat blade is inserted into cohesionless soils, at a fixed depth of insertion and constant soil surface (horizontal), sets of forces required to fail the soil at various attack angles are recorded. The problem then is reduced to finding estimates of the physical soil properties given these sets of data pairs $\{\alpha_n, F_n\}$: where α_n is the tool angle for the n th measurement and F_n is the force required to move the embedded plate and fail the soil. Using these data pairs, the goal is then to invert the soil models to determine the estimates $\hat{\phi}$, $\hat{\delta}$, and $\hat{\gamma}$ which would account for these measurements.

Hong used a nonlinear optimization methods (weighted sum squared error) presented in eq. (2.15), and discussed that the mapping of parameters to forces are non-unique.

$$WSSE(\phi, \gamma, \delta) = \sum_n \left(\frac{F_n - F_{pred}(\alpha_n, \phi, \gamma, \delta)}{F_n} \right)^2 \quad (2.15)$$

To overcome this problem, he developed the Parameter Space Intersection

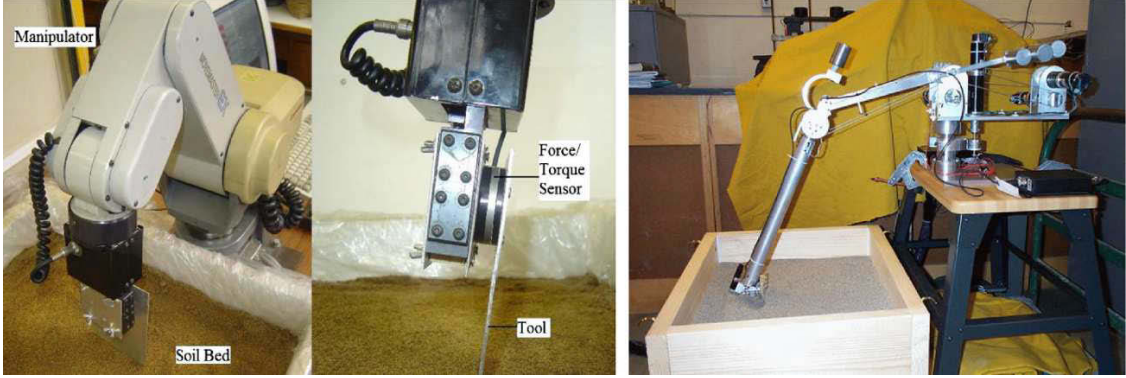


Figure 2.14: Robotic Arms Used for Soil Parameter Estimation in [Althoefer et al., 2009] (left and middle) and [Hong, 2001] (right).

Method (PSIM), a graphical method for model inversion. PSIM uses pre-computed tabulated model predictions for the estimation of the properties of the cohesionless soils in the parameter space (ϕ , γ , and δ) which are consistent with a given set of measurements with associated uncertainties. Hong claimed that the estimated values are in agreement with the direct shear results to within approximately 3° .

Exploring other non-linear optimization techniques for model inversion, Tan *et al.* applied Newton-Raphson Method (NRM) on the same data from Hong's experiments [Hong, 2001] and estimated two parameters of ϕ and γ for some cohesionless soil samples. They reported the same accuracy as in PSIM, but 25 times faster when

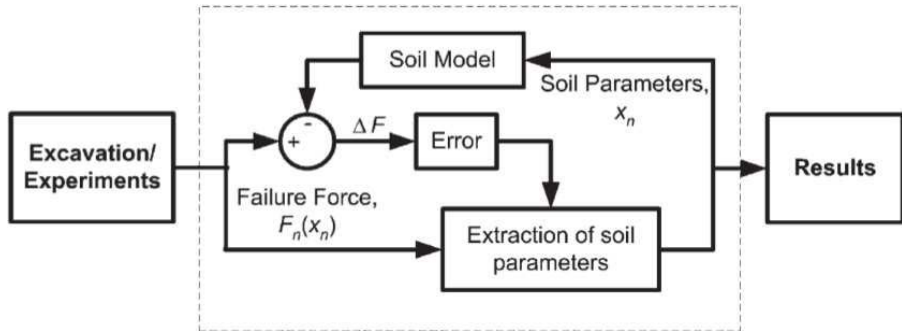


Figure 2.15: Soil Property Estimation Scheme Based on Newton-Raphson Method Adopted from [Tan et al., 2005b].

using Mohr-Coulomb model (in the order of 0.05 s) and 2000 times faster when using Chen & Liu CLUB model (in the order of 0.2 s) [Tan et al., 2003]. Using a combination of Coulomb's model and Chen & Liu Upper Bound (CLUB) model, Tan *et al.* applied the Newton-Raphson optimization technique to replicate the results presented in [Hong, 2001]. The optimization technique was used to minimize the failure force prediction error as depicted in fig. 2.15, and estimated two parameters of ϕ and γ for some cohesionless soil samples [Tan et al., 2003, 2005a]. It was also found that the Mohr-Coulomb model provides much better prediction once the attack angles $\alpha \leq 80^\circ$.

Modifying their estimation method, Althoefer *et al.* used a robotic manipulator to conduct a series of dig and estimate four parameters: (δ) and (γ) from two separate force reading, and then using the two estimated parameters and two additional cutting force reading to estimate the remaining parameters of (ϕ) and (c) depicted in fig. 2.16 [Althoefer et al., 2009, Tan et al., 2005b]. Applying the Modified Newton-Raphson Method (MNRM) on non-cohesive material ($c = 0$), they observed relative error of up to 22.1% in the three remaining parameters estimates. They also applied the method on moderately cohesive material (watered soil sample), where the convergence and accuracy of the estimates required initial values that were sufficiently close or the same as the actual values.

2.2 Maintenance & Condition Monitoring

Reliability is defined as the ability of a component or a system to perform its required functions under the desired conditions of operation within a given time frame. Therefore most equipment maintenance programs are designed around the philosophy of delivering reliable equipment consistently [Tomlinsion, 2009]. These maintenance programs are aimed to improve equipment reliability, to lower the downtime and also to allow realizing the productivity built into the equipment

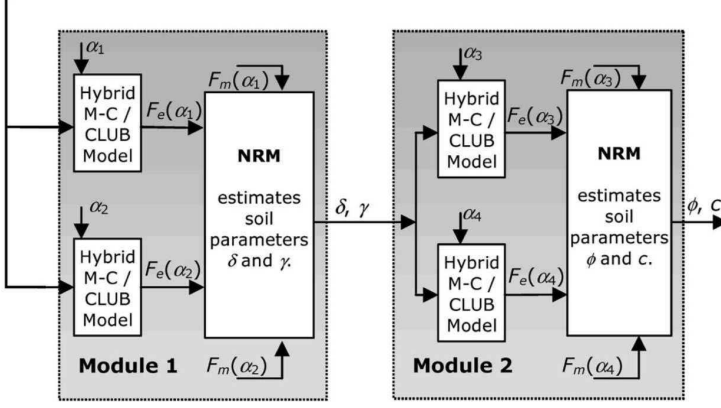


Figure 2.16: MNRM Using the Hybrid Soil Model: Each Module Computes Estimates for the Two Soil Parameters, Reducing the Error Between Estimated Forces F_e and Measured Forces F_m at Different Attack Angles α_1 , α_2 , α_3 , and α_4 at Each Iteration. The Cycle Is Repeated Until the Overall Force Error Is Below a Predefined Threshold. After [Althofer et al., 2009]

[Sottile and Holloway, 1994].

Traditional maintenance strategies were developed solely on time-based actions such as inspections, component replacements, and overhauls, assuming the equipment's reliability degrades proportional to the time in service. This is not necessarily the right assumption for equipment and machines that operate in variable conditions. For a given earthwork activity, carried out with a piece of earthmoving equipment, of the proper power capacity, the active force delivered to the tool must be greater than the resistive force of the medium. However, if the resultant of the excavating force is greater than the capacity of the excavating machine (in terms of power, or rigidity of the elements) it can cause damage to the elements of the power terrain (motor/engine, hydraulic system, gears and bearings) as well as the structural components of the equipment [Hemami, 1995]. In addition to the excessive external loading, there are a handful of other sources that could cause component and machine level failure. Infant mortality, reaching the end-of-service life of the parts, poor maintenance, equipment misuse or poor operating method, and pre-existing conditions are some of the examples or the failure root cause. A

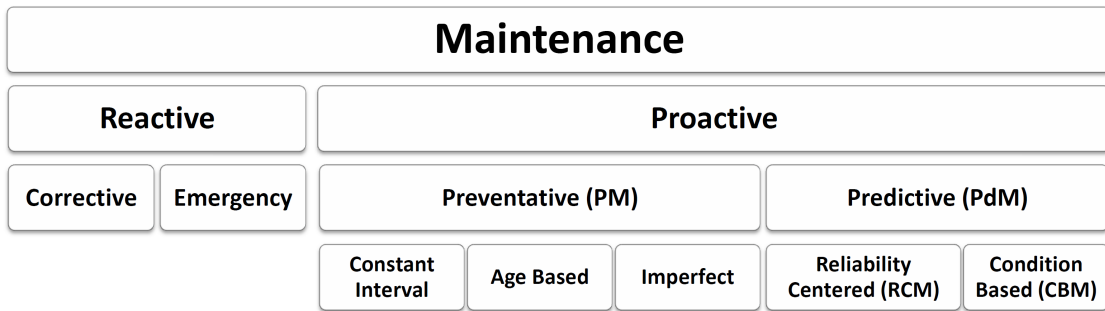


Figure 2.17: Taxonomy of Maintenance Philosophies According to [Kothamasu et al., 2006].

component failure may lead to consequential damage to other parts of the machine, long and costly shutdowns, and a high opportunity cost of lost production [Majumdar, 1995, Dhillon, 2008, Hall and Daneshmend, 2003, Dhillon, 2002, Edwards et al., 2002]. Depending on the criticality of the equipment, implementation of the maintenance program could vary from simple reactive maintenance based on “Fail and Fix” approach, to more complicated proactive maintenance approaches that employ advanced condition monitoring techniques. In preventative (time-based) and Predictive (condition-based) methods, potential failure could be predicted early enough to take action and avoid system/functional break down. Figure 2.17 demonstrates the reactive and proactive trends in maintenance practices [Girdhar, 2004].

2.2.1 Condition-Based Maintenance

One of the most cost efficient methods for critical equipment maintenance is Predictive Maintenance (PdM), with the focus on the equipment condition as it is operating. It relies on incipient failures and the resultant change in some of the monitored parameter [Randall, 2011]. Condition-based maintenance (CBM) is commonly used for diagnostic (identifying the nature or cause of a failure) and prognostic (prediction about how a failure will develop) [Jardine et al., 2006], through detection of a change

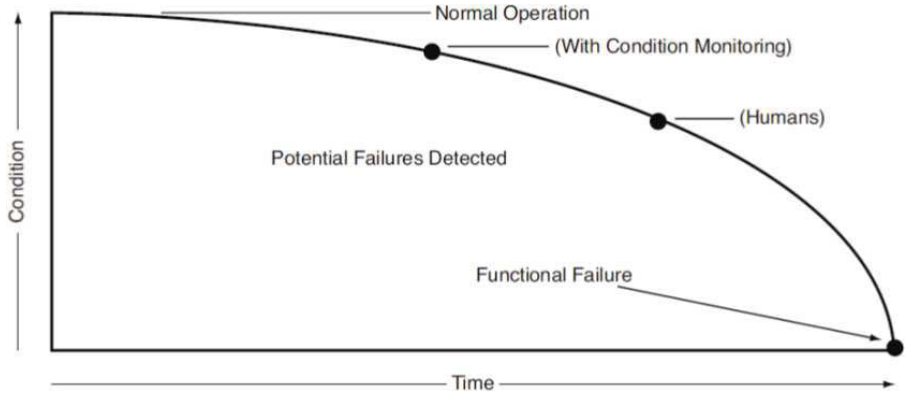


Figure 2.18: Condition Monitoring Allows Early Detection of Potential Failures [Tomlinsong, 2009].

in the features of a system (potential failure/fault) that could be an indication of a functional failure down the road, as shown in fig. 2.18. Any fault detection system comprises of data collection, feature extraction and assessment of the features. The two main streams in fault detection are *pattern-based methods* and *model-based methods*. Model-based methods can only be applied to systems where the complete physics of the system is understood well enough to construct a model under both acceptable and unacceptable operations. On the other hand, pattern-based methods function by distinguishing the patterns of ‘acceptable’ from ‘unacceptable’ based on a limited knowledge of the system, gained from system’s behavior, operation or certain parameters. The change in the pattern of the system, compared to the frame of reference (often the normal operating condition), is an indication of fault presence. Fault diagnostic (or pattern recognition) is commonly described as a mapping between the information from measurement space or feature space to machine faults in the fault space [Jardine et al., 2006], and is tied very closely to the detection concept. Vibration is the main parameter for monitoring many mechanical systems. Other parameters of interest are the lubricant composition, temperature and noise.

2.2.2 Vibration Analysis

Mechanical vibrating systems can be modeled with three elements: inertia element, elastic element, and damping element [Bobrovnikii, 2007]. The dynamic state of such systems can be fully described by one variable that characterizes deflection of the inertia element from the equilibrium position as shown in fig. 2.19.

It is commonly accepted to represent a general Single-Degree-of-Freedom (SDOF) system as the mass-spring-dashpot system shown in fig. 2.19 with:

$$m\ddot{x}(t) + c\dot{x}(t) + kx(t) = f(t) \quad (2.16)$$

where $x(t)$ is the displacement of the mass from the equilibrium position, and $f(t)$ is an external force applied to the mass - in the form of $\text{Re}(fe^{j\omega t})$ for harmonic vibrations. The three terms in the left-hand side of the equation represent the force of inertia, dashpot reaction force, and the force with which the spring acts on the mass. Common for all types of vibration is that the mass gives rise to an inertia force, the spring acts as an elastic restoring force, and the damper acts as a converter of mechanical energy into some other form, most commonly heat. To apply the results to physically different SDOF systems, the parameters m , k , c , and the displacement x should be replaced by the corresponding quantities as shown in fig. 2.19. Equation (2.16) can be generalized to represent the equation of motion of Multi-Degree-of-Freedom (MDOF) systems with N degrees of freedom as well:

$$\mathbf{M}\ddot{\mathbf{x}}(\mathbf{t}) + \mathbf{C}\dot{\mathbf{x}}(\mathbf{t}) + \mathbf{k}\mathbf{x}(\mathbf{t}) = \mathbf{f}(\mathbf{t}) \quad (2.17)$$

where $\mathbf{x}(\mathbf{t})$ and $\mathbf{f}(\mathbf{t})$ are the displacement and external force vectors associated with each element.

$$\begin{aligned} \mathbf{x}(\mathbf{t}) &= [x_1(t), x_2(t), \dots, x_n(t)]^T \\ \mathbf{f}(\mathbf{t}) &= [f_1(t), f_2(t), \dots, f_n(t)]^T \end{aligned} \quad (2.18)$$

Vibration in most mechanical systems involves the periodic oscillation of energy from potential to kinetic [McBain, 2012]. Linear mechanical vibrations can be

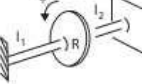
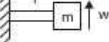
Vibratory System	Inertia Element	Elastic Element	Damping Element	Variable	
	Mass-spring-dashpot system	Mass, m (kg)	Spring with stiffness k ($N\ m^{-1}$)	Dashpot with damping coefficient c ($kg\ s^{-1}$)	Linear displacement x (m)
	Disc-shaft system	Moment of the disc inertia $\frac{mR^2}{2}$ ($kg\ m^2$)	Static torsional stiffness of the shaft $G \frac{\pi a^4}{2} \left(\frac{1}{I_1} + \frac{1}{I_2} \right)$ ($N\ m$) G = shear modulus a = radius of the shaft	Losses in shaft material	Angular displacement of the disc ϕ (rad)
	Cantilever beam with a mass at the end	Mass, m (kg)	Static flexural stiffness of the beam $\frac{3EI}{l^3}$ ($N\ m^{-1}$) E = Young's modulus I = moment of inertia	Losses in beam material	Linear displacement of the mass w (m)
	Pendulum	Moment of inertia ml^2 ($kg\ m^2$)	Angular stiffness due to gravity $g = 9.8$ ($m\ s^{-2}$) mgl ($N\ m$)	Friction in suspension axis	Angular displacement ϕ (rad)

Figure 2.19: Examples of Single Degree of Freedom (SDOF) System (after [Bobrovitskii, 2007])

described in exponential form [Pettersson, 2007]:

$$\xi(t) = \text{Re}[Ae^{j\omega t}] \quad (2.19)$$

where A is the amplitude - which is complex in general - and it has a phase shift relative to some reference, and ξ is the mass displacement. Vibration power represents the energy transmitted per unit of time along continuous lines or discrete points in vibrating structures [Heo and Kim, 2015]. Non-stationary processes such as vibrations resulting from impacts encompassing a finite amount of energy are assessed by means of

$$\begin{aligned} E &= \int_0^{T_p} F(t)\xi(t)dt = \int_0^{T_p} \text{Re}[\hat{F}^{j\omega t}] \text{Re}[\hat{\xi}e^{j\omega t}]dt \\ &= \frac{1}{2} \text{Re}[\hat{F}\hat{\xi}^*] \end{aligned} \quad (2.20)$$

where $F(t)$ is the excitation force, and the $*$ denotes the complex conjugate. Similarly, those processes that can be considered stationary, can be assessed by

means of the power averaged over time:

$$\begin{aligned}
 \bar{W} &= \lim_{T \rightarrow \infty} \frac{1}{T} \int_0^T F(t) \frac{\partial \xi(t)}{\partial t} dt \\
 &= \lim_{T \rightarrow \infty} \frac{1}{T} \int_0^T \operatorname{Re}[\hat{F}^{jwT}] \operatorname{Re}[\dot{\xi} e^{jwT}] dt \\
 &= \frac{1}{2} \operatorname{Re}[\hat{F} \dot{\xi}^*]
 \end{aligned} \tag{2.21}$$

where $\dot{\xi}$ is the velocity in the direction of the force F . The advantage of using energy or power is seen in the fact that the transmission process involves both kinematic (motion) and dynamic (force) quantities.

The mechanical vibration process can be summarized into four main steps as depicted in fig. 2.20: A mechanism triggers the vibration (generation), oscillatory energy transfers from the mechanisms of generation to a passive structure (transmission), energy distributes throughout the structural system (propagation) and finally power imparts to the environment (radiation). Rotating and reciprocating equipment, even in good condition, can generate vibrations. These vibrations can be directly linked to periodic events in the machines operation, such as rotating shafts, meshing gearteeth, rotating electric fields, and so on [Randall \[2011\]](#).

Imparted energy flows into the subsystems, whereas parts of it turns into energy losses. The power balance for two coupled subsystems is illustrated in fig. 2.21 where power is injected in subsystem 1 W_{1in} . This is partially transmitted to subsystem 2 W_{21} , and partially dissipated W_{1diss} . Similarly, the power transmitted to subsystem 2 is partially retransmitted to subsystem W_{12} and partially dissipated W_{2diss} . This

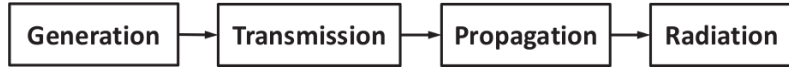


Figure 2.20: Mechanical Vibration As A Process (after [\[Petersson, 2007\]](#))

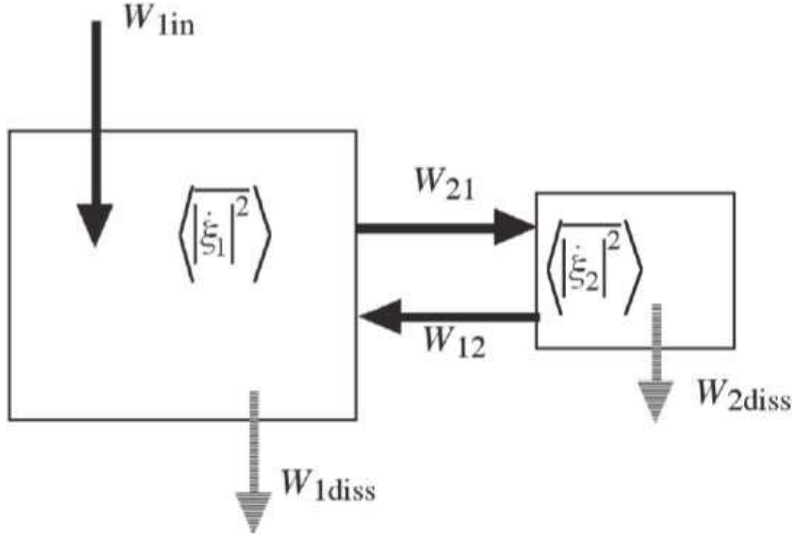


Figure 2.21: Energy Flows in Two Coupled Subsystems (after [Petersson, 2007])

means that the power balance for the system can be written as:

$$\begin{aligned} W_{1in} + W_{12} &= W_{21} - W_{1diss} \\ W_{21} &= W_{12} + W_{2diss} \end{aligned} \quad (2.22)$$

When the number of modes in a frequency band (modal density) gets sufficiently large, it is often more appropriate and convenient to consider an energetic description of the vibration [Petersson, 2007]. This way, the distribution of the energy throughout the vibrating system can be estimated. A remarkable feature of this description is its capability to capture the variation in the vibration characteristic of the system. For example, small geometrical deviations from a nominal design have a strong influence on the transmitted vibration frequency [Petersson, 2007]. Note that the power transmitted between two subsystems is proportional to the energy of the emitting subsystem and, hence, to the average mean square velocity, where the equality of kinetic and potential energies for resonantly vibrating systems is invoked [Petersson, 2007]. A spatial average is denoted by $\langle \rangle$ enclosing the variable. Accordingly, the

energy flows can be written as:

$$\begin{aligned} W_{21} &= C_{21} \langle \overline{\dot{\xi}_1^2} \rangle \\ W_{12} &= C_{12} \langle \overline{\dot{\xi}_2^2} \rangle \end{aligned} \quad (2.23)$$

where C_{21} and C_{12} are coefficients that are dependant of the spatial and temporal coupling of the two vibration fields.

Vibration analysis works on the premise that defects in a machine change the normal vibration signature in a way that can be related to the fault [Tomlingson, 2009, Randall, 2011]. Mechanical objects vibrate in response to the pulsating force of a machine defect. An increase in the vibration amplitude, can signify the growth of a potential defect. Vibration monitoring can reveal problems in machines involving unbalance, misalignment, looseness and impact. It can uncover and track the development of defects in machine components such as bearings, gears, belts, and drives Tomlingson [2009]. In moving systems, potential energy can be temporarily stored in rotor shaft deflection, bearing deflection, or the deformation of the machine elements [McBain, 2012]. Temporary spring-like storage can be found in virtually every component of the machinery [McBain, 2012], and which can cause vibration when released. The basic problem of the condition monitoring is further explained next.

Source of information in Vibration signal

Measured vibration signals are always a combination of source effects and transmission path effects. The contribution to the response at one measurement point from one source, in the time domain, is a convolution of the force signal with the impulse response function (IRF) of the transmission path from the source to the measurement point [Randall, 2011]:

$$x_i = \sum_j s_j * h_{ij} \quad (2.24)$$

where s_j is the source, and x_i is the measured impulse response. In the frequency domain this simplifies to a product of their respective spectra, the spectrum of the

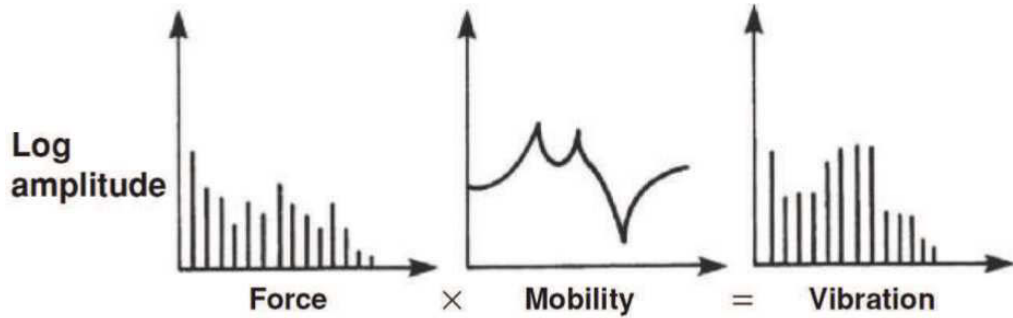


Figure 2.22: Combination of Forcing Function and Transfer Path to Give Response Vibration for One Source (after [Randall, 2011]).

IRF being equal to the corresponding frequency response function (FRF), and can be presented as:

$$X_i = \sum_j S_j H_{ij} \quad (2.25)$$

where S_j , and X_i are the Fourier transform of their respective signals in eq. (2.24). Figure 2.22 depicts the combination of forcing function and transfer path to give response vibration for a single source. Here, ‘mobility’ is the FRF corresponding to force input and vibration velocity output. Identifying a change in response vibration, the diagnosing problem is to decide whether the change has occurred at the ‘source(s)’ or in the ‘structural’ transmission path. While in many cases, the change at the source (e.g. increase in imbalance, change in the gear meshing force, etc.) is the root cause of the change in the condition, there are also instances where the changes in the structural response can be due to other types of faults (e.g. a developing crack in a machine element) [Randall, 2011].

An example with a combined effect is a developing tooth root crack that affects the local structural properties (i.e. the stiffness), but in terms of responses at the bearings this can be interpreted as a change in the forcing function at the tooth mesh. Another example is the case of a crack in a moving element, if the crack is breathing, that is opening and closing every revolution of the shaft, the character of the forcing function changes (increases or decreases) as the crack opens and closes,

which would change the magnitude of the responses at each those instances [Randall, 2011, Shih and Chung, 2013].

Signal Classes

Most machine components (e.g. gears, bearings, etc.) give rise to specific vibration signals that characterize the behavior of the component. This allows to distinguish them from other components. It is well-known that gear-generated signals are usually at harmonics (integer multiples) of the associated shaft rotation speeds, whereas the frequencies associated with the bearings are not [Randall, 2011]. The presence of a defect in machine parts can change this characteristic of the component, depending on the failure mode. Signals are often distinguished by the repetition frequencies of periodic events, which justifies the use of frequency spectrum for studying how their constitutive components are distributed with frequency.

The characteristics of the signal under study determines what signal processing techniques should be used. Signal classes can basically be broken down into two classes of ‘stationary’ and ‘non-stationary’ as is presented in fig. 2.23. Stationary signals have statistical properties that are invariant with time. If the signal does not satisfy the conditions for stationarity, it is considered non-stationary.

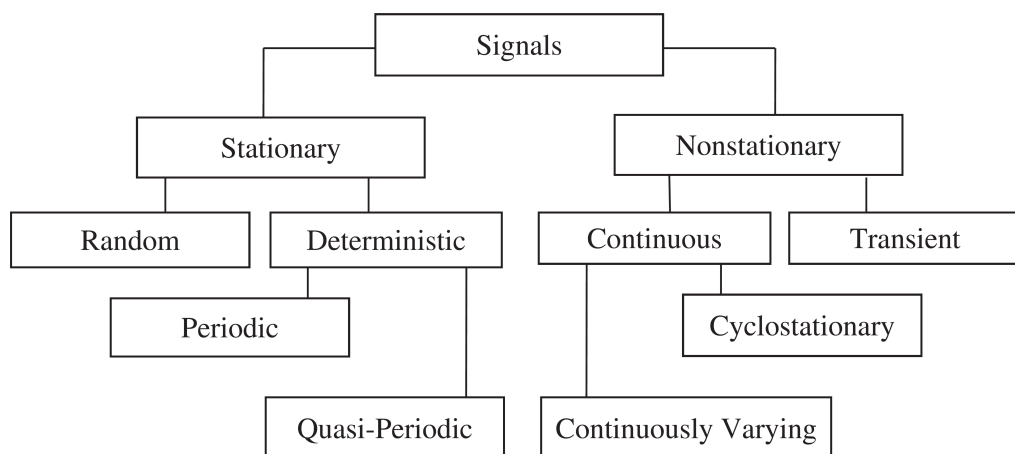


Figure 2.23: Main Signal Categories (after [Randall, 2008])

Stationarity condition for deterministic signals means that they are composed entirely of discrete frequency sinusoids, and their value can be predicted. The frequency spectrum of deterministic signals (i.e. Periodic and Quasi-periodic) consists of discrete lines at the frequencies of those sinusoids as shown in fig. 2.24. On the other hand, the value of the random signals cannot be predicted, however they have unchanging statistical properties. Stationary random signals do not appear very different in the time domain from the quasi-periodic signal, but their spectrum is entirely different, with no discrete frequencies as shown in fig. 2.24.

Non-stationary signals can be divided into two main classes, continuously varying and transient. Transient signals only exist for a finite length of time and are typically analyzed as an entity. Typical example of transient signal is the impulsive force, and the impulse response of the structure to which the force is applied. The energy and power of the signal can be used to distinguish between transient and continuous signals. The true power associated with a vibration signal is related to the square of its amplitude. A transient signal has an instantaneous power at each point in time but is characterized by the integral of this power over its whole length in time, this being called its energy. Energy of the non-stationary transient signal is finite and explained earlier in eq. (2.20). Cyclostationary signals by definition have power which is always positive but varies periodically with time, and so their total energy is infinite.

Vibration signals measured during the run-up or coast-down of a machine, also have a finite length, but are considered as continually changing non-stationary signals, rather than transients. They are analyzed by being divided into short quasi-stationary sections, to see how their power varies with time (time/frequency analysis). Continuously varying non-stationary signals will often be treated by the techniques of time/frequency analysis.

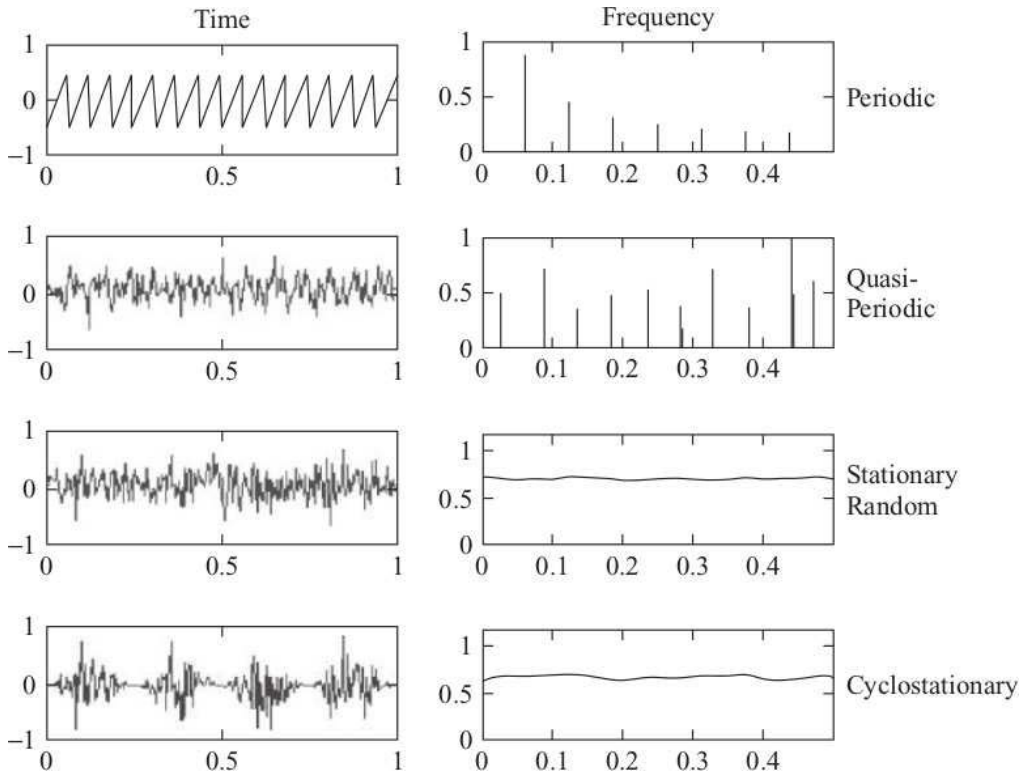


Figure 2.24: Typical Signals in the Time and Frequency Domains (after [Randall, 2008])

2.2.2.1 Vibration Signature and Failure Modes

Every machinery can be considered as a mechanical multi-body systems which is made of several components. These components can be divided in two major groups: links, that is, bodies with a convenient geometry, and joints, which introduce some restrictions on the relative motion of the various bodies of the system [Flores et al., 2011]. Signals generated from machines during constant speed and load condition, are typically stationary and/or cyclostationary, whereas start-up and coast down signals are non-stationary signals. Most faults manifest themselves at a frequency corresponding to the speed of the shaft in question, e.g. $1\times$ (one time), $2\times$ (two times), and so on. Changes in vibration signals are ascribed to changes in condition, so it is important to pick up the fault signature incorporated in these signals through

Unbalance	Gear defects	Cavitation
Bent shaft	Misalignment	Bearing defects
Eccentricity	Shaft cracks	Oil whip/whirl
Looseness	Rotor rubs	Belt drive problems

Figure 2.25: Some of the Machinery Defects Detected using Vibration Analysis.

the use of proper transducers (i.e. proximity probes, accelerometers, encoders). Radial vibration is in the plane perpendicular to the axis of rotation, and can be detected by radial vibration transducers (accelerometers and proximity probes) as a result of their radial component. Some failures in machine components occur because of excessive torsional vibration. Torsional vibrations, are variations in angular velocity of the shaft, result directly from the fluctuating torque (that can be associated with a varying loading in a reciprocating system).

Vibration signal generated by the machine components defect - depending on their geometry - can be produced at different harmonics of the rotating shaft and in different direction, e.g. the unbalance gives a response primarily at $1\times$ in the radial direction, and the vibration from misalignment amplifies a response at $2\times$ and in the axial direction. Figure 2.25 summarizes the commonly witnessed machinery faults diagnosed by vibration analysis.

Unbalance and misalignment are two very common type of faults, where the asymmetric mass distribution of the rotor produces centripetal forces that rotate with the rotor and causes high vibration. These faults along with mechanical looseness, rotor rub, bearing and gear faults often produce an axial or radial vibration response. Torsional/angular vibration - in the direction parallel to the axis of rotation - most often experienced often because of variations in gear geometry, periodic rotor-to-stator contact, misaligned couplings, reciprocating drivers or loads, or because of radial vibration [Girdhar, 2004].

Some of the more common failure modes of interest associated with multi-body mechanisms are excessive clearance in joints, cracks in load-bearing elements, and faults related to gearbox. These failure modes are further described next.

Joint Clearance

Mechanical looseness in rotating equipment can occur at three locations: internal assembly looseness, looseness at machine, and structure looseness. This category of fault could be between a bearing liner in its cap, a sleeve or rolling element bearing (this is discussed later), or an impeller on a shaft. The functionality of a joint relies upon the relative motion allowed between the connected components, with inevitable clearance between the mating parts. This leads to surface contact, shock transmission, and the development of friction and wear. No matter how small that clearance is, it can cause vibration and fatigue phenomena, lack of precision or, even random overall behavior [Flores et al., 2011]. To study the loss of contact due to joint clearance proximity probes and accelerometers can be used [Haines, 1985, Dubowsky et al., 1984, Soong and Thompson, 1990].

For an ideal or perfect revolute joint, with small or no clearance, the journal and bearing centers coincide. The inclusion of the clearance (c), the difference between

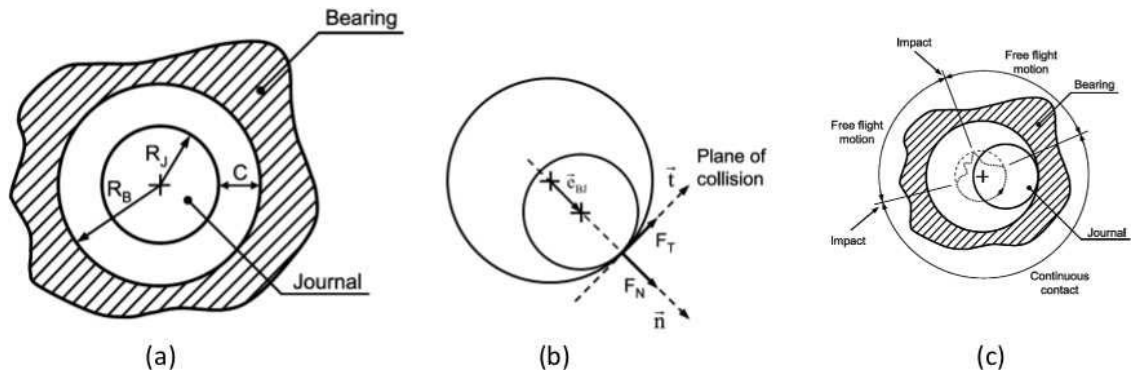


Figure 2.26: (a) Representation of a revolute Joint with Clearance, (b) Normal and Tangential Forces Due to the Impact Between the Journal and Bearing Surfaces, (c) Different Types of Journal Motion Inside the Bearing (after [Flores et al., 2011]).

the bearing radius R_B and the journal radius R_J , allows for the separation of these two centers as shown in fig. 2.26(a). In a dry contact situation, the journal can move freely within the bearing until contact between the two bodies takes place. Figure 2.26(b) illustrates the normal and tangential force components due to the impact between the journal and the bearing wall. This would create a normal contact force together with a friction force that can be evaluated to obtain the dynamics of the journal-bearing. These forces are of a complex nature, and their corresponding impulse is transmitted throughout the mechanical system [Flores et al., 2011]. In a revolute clearance joint, three different modes of motion between the journal and the bearing can be considered, as shown in fig. 2.26(c): continuous contact mode, free flight mode, and impact mode. In the continuous contact mode, the journal and the bearing are in contact and a sliding motion related to each other is assumed to exist. This mode is ended at the instant when the journal and bearing separate and the journal enters the free flight mode. In the free flight mode, the journal can move freely inside the bearing boundaries, i.e., the journal and the bearing joint are not in contact, and hence there is no reaction force between these two elements. After the end of the free flight mode, the journal enters the impact mode, in which impact forces are applied and removed. At the termination of the impact mode, the journal can enter either free flight or following mode. Measuring the acceleration of the moving element, the impact force between the journal and bearing can be measured and monitored indirectly.

Revolute joint with clearance has been investigated through a Crank-Slider mechanism in a number of studies [Flores et al., 2011, Erkaya and Uzmay, 2010, Sun and Xu, 2013, Gummer and Sauer, 2014]. Experimental results indicates that the force variations on the mechanism can reach beyond the expected design values due to the impact force acting only during a small time interval of contact, which can cause a sudden increase in the vibration amplitude. The number and magnitude of the contribution of the dominant frequencies increase with the crank speed and

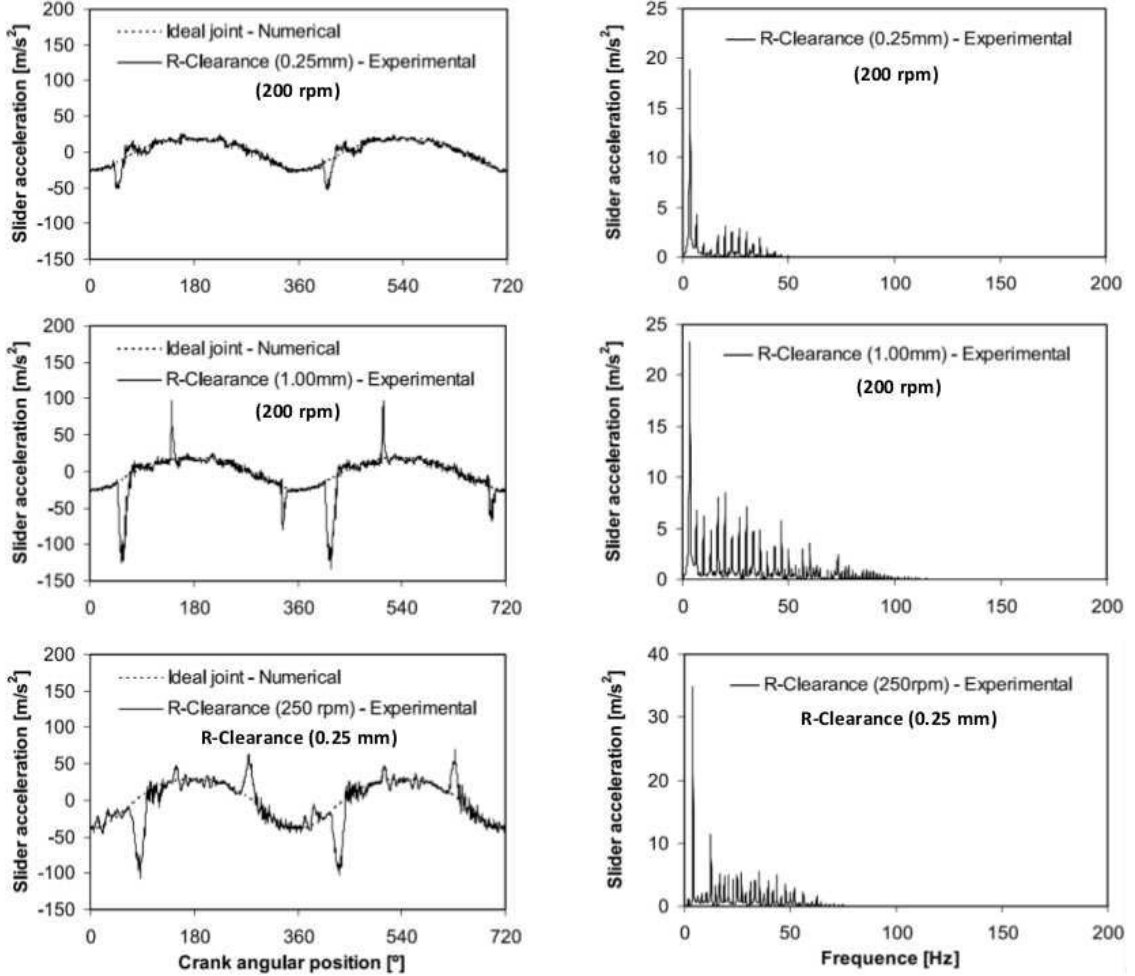


Figure 2.27: Effect of Revolute Joint Clearance on Acceleration Signal: $c=0.25$ mm, $\omega=200$ rpm (top), $c=1.00$ mm, $\omega=200$ rpm (middle), $c=0.25$ mm, $\omega=250$ rpm (top) (after [Flores et al., 2011]).

the clearance size. Furthermore, the maximum slider acceleration increases with crank speed and clearance, as illustrated in fig. 2.27.

Once a journal bearing goes through excessive wear, it may display a whole series of running speed harmonics, which can be up to $10\times$ or $20\times$. At this point, the FFT spectrum of the clearance looks very much like that of mechanical looseness. Presence of minor unbalance or misalignment can exacerbate the condition and cause higher vibration amplitudes compared with bearings having a normal clearance with

the journal [Girdhar, 2004].

Breathing Crack

The basic principle during crack development is that the rotor loses stiffness in the direction perpendicular to the crack direction. If a crack develops on the circumference of a rotor, transverse to the shaft axis, the stiffness in the plane perpendicular to the crack decreases and remains the same in the other orthogonal plane. This would cause two major deflections per revolution, which would cause the $2\times$ rpm vibration frequency. There are two fundamental symptoms of a shaft crack: An unexplained changes in the $1\times$ shaft relative amplitude and phase, and occurrence of a $2\times$ vibration frequency.

While many have studied the presence of a crack in a rotor [Ishida, 2008, Bachschmid et al., 2010, Babu et al., 2008, Stoisser and Audebert, 2008], and beams [Saavedra and Cuitino, 2001, Douka and Hadjileontiadis, 2005] not many studies are carried out on a developing crack on elements of a multi-body system [Yin et al., 2007, Shih and Chung, 2013, Raza and Frimpong, 2013]. The existence of a crack in an element of a linkage not only influences the rigidity of the component, but also changes dynamic characteristics of the system. Considering the crank-slider

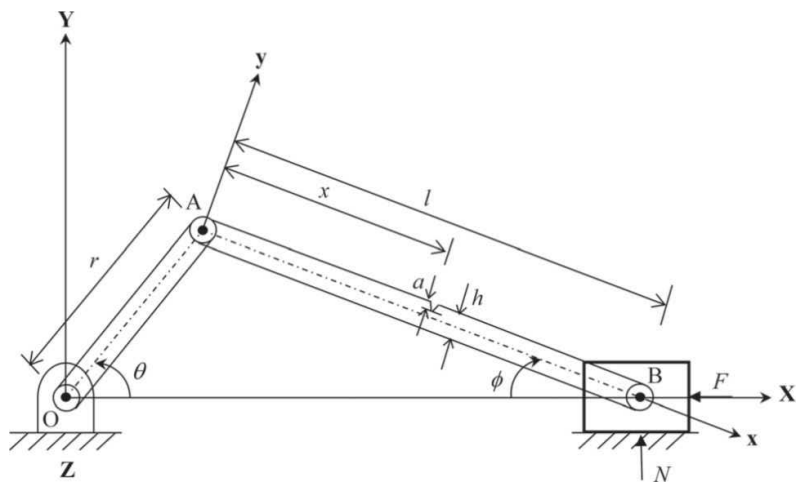


Figure 2.28: Slider-Crank Mechanism with a Flexible Cracked ($x=1/2$) Connecting Rod Under Undeformed Configuration (after [Shih and Chung, 2013]).

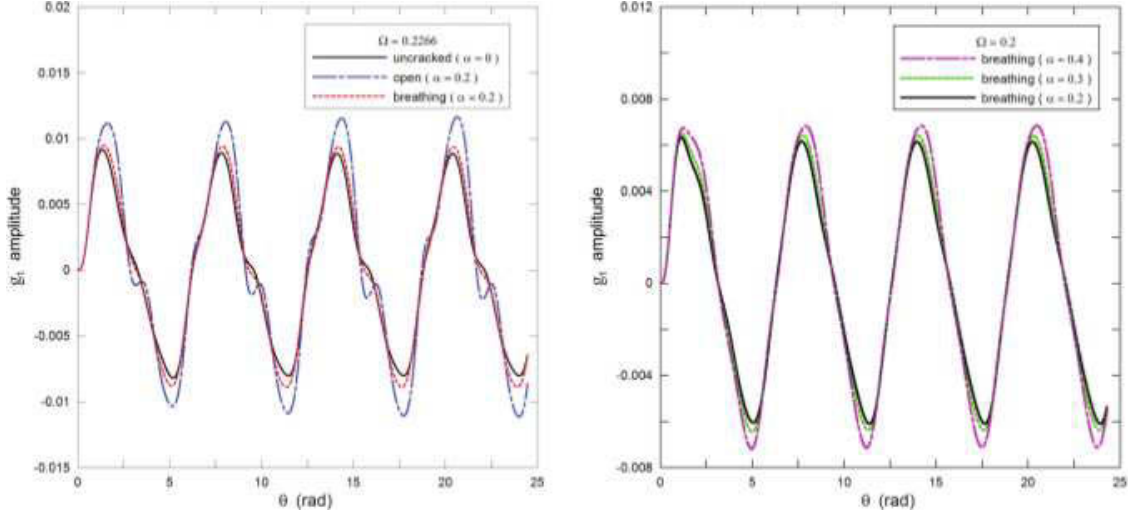


Figure 2.29: Left: Comparison Among the Uncracked, Open, and Breathing Crack Models of Transverse Amplitude Under Constant Crank Angular Speed Ω_1 . Right: Transient Transverse Amplitude for the Breathing Crack Model with Different Crack Depth Ratios Under Reduced Angular Speed $\Omega_2 = 0.9\Omega_1$ (after [Shih and Chung, 2013]).

multi-body system shown in fig. 2.28, presence of crack in the connecting rod has been studied in [Fung, 1997, Chondros et al., 2001, Shih and Chung, 2013].

To analyze the behavior of a cracks, two breathing crack models are commonly used: an open crack model and a breathing crack model. The breathing crack model assumes that the stiffness of the link varies between a maximum (closed crack under compressive load) and a minimum (open crack under tensile load). When a crack locates at the surface of the connecting rod, the natural frequency of the cracked connecting rod is influenced by the crack depth. The transverse vibration of the connecting rod with a breathing crack, is directly influenced by the crack severity, and the rotating speed of the crank (ω).

Figure 2.29 demonstrates that the larger the crack severity index (α) is, and the greater the angular velocity ratio (Ω), the greater the increase in the vibration amplitude will be.

Gearbox Faults

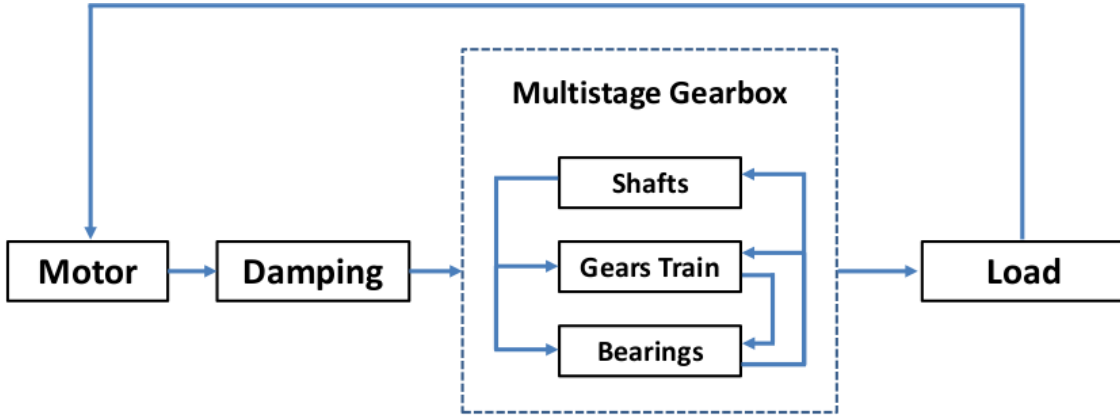


Figure 2.30: Interaction Between Components in Multi-Stage Gearbox System and External Components to the Gearbox Such As: Motor, Damping Coupling, External loading (after [Bartelmus and Zimroz, 2014]).

Gearboxes often act as the link between the driving and driven machine, therefore they have to be designed for high reliability. A common type of gearbox has parallel shafts and consists of several elements - gears, bearings and shafts - that interact with each other as illustrated in fig. 2.30. Hence, gearbox needs to be treated as a system, and not as individual gears and bearings. In monitoring the gearbox system, factors influencing the vibration, i.e. change of condition and operation factors, and the effect of elements on each other should be taken into account as demonstrated earlier in fig. 2.2 [Bartelmus and Zimroz, 2009a, Bartelmus et al., 2010, Bartelmus and Zimroz, 2014]. Gearbox degradation can be contributed to two groups of failure: Primary unbalance and misalignment associated with the way the gearbox is coupled with the motor or the load at the beginning of operation; and Secondary misalignment - also known as the inner gearbox shafts and gears misalignment (IGSGM) - due to frictional wear of bearings and linear increase of inter-teeth forces [Bartelmus and Zimroz, 2014]. The main cause of gearbox failure is often the secondary misalignment which can trigger the degradation process of the gear tooth.

A looseness (between a bearing liner in its cap, a sleeve or rolling element

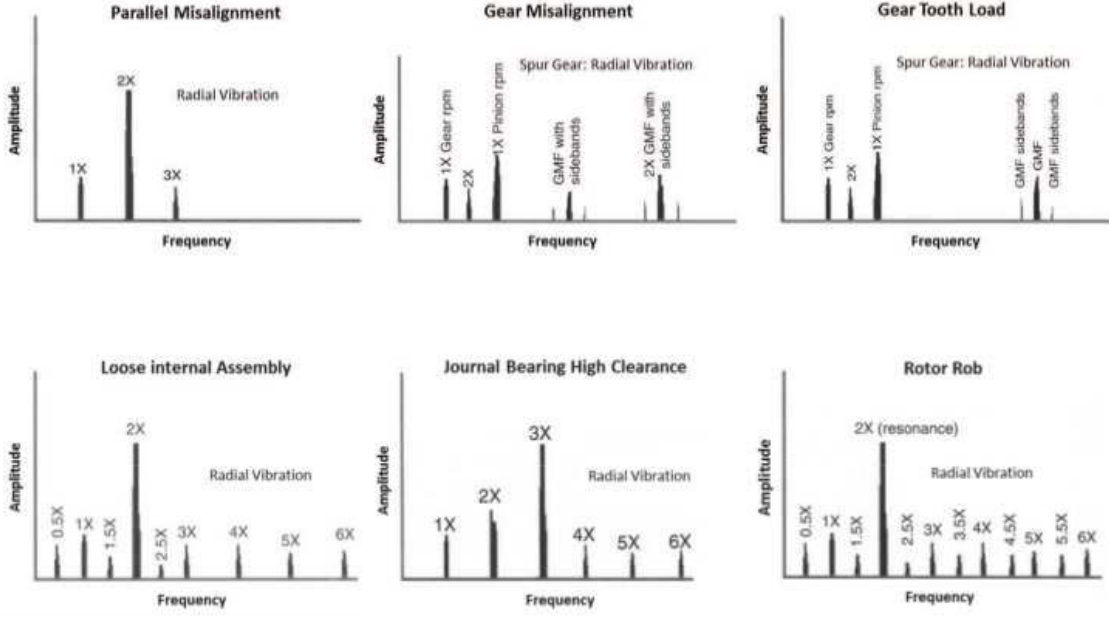


Figure 2.31: FFT of the Vibration Signal Associated with Some of the Common Failure Modes of the Gearbox System (after [Girdhar, 2004]).

bearing), can cause the inner misalignment and turn into the rubbing between shafts and stationary parts (due to misalignment under severe pre-loading) and cause sever damage to gearbox assembly and must hence be identified immediately. In many cases gearbox systems operate under non-stationary load/speed conditions during their normal state, e.g. in wind turbines and excavators. In such systems the vibration signal is directly linked to the operation factor - instantaneous speed or the external load variation [Bartelmus et al., 2010].

FFT spectrum of the vibration signal associated with some of the common failure modes of the gearbox system under stationary condition is illustrated in fig. 2.31. For fault diagnosis of gearboxes under non-stationary operations, researchers have proposed other statistical analysis [Samuel and Pines, 2005], time domain averaging [McFadden, 1991], Time - Frequency analysis [Williams and Zalubas, 2000], Cyclostationary analysis [Zimroz and Bartelmus, 2009, Bartelmus et al., 2009]. Extraction of the diagnostic features from vibration signal often requires extensive

signal conditioning, i.e. filtering, modeling or decomposition. One of the most recent approaches in gearbox monitoring is a novel decomposition method called Empirical Mode Decomposition (EMD) and has shown its effective application in many diagnostic tasks [Ricci and Pennacchi, 2011, Lei et al., 2013, Amarnath and Krishna, 2014, Dybala and Galezia, 2014, Li et al., 2015, Liu et al., 2015].

2.2.2.2 Signal Processing

The type of the signals emitted from a machine is the primary factor in the selection of an appropriate processing method. This becomes more important knowing that time and frequency manifestation of various signals can be significantly different. In rotating equipment, faults such as imbalance and misalignment manifest themselves at shaft speed and its harmonics. Power spectra of the signal in time domain or frequency domain can be used for detection of these faults, if the signal is stationary. In reciprocating machines, signal varies both in time and frequency domains due to variable loading/speed conditions and the signal that is measured during one shaft rotation may be severely non-stationary [Randall, 2011]. Furthermore, faults with short duration transient effect have an intermittent or transient characteristic and give rise to sudden and brief changes in signal amplitude or phase. Impacts of this nature will hardly be visible in the spectrum, because energy is dispersed in the temporal averaging process.

One appropriate group of signal processing methods for continuously varying non-stationary signals is the family of time-frequency methods, such as the STFT (Short Time Fourier Transform), which will be discussed later.

Time Domain

Vibration signals are initially obtained as time series representing proximity, velocity, or acceleration in the time domain. Time domain feature extraction has 3 main categories: Raw signal method, filter-based method, and stochastic/advanced methods [Yang et al., 2003]. The most commonly used approach in time domain is

Table 2.1: Time-Domain Features Extracted Based on Statistical Method

Order	Feature	Description
Fr_1	Standard deviation	$\sigma^2 = \int_{-\infty}^{\infty} [x - \mu]^2 p(x) dx$
Fr_2	Skewness	$S = \frac{\int_{-\infty}^{\infty} [x - \mu]^3 p(x) dx}{\sigma^3}$
Fr_3	Kurtosis	$K = \frac{\int_{-\infty}^{\infty} [x - \mu]^4 p(x) dx}{\sigma^4}$
Fr_4	Peak to Peak	$P2P = \text{Max}(x) - \text{min}(x)$
Fr_5	Mean	$\mu = \int_{-\infty}^{\infty} x p(x) dx$
Fr_6	Peak to Mean	$P2M = \frac{Fr_4}{Fr_5}$
Fr_7	Root Mean Square	$RMS = \sqrt{\text{Mean}(x^2)}$
Fr_8	Crest Factor	$CF = \frac{\text{Max}(x)}{RMS(x)}$
Fr_9	Shape Factor	$SF = \frac{RMS(x)}{\text{Mean}(x)}$
Fr_{10}	Impulse Factor	$IF = \frac{\text{Max}(x)}{\text{Mean}(x)}$

the statistical method, which is used to define certain features of the signal that are sensitive to certain characteristics in the signal. Statistical features of the signals are generally a good indicator for change detection in stationary signals (such as fault) or a change in the state of the signal from stationary to non-stationary. In the statistical approach it is assumed that $p(x)$, the underlying probability density function (pdf) of the monitored variables $x(t)$, under normal and faulty states will show a noticeable difference. The success in detection of change depends on the significance of the deviation and effectiveness of the algorithm that is used for the interpretation of the data [Lebold et al., 2000, Randall, 2011].

The *root mean square* (RMS) of a vibration signal is a statistical feature that measures the power content in the vibration signature. It is the most basic approach to measuring defects (e.g. imbalance) in the time domain, but it is not sensitive enough for detection of incipient faults. *Crest factor* is an effective measure of the impulsiveness of the signal, as is defined as the ratio of the peak level of the input signal to the RMS level. *Mean*, *variance*, and *skewness* are the first, second, and third moments of probability distribution function (*pdf*) and are some of the other features used in the time domain. *Kurtosis* is defined as the fourth moment of the *pdf* and measures the relative peakedness or flatness of a distribution as compared to a normal distribution. Kurtosis provides a measure of the size of the tails of distribution and is used as an indicator of major peaks in a set of data. As rotating machinery faults present themselves, Kurtosis should signal an error due to the increased level of vibration. Various other statistical features such as *Shape factor*, *Absolute mean*, *Zero crossing rate*, *Maximum Peak*, and *Peak to Peak* can be computed from the information obtained from the spectrogram representation of different faults. These features can be calculated from the raw, synchronous or time averaged signal. Some of the statistical features that can be applied in time-domain are presented in table (2.1). When the number of features are large, multivariate statistical techniques can be applied to compress data and reduce the dimensionality problem. Techniques such as the Principal Component Analysis (PCA) are used to transform a number of related process variables to a smallest set of uncorrelated variables; in other words reproduce factors with lower dimensions that can still describe the trend in the data set [Venkatasubramanian et al., 2003].

Frequency & Time-Frequency Domains

The conventional diagnostic technique is based on the Frequency-domain or spectral analysis. Traditional spectral analysis based on Fourier Transform (FT) transforms a time-series signal $x(t)$ from time-domain to frequency-domain and generates its

spectrum $X(\omega)$ defined as:

$$X(\omega) = \int_{-\infty}^{\infty} x(t)e^{-i\omega t} dt \quad (2.26)$$

Fourier analysis works on the premise that the signal can be expressed as a summation of sinusoidal components, and hence all signals can be decomposed in this way. Fast Fourier Transform (FFT) allows to study the fundamental and harmonic frequencies existing in a signal. With such capability, failure modes with pronounced frequencies of repetition or fault that change the frequencies of the normal signal can be identified. An important condition for application of the FFT is the invariability of load/speed of the operation. FFT assumes the frequency does not change over time and hence it is incapable of handling non-stationary signals (i.e. frequency-modulated signals with underlying time-varying phenomenon, and transient signals with short duration and unpredictable time behavior). It is also known that the presence of localized fault introduces non-stationary property into the vibration signal [Li, 2012].

Order Analysis (OA) is another FFT-based technique that transforms the revolution domain into an order spectrum and tries to overcome the effect of frequency changes. OA works on the premise that the frequency change within each time interval is small, and hence the signal behaves stationary at those intervals. This assumption fails if the frequency changes within time intervals are significant.

To overcome the deficiencies of the FFT, time-frequency transformations are developed that account for the time dependence of the signal. Short-Time Fourier Transform (STFT), Spectrogram (Power of the STFT), Wigner-Ville distribution, Wavelet and Hilbert-Huang transform are examples of such methods.

a. Short-Time Fourier Transform

Short-Time Fourier Transform (STFT) transforms the time-series signal into a two-dimensional map of time and frequency. STFT works by moving a short time

window along the signal and perform the Fourier transform as a function of the time shift as explained in equation eq. (2.28):

$$X(\tau, \omega) = \int_{-\infty}^{\infty} x(t)\omega(t - \tau)e^{-i\omega t}dt \quad (2.27)$$

The amplitude squared $|X(\tau, \omega)|^2$ is known as the spectrogram. It should be noted that the window $\omega(t)$ is fixed, and thus the resolution of the spectrum is fixed.

b. Continuous Wavelet Transform

Wavelet transform offers a better frequency resolution compared to STFT, as it uses a more general function as the basis to construct the signal. Therefore, it offers a better timefrequency localization. The transformation of a signal from the time domain to wavelet coefficients allows for signal decomposition. Continuous Wavelet Transform (CWT) is defined in the following way:

$$CWT(a, \tau) = \frac{1}{\sqrt{|a|}} \int_{-\infty}^{\infty} x(t)\psi^*(\frac{t - \tau}{a})dt \quad (2.28)$$

where τ is the position parameter (time shift of the mother wavelet), a is the scaling parameter (or pseudo-frequency), ψ is the mother wavelet, and ψ^* is the complex conjugate of ψ . The mother wavelet is a function that is used to create a set of wavelets by changing the scaling parameter a and the wavelet position parameter τ . The wavelet coefficients are interpreted as the correlation measure of signal and wavelet, and are obtained by comparing the wavelet with the signal. Accuracy of the results from classic wavelet techniques such as Discrete Wavelet Transform (DWT) and Wavelet Packet Transform (WPT) depends on the proper choice of the mother wavelet (i.e. Haar, Daubechies, Morlet, Mexican hat,etc.). In principle, the wavelet decomposition would achieve a better result if the wavelet basis is similar to the signal under analysis [Loutas and Kostopoulos, 2012]. A variety of Second Generation Wavelet Transform (SGWT) are being developed which are independent of the choice of the mother wavelet.

c. Hilbert-Huang Transform

Unlike the other time-frequency methods that take a predetermined structure either through time or frequency (i.e STFT and Wavelet transform), Hilbert-Huang Transform (HHT) is a self-adaptive technique designed to extract the instantaneous frequency of non-stationary and nonlinear time-series [Huang, 2005]. Application of the EMD and other extended forms of it for fault diagnosis of rotating equipment has become a very hot topic and many researchers are investigating it [Bin et al., 2012, Georgoulas et al., 2013, Feng et al., 2013, Zheng et al., 2013, Ricci and Pennacchi, 2011, Lei et al., 2013, Amarnath and Krishna, 2014, Dybala and Galezia, 2014, Li et al., 2015, Liu et al., 2015]. HHT specifically developed to analyze data from non-stationary and nonlinear signals consists of two main steps: the empirical mode decomposition (EMD) that decomposed the signal into a number of orthogonal components called intrinsic mode function (IMF) and the Hilbert Spectral Analysis (HSA) that applies Hilbert-transform and computes the instantaneous frequencies embedded in the signal [Huang et al., 1998, Huang, 2005, Lei et al., 2013]. The steps taken can be summarized as follows:

1) IMF extraction: Also known as sifting, the EMD algorithm first decomposes the signal into its IMFs. Algorithm starts by feeding the signal $x(t)$, and generates a residue ' r_n ' where $r_n = r_{n-1} - c_n$ and a collection of n IMFs ' c_j ' ($j = 1, 2, \dots, n$):

$$x(t) = \sum_{j=1}^n c_j + r_n \quad (2.29)$$

2) Hilbert Spectral Analysis: Applying the Hilbert transform (HT) on each IMF, instantaneous frequency can be computed as the derivative of the phase function. Repeating this procedure for all IMFs, the original data can be expressed as:

$$x(t) = \text{Real Part} \sum_{j=1}^n a_j(t) e^{i \int \omega_j(t) dt} \quad (2.30)$$

The time-frequency distribution is designated as the Hilbert-Huang spectrum

$H(\omega, t)$:

$$H(\omega, t) = \text{Real Part} \sum_{j=1}^n a_j(t) e^{i \int \omega_j(t) dt} \quad (2.31)$$

From the Hilbert Spectrum (HS) $H(\omega, t)$, it is also possible to estimate the Marginal Hilbert Spectrum (MHS), $h(\omega)$, defined as

$$h(\omega) = \int_0^T H(\omega, t) dt \quad (2.32)$$

where T is the total data length. While the Hilbert spectrum (HHS) offers a measure of amplitude contribution from each frequency and time, the marginal spectrum (MHS) offers a measure of the total amplitude contribution from each frequency [Yang et al., 2013, Chen and Jegen-Kulcsar, 2007]. The important difference between HT and FFT is visible in this expanded form of the equation (2.30). In HHT, each IMF component is described with their own different amplitude and frequency (which are time-varying functions of time and frequency), whereas in FFT each component would have a constant amplitude and frequency. Hunag also showed that the EMD method is equivalent to an adaptive wavelet, and hence avoids the shortcoming of using a priori-defined wavelet basis. A comparison of the HHT to FFT and Wavelet methods can be found in [Huang, 2005].

2.3 State of the Art in Earthmoving Equipment Monitoring

Performance measures of the earthmoving equipment, typically from drives and engines, are used to monitor the status of the equipment. Information about the payload, cycle times, and number of loads hauled are collected and stored in on-board computers during each cycle or working periods and can be downloaded to a computer for subsequent analysis [Tomlinsion, 2009].

Many studies have applied vibration analysis to monitor the condition of mining equipment such as shovels and trucks, and used to detect and diagnose faults [Brown

and Jorgensen, 1988, Burrows, 1996, Saavedra and Molina Vicuna, 2007].

One of the first applications of the vibration monitoring technique for shovels is reported in the pioneering work by Brown and Jorgensen [Brown and Jorgensen, 1988]. By comparing the Fast Fourier Transform of the vibration signals acquired from the equipment (healthy and faulty states), imbalance and misalignment in power and transmission components, and faults in bearings were detected. The authors were aware of the fact that their method is limited to the period when the speed is constant.

Burrows conducted a review of the automatic detection of anomalies and diagnosis for mobile mining equipment, with a focus on the application of vibration analysis [Burrows, 1996]. He summarized the time-based vibration analysis techniques that can be used for monitoring, e.g. the signal RMS, peak level detection for signal impulsiveness, Crest factor, Spike energy, Kurtosis, and envelope detection. The study also covered frequency-based vibration analysis techniques such as spectrum analysis (FFT: Fast Fourier Transform, CPB: Constant Percentage Band Filtering), Spectral mapping (waterfall plot), Cepstrum analysis, Spectrum comparison and Trending of the spectral differences.

On a different scale and in the industrial front, *P&H* was the first mining equipment manufacturer to offer predictive technology solutions for shovels. Through collaboration with Emerson process management, *P&H* also utilize portable vibration analyzers to detect impending mechanical defects in mechanical components of the machine. This was done by taking the machine out of service, once a month to go through routine maintenance for such inspections [Nower, 2013]. *P&H* expanded their line of product to include health monitoring and diagnostic features, for faults i.e. bearing, gears, alignment and structural defects. For continuous monitoring, they have been developing systems based on the PreVail ® platform [Nower, 2013], a remote health monitoring packages for electrical driven equipment, as well as Centurion ® control system, for monitoring and fault detection. These systems

are equipped with accelerometers mounted close to bearings and gearbox on the shovel. Measurements are only conducted when shovel makes particular movements at particular speeds, and still acquiring the proper data is very challenging (out of 300 cycles that a shovel completes in a shift only 3 cycles meet the criteria for data collection). A key step in this method is the so called ‘Staged Testing’ which is data collection during a simulated cycle of machine operation with no loading while the machine is waiting for a truck [Nower, 2013].

Earthmovers and ground engaging equipment, operate under transient conditions and they have short work cycles with variable load and speed, with some very slow speed shafts. This poses a challenge for applying methods such as Fourier Transform on the vibration data. Saavedra and Salamanca addressed the transient nature of the shovel’s operation, and proposed to use vibration analysis to monitor electromechanical Shovel components, i.e. the hoist, crowd, swing and propel transmissions [Saavedra and Salamanca, 2002]. They demonstrated how the effect of variable rotational speed causes the spectral components to spread over a number of adjacent spectral lines, which makes it impossible to perform a diagnostic procedure. Accounting for the variability in load or speed, they investigated how Revolution-Order Transform (ROT) and Time-Frequency Transformation (TFT) can be used to recover the diagnostic features of the signal purpose while the shovel is still in operation [Saavedra and Gonzalez, 2005, Saavedra and Molina Vicuna, 2007].

The findings of these studies and two unpublished masters thesis by Ramirez [Ramirez, 2003] and Vicuna [Molina Vicuna, 2006], eventually turned into SiAMFlex. SiAMFlex is a commercial vibration monitoring system specially designed for the electro-mechanical mining shovels, and developed by Cadetech based on a National Instrument platform [Ramirez, 2009, 2010]. SiAMFlex was used to identify failure modes such as defects and faults in gears and bearings, misalignment in engine-input shaft, looseness of components (all based on vibration signal), and crack in shovel’s structure (based on strain gauge reading). Vibration signal is acquired from

strategic locations on certain components (e.g transmission). While the shovel is in operation, the algorithm in the program identifies intervals of time where the rotational speed remains approximately constant, and then processes the data to compute a classic FFT spectrum. The data is also processed through the OSA and TFT during the non-stationary period. It also performs time-domain analysis and extracts features of the vibration, strain, acceleration and rotational signals, such as RMS, peak, peak-to-peak, average, minimum, maximum and crest factor. The application records data, and then analyzes it to find the best measurement period, where interpretations will be made. They also proposed to use the SiAMFlex as a visual tool for crack monitoring. Proposed parameters of interest during a load cycle of the dipper were the strains (measured with strain gauges located in the rear right and left post of the shovel's frame) and rotational accelerations of the hoist, crowd, and swing transmission motors.

Timusk, Lipsett and Mechefske also investigated the application of the vibration analysis for machinery in transient operating modes [Timusk et al., 2008]. They developed a laboratory apparatus with variable speed and loading capability to replicate the duty cycle of the excavator swing machinery. Unlike the studies conducted by Saavedra and his team [Saavedra and Salamanca, 2002, Saavedra and Molina Vicuna, 2007] who used the characteristics of the normal operating condition as a prior information, they adopted a novelty detection scheme for fault detection. In this context the novelty detection algorithm has a training period, where it will be considered as the baseline for the normal operating condition. Any condition with significant difference will receive a novelty score.

Appreciating the effect of the operating mode on the physical response of the system and the diagnostic parameters, Timusk et al. investigated a number of classification methods to obtain real-time information regarding the shovel operating modes [Timusk et al., 2008, 2009b]. McBain and Timusk reported that the speed changes have a strong relation with the vibration responses acquired by accelerome-

ters [McBain and Timusk, 2009]. They proposed that segmentation of the vibration signal based on speed segments will improve the classification method adopted in their novelty detection algorithm.

Operation of the gearbox in Bucket-Wheel Excavator provides a platform to study different vibration monitoring algorithms in an environment with highly variable load/speed, and has attracted many researchers in recent years [Bartelmuš and Zimroz, 2009a,b, 2014, Wyłomanska et al., 2014, Vicuna, 2014]. These studies reported that time-frequency methods can be successfully applied to detect local damage for such systems under time varying cyclic load. Carrying out excavation with different loads and rotational speeds, it is reported that at lower rotational speeds, the influence of the load in the resulting signal can be significant. This is while at higher rotational speeds, the influence of the load is masked by the influence of the rotational speed [Vicuna, 2014].

As illustrated earlier in fig. 2.2, the vibration signal can be influenced by the change of condition (e.g. in presence of fault) and change of operation. Many studies have recognized the importance of the load and rotational velocity variability as contributing factors to the change of operation. However, none has looked into the environmental variability, which is the main source of load variability in many cases. A change in the environmental parameters not only can impact the interaction load experienced by the equipment and its elements, it can also affect the overall vibration response of the system through changing the elastic and damping parameters of the base. Therefore, a complete condition monitoring system for mobile equipment, should not only monitor the condition of the equipment, but also it must be able to continuously assess the environmental condition of the operation.

Furthermore, reviewing the condition monitoring literature in the area of earth-moving equipment, it is found that most successful detection algorithms often require a variety of sensors (accelerometers, strain gauges, encoders, load sensors, etc.), and

in several locations. Each of these probes are then tasked with detection of certain localized failure mode in their vicinity (e.g. misalignment, looseness and rubbing, rotor crack development), and yet successful detection depends on the proximity of the probe to the faulty component. Hence, establishing an effective monitoring system for these equipment requires extensive data acquisition infrastructure and sophisticated processing algorithms, which becomes very costly and time consuming. Additionally, most studies are focused on certain failure modes (i.e. gears and bearings) and there is a need to study and develop methods for monitoring the equipment for other more complex failure modes such as crack development in a structural element, or a progressively wearing joint.

Chapter 3

Methodology

Many types of industrial equipment operate under stationary condition, that is, constant state of loading and invariable rotating speed. These machines behavior are well studied and their performance can be easily monitored to detect any change in their normal status due to a change of condition - presence of fault. Therefore, maintenance system can be developed with relative ease, and high cost unplanned shut downs can be avoided or minimized.

Machinery with non-stationary behavior however, that operate in a time-varying manner and often exposed to operational and environmental changes, belong to a different class of equipment that are much harder to monitor, and therefore are more prone to experience costly down times. They might undergo a change in the way they operate, due to variability in the external loading, rotational speed or changing environmental conditions. Examples of such machinery are earthmovers and wind turbines, shown in fig. 3.1. While this is becoming an active research area, efforts are largely focused on the variability of the loading and the rotational speed, and not many has considered the environmental side of the equation.

Internal and external changes can affect the operating envelope, and therefore a formerly safe operating mode becomes unsafe, as can be seen in fig. 3.2. The root



Figure 3.1: Wind Turbine and Earthmovers Are Exposed to Excessive Environmental and External Loading Variabilities, Which Affects Their Performance and Mode of Operation. Simulation courtesy David Bock [Bock, 2014, Stevens et al., 2015].

cause for the change in the operating envelope can be a change in one or multiple critical parameters of the environment (a change in the speed of the wind, change in the environmental property, etc.) or a change in the equipment (Structural defect, Fluctuation of the available Power, Change in the operating speed, etc.). In some cases, a change in the operating mode might allow to recover from the operating envelope change and bring the system back into a newly identified safe zone. Therefore, identification of the safe operating envelope, a combined set of equipment and environment parameters, becomes very critical.

Operating conditions of ground engaging equipment are often non-stationary, randomly changing, and severe in terms of the interaction loads. The correlation

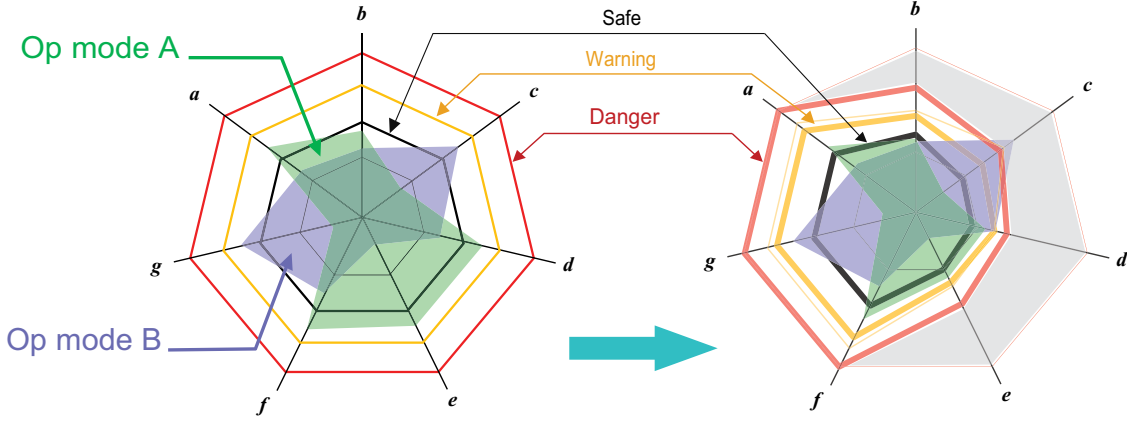


Figure 3.2: Internal and External Changes can Affect the Operating Envelope, and Therefore a Formerly Safe Operating Mode Becomes Unsafe. Change of Operating Mode Might be Feasible for Some Operation, while the others Might Remain Unsafe Under the New Condition.

between the magnitude and variability of the loading due to variability in the terrain, and the equipment structural damage is well documented [Yin et al., 2007, Allen and Sundermeyer, 2005, Raza and Frimpong, 2013, Hall, 2002, Frimpong and Li, 2007, Frimpong and Hu, 2004]. Some studies suggested that the change in the property of the material being dug can result in varying mechanical energy input to the machine, and deteriorate equipment's health and longevity [Frimpong et al., 2008a, Frimpong and Li, 2007]. Therefore, it is very important to detect how environmental properties change over time, whether such changes impact the operating envelope or not, and if they necessitate a change in the operating mode. This means that the interaction force, and environmental properties are critical parameters that needs to be monitored.

Collecting real-world data from ground engaging equipment, such as shovels, is nearly impossible due to the harsh environment of operation and the inaccessibility of the condition data. Also, conventional methods of environmental property assessment, are very time consuming which makes the measured values useless for continuous assessment. Therefore study of the new methods for equipment and environmental monitoring is very difficult. To overcome these challenges in the

present study, it is proposed to investigate them on a simplified experimental set up in a well-controlled environment of a laboratory where equipment's condition, modes of operation and environmental parameters can be varied and experimented in a desired fashion.

A special ground engaging equipment based on a crank-slider mechanism is designed and fabricated that operates under time-varying behavior, and allows to

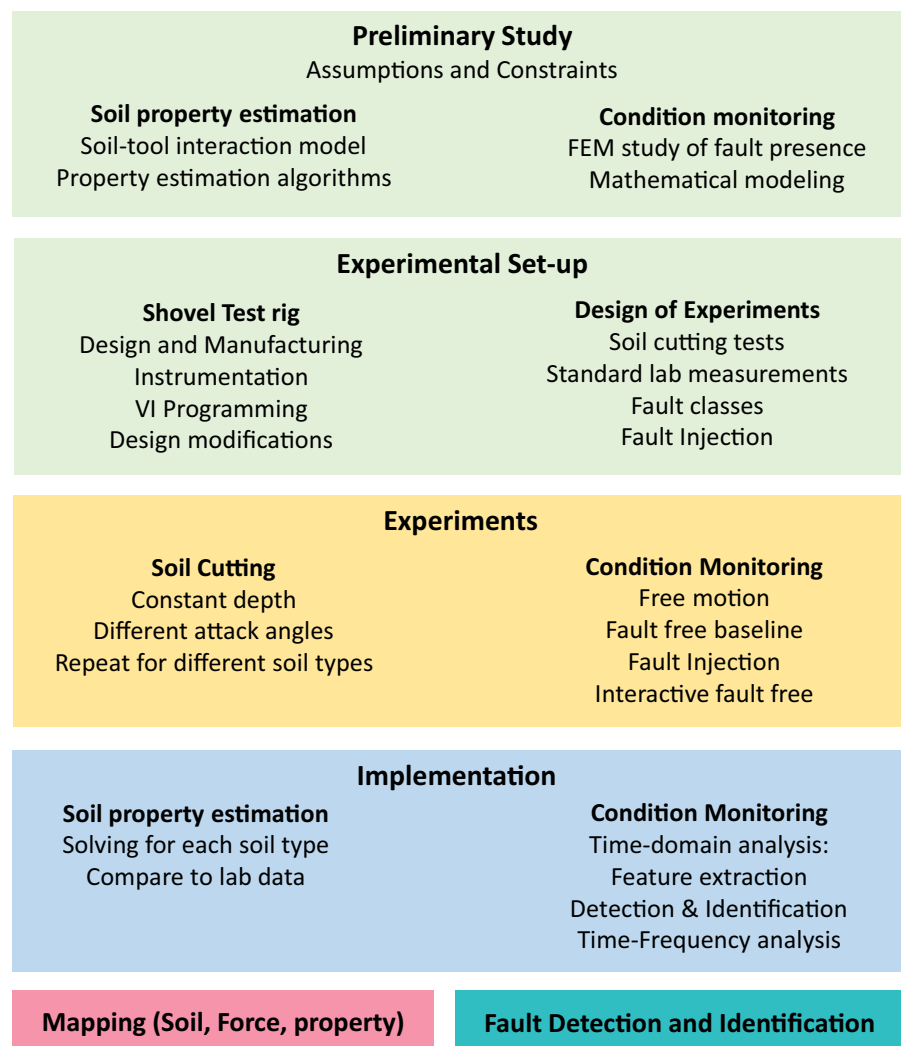


Figure 3.3: Research Road Map: Preliminary Study, Experimental set-up and Design of Experiment, Experiments and Data Collection, Implementation of Monitoring Methods, System Level Monitoring: Environment Characterization and Fault Detection

simulate the underlying non-stationary operating condition of the ground engaging equipment. For the case studied in this work, monitoring the environment offers continuous assessment of the physical properties of the medium being dug, and this will be done during ground-tool interaction. For the equipment monitoring, a slightly different approach from the classical vibration monitoring methods is proposed, which explores the fault signatures through certain dynamic parameter of the system, i.e. acceleration.

For the conduct of this research a preliminary analysis was completed, where assumptions and constraints were identified. It was decided to focus on the granular material, where soil-tool interaction models can be used reliably for the interaction force prediction and soil property estimation. Shortcomings of the existing estimation algorithms were studied, and a few creative suggestions were made and tested. Additionally, a numerical study was carried out and observability of the fault signature was evaluated using a combination of finite element analysis and MATLAB Simulink tool box as presented in appendix [B](#).

Findings of the preliminary study was used for the development of the experimental set-up, where general and task specific requirements were identified and addressed in the design. Acknowledging the limitations of the equipment and tools, a series of experiments were designed. This included the cutting force measurements during the interactive period of operation, and acceleration-based monitoring during the interactive and non-interactive period of operation.

Results from both series of experiments were recorded and post-processed using the proposed methods. Cutting force measurements were fed to the proposed estimation algorithm and the acceleration data was used for condition monitoring.

Research road map and steps are summarized in fig. [3.3](#). These steps are broken down into three major phases: experimental platform design, experiments and numerical analysis for the soil property estimation, and experiments, and signal processing work for fault detection and condition monitoring.

3.1 Experimental Platform Design

The test apparatus was designed to simulate the simplified operation of an earth-moving equipment with a simple back and forth motion. There were a number of competing objective that shaped the design criteria. Test rig must:

- Produce a soil pushing action in a continuum at different attack angles and depth
- Produce a time-varying behavior (through speed and/or load)
- Offer potential for structural integrity manipulation (controlled failure modes)

Accordingly, the apparatus was designed based on an offset crank-slider mechanism that would produce the time-varying behavior throughout its reciprocal motion. A shovel assembly was designed to provide the dozing action, where the blade's attack angle α , and the depth of penetration h can be adjusted manually. Also, the modular design of the test rig, allowed to offer potential failure modes at the shovel assembly joint and link, and also on the elements of the power train. The test rig was equipped with a variety of off-the-shelf and in-house sensors that would support the data collection required for the property estimation and fault detection experimentations.

3.2 Environment Monitoring

There are a number of medium property estimation methods described in the literature, mostly for non-cohesive methods. In this work, an improved algorithm is developed, which can be used for both cohesive and non-cohesive material. Selection of the non-cohesive and low-cohesion medium types (Glass beads and Play sand) was based on the relative similarity of the soil samples available and soils used in studies reported in the literature. Oil sands, a highly cohesive material, is the sole

cohesive material of interest, due to the massive application they have in Alberta's surface mining operations.

An important measurement for this algorithm is the measure of the failure force for different attack angles, during the soil-tool interaction. The description of the failure force and the methods used for measuring and processing the force, are further explained in section 5.1. Similar to the approach used in literature, several measurements are made and averaged. The cutting force required for two types of medium (Play sand and Glass beads) are measured at multiple attack angles. These measurements are then fed into the proposed property estimation algorithm. At the first step, soil samples are assumed to be non-cohesive, in order to construct and validate the algorithm used in the literature. The estimated properties obtained from this approach, are compared and verified against the results obtained from the standard lab measurements. Next, accounting for cohesion, the proposed estimation algorithm was used to predict the properties of all the same soil samples (Glass beads and Play sand), and relative estimation error are calculated. At the end, the validated estimation algorithm was used to predict the properties of highly cohesive oil sands samples. The actual oil sand properties are also directly measured, and used to measure the accuracy of the estimation algorithm.

3.3 Equipment Monitoring

Despite the primary role the shovels have in surface mining, there is hardly any study focused on monitoring the health of the equipment. In rotating equipment, where most of the literature comes from, equipment monitoring focuses on the energy-out representations, e.g., a vibration signal emitted from the equipment, either from the casing or close to the moving parts. In those studies, the most common methods used for processing the vibration data are based on time-domain analysis, and some FFT-based (fast Fourier-transform) methods.

Unlike the conventional vibration monitoring method that uses the casing vibration, the approach presented in this work relied on the displacement (x_s) and acceleration (A_s) signals from the slider. A few studies demonstrated how presence of fault changes the acceleration of a crank-slider mechanism. So the motivation for the choice of signal, was to investigate the effectiveness of the acceleration signal as a monitoring tool. In crank-slider, the acceleration signal can be directly linked to the kinetic energy. Thus, monitoring the acceleration of the slider, allows to monitor the changes in the kinetic energy in presence of energy sinks (i.e. failure modes).

To investigate this, the following methodology was adopted: First, displacement, acceleration and angular displacement signals $(x_i, A_i, \phi_i)_N$ were acquired during the free motion of the shovel under *Normal* (fault-free) state to develop a baseline for the healthy state of the equipment. Next, failure modes (F_X) were introduced one by one, and the signals $(x_j, A_j, \phi_j)_{F_X}$ were collected under each *Faulty* state. Signal processing techniques were applied in time and frequency domain, and certain features of the collected signals were compared. Features were correlated to certain faulty conditions, and used to detect fault presence and identify fault type. The signals of interest were collected with a potentiometer, accelerometer and an encoder. For each trial, signals were acquired for several cycles (1 cycle= One full rotation of the crank), where the slider moved back and forth.

For the equipment monitoring, some of the less studied, but equally important failure modes, i.e. breathing crack, extreme clearance and misalignment, were investigated through advanced signal processing techniques. Each of the three faults (F_A, F_B, F_C) were introduced separately and the data was collected over several cycles of free motion. Some of these failure modes, do not display themselves in every cycle. To accommodate the property estimation investigation, the rig was designed to simulate a slow process, e.g. operating at $f \leq 1$ Hz. Hence, the signatures associated with the faults needed several cycles to appear in the signals recorded.

Each of the faulty were repeated and data collected from several runs.

Signal processing techniques in time and frequency were applied to evaluate the changes in the signal, caused by presence of these faults. Signals under study were not necessarily at the close proximity of the faulty component. Hence, the modulation effect caused by a particular fault, may disappear in the carrier signal. Other imperfection in the system were also combined with the fault signature and added to the noise level. Additionally, some of the failure modes under investigation demonstrated a transient behavior, which made the detection even harder. To get rid of the unwanted noise and to extract the valuable information, some signal conditioning was necessary. A variety of time, frequency, and time-frequency signal processing methods were applied and their effectiveness in fault detection is discussed. Acceleration signal calculated from the displacement is the primary signal of interest. However, some of the results from the other two signals are also considered for monitoring.

Chapter 4

Experimental Platform

This chapter discusses the evolution of the test rig from a simple soil cutting tool to the final design of an equipment that is used for property estimation and fault detection.

It starts with an overview of the design requirements for the property estimation experiments, and additional requirements for the structural monitoring study. The process by which these requirements are incorporated in the test apparatus design also will be reviewed. The limitations of the test rig resulting from design choices and how those limitations exhibit themselves in data collection are outlined.

In addition to the test rig itself, the development of the supporting hardware for sensing, and recording the data is presented. Finally, the structural failure modes that are studied and their seeding method is discussed.

4.1 Design Requirements

The movement of a single blade in a granular material (e.g. soil and sand) is the basis for generating the interaction force in our investigation. Other material type

such as gravel and rock has not been studied. Once the tool is engaged in the medium and moves horizontally, it can break the internal bonding of the medium, and the tool-ground interaction force can be measured. The first peak represent the cutting force and is of interest. The following peaks - associated with successive failure surfaces are not of interest. Two main parameters affecting the interaction force, are the depth of penetration H and the attack angle of the blade α . A drive train mechanism (electro-motor and a reducing gearbox) can be coupled with a shovel assembly through a crank-slider mechanism to provide the power required for the soil cutting and the horizontal motion in the x direction.

4.1.1 System Dynamic & Time-Varying Behavior

An interesting feature of a centered crank-slider mechanism is that the crank angle, with respect to horizon, is the same in both forward and return stroke of the slider, e.g. zero at either of the limiting positions of the stroke. However, in an offset crank-slider, the crank angle for executing the forward stroke is different from that of the return stroke [Bautista, 2009]. This feature is widely used to design quick return mechanisms where the period of the working stroke will be greater than period of the return stroke. In other words, speed and acceleration signals are time-varying.

In addition to external load due to the interaction, inertial forces are also another source of load variability in the system. Fast-moving machinery with rotating and reciprocating masses, produce fluctuating forces in presence of unbalance, which is a significant source of vibration excitation [Arakelian and Briot, 2015]. This force is also known as shaking force (SF). An off-set crank-slider mechanism (with eccentricity e) is illustrated in fig. 4.1. It produces a shaking force F_B^{sh} due to internal unbalance of system. The shaking force of the reciprocating motion, crank moves from A' to A while slider moves from B' to B , can be expressed as:

$$F_B^{sh} = -m_3\ddot{x}_B = F_1 + F_{1'} + F_2 \quad (4.1)$$

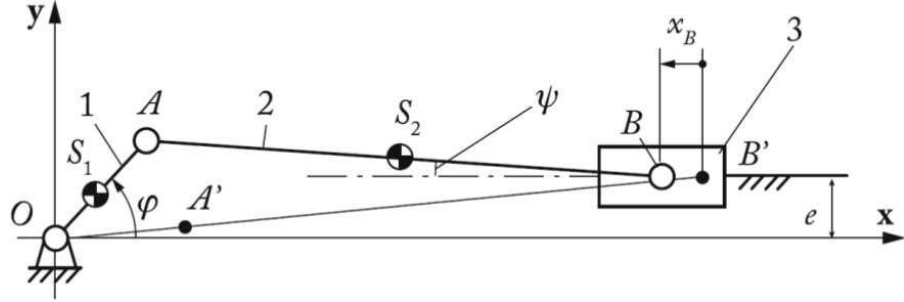


Figure 4.1: Offset Crank-Slider Mechanism: Once crank rotates from A' to A , slider moves from B' to B . φ is the angle of the rotation of the crank, ψ is the angle of the connecting rod with horizontal axis, e is the offset, and S_1 and S_2 are the center of gravity of the Crank and the Connecting rod respectively.

where,

$$\begin{aligned} F_1 &= -m_B \dot{\varphi}^2 r \cos \varphi \\ F_{1'} &= -m_B \dot{\varphi}^2 \lambda e \sin \varphi \\ F_2 &= -m_B \dot{\varphi}^2 \lambda r \cos 2\varphi \end{aligned} \quad (4.2)$$

where $r = l_{OA}$, $l = l_{AB}$, $\lambda = r/l$, $m_B = m_2 l_{AS_2}/l + m_3$, m_2 is the connecting rod's mass, and m_3 is the mass of the slide [Arakelian and Briot, 2015].

Replacing the crank bar in fig. 4.1, with a disk with mass m_1 and radius r , and for the connected rod with mass m_2 and length l , and the slider with mass m_3 are, the kinetic energies of the crank (T_1), connecting rod (T_2), and slider (T_3),

$$\begin{aligned} T_1 &= \frac{1}{2} I_1 \dot{\varphi}^2 = \frac{1}{2} \left(\frac{1}{2} m_1 r^2 \right) \dot{\varphi}^2 = \frac{1}{4} m_1 r^2 \dot{\varphi}^2, \\ T_2 &= \frac{1}{2} I_2 \dot{\psi}^2 + \frac{1}{2} m_2 \dot{x}_{2cg}^2 + \frac{1}{2} m_2 \dot{y}_{2cg}^2 \\ &= \frac{1}{6} m_2 l^2 \dot{\psi}^2 + \frac{1}{2} m_2 r^2 \dot{\varphi}^2 \sin^2 \varphi + \frac{1}{2} m_2 r l \dot{\varphi} \dot{\psi} \sin \varphi \sin \psi, \\ T_3 &= \frac{1}{2} m_3 \dot{x}_3^2 = \frac{1}{2} m_3 r^2 \dot{\varphi}^2 \sin^2 \varphi + m_3 r l \dot{\varphi} \dot{\psi} \sin \varphi \sin \psi + \frac{1}{2} m_3 l^2 \dot{\psi}^2 \sin^2 \psi. \end{aligned} \quad (4.3)$$

Then, the total kinetic energy of a the entire shovel assembly can be obtained as

$$T = T_1 + T_2 + T_3. \quad (4.4)$$

We also know that (ψ) can be described in terms of (φ) : $r \sin \varphi = l \sin \psi + e$. Which yields to,

$$\psi = \sin^{-1} \left(\frac{r \sin \varphi - e}{l} \right). \quad (4.5)$$

In other words, $\dot{\psi}$ can be described in terms of φ

$$\dot{\psi} = \frac{r \cos \varphi}{l \cos \psi} \dot{\varphi}. \quad (4.6)$$

Also,

$$\ddot{\psi} = \frac{r \ddot{\varphi} \cos \varphi + l \dot{\psi}^2 \sin \psi - r \dot{\varphi}^2 \sin \varphi}{l \cos \psi}. \quad (4.7)$$

Assuming $Q = [\psi \ \varphi]^T$, as the vector of generalized coordinates, the equation of motion of the crank-slider system can be derived as,

$$M(Q) \ddot{Q} + N(Q, \dot{Q}) + \Phi_Q^T = Q^A, \quad (4.8)$$

where

$$M = \begin{bmatrix} A & E \\ E & B \end{bmatrix}, \quad N = \begin{bmatrix} K_W \\ P_W \end{bmatrix}, \quad Q^A = \begin{bmatrix} F_{ext} l \sin \psi \\ F_{ext} r \sin \varphi - \tau \end{bmatrix} \quad (4.9)$$

Discounting for frictional force, F_{ext} represents the external force [Ha et al., 2006].

Also, $\Phi_Q = [-l \cos \psi \ r \cos \varphi]$, and

$$\begin{aligned} A &= \frac{1}{3} m_2 l^2 + m_3 l^2 \sin^2 \psi, \\ B &= \frac{1}{2} m_1 r^2 + (m_2 + m_3) r^2 \sin^2 \varphi, \\ E &= (\frac{1}{2} m_2 + m_3) r l \sin \varphi \sin \psi, \\ K_W &= m_3 l^2 \dot{\psi}^2 \sin \psi \cos \psi + (\frac{1}{2} m_2 + m_3) r l \dot{\varphi}^2 \cos \varphi \sin \psi + \frac{1}{2} m_2 g l \cos \psi, \\ P_W &= (\frac{1}{2} m_2 + m_B) r l \dot{\psi}^2 \sin \varphi \cos \psi + (m_2 + m_B) r^2 \dot{\varphi}^2 \sin \varphi \cos \varphi \end{aligned}$$

4.1.2 Task-Specific Requirements

The offset of the slider rail to the center of the crank (e), also allows to house a sandbox, where mediums with different property will be subject to the dozing.

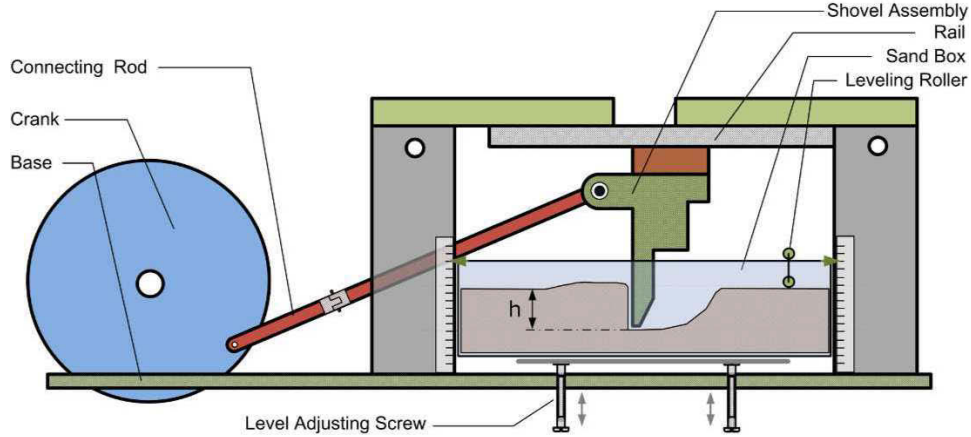


Figure 4.2: Shovel Assembly Driven by the Slider-Crank: Depth of Penetration h , and Blade's Angle of Attack $\alpha = 90^\circ$

The sandbox can be adjusted to accommodate different depth of penetration (h), as shown in fig. 4.2. Also, the blade angle of attack (α) is another controlled parameters that is discussed further in section 4.2.1. The signals of interest for property estimation are interaction force (F_{int}) and the displacement (x), which are collected with a potentiometer and a force sensor.

The design of this multi-linkage mechanism would present various opportunities to simulate common structural defects of a ground engaging equipment as discussed in section 2.2.1. In particular, three failure modes are proposed and can be implemented for the fault detection experiment: excessive clearance in the revolute joint between the connecting rod and the slider (F_A), a breathing crack in the connecting rod (F_B), and an excessive looseness/misalignment in the intermediate parallel shaft of the gearbox (F_C). These failure modes are further discussed in section 4.3.

Note that, for a full clockwise rotation of the crank, the slider makes a forward (\leftarrow) and a return (\rightarrow) stroke as illustrated in fig. 4.3. Necessary signals to be acquired are slider's displacement (x), acceleration (A), and angular velocity of gearbox input ($\dot{\phi}_i$) and output ($\dot{\phi}_o$) shafts. These signals of interest are collected with a potentiometer, an accelerometer, a tachometer and a digital encoder, and

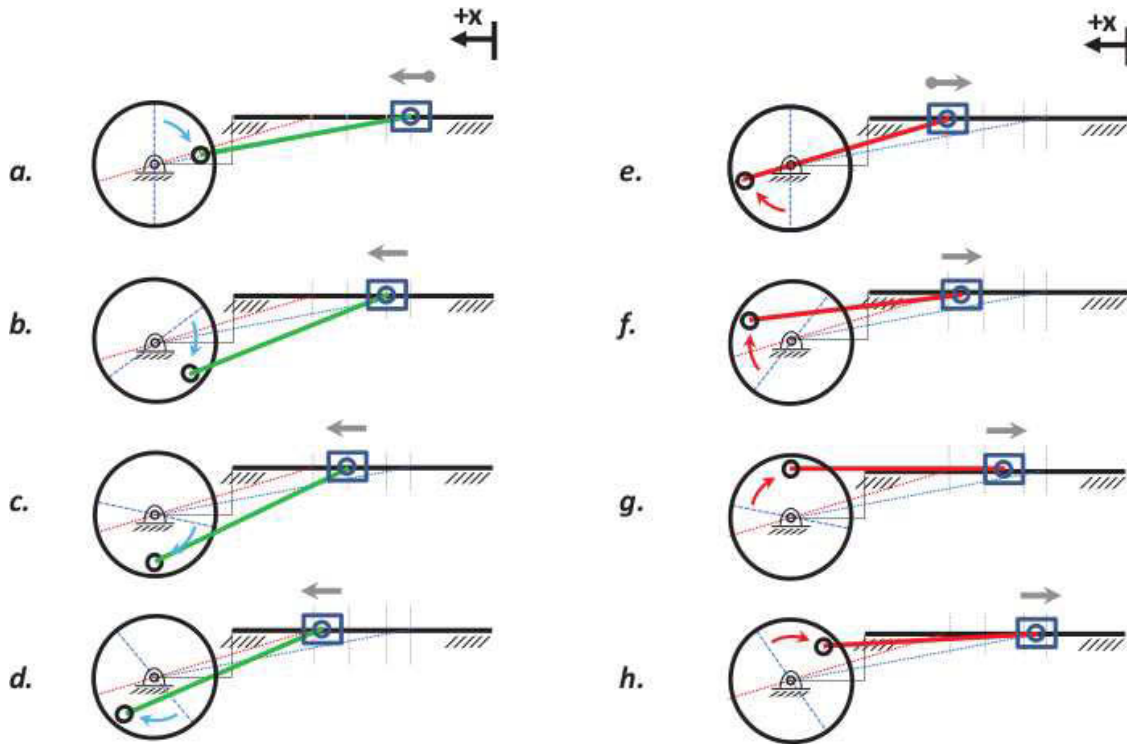


Figure 4.3: A full Cycle of the Crank-Slider Motion: (a-d) Connecting rod is under tensile load, and slider is moving to the left with $\dot{x}_S \geq 0$; (e-h) Connecting rod is under compressive load, and slider is moving to the right with $\dot{x}_S \leq 0$. Note that the positive and negative Max $|\ddot{x}_S|$ occurs at (a) and (e) at the either ends of the reciprocal motion, where $\dot{x} = 0$. $\ddot{x}_S = 0$ occurs twice in each cycle in the mid way.

will be discussed in depth in section 4.4.

4.2 Structure and Subsystems

The test rig is comprised of the following subsystems: the implement assembly, which provides the soil-tool interaction; the support structure for the mechanism (including the frame); the power train to provide the digging power, and a sensing and data acquisition system to acquire and process data from the rig.

4.2.1 Structure & Implement Assembly

The implement assembly uses a flat metal blade as the soil engaging tool, that is mounted on the slider. Assembly's motion is constrained in the x direction through a prismatic joint. Blade passes through a bed of granular material in a prismatic container with vertical walls. The flat blade was chosen for its similarity to theoretical cutting and failure models, such as the Mohr-Coulomb model for planar soil failure. The blade is designed to be sensitive to applied loads in bending, so that force can be measured. This configuration constrains the blade in the y direction, and the load through the mechanism varies in the x direction.

The soil accumulated in front of the blade applies a normal force in the x direction and shear force components in the y & z directions. However, the amount of shear force from friction is low compared to the cutting force for low-cohesion soils.



Figure 4.4: Shovel Assembly with the Blade at an Attack Angle of $\alpha = 70^\circ$

Depending on the type of medium and the depth of penetration, the interaction force F_{int} may vary from 0.1 N up to 100 N for a small digging implement (depending on the H , α , and the medium type). Preliminary trials with the test rig, suggested that for cutting through soil and pushing it at low speed $\dot{x} \leq 0.5$ m/s until it fails, a distance of 0.2 m to 0.5 m proved to be sufficient.

The shovel assembly is driven by a connecting rod (con-rod) attached to a flywheel, producing a reciprocal motion along the slider rail. One full rotation of the crank allows the blade to cut and doze the medium over a range of 0.26 m. Table 4.1 presents the geometrical properties of the crank, the con-rod and the slider. For the implement, four attack angles ($\alpha_i=60^\circ, 70^\circ, 80^\circ, 90^\circ$), may be attained by manually changing the orientation of the blade. These angles were used to compare the results with the ones reported in the literature. Once the blade is in position, the medium will be deposited in the sandbox. Negligible adhesion of the medium allows free flow motion of the medium grains. The depth of penetration h can be adjusted between 0.001 m to 0.003 m by changing the height d of the sand box, using leveling screws

Table 4.1: Properties of the Crank-Slider System

Properties	Value
e	0.15 m
r	0.135 m
l	0.65 m
$m_c = m_1$	3.750 kg
$m_r = m_2$	2.760 kg
$m_s = m_3$	1.350 kg
$I_c = I_1$	$\frac{1}{2}m_1r^2 = 0.0341$
$I_r = I_2$	$\frac{1}{3}m_2l^2 = 0.3887$
$I_s = I_3$	$\frac{1}{12}m_s(a^2 + b^2) = 0.069$

as illustrated in fig. 4.2. The surface of the medium is leveled manually using a roller before each trial, and in excess of the overburden, that is above the level line, is removed.

4.2.2 Power & Transmission

The drive system used to power the shovel assembly is the Gearbox Dynamic Simulator (GDS) by SpectraQuest Inc. It is built and assembled using high tolerances so that it would not be affected by undesired vibration. GDS consists of an electric motor and a parallel shaft gearbox system. The speed of the electromotor can be controlled via a variable frequency drive (VFD). The motor provides power up to a maximum of 1 hp which is far greater than the maximum power required for the low-speed soil cutting:

$$100 \text{ N} \times 0.5 \text{ m/s} = 50 \text{ Nm} = 0.07 \text{ hp.}$$

The gearbox is filled with SAE 80W-90 lubricant in order to minimize gear wear. There are two sets of gears in the GDS, and both sets are spur gears. The parallel shaft gearbox is set up as a speed reducer, with the first stage consisting of a pinion with 24 teeth and a gear with 60 teeth, and the second stage consisting of a pinion with 36 teeth and a gear with 48 teeth, as shown in table 4.2. The bearings used in the GDS are rolling element bearings, with bushing that house the bearing on the gearbox walls. The complete shovel rig, shovel assembly and the power train, is depicted in fig. 4.5.

4.3 Failure Modes of Experimental Apparatus

The original condition of the equipment (which is free of any physical faults) is considered as healthy or normal state. Different failure modes can produce different

Table 4.2: Gear Numbers in the Parallel Shaft Gearbox

Gear Location	No. of Teeth
Input shaft	24
Intermediate shaft	60
Intermediate shaft	36
Output shaft	48

types of response. Some faults generate a linear forced response (LFR), in presence of an external harmonic force $f(t)$. Some other faults will generate a transient response whenever the forcing function is not purely harmonic (e.g., a chipped gear, rapid speed ramp), or when the system is demonstrating non-linear behavior (e.g., seal rubs, ball bearing deadband) [John M. Vance, 2010].

To evaluate the hypothesis, three classes of structural faults were selected: excessive looseness in a joint, a crack in a link, and misalignment/rubbing of the rotating shaft. These faults are selected because they represent similar failure modes

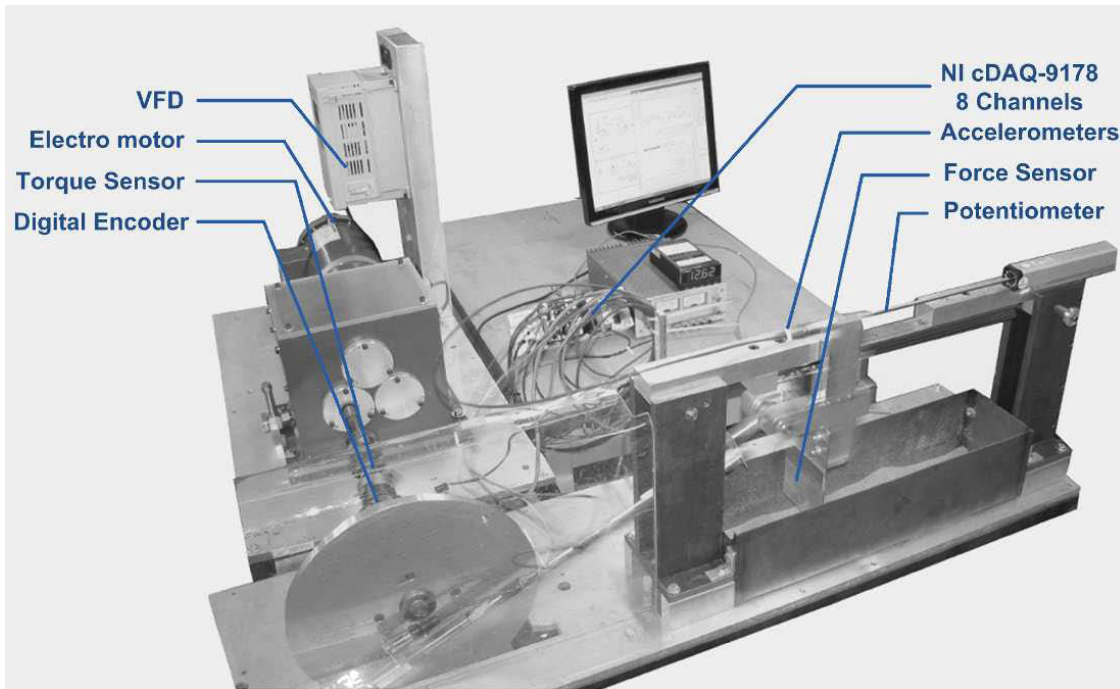


Figure 4.5: Commissioned Shovel Test Rig and Data Acquisition System

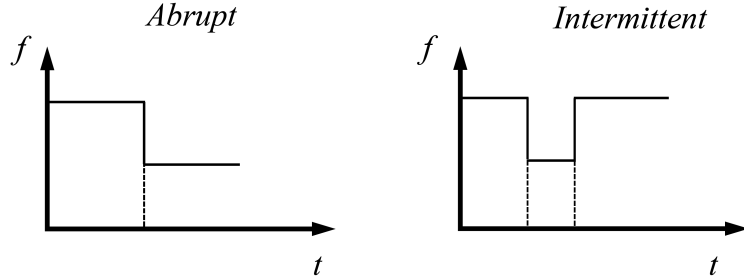


Figure 4.6: Characteristic of Intermittent vs. Abrupt faults

that occur in a real shovel components. Another reason for choosing these different faults is that they have different characteristics: shaft misalignment has an abrupt nature, whereas the crack and looseness have an intermittent nature. As illustrated in Fig. (4.6), abrupt faults have a step-like behavior, where the signal changes abruptly from the nominal value to a faulty value, and may stay at or near the new value (continuous). In contrast, intermittent faults have a temporary effect: the signal changes from the nominal value to a faulty value, and returns to the nominal value after a short period of time (transient) [Contant et al., 2004, Donders, 2002]. This choice, allows us to test the viability of the hypothesis over different fault types.

Three fault classes used in this research were earlier introduced in section 2.2.2.1. The first fault under study (\mathbf{F}_A) is described by excessive looseness in the revolute joint as illustrated in fig. 2.26. It is seeded in the test rig by reducing the radius of the journal (R_J) inside the bearing. Under repeated cyclic motion and over time, this fault can cause excessive wear of the bearing housing.

The joint between the connecting rod and the slider consists of three bearings mated at two parallel planes as illustrated in fig. 4.7. The bearing on the end of the connecting rod fits in between the two bearings on the slider, and the journal (pin) goes through the three bearings. The journal is held in place with two snap rings on either end. Under normal condition, the journal has a diameter of $D_{J1}=9.5$

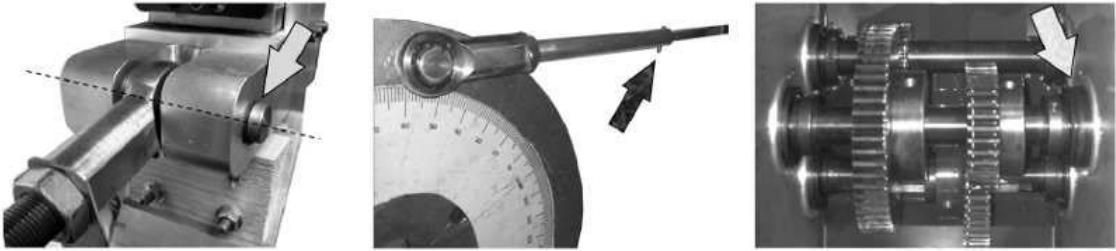


Figure 4.7: Select Structural Fault Locations: Fault A (left), Fault B (middle) and Fault C (right)

mm, with each of the bearings diameter $D_B=10$ mm, and offers 1 degree of freedom (DOF). Under F_A , a new journal is installed that has about 50% of the previous diameter $D_{J2}=5$ mm. This fault not only significantly increases the looseness of the joint connecting the con-rod to the slider but also changes the DOF. This is because the new journal not only can rotate, but also can now move in vertical and horizontal directions. Once the con-rod is moving from a resting position, the journal starts to move with the bearing on the con-rod in a plane. It would not move the slider, until the DOF in the horizontal direction is lost. At that point, the slider starts to move with the connecting rod. The contact between the surfaces of the journal and the bearings, generates normal and tangential forces which would have a greater appearance in the form of impact once the slider reaches its limits. At that point, the connecting rod is still in motion.

Therefore, F_A is expected to represent an intermittent class of faults that manifests itself with a greater magnitude at either end of the reciprocal motion and disappears/weakened in between. By definition, intermittent faults have a transient behavior, and if appear periodically can manifest itself as a cyclostationary effect.

The second fault under study (**F_B**), is described as a crack in a link as illustrated in fig. 2.28. As noted in section 2.2.2.1, a crack in a link often demonstrates a breathing effect, which means that the stiffness of the link varies between a maximum (closed crack under compressive load) and a minimum (open crack under tensile load). Observability of the crack through vibration signal is directly proportional to the

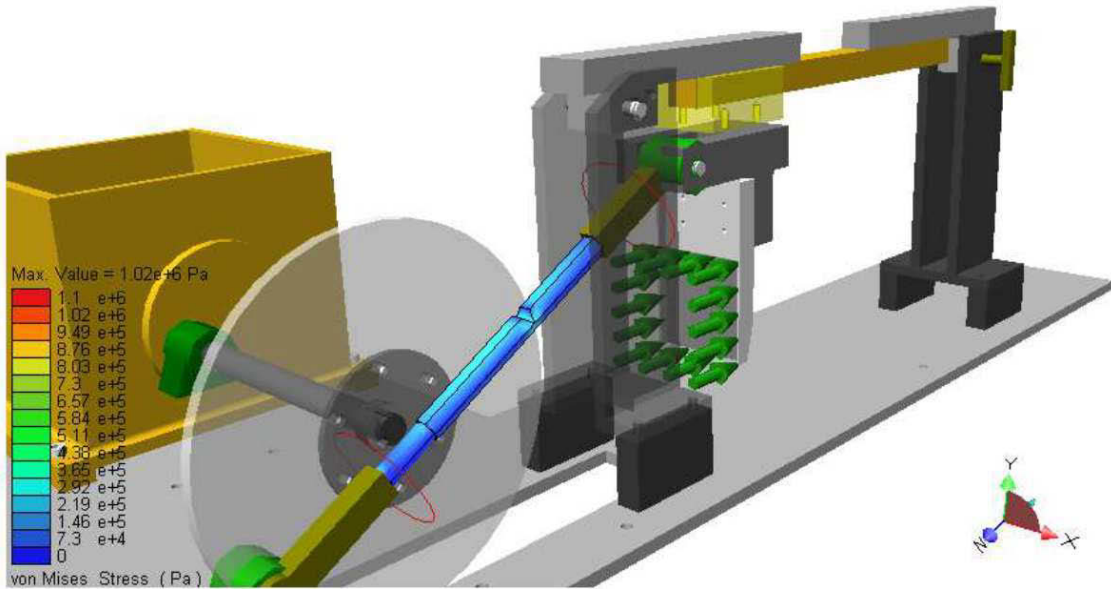


Figure 4.8: Finite Element Analysis of a Defective Connecting Rod (Crack size $a = 0.25h_2$): It Shows that the Highest Stress Concentration Occurs When the Connecting Rod is Under Tensile Loading.

ratio of the crack to link size, and the angular velocity and the load applied to the link [Shih and Chung, 2013]. In the test rig design, the connecting rod is made of 3 pieces of metal shafts that are rigidly connected to each other. The middle piece has a different thickness compared to the other two ends ($h_1 = h_3 = 15$ mm, $h_2=10$ mm), and can be disconnected and replaced. This design allows to removed the middle piece and install a faulty one, where a crack with the depth of $a = 0.25h_2$, is seeded. This ratio is large enough to have noticeable signature in the acceleration signal as studied in [Shih and Chung, 2013] and also demonstrated in the preliminary finite element modeling study in fig. 4.8. The impact of this fault is further investigated, and the results are presented in appendix B.

The third fault under study (\mathbf{F}_C) is described by the misalignment of the intermediate shaft in the gearbox and the associated rub between the shaft and the gearbox wall. This fault is seeded in the test rig by removing the supporting bearing on one end of the intermediate shaft. By hindering the tolerance required for shaft

Table 4.3: Description of the Failure Modes Under Study

	Fault A	Fault B	Fault C
Location	Joint (Slider/Conrod)	Link (Connecting Rod)	Rotating Shaft (Gearbox)
Description	Excessive Looseness	Breathing Crack	Misalignment/Rub
Behavior	Cyclostationary	Transient	Abrupt/Transient

alignment, it will cause the spur gears on the shaft to depart from their ideal involute profiles and will disrupt the gear meshing. As a side effect, the rotating shaft may come in contact with the non-rotating parts (i.e. bearing bushing on the gearbox wall), and cause a rubbing effect (see section 2.2.2.1). While the misalignment demonstrates an abrupt behavior, the rub - if occurs - will have a transient behavior. Abrupt faults have a step-like behavior, where the signal changes abruptly from the nominal value to a faulty value, and often is observed through truncated waveform.

4.4 Data Acquisition and Sensors

The monitored parameters of the system are the interaction force between the blade and the medium f_{int} , displacement x_s and acceleration of the slider assembly \ddot{x}_s , the angular displacement of the crank ϕ , effective torque applied on the crank shaft τ . As shown in eq. (4.8), monitoring these parameters provides complete observability of the system. Fig. (4.9) illustrates the sensing, data acquisition, and actuation elements of the system.

For the test rig, in order to study the kinematics of the end-effector, the slider position and its vibration are recorded. Displacement can be measured through LVDT (linear variable differential transformer). LVDT has low susceptibility to noise and interferences and it can offer infinitesimal resolution. Since the operation of the shovel rig is within the low-frequency range (having a bandwidth on the

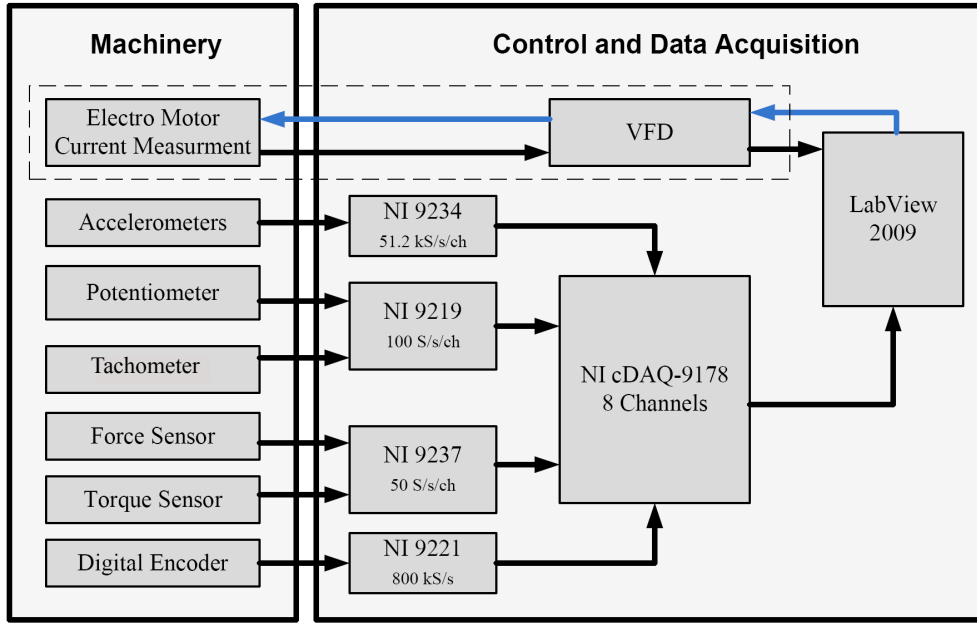


Figure 4.9: Sensing and Data Acquisition Element

order of 1 Hz), position and displacement measurements provide good accuracy [Fraden, 2010]. The slider's position along the x axis is measured through a linear potentiometer, and the signal is captured in a NI9219 analogue input module at a rate of 100 S/s.

It is common practice to have seismic transducers, such as accelerometers and velocity sensors, mounted on machine housing components to measure their vibration level, often in ips and gs [John M. Vance, 2010]. The output signal from an accelerometer is both amplitude and frequency modulated since the transducer produces a voltage proportional to the instantaneous vibration. To pick up the vibration signature of the failure modes, a piezoelectric accelerometer is mounted on the slider. The signal recorded from the accelerometer goes to a NI9234 IEPE module.

Some failures in machines occur because of excessive torsional vibration. When there are gearbox and couplings in the drive train, torque fluctuations have to be supported by the housing and foundation, giving rise to lateral vibrations. Shaft

Table 4.4: Shovel Rig Sensors

Transducer	Model Spec.	Module
Optical Encoder	BEI HS35 5000 cpt	NI9221 C series
Torque transducer	In-house	NI9237 simultaneous bridge
Force plate (In-house)	In-house	NI9237 simultaneous bridge
Accelerometer	ICP(R) 603C01	NI9234 iepe
LVDT Potentiometer	Omega LP801	NI9219 analogue input

encoders are not considered torsional vibration transducer, but they can carry information about torsional vibration (i.e. angular velocity variations) that can be obtained by analyzing the shaft encoder signals. The angular position of the crank is measured through an incremental encoder that is mounted on the output shaft of the gearbox. The digital signal from the encoder goes to a C Series NI9221 module.

To measure the soil-cutting force, a strain-gauge-based force sensor is mounted on the back of the shovel blade. Signals from the force plate are acquired at a rate of 50 kS/s, through an NI9237 simultaneous bridge module connected to the same microcomputer. The force sensor was calibrated using a hydraulic press, applying known forces within the sensor's elastic range.

The input torque τ applied by the gearbox was captured by a set of shear strain gauges mounted on the shaft. For the torque sensor, a calibration device with a lever arm and weights was used to produce specific values of torque, and then the calibration curve was used to correlate the voltages to the associated torques.

Table 4.4 summarizes the sensors and modules of the data acquisition system. All the collected signals are routed to the NI cdaq-9178 chassis, and then forwarded to the LabView VI developed for data collection and pre-processing. The VI program is presented in appendix C. Preliminary signal processing is carried out to convert collected voltage and current signals to the proper parameters of interest.

Acknowledging the limitations of the test rig, the next two chapters presents the

experimental approach and data analysis methods used to evaluate the hypothesis and the idea of environment and equipment monitoring. Chapter 5 introduces how the rig is used to dig through a variety of soil types, and how the cutting force is measured, and describes the methodology developed to obtain information about the environmental properties of the site of operation. The rig is also used to perform a time-varying behavior and the data collected from the equipment is analyzed to monitor the condition of equipment through vibration analysis.

Chapter 5

Soil Parameter Estimation

Equipment situation awareness is an important system level monitoring [Lever, 2011]. Knowledge of the environment of operation is not only important for dig planning [Cannon and Singh, 2000] and production optimization [Tatum et al., 2006b], but it also contributing factor to the greater cause of autonomous digger [Lever, 2011]. Additionally, environmental factors has been identified as a source of operational variabilities that should be accounted when addressing equipment monitoring [Bartelmus, 2012]. In this context, the present study considers soil property estimation as an important component of the environment monitoring.

This chapter presents the methodology and formulation developed for property estimation of cohesive and noncohesive medium.¹ Using the shovel test rig developed for this study, these methods will be applied and experimentally tested for property estimation. At the end of this chapter, the estimated properties are compared to physically measured ones for cohesive and noncohesive material.

Material covered in this chapter help to gain a better understanding of the environment of operation, and allows to have a better estimation of the machine-

¹Parts of this chapter have been published in Journal of Terramechanics, [Yousefi et al., 2012], Contributing authors: Yousefi, R. and Kotchon, A. and Lipsett, M. G., Online publication date: 1-Jun-2012.

ground interaction force, and thus the effect on machine dynamics.

5.1 Machine-Ground Interaction

Property estimation, is the inverse of the interaction force model. As explained in the literature, and due to complexity of these models, they can not be analytically inverted. Hence, most property estimation schemes work on the principle of minimizing the error between the predicted force (computed from an interaction model) and the actual measured failure force from the interaction.

Other estimation methods, attempt to numerically solve the non-linear system of equations that can be constructed by multiple digits. Newton-Raphson method, is an example of such methods. For each unknown parameter that is to be estimated, a unique function is required. However, there are more than one parameter to be estimated, while there is only one equation to describe the interaction system. This can be solved by including an additional measurement of the cutting force forces - at a new rake angles - for each additional unknown and expand the equation around those points. This effectively creates multiple independent equations, which can be used to obtain the desired soil parameters. Figure 5.2 shows how the rake angle α is set to 70° and 80° for the experiments. These two angles are selected, because the Mohr-Coulomb method gives more accurate estimations below 80° [Hong, 2001].

To calculate the failure force based on the Mohr-Coulomb equation presented in eqs. (2.10) and (2.11), the required soil parameters are: soil density γ , soil-tool interface (external) friction angle δ , soil-soil internal friction angle ϕ , and soil cohesion c . The required geometric properties of the tool include: the height of the blade H , the rake angle of the blade with respect to the horizontal axis α , and the angle of the soil surface β . These parameters are illustrated in fig. 5.1. The Mohr-Coulomb model assumes that the soil or substance fails on a flat plane in a wedge-like shape, starting from the tip of the blade and proceeding to the surface of

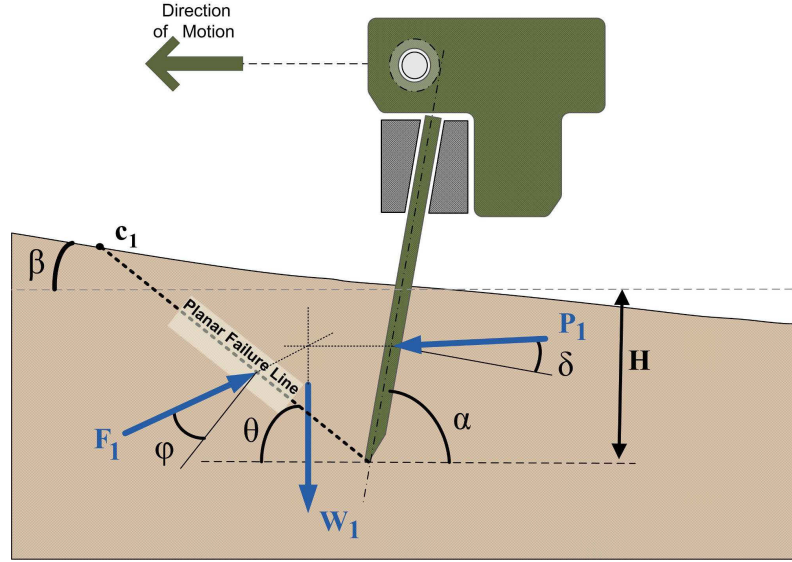


Figure 5.1: Planar Failure Surface According to Coulomb Theory: Internal Friction Angle ϕ , External Friction Angle δ , Attack Angle α , Planar Failure Line θ , Surface angle β , and Depth of Penetration H

the soil. This approximation works well for granular material with low cohesion. Previous experiments has shown that the Mohr-Coulomb method is accurate for rake angles between 50° and 80° [Hong, 2001].

The failure force of the material during the soil-tool interaction is described as the maximum amount of pressure the soil wedge can withstand during cutting before it fails in shear. During the soil-tool interaction, the exerted load on the

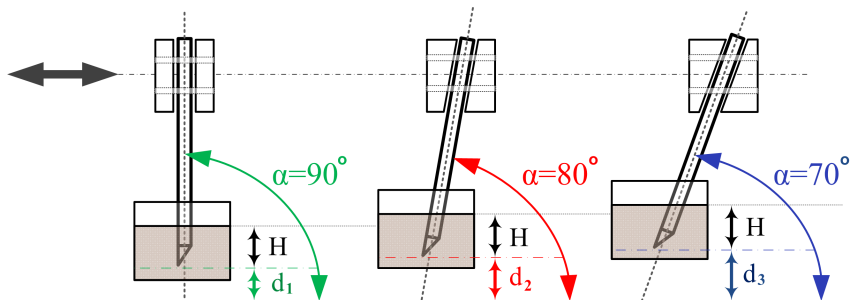


Figure 5.2: While Changing the Attack Angle (α_i), by Changing d_i , Depth of Penetration is Kept Constant at H .

medium will incrementally increase before the failure, while the blade is still in place. As a result, the force required to cut the soil will have an obvious peak right before the soil fails for the first time. After the soil failed, if the soil overburden is pushed with the blade horizontally, then the soil will fail continually and at intervals [Singh, 1995].

5.2 Modified Newton-Raphson Method (MNRM)

Non-linear terms in the Mohr-Coulomb model described in eqs. (2.10) and (2.11) makes it impossible to obtain an analytical inverse. Therefore, a non-linear iterative solving method must be applied to obtain the two unknown parameters (Internal and external friction angles: ϕ, δ). The Newton-Raphson iterative method operates by making a series of guesses to improve an initial estimate [Gilat, 2010].

For the following system of equation,

$$F(z) = f(z) - z = 0 \quad (5.1)$$

we can expand it about an arbitrary point z_i ,

$$z = f(z) = f(z_i + (z - z_i)) \quad (5.2)$$

using the Taylor expansion, and some simplification, the iterative method will become,

$$z_{i+1} = z_i - \left(I - \frac{\partial f}{\partial z} \right)^{-1} [z_i - f(z_i)], \quad i = 0, 1, \dots, \quad (5.3)$$

This is known as the Newton-Raphson method. For a system of equation, it can be written as,

$$F(z) = F(x, y) = \begin{bmatrix} F_1(x, y) \\ F_2(x, y) \end{bmatrix} \quad (5.4)$$

and the Jacobian matrix,

$$\frac{\partial F}{\partial z} = J(x, y) = \begin{bmatrix} \frac{\partial F_1}{\partial x} & \frac{\partial F_1}{\partial y} \\ \frac{\partial F_2}{\partial x} & \frac{\partial F_2}{\partial y} \end{bmatrix} (x, y) \quad (5.5)$$

This estimate is then refined until the difference between the current and previous estimation falls beneath a chosen value.

$$\Delta z = z_{i+1} - z_i \quad (5.6)$$

The challenge in the implementation of the Newton-Raphson method is the extensive computation power, as it needs to compute and evaluate the entire Jacobian matrix $\frac{\partial f}{\partial z}(z_i)$ at every iteration. Moreover, each Newton-Raphson iteration requires the inverse of the Jacobian. To avoid these two challenges, a modified Newton-Raphson method can be applied (See appendix D)). In the modified Newton-Raphson method, the Jacobian is approximated by a fixed matrix e.g. $\frac{\partial f}{\partial z}(z_0)$. Therefore, we no longer need to compute the Jacobian in every iteration, nor do we need to solve the linear system (invert the Jacobian) in every iteration [D. Vaughan Griffiths, 2006, Anandarajah, 2010].

For our system of equations $f_i(\phi, \delta, \alpha_i)$, the Newton-Raphson method can be expressed as follows:

$$\begin{bmatrix} \phi \\ \delta \end{bmatrix}_{k+1} = \begin{bmatrix} \phi \\ \delta \end{bmatrix}_k - \lambda \left[\begin{bmatrix} \frac{\partial f_1}{\partial \phi} & \frac{\partial f_1}{\partial \delta} \\ \frac{\partial f_2}{\partial \phi} & \frac{\partial f_2}{\partial \delta} \end{bmatrix}^{-1} \right]_{\phi, \delta} \times \begin{bmatrix} f_1(\phi, \delta, \alpha_1) \\ f_2(\phi, \delta, \alpha_2) \end{bmatrix}_k \quad (5.7)$$

Including a relaxation factor of $\lambda = 0.5$ [Althoefer et al., 2009], the change in each desired parameter is:

$$\Delta \delta = \lambda \frac{-f_1 \left(\frac{\partial f_2}{\partial \phi} \right) + f_2 \left(\frac{\partial f_1}{\partial \phi} \right)}{J(f_1, f_2)} \quad (5.8)$$

$$\Delta \phi = -\lambda \frac{-f_2 \left(\frac{\partial f_1}{\partial \delta} \right) + f_1 \left(\frac{\partial f_2}{\partial \delta} \right)}{J(f_1, f_2)}$$

$\Delta\phi$ and $\Delta\delta$ are the incremental improvements of the desired parameters; and f_1 and f_2 are the failure force functions and different angles of α .

5.2.1 Proposed Estimation Scheme

Building upon the method of estimation for 2 unknown parameters, a new estimation scheme is proposed that can account for cohesion as well. In this method, and to predict all three soil parameters, ϕ , δ , and c , three sets of equations are required. However, when using three sets of Mohr-Coulomb equations at different rake angles as the input equations, solution of the Newton-Raphson method will become wildly unstable or divergent. Hence, a modified parameter estimation method is required to obtain a solution, and similar to the interaction model, the modification comes from soil mechanics.

The soil-tool friction angle represents the tool roughness. For cohesionless soil, $\delta = 0$ models a perfectly smooth wall, while $\delta = \phi$ indicates a completely rough wall [Shiau et al., 2008]. In the soil mechanics field, it is commonly accepted to consider the soil-tool friction angle δ equal to $\frac{2}{3}$ of the soil-soil friction angle ϕ [Shiau et al., 2008, Look, 2007]. This relationship is adopted and used as a third equation in the proposed parameter estimation scheme.

As a result, the parameter estimation algorithm returns a set of values for ϕ

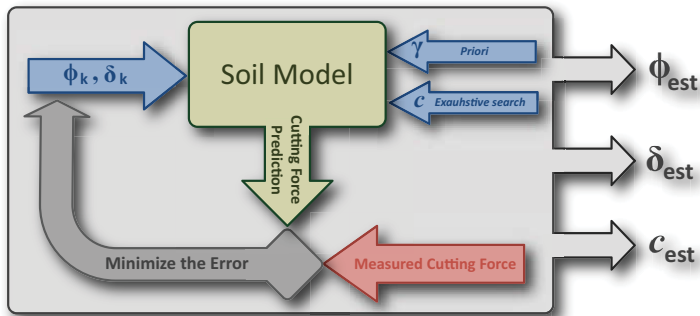


Figure 5.3: Proposed Material Property Estimation Scheme: It Takes Force Measurements from Two Different Attack Angles, and Estimates for up to 3 Soil Parameters.

and δ , choosing a cohesion value c that results in a δ that is $\frac{2}{3}$ the magnitude of ϕ . Figure (5.3) demonstrates how the proposed estimation scheme operates.

5.3 Experiments & Results

The main objective of the experimental work is to obtain failure forces required for a medium, at multiple rake angles, under controlled conditions (i.e. temperature, humidity, input power and cutting speed) for each experiment. Soil cutting tests were performed on three soil samples: *Play sand*, *Glass beads*, and *Oil sand*. It is important to note that the first two material are assumed to be cohesionless, while the Oil sand is highly cohesive. To account for this, the following two steps were taken for processing the data:

Step 1 For the first approach, play sand and glass beads are treated to be cohesionless ($c = 0$). This way the NRM algorithm for the estimation of two friction angles (ϕ) and (δ) proposed in [Tan et al., 2003] is applied. This step, allows to validate the estimation algorithm, and also to establish a baseline.

Step 2 In the second approach, the new estimation scheme is applied on all soil samples (including Oil Sands), assuming non-zero values for cohesion ($c \geq 0$). Using two sets of failure force readings and an auxiliary equation, frictional angles (ϕ) and (δ) and the cohesion (c) values are estimated for all soil samples..

Shear box tests were also performed to measure of the friction angles where it was possible, for comparison purpose and to assess the estimation error.

Under similar experimental procedure, failure forces are recorded for Oil Sand samples. Characterizing Oil Sand is difficult because it is highly cohesive and inhomogeneous, hence the failure force might significantly fluctuate.

5.3.1 Shearbox Measurement of Soil Properties

Shearbox test provide a direct but lengthy measurement of the soil parameters (density, friction angle and cohesion), which can be used as a baseline to compare and validate the estimation results. A direct shear test is a controlled set up for testing and measurement of the shear strength properties of a medium over an extended period of time. In this procedure, the material is sheared slowly, at a speed of less than 5 mm/min, at different loading pressures. The slope of the failure force versus the loading pressure is taken to be the shear angle of the material (ϕ), while the y-intercept provides the cohesion (c) [Craig, 1990]. For Glass beads and Play sand samples, Shear angle (ϕ) and cohesion (c) were obtained using a standard shear box test. Soil-tool friction angle (δ) was measured using the procedure described by McKyes [McKyes, 1985]. The results of these measurements are presented in table 5.1.

Hong [Hong, 2001] and Tan *et al.* [Tan *et al.*, 2005a] used glass beads and Ticino samples. The measured values of the mechanical properties of soil samples reported in their studies are presented in table 5.2.

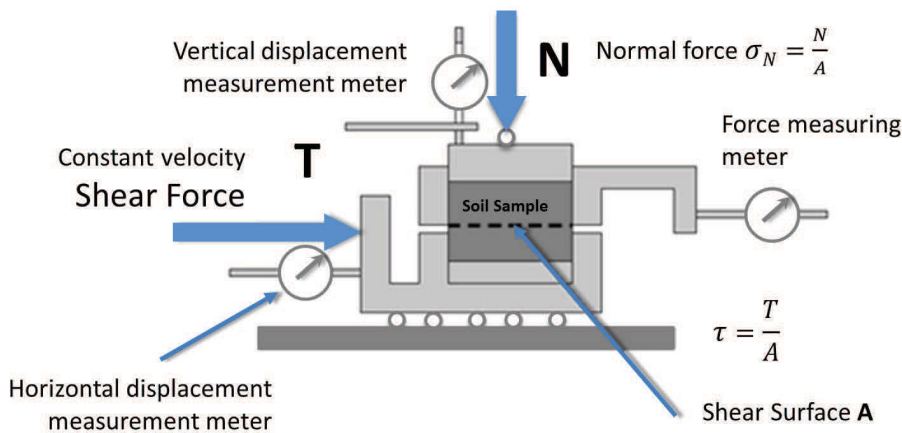


Figure 5.4: Principles of Direct Shear Testing (after [Mecsi, 2009])

Table 5.1: Measured Density and Friction Angles for Soil Samples

Parameter	Glass beads	Play Sand
γ (kg/m^3)	1460	1650
ϕ ($^\circ$)	27	36
δ ($^\circ$)	20	22

Table 5.2: Reported Density and Friction Angles of Soil Samples Used in [Tan et al., 2005a]

Parameter	Glass beads	Ticino
γ (kg/m^3)	1460	1430
ϕ ($^\circ$)	31	42.3 \sim 45.4
δ ($^\circ$)	18	22 \sim 24

5.3.2 Cutting Force

Play sand and glass beads were tested for two different attack angles, $\alpha_1 = 70^\circ$ and $\alpha_2 = 80^\circ$, at a penetration depth of $H = 0.0254$ (m), as shown in fig. 5.2, with a blade of width 0.10 (m). These values were assumed, to replicate the experimental conditions similar to [Tan et al., 2005a]. Figures 5.5 and 5.6, demonstrates the soil-tool interaction forces measured from multiple soil cutting trials on Play Sand at $\alpha_1 = 70^\circ$ and $\alpha_2 = 80^\circ$. The first peak value for each trial indicates the failure force. Interaction forces from soil cutting trials on Glass beads for 70° and 80° rake angles are also illustrated in figs. 5.7 and 5.8, failure forces are similarly extracted, and presented in table 5.3. The averaged failure force for each specific rake angle is then calculated, and fed to the estimation scheme for each of the soil samples.

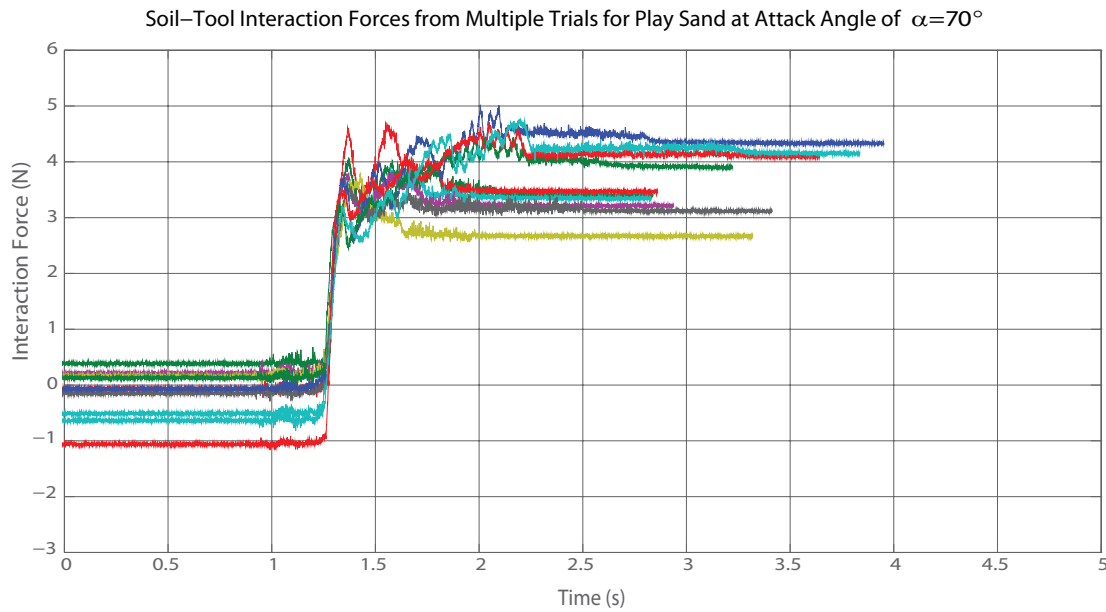


Figure 5.5: Interaction Force Experienced from Multiple Play Sand Cutting Trials at 70° .

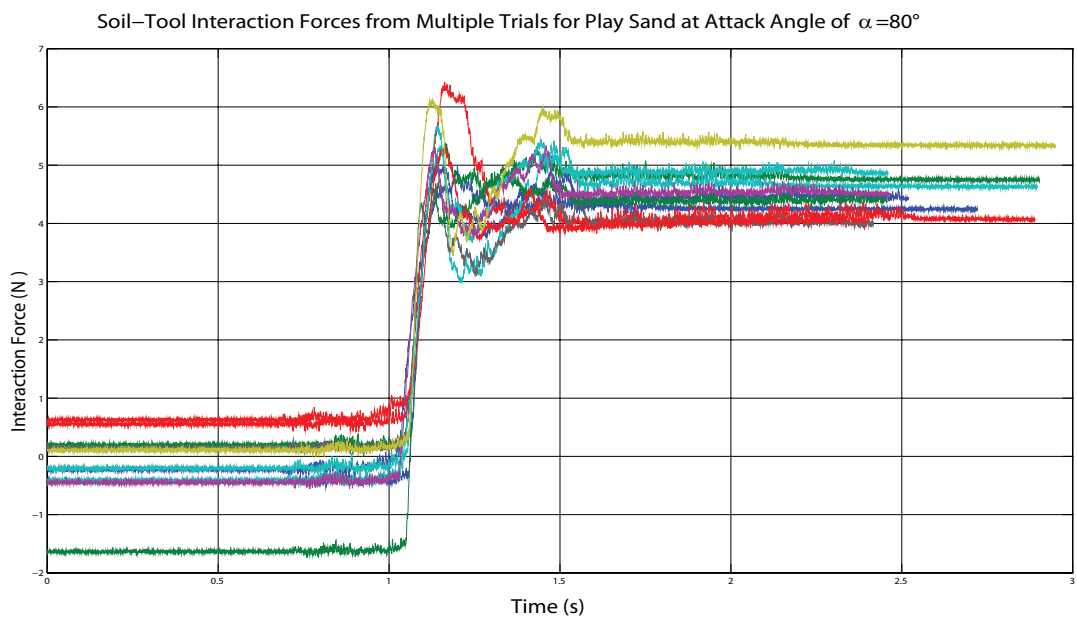


Figure 5.6: Interaction Force Experienced from Multiple Play Sand Cutting Trials at 80° .

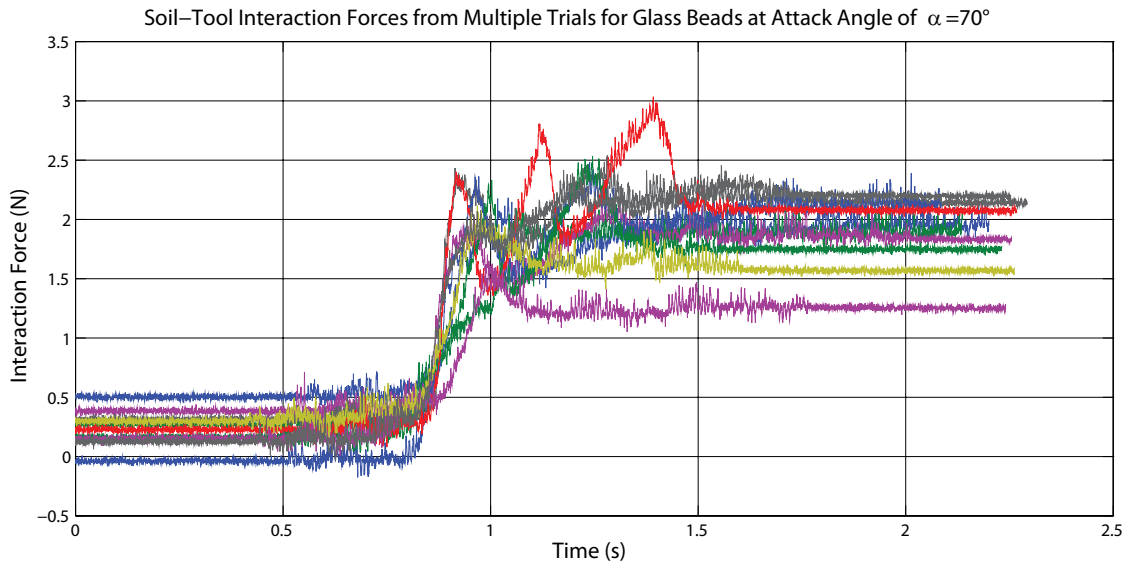


Figure 5.7: Interaction Force Experienced from Multiple Glass Beads Cutting Trials at 70° .

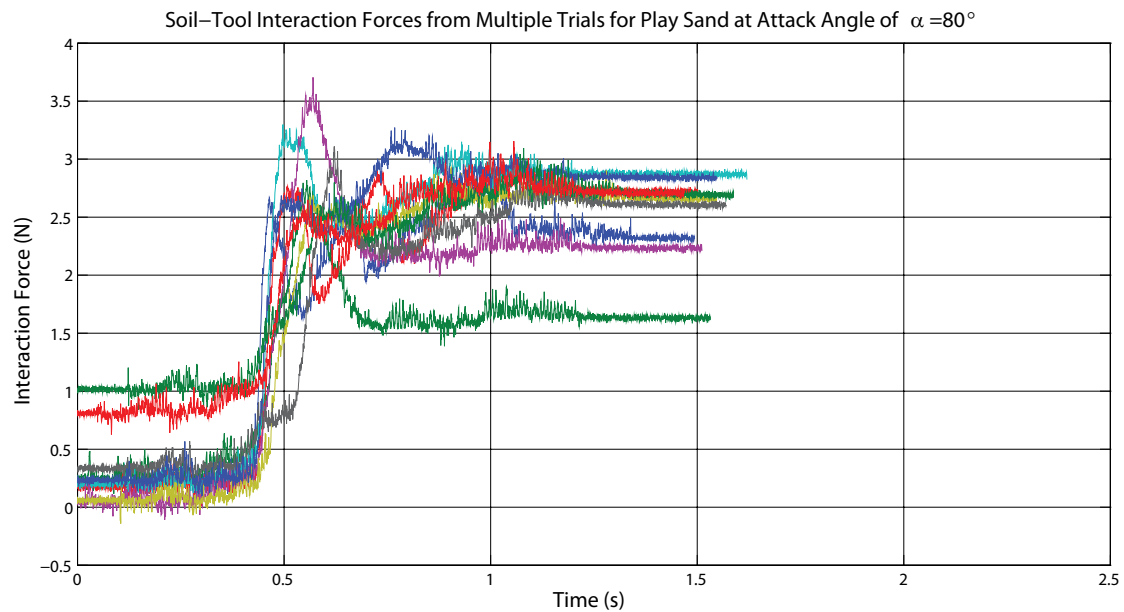


Figure 5.8: Interaction Force Experienced from Multiple Glass Beads Cutting Trials at 80° .

Under similar experimental procedure, failure forces are recorded for highly cohesive Oil Sand samples. This material can be difficult to characterize because it is not only cohesive but also inhomogeneous. Cutting the more dense and cohesive Oil Sand required higher amount of input energy, and interaction forces. Figures 5.9 and 5.10 show the Oil Sand demonstrated much higher resistive force before it failed. It is noticeable, that the interaction force did not show as much fluctuation as the other two soil samples. The averaged cutting forces recorded for Oil Sand at 60° , 70° , and 80° rake angles, are 22 (N), 45 (N) and 58 (N) respectively, and presented in table 5.4).

Table 5.3: Cutting Force Measurement for Glass Beads & Play Sand at $\alpha_1 = 70^\circ$ & $\alpha_2 = 80^\circ$. Averaged Value from Multiple Trials Is Used for Estimation.

i	Glass beads		Play sand	
	70°	80°	70°	80°
1	2	2.65	3.3	5.4
2	2.2	2.75	4.2	6.4
3	1.9	2.7	3.2	4.1
4	2	3.2	3.3	4.1
5	2.3	3.5	4.1	4.7
6	2.25	2.65	3.7	4.6
7	2.3	3.05	3.8	5.3
8	2.45	2.65	4.6	5.7
9	1.6	2.65	3.7	5.3
10	1.95	2.6	3.6	6.2
Average	2.1	2.85	3.75	5.2

Table 5.4: Averaged Oil Sand Cutting Force at 60° , 70° , and 80° .

Attack angle	Cutting Force
60°	22 N
70°	45 N
80°	58 N

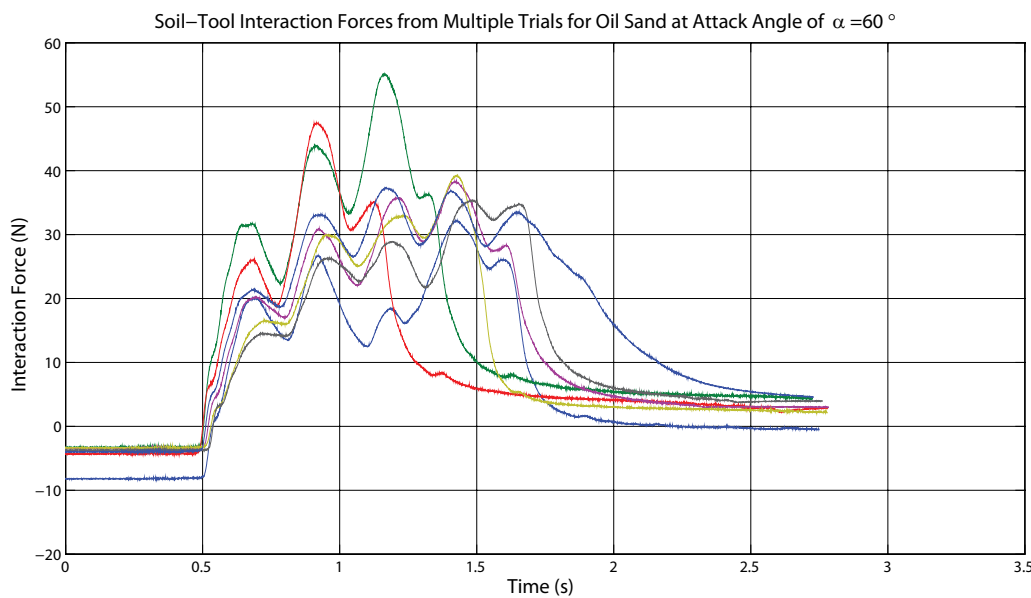


Figure 5.9: Interaction Force Experienced from Multiple Oil Sand Cutting Trials at 60° .

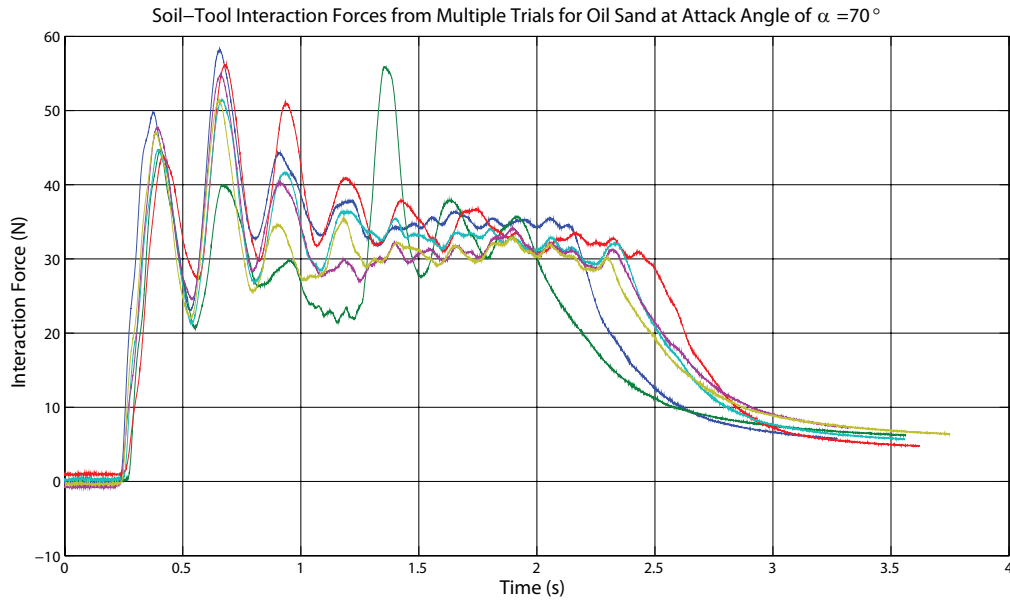


Figure 5.10: Interaction Force Experienced from Multiple Oil Sand Cutting Trials at 70° .

5.4 Discussion and Chapter Summary

While Glass bead and Play sand have each been treated as cohesionless material, on the other hand, materials such as oil sand are known to be highly cohesive. This means that previous algorithms developed for property estimation of cohesionless material cannot be used for cohesive materials such as oil sand. Therefore, an effective estimation scheme for such soils needs to incorporate the cohesion term.

The proposed estimation scheme allows to account for cohesion, hence Glass beads and Play sand are tested under two scenarios. First as cohesionless material (assuming $c=0$), and the with cohesion (assuming non-zero cohesion). This feature also allows estimating the mechanical properties of the highly cohesive oil sand. Note that the starred values for the oil sand are from [Wong, 2001]. Applying the proposed estimation scheme, described in section 5.2.1, all of the three soil parameters, ϕ , δ , and c , could be estimated as presented in table 5.5. As can be seen in table 5.5, cohesion values for play sand and glass beads is less than 5 kPa,

Table 5.5: Property Estimation Result for Cohesive and Non-Cohesive Soils

Non-Cohesive	ϕ°	ϕ_{est}°	ϕ_{err}°	δ°	δ_{est}°	δ_{err}°			
Glass Beads	27	32	5	20	26	6			
Play Sand	36	62	26	22	20	2			
Cohesive	ϕ°	ϕ_{est}°	ϕ_{err}°	δ°	δ_{est}°	δ_{err}°	$c(kPa)$	$c_{est}(kPa)$	$c_{err}(kPa)$
Glass Beads	27	32	5	20	26	6	0	0	0
Play Sand	36	39	3	22	25	3	2.85	4.4	1.55
Oil Sand	60	56	4	–	33	–	94	95	1

this classifies them as cohesionless or low-cohesion materials.

Table 5.5 compares the estimated values of the three parameters, with shear box measurements and previously reported values, and provides a relative error for each estimation. Previously reported error in estimated parameters is between 10% and 30% [Tan et al., 2005a]. In a field setting, this is sufficient to provide useful information for design and for control of equipment such as an automated excavator.

Treating the soil samples to be cohesionless provides a shear angle estimation for the glass beads within the range of acceptable error (i.e. $\leq 30\%$), but not for the play sand (indicating that the assumption that play sand is cohesionless is not appropriate). Taking cohesion into account significantly brings down the associated error of the friction angles of the play sand. The error in the predicted cohesion of the play sand is comparable to that of other parameter estimation methods for sands [Tan et al., 2005a].

There is a considerable range of reported properties for oil sand in the literature. Brookere reported an angle of shearing resistance below 45° , with a cohesion intercept of 80 (kPa) [Brookere, 1975]. Agar performed triaxial tests on Athabasca oil sand samples, where friction angles ranging from $27^\circ - 55^\circ$ were reported [Agar et al., 1987], under the assumption that oil sand was cohesionless. These are similar to results from Wong, who reported a peak friction angle of 48° and a cohesion of

94 (kPa) [Wong, 2001] for oil sand samples from Fort McMurray - similar to the samples used in our experiment. Compositional differences between types of oil sand are likely responsible for the wide range of reported values. Additionally, there are multiple sets of test conditions, sampling methods, and sample preparation techniques used, which could contribute to the variability in the results.

Shear-box tests performed on the sample also showed that there can be a wide range of shear angles obtained for oil sand, depending on the type of oil sand tested and the methods used for sample preparation and testing. This is particularly complicated by the lack of a clear failure peak in shear box testing for this material. While the loose, non-cohesive materials had a well-defined failure peak in the shear box tests, the oil sand did not, and the failure peak was considered to occur when the sample strain dropped to 10% of its original value. Due to the change in shear box test procedure, the calculated friction angle for the oil sand may not represent the failure condition of the material in the same manner that it represents the failure of the loose, non-cohesive materials.

There are two discrepancies between the theoretical model used to approximate the cutting process and the experimental apparatus, which contribute to the error in the parameter estimation. First, the Mohr-Coulomb model does not take into account boundary conditions or edge effects caused by the walls of the soil container. Second, the model considers density to be a fixed parameter during the cutting process; and the estimation method does not account for compaction of the material due to the movement of the cutting blade. Additionally, the Mohr-Coulomb model does not account for the adhesion of the oil sand. Unlike the play sand and glass beads, oil sand adheres strongly to the cutting blade and soil container. The adhesion between the oil sand and the walls of the container could cause an increase in cutting force not represented in the Mohr-Coulomb model. It may also affect the shape of the failure plane, causing a more complex failure. Furthermore, the cohesion and adhesion of the oil sand also affect the shear box tests used to determine the

properties of the materials investigated in this experiment.

Summary of the findings of this chapter is as follows

- Using the principals of the Soil Mechanics, the theoretical relationship between internal and external friction angles is adopted as an auxiliary equation to initiate the soil property estimation scheme. This would allow expanding the estimation for three unknown parameters.
- The proposed estimation scheme takes two force readings and produces an estimate for three soil parameters: Cohesion (c), Internal friction angle (ϕ), and external friction angle (δ). Accounting for the cohesion is a significant improvement over previous estimation schemes reported in the literature, which were only suitable for cohesionless material. Material such as Play sand (with low cohesion) has been previously treated as cohesionless, which produces inaccurate estimate.
- Proposed scheme provides an acceptable estimate (error $\leq 30\%$) for non-cohesive material such as Glass beads, and offers significant improvement for property estimation in relatively cohesive material such as Play sand (error $\leq 15\%$).
- Using the new estimation scheme, mechanical properties of highly cohesive oil sand were successfully estimated for the first time, which are in agreement with directly measured values in literature.

Chapter 6

Monitoring and Fault Detection

Structural health monitoring and prognosis, along with the environmental monitoring, is another important side of the equipment situation awareness [Lever, 2011]. Knowledge of the equipment condition, allows to better predict machines response to the environment, external and internal forces, and ultimately better planning of the operational strategy. In the context of the system level monitoring, equipment condition monitoring is defined by identifying the influential factors such as wear and degradation and the effect of variable operating condition (load, and speed). These factors can affect equipment structural integrity, reliability, and machine availability to perform certain tasks (i.e. pay load capacity, cycle time, dig energy) as shown in fig. 1.1. Through application of environmental monitoring, changes associated with the environment can be successfully identified, and hence its contribution to the operational variability (whether it is the load variability, or change in the monitored signal) can be isolated. As a result, any change in the operating condition of the system then can be identified as a change in the condition of the equipment, as was portrayed in fig. 1.2.

This chapter presents a new look at equipment monitoring from the perspective of system dynamics. Using the shovel test rig developed for this study, conventional

vibration analysis is adopted to monitor the variation in two of the dynamic parameter of the system (i.e., acceleration of the slider, and crank angular velocity). It is widely accepted in the literature that some faults can potentially change the dynamics of the entire system. The slider, that is the end-effector located at the end of the kinematic chain, is a good location for monitoring such changes, because it responds to deviations from normal state caused by faults in other machine elements. Angular velocity of the crank is a state variable of the system that was also monitored. The crank, being in the middle of the mechanism, allows assessment of the impact of the proximity of the sensor on the fault identification outcome at the tool.

The effectiveness of the condition monitoring through acceleration signal will be discussed and application of different signal processing methods for detection and identification of the faults will be reviewed. This approach views the condition monitoring problem from a energy balance point of view, and promotes the use of dynamic parameters of the system for fault detection and condition monitoring.

This chapter is structured as follows. The time-varying behavior of the system is first studied, which impacts the choice of the signal processing technique. Using the statistical features of the waveform, a time-domain analysis is carried out on the acceleration signal to identify fault presence. Features extracted from this step are then used to establish a baseline and to separate failure modes using a dimension reduction technique. Following the time-domain analysis, Frequency and Time-Frequency domains analyses are considered. Time-Frequency signal processing techniques are applied on the both acceleration and angular velocity signals, and their effectiveness in fault detection is compared. Interactive phase of operation (when the shovel engages with the medium) has not been the focus of the monitoring study. However, some preliminary results from the interactive period are presented in appendix E.

6.1 Non-Stationary Behavior

As discussed earlier in section 2.2.2 stationary signals have statistical properties that are invariant with time. Signals that lack such characteristic are considered non-stationary and are categorized into continuously varying and transient.

The monitoring process starts with establishing a baseline for the normal operating condition during free motion (non-interactive). Signals from the displacement of the slider (x_s , A), and rotation of the crank ϕ are acquired for several cycles (one cycle being one full rotation of the crank). With each rotation of the crank, the slider completes a forward and return stroke, as was shown in fig. 4.3. Normal operating condition trials were repeated and four sets of signals were collected to develop a reliable baseline.

The effect of the offset design and shaking force, which is the unbalanced force acting on the frame of machine, are discussed in section 4.1.1. Figure 6.1 illustrates the response of x_s , A and $\dot{\phi}$ for $10(s)$, equal to about six cycles of operation under normal conditions (with $T \approx 1.5 s$). The effect of the offset is clear in the asymmetric shape of the slider's acceleration signal, where it demonstrates different behavior in the forward and return strokes. Also, the disturbance in the acceleration signal, while the the slider reaches its left limit, is the passing of the connecting rod through its singularity point. The crank angular velocity varies as well, as it completes one full rotation (one cycle).

This variability is primarily due to the unbalance and the effect of the shaking force, as previously discussed. Using eqs. (4.2) and (4.2), the shaking force is calculated and plotted for the same cycles. Shaking force under normal condition (F_N^{SH}) demonstrate a near-symmetric sinusoidal waveform. The magnitude of the maximum shaking force during the free motion is of the same order of magnitude experienced when the apparatus is cutting cohesionless medium. Also, it is observed that the maximum shaking forces experienced at the end of the return stroke (\rightarrow), is slightly higher ($\sim 15\%$) than the ones at the end of the forward (\leftarrow) stroke. Also

as expected, it is observed that the maximum shaking force, and maximum slider's acceleration is happening at the same instance.

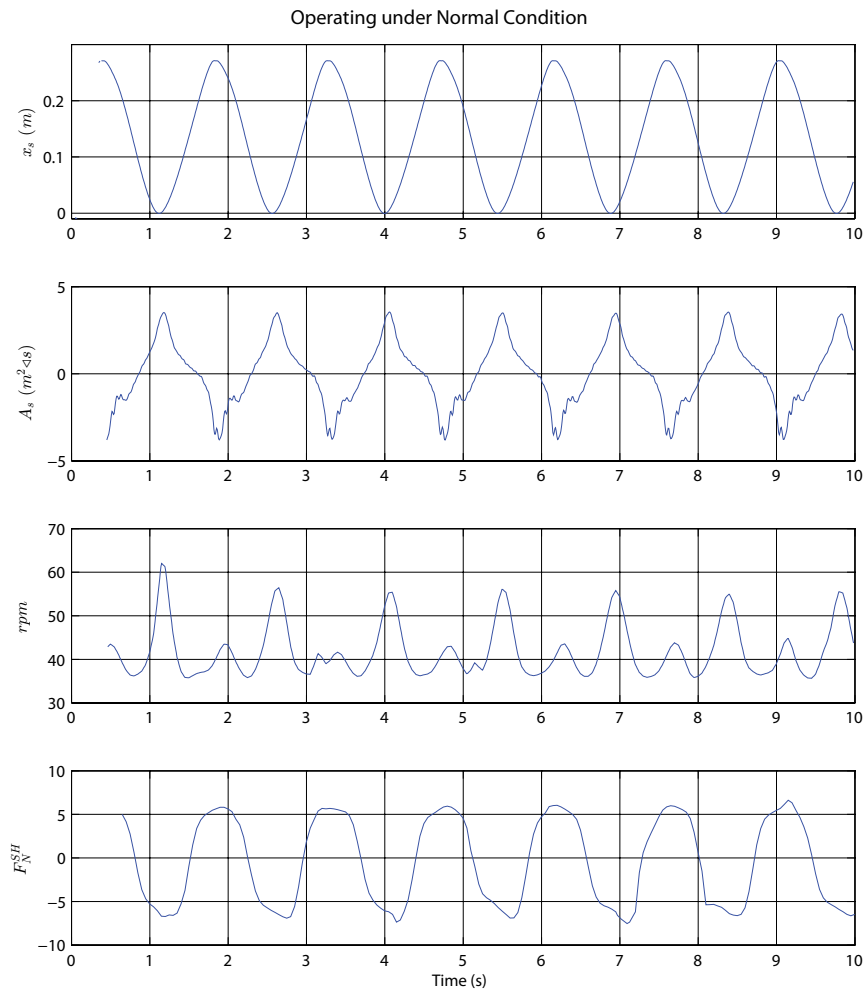


Figure 6.1: Slider's Displacement x_s , Acceleration signal A_s , Crank Angular Velocity $\dot{\phi}$, and Shaking Force F_N^{SH} for 10 (s) under Normal Condition.

6.2 Fault Diagnostic

Once the baseline was established, faulty components were seeded and the signals of interest (x_s , A and $\dot{\phi}$) were collected. For each faulty condition, similar to the normal operating condition, four sets of samples were collected.

Shaking forces (F_{FX}^{SH}) were calculated and plotted along with the other signals, as illustrated in figs. 6.2 to 6.4. There are a number of differences in the time series data that can be seen immediately. As discussed in the literature, a number of data processing techniques are available to analyze these signals. Time-domain analysis, Frequency-domain analysis, and Time-Frequency analysis will be applied and the results will be discussed in the following sections.

6.2.1 Time-Domain Analysis

The time domain approach taken in this section was based on statical feature extraction, explained earlier in section 2.2.2. Statistical features presented in table 2.1 can be used to separate normal from faulty states based on the assumption that the presence of faults will change such features. These features were calculated for the acceleration signal from all four operating conditions measured as presented in table 6.1.

To assess the changes made to the acceleration signal due to the presence of faults, Standard deviation ($Fr1$) and Mean ($Fr5$), provides the first insight. Comparing the distribution of the acceleration signal in Normal and Fault conditions, it can be seen in fig. 6.2 that the signal is largely distorted under Fault A, whereas in Faults B and C, it is not deviating from the normal signal as much, as depicted in fig. 6.3 and fig. 6.4. This explains the relative changes in the ‘standard deviation’ and ‘mean’ values. The changes in the signal ‘mean’ and ‘standard deviation’, can be contributed to the rubbing effect that occurs at the either end of the slider’s movement in presence of Fault A. This is evident in the displacement signal shown

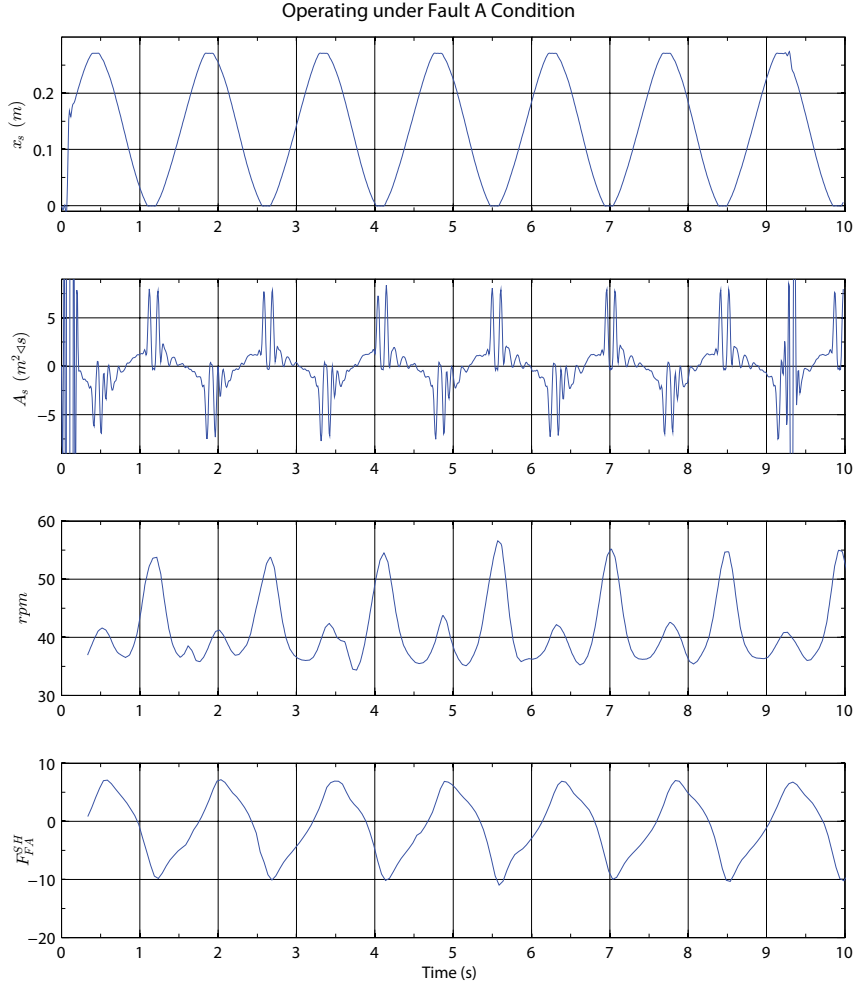


Figure 6.2: Slider's Displacement x_s , Acceleration Signal A_s , Crank Angular Velocity $\dot{\phi}$, and Shaking Force F_{FA}^{SH} for 10 (s) under Fault A Condition.

in fig. 6.2, which is flattened on both ends of the motion. The excessive clearance in the revolute joint, activates the additional DOF of the revolute joint, which disrupts the continuity of the slider motion in the x direction. Allowing the revolute to move freely, increases the chance of contact and causes impact. On the other hand, under Fault B, this only happens when the slider starts its forward stroke. At that point, the compressive load on the connecting rod becomes tensile which activates the ‘open mode’ of the breathing crack.

The next three features, Peak to Peak ($Fr4$), Peak to Mean ($Fr6$) and RMS ($Fr7$), are conventionally used for vibration monitoring. While RMS values are pretty much the same as the standard deviation (by definition), $Fr4$ and $Fr6$ offer interesting information about the failure modes. Acceleration signal under Fault A demonstrates a significant amount of increase to both features (around $8\times$ the normal). While the change in these two features are noticeable for Fault C, ‘peak

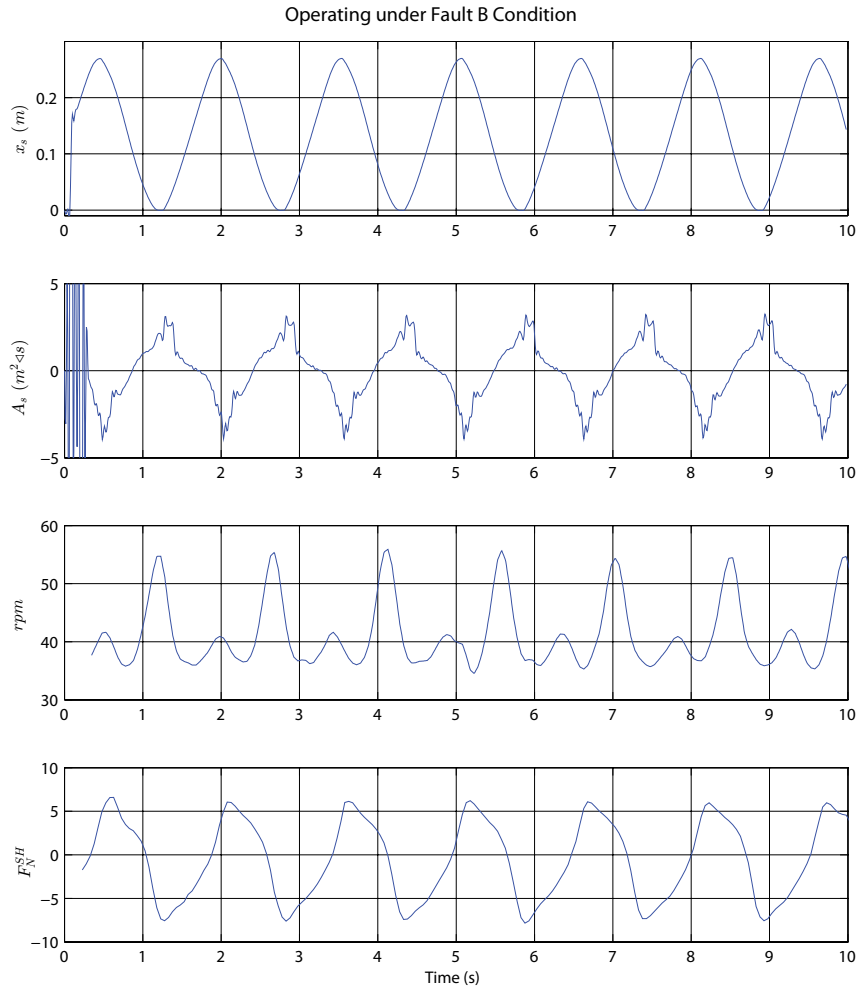


Figure 6.3: Slider’s Displacement x_s , Acceleration Signal A_s , Crank Angular Velocity $\dot{\phi}$, and Shaking Force F_{FB}^{SH} for 10 (s) under Fault B Condition.

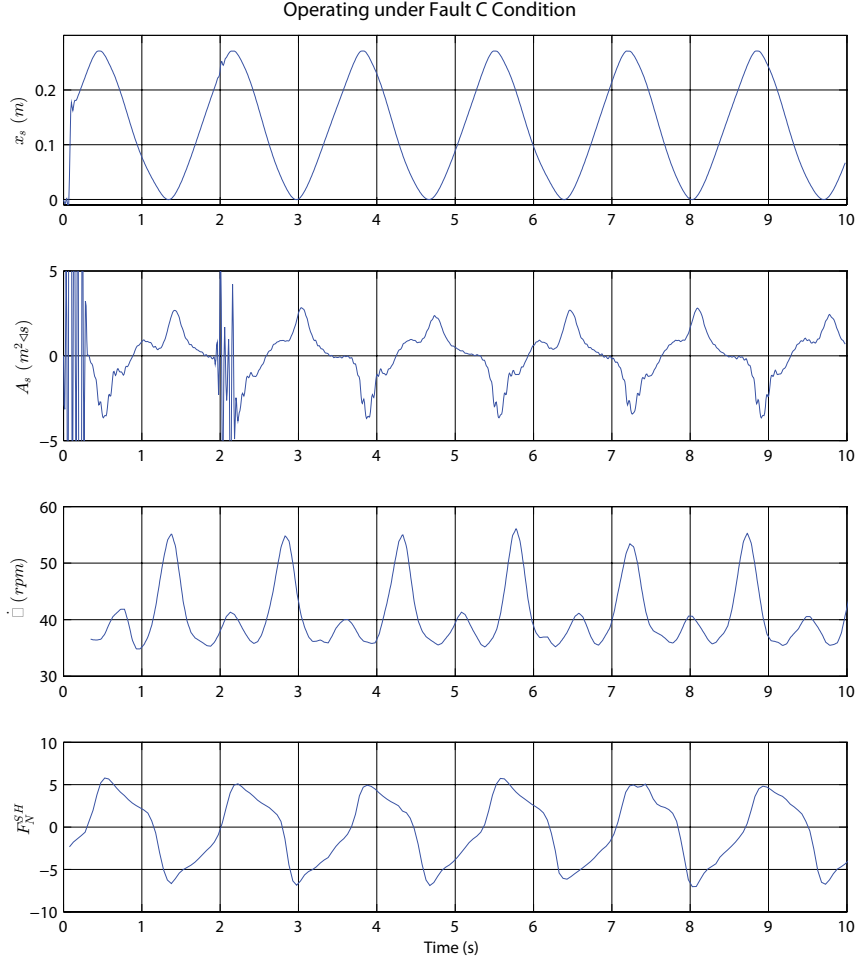


Figure 6.4: Slider's Displacement x_s , Acceleration Signal A_s , Crank Angular Velocity $\dot{\phi}$, and Shaking Force F_{FC}^{SH} for 10 (s) under Fault C Condition.

to peak' and 'peak to mean' values demonstrate no significant change in presence of fault B.

Skewness ($Fr2$) and Kurtosis ($Fr3$) are descriptors of the shape and symmetry of the probability distribution. Skewness, the third centered moment of inertia, is zero for symmetrical functions and large for asymmetrical functions. Kurtosis, fourth centered moment of inertia, is large for 'spiky or impulsive signals, because of the considerable weighting given to local spikes by taking the fourth power [Randall,

Table 6.1: Typical Statistical Features Extracted from the Acceleration Signal

Feature	Description	Normal	Fault A	Fault B	Fault C
Fr1	Standard Deviation	2.0	2.6	1.8	1.6
Fr2	Skewness	-0.1	-0.9	-0.2	-0.5
Fr3	Kurtosis	2.5	10.9	2.5	3.8
Fr4	Peak to Peak	8.6	37.7	8.5	11.8
Fr5	Mean(abs)	1.6	1.8	1.4	1.2
Fr6	Peak to Mean	5.4	21.2	6.0	10.1
Fr7	RMS	2.0	2.6	1.8	1.6
Fr8	Crest factor	2.0	6.0	2.1	4.1
Fr9	Shape factor	1.2	1.5	1.2	1.3
Fr10	Impulse factor	2.4	8.8	2.6	5.5

[2011]. The acceleration signal for the normal operating condition, demonstrate near zero ‘skewness’ value, while signal under Fault A conditions has a skewness of about $10\times$ the normal. Fault B shows the least amount change, and this can be confirmed by looking at the waveform signal as well. Kurtosis is a good indicator of spikiness of the signal [Randall, 2011], the large spikes in the acceleration signal under Fault A are clear evidence of such high kurtosis value ($5\times$ the normal). Note that the negative skew indicates that the probability density function (*pdf*) has a longer left-side tail.

The simplest measure of impulsiveness is the crest factor (*Fr8*), which is defined as the ratio of ‘Peak’ or ‘Max’ to the ‘RMS’ value of a the waveform. The crest factor for a sinusoidal waveform is 1.414, because the peak of a true sinusoid is 1.414 times the RMS value. Crest factor is a less stable feature than the kurtosis, as it relies on the maximum value of the measured signal which can change from one reading to another. However, the next two features, *Fr8* and *Fr10*, match the same trend found earlier in Crest Factor: $3\times$ higher in the presence of Fault A and $2\times$ higher in the presence of Fault C.

6.2.1.1 Dimension Reduction and Classification

Extracting the statistical features from all trial constructs a 16×10 matrix (16 sets of data, each with 10 features). Multivariate statistical techniques are useful in compressing data and reducing its dimensionality. Using such techniques essential information can be retained, that is easier to analyze than the original larger data set. Transforming a number of related variables to a smaller set of uncorrelated variables is one of the key functions of multivariate statistical techniques. Principal Component Analysis (PCA) is a standard multivariate technique that was used to develop the baseline by reducing the dimension of extracted features [Jolliffe, 2002, Abdi and Williams, 2010]. Three sets of data from normal operating condition were used to train the PCA and to extract the linearized transformation that would best represent the normal condition data. Figure 6.5 demonstrates that using the first two principal components 99.9% of the variation in the ten features can be captured. Hence, these two principal components suffice to describe the baseline with high confidence. The linear transformations to express first and second principal components are presented in eqs. (6.1) and (6.2). These two principal components (PC_1 and PC_2) are then used to map all the statistical features extracted earlier, into a two-dimensional map.

$$PC_1 = 0.3136Fr_1 - 0.0823Fr_2 + 0.4962Fr_3 - 0.423Fr_4 \\ + 0.218Fr_5 - 0.17Fr_6 + 0.314Fr_7 + 0.29Fr_8 + 0.218Fr_9 + 0.407Fr_{10}, \quad (6.1)$$

$$PC_2 = -0.201Fr_1 - 0.108Fr_2 - 0.346Fr_3 - 0.392Fr_4 \\ - 0.211Fr_5 + 0.745Fr_6 - 0.201Fr_7 - 0.127Fr_8 + 0.103Fr_9 - 0.082Fr_{10}, \quad (6.2)$$

The remaining normal data set was used to validate the principal components construction, and it's effectiveness for clustering the normal data. Figure 6.5 shows the training data in red circles and the validation data in cyan circle. Also, four

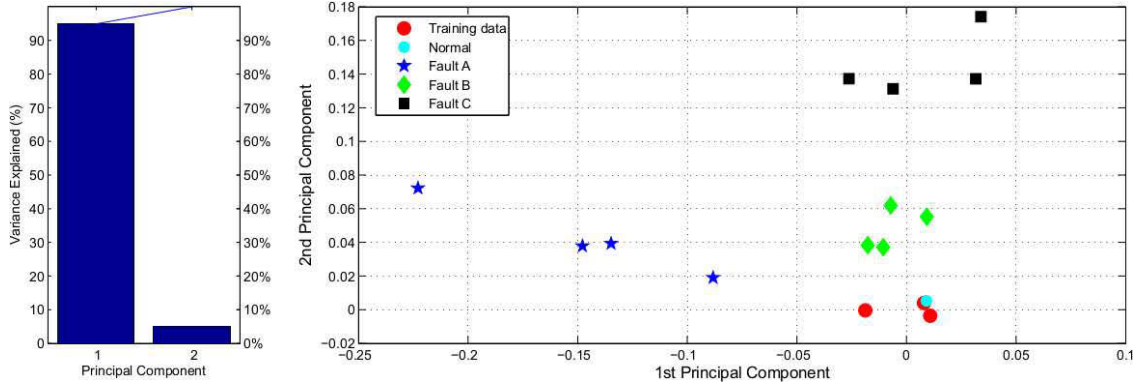


Figure 6.5: Feature Extraction and PCA Are Applied on Acceleration Signal (A) to Separate Healthy and Faulty states. Four Health Classes Are Separated Using PC_1 and PC_2

classes of operating condition (N, F_A, F_B, F_C) can be successfully separated from the normal data, for all four sets of trials (total of 16 data sets).

Furthermore, using these two principal components (PC_1 and PC_2), all four classes of operating condition can be separated using a linear classifier. The linear

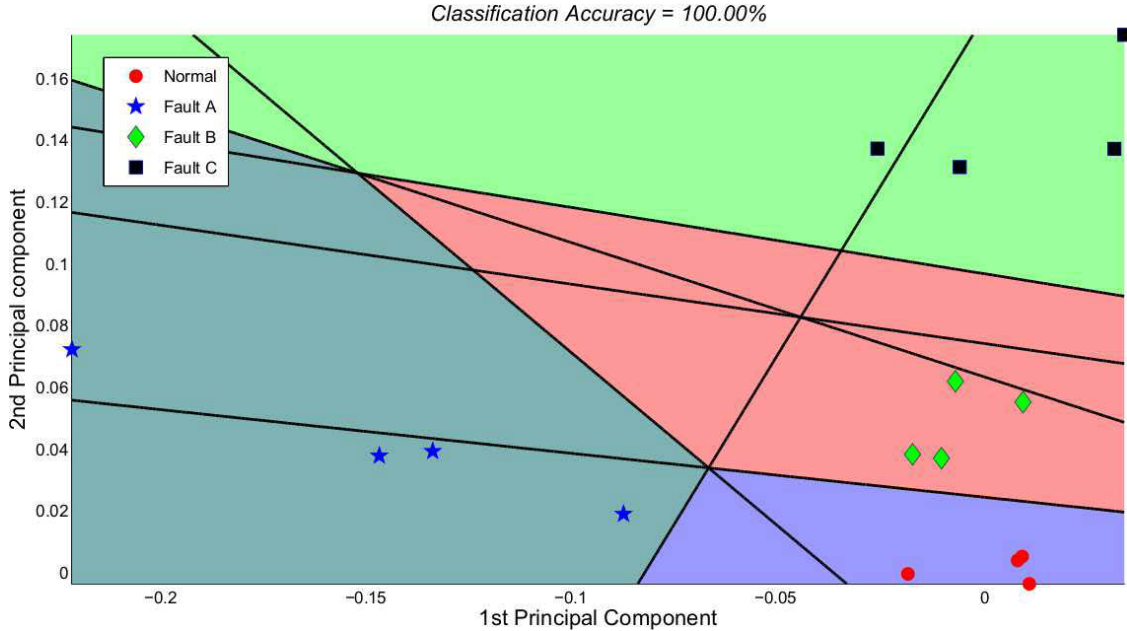


Figure 6.6: Normal (circles), Fault A (stars), Fault B (diamonds) and Fault C (squares) Operating Conditions Can Be Separated Using A Linear Classifier.

classifier in Matlab R2012a - `classify(sample, training, group, 'linear')` - fits a multivariate normal density to each of the four groups of condition, with a pooled estimate of covariance. The result of the classification is presented in fig. 6.6.

6.2.2 Frequency and Time-Frequency Domain

The Fast Fourier Transform (FFT) is the most widely used spectral analysis method used for fault detection in sample data sequence for stationary or nearly stationary systems. It was discussed in section 2.2.2.2 that if the stationary condition is not met, results obtained from the FFT are not reliable. For all the trials, motor nominal speed was set constant at 126 rpm (~ 2.1 Hz). With the gearbox ratio of 0.3, the output shaft of the gearbox rotates at the speed of 37.8 rpm (~ 0.63 Hz). Fourier transform was applied on 15 (s) of the acceleration signal, about 10 cycles, from all 4 health conditions and the spectra are presented in fig. 6.7. Spectrum of the normal condition, demonstrate a dominating frequency of 0.67 Hz which is close to the $1\times$ of the rotation of the crank. Second peak is at 2.1 Hz, which is about $3\times$. There are also many harmonics at half and full cycles, but they are all smaller peaks. Spectrum of the signal under Fault A demonstrates the $1\times$, at a slightly smaller frequency (0.64 Hz), but many larger spikes can be seen at high frequency range.

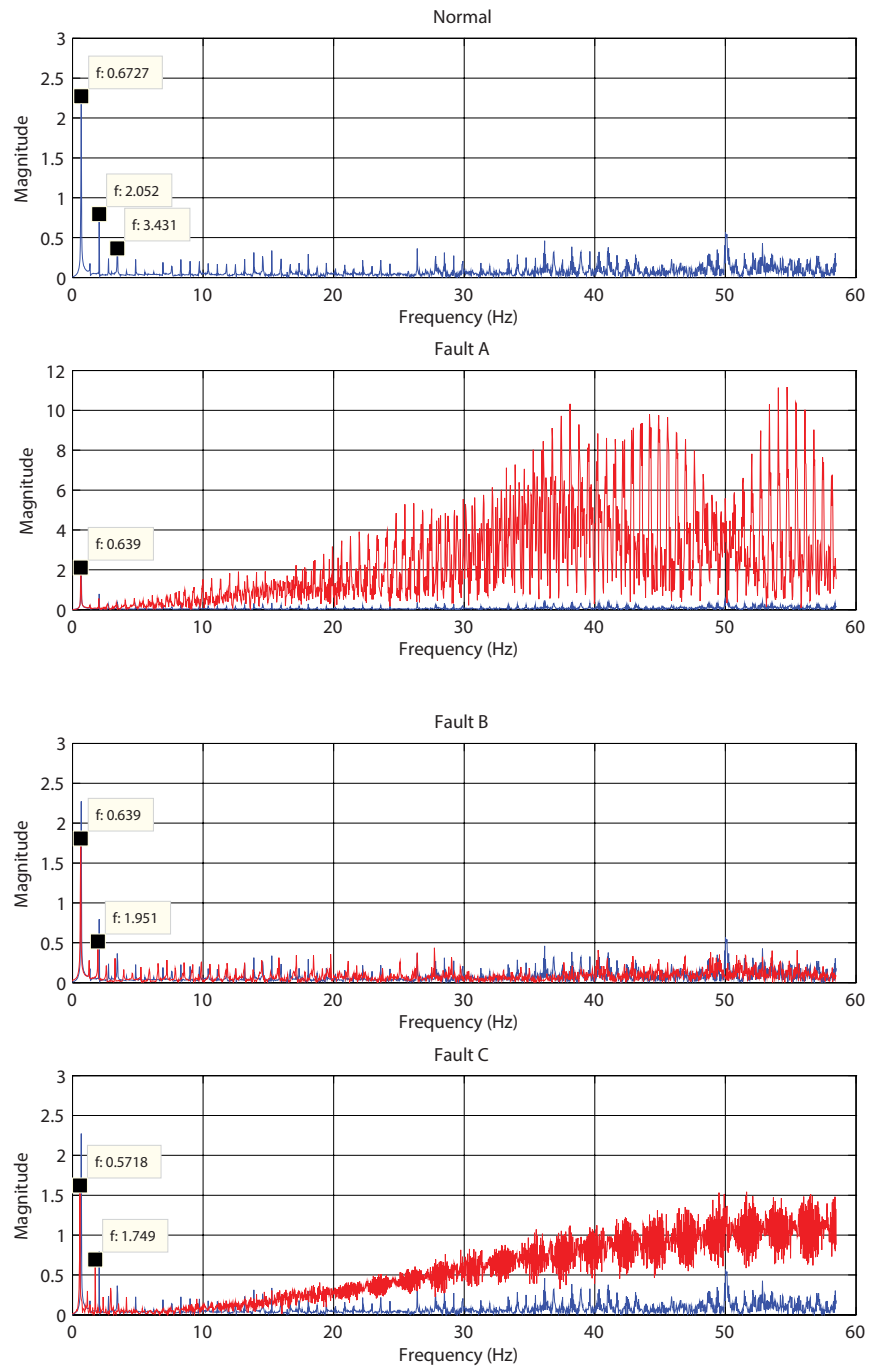


Figure 6.7: FFT Spectrum of the Acceleration signal for Normal (Blue), Fault A, Fault B and Fault C conditions (in Red). Spectrum of the Normal condition is Plotted in the Background.

This is primarily due to the impulsive and spiky nature of fault A. In the presence of Fault B, acceleration signal shows a lot of harmonics at $1\times$, $2\times$, $3\times$, ..., but the spectrum is not much different from Normal condition. In presence of Fault C, the dominating frequency of the signal reduces by about 18%. Additionally, and similar to Fault A, Fault C demonstrates a whole array of high frequency content. Although, some changes are observed in the spectra, the non-stationary condition of the signal prevents it from being used as a reliable tool for detecting fault presence.

Just as like as purely time-based approach to monitoring, which loses the frequency information, a purely frequency based method, will lose the time information; whereas a time-frequency approach conserves both time and frequency information [Randall, 2011]. Among many time-frequency methods, Short Time Fourier Transform (STFT), has been widely used for fault detection for non-stationary signals. The STFT uses sliding windows in time to capture the frequency characteristics as functions of time. Therefore, spectrum is generated at discrete time instants (which allows to regard the signal stationary at such a short time span) and provides a better tool to deal with the non-stationary signals as noted earlier in section 2.2.2.2.

To evaluate the effectiveness of the STFT for the time-varying behavior of the test rig, 'Spectrogram' of the acceleration signal was generated. The failure modes of the interest demonstrate themselves in terms of harmonics of the rotational speed. Because of the low angular speed of the system (under 1 Hz), and to focus on the low frequency events (fault signatures), a low pass filter was applied on the signal. In fig. 6.8 the STFT provides a time-frequency distribution of the signal under all four conditions. Under normal condition $1\times$, and $3\times$ components are visible. Spectrogram of the signal under Fault A and Fault B reveal several concentrated high frequency events. The high magnitudes of these events, affect the frequency content of the signal. The impulsive nature of the phenomena indicates the presence of a large transient (i.e. impact), which is the characteristic of Fault A and Fault B. Figure 6.8c and fig. 6.8d demonstrate that the frequency has a modulating

characteristic, which can be used for fault detection and to further separate these two faulty modes (Fault B and Fault C) from Fault A. To further investigate this, signal is analyzed using Empirical Mode Decomposition (EMD) and Hilbert-Huang Transform (HHT) in the next section. As discussed in section 2.2.2.2, EMD is specifically developed to analyze data from non-stationary and nonlinear signals and uses a self-adaptive approach to deal with signal.

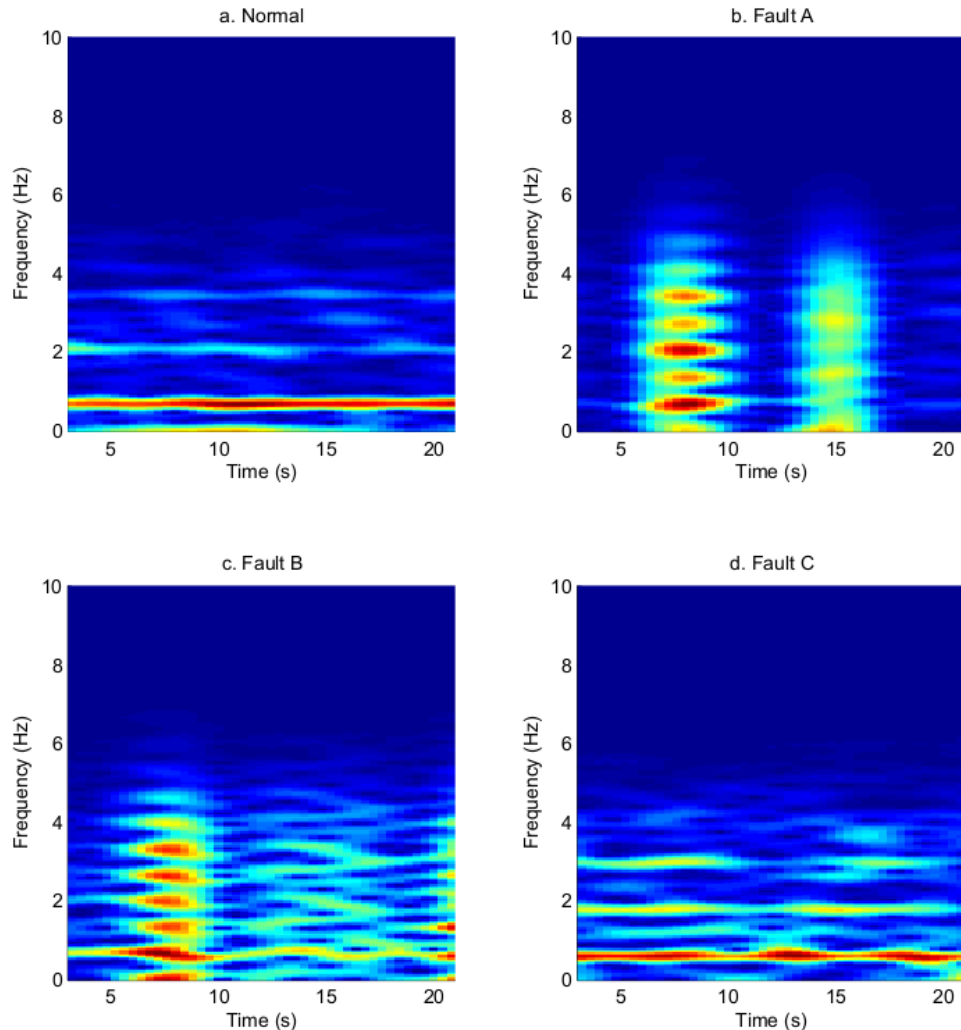


Figure 6.8: Spectrogram (stft) of the Acceleration Signal for All Four Health Conditions. Figures (b) and (c) Demonstrate Significant Impact. Also, in figures (b) and (c) It is Observed that the Dominating Frequency is Modulating Along the Time Axis.

6.2.2.1 Hilbert-Huang Transform (HHT)

Principles of HHT are explained in section 2.2.2: HHT represents the signal in the time-frequency domain by combining empirical mode decomposition (EMD) with the Hilbert transform. In contrast to FT which uses constant amplitude sine and cosine functions to represent each constituent frequency components, HHT first extracts the instantaneous frequency (IMF) using the EMD (which offers smoothing the nonstationary signals), and imposes Hilbert Transform on the IMFs. Hilbert spectrum and its marginal spectrum are extracted for the four cases based on the acceleration signal.

a. HHT analysis of the signal under Normal Condition

Decomposition results of the acceleration signal in normal condition is demonstrated in fig. 6.9, which shows eight IMFs and one residue.

IMF1 shows a very small localized disturbance representing an impact type force, which is synchronized with maximum negative acceleration. This represents the rotation of the crank as it passes through its singularity point (end of forward stroke of the slider). IMF2 shows a distributed disturbance, which has its maximum at the end of the forward stroke of the slider. Comparing it to the waveform signal, it can be seen that it represents the shaking force effect. IMF3 also shows a periodic noise. IMF4 is the $1\times$ component of the acceleration.

Hilbert spectrum (HHS) demonstrates a measure of amplitude contribution from each frequency and time. Marginal spectrum (MHS) offers a measure of the total amplitude contribution from each frequency. Figure 6.10 shows the HS of the signal under normal operating condition. It can be seen that the instantaneous frequency of the signal is unstable noticeably. This reflects the fluctuation of the rotational speed of the test rig due to the unbalance of the system, as noticed and illustrated in fig. 6.1. The main energy peak in the marginal Hilbert spectrum appears at the 0.625 Hz, with two smaller sidebands observed at 0.375 Hz and 1 Hz.

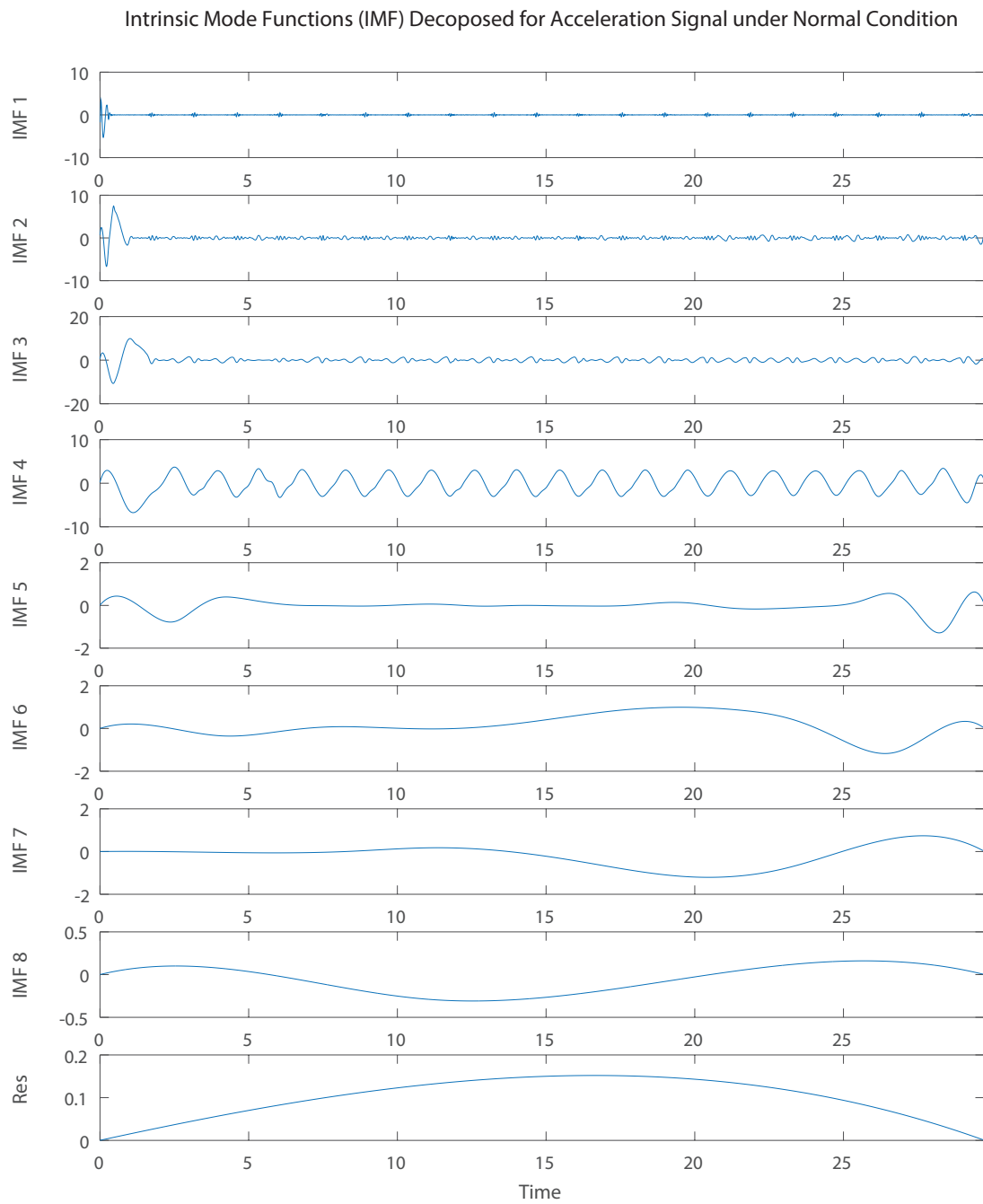


Figure 6.9: EMD Decomposed the Acceleration Signal into eight IMFs for Normal Condition.

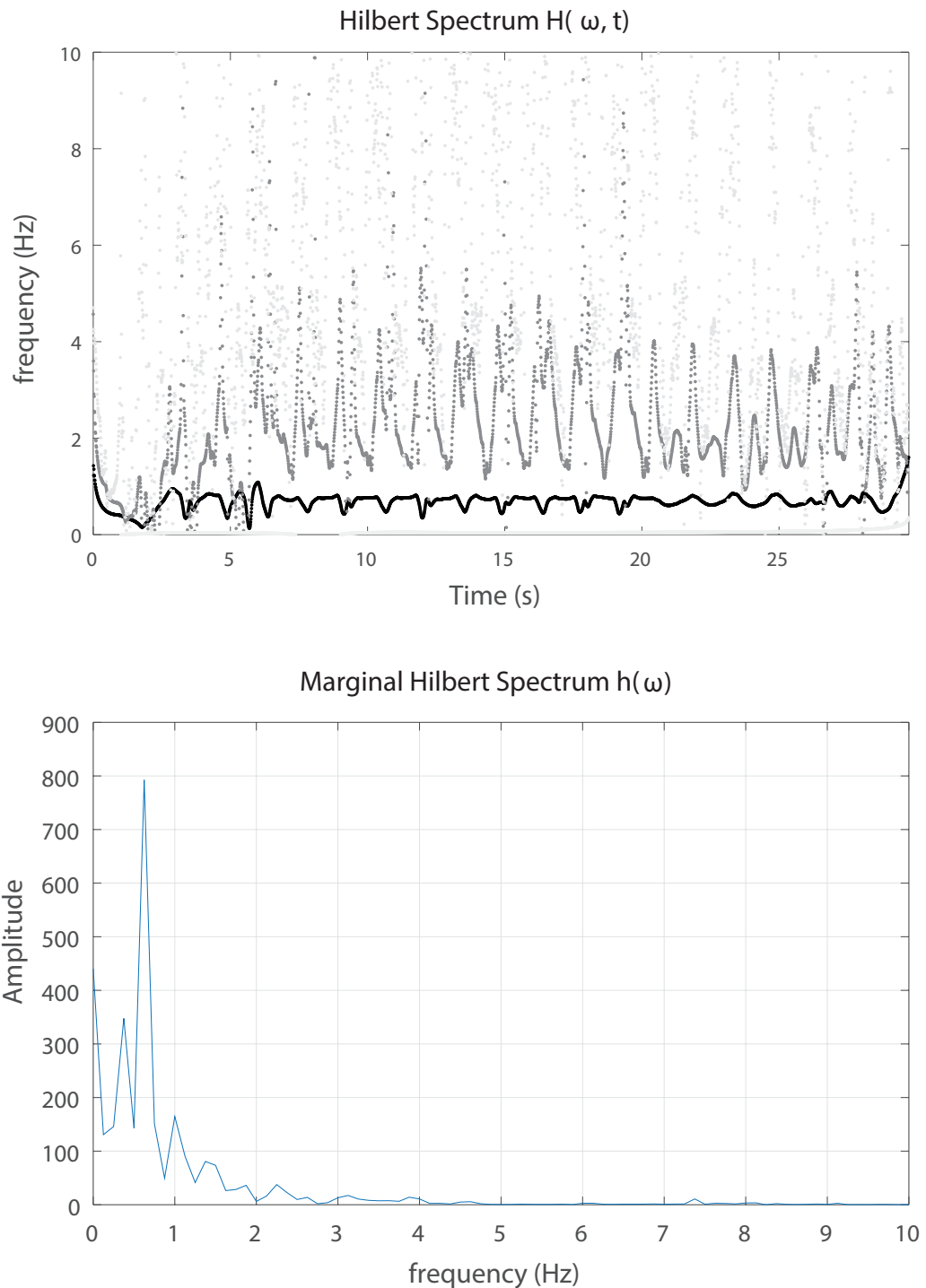


Figure 6.10: HHT analysis of the Acceleration Signal for Normal Condition (a) Hilbert Spectrum is the instantaneous frequency of each IMF (top), (b) Marginal Spectrum of the entire IMFs (bottom).

b. HHT analysis of the signal under Fault A Condition

Decomposition results of the acceleration signal under Fault A (excessive clearance) condition is demonstrated in fig. 6.11, which shows nine IMFs and one residue.

IMF1 to IMF4 are the localized high magnitude disturbances, that represent the impulse components caused by the failure mode. IMF5 is the $1\times$ component of the acceleration, which is completely disrupted at $t=10$ (s) and after $t=20$ (s), in presence of impact.

The transient nature of this failure mode is completely evident in the first four IMFs. Figure 6.12a shows the Hilbert spectrum of the signal under Fault A condition. From this figure it can be seen that the instantaneous frequencies of high-frequency components appear and scatter the time-frequency spectrum of the acceleration signal.

Figure 6.12b shows the main energy peak appears in the frequency 0.5 Hz, followed by a number of sub-harmonics. Note the energy of the peak spectrum is reduced from 800 (in normal condition) to 500, and is spread around the higher frequency components.

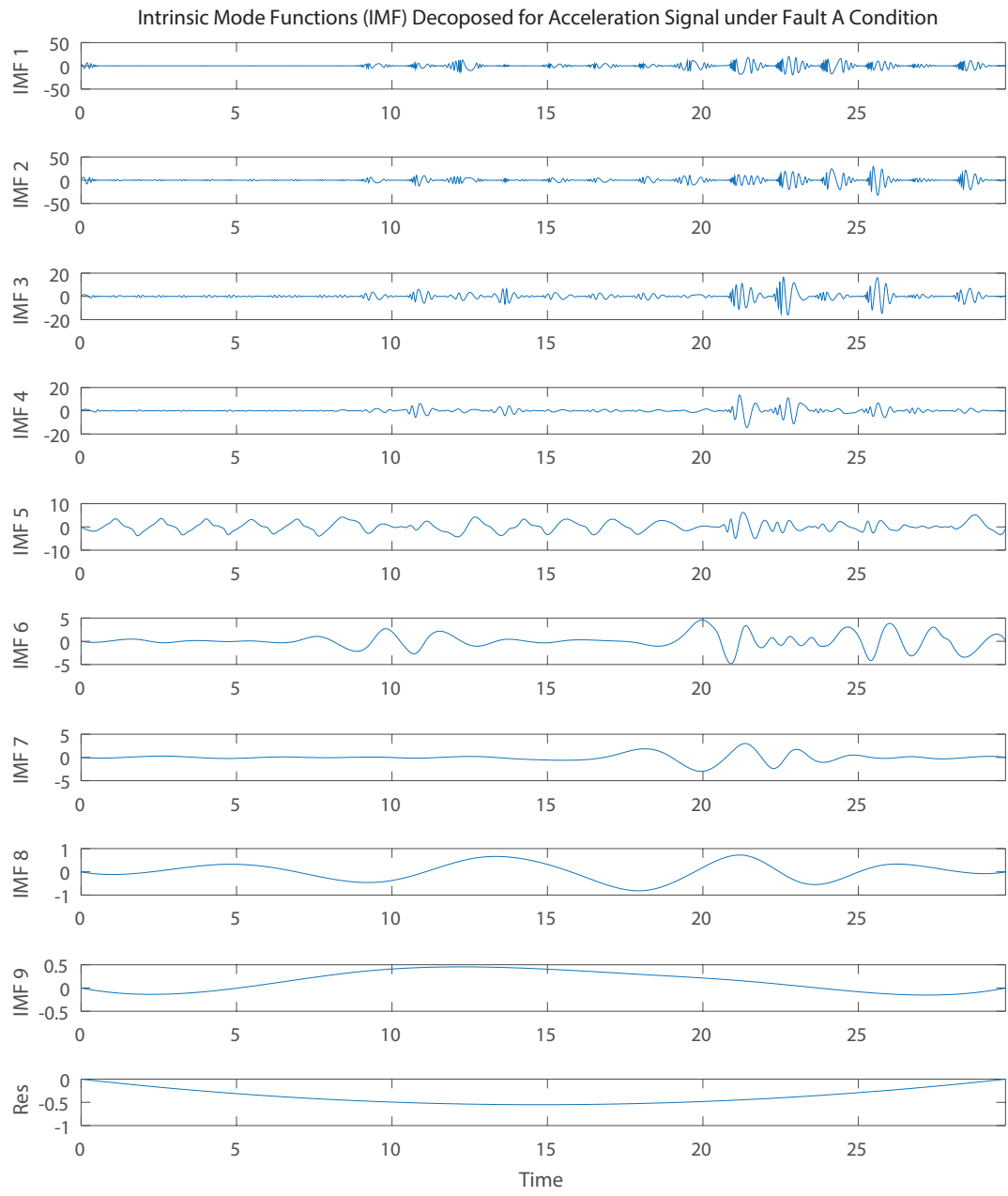


Figure 6.11: EMD Decomposed the Acceleration Signal into nine IMFs for Fault A Condition. The first four IMFs carry signatures of Fault A.

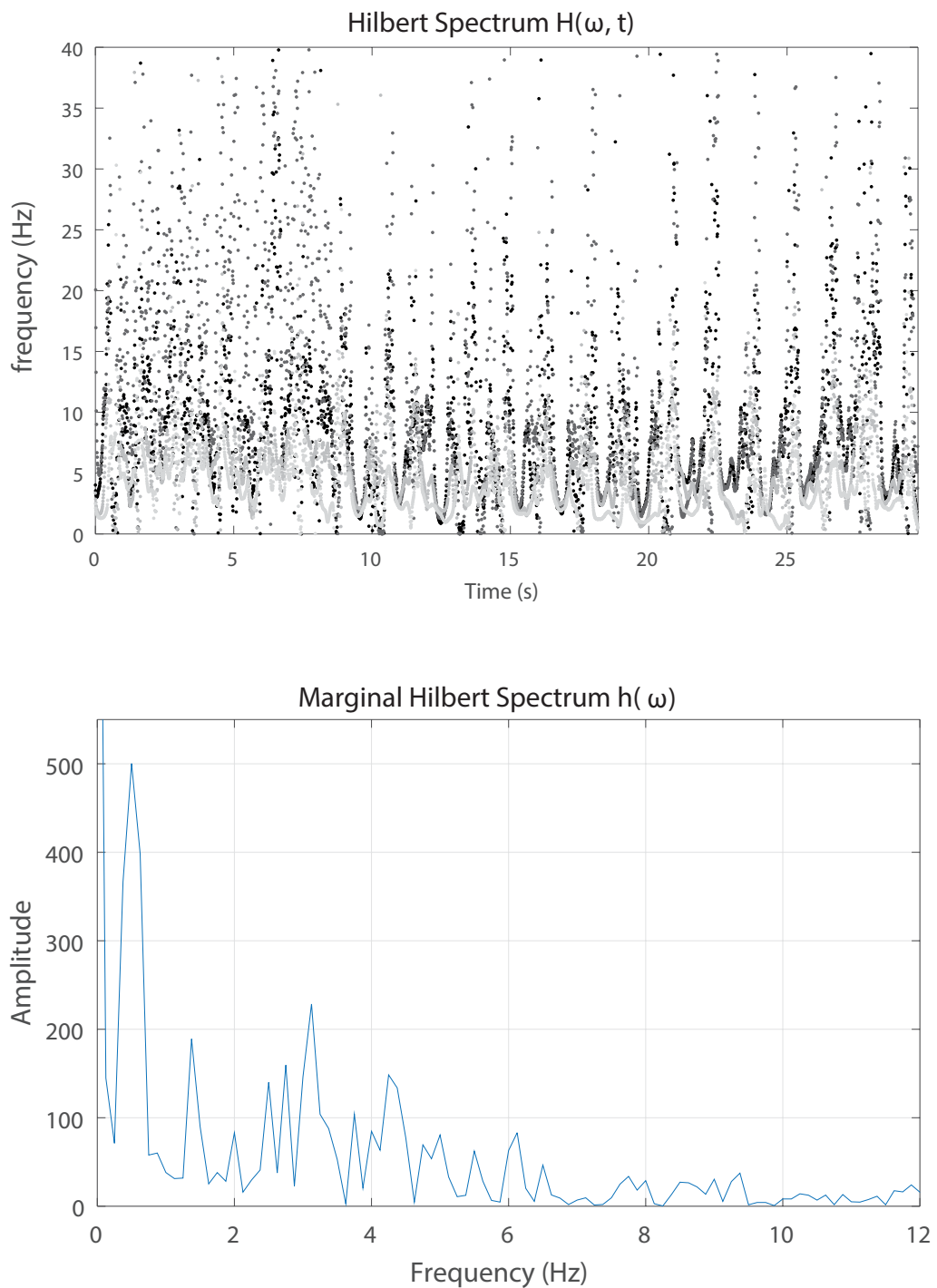


Figure 6.12: HHT analysis of the Acceleration Signal for Fault A Condition (a) Hilbert Spectrum is the instantaneous frequency of each IMF (top), (b) Marginal Spectrum of the entire IMFs (bottom).

c. HHT analysis of the signal under Fault B Condition

Decomposition results of the acceleration signal under Fault B (breathing crack) condition is demonstrated in fig. 6.13, which shows seven IMFs and one residue. In addition to the impulse observed in normal condition, which is at the end of forward stroke of the slider, IMF1 demonstrate a new and greater impulse synchronized with maximum positive acceleration. This is at the beginning of the forward stroke, when the compressive loading of the connecting rod changes to a tensile loading, and as a result activates the ‘open mode’ of the breathing crack in the connecting rod.

IMF2 also shows two sets of disturbances at those instances. There is larger impact at the end of the forward stroke, which can be correlated to the breathing crack switching back to the closed more, and a distributed disturbance that can be contributed to the shaking force. The cyclic behavior of this failure mode is evident in the first two IMFs. IMF3 also shows a periodic noise. IMF4 is the $1\times$ component of the acceleration, with little to no sign of the impulsive force.

Figure 6.14a shows the Hilbert spectrum of the signal under Fault B condition. From this figure it can be seen that the instantaneous frequency of the acceleration signal is modulating noticeably. Figure 6.14b shows the main energy peak appears in the frequency 0.63 Hz, followed by a $3\times$ harmonic at 1.6 Hz. Note the energy of the peak spectrum is concentrated at the dominating frequency components, increasing it to 1150 from 800 (in normal condition).

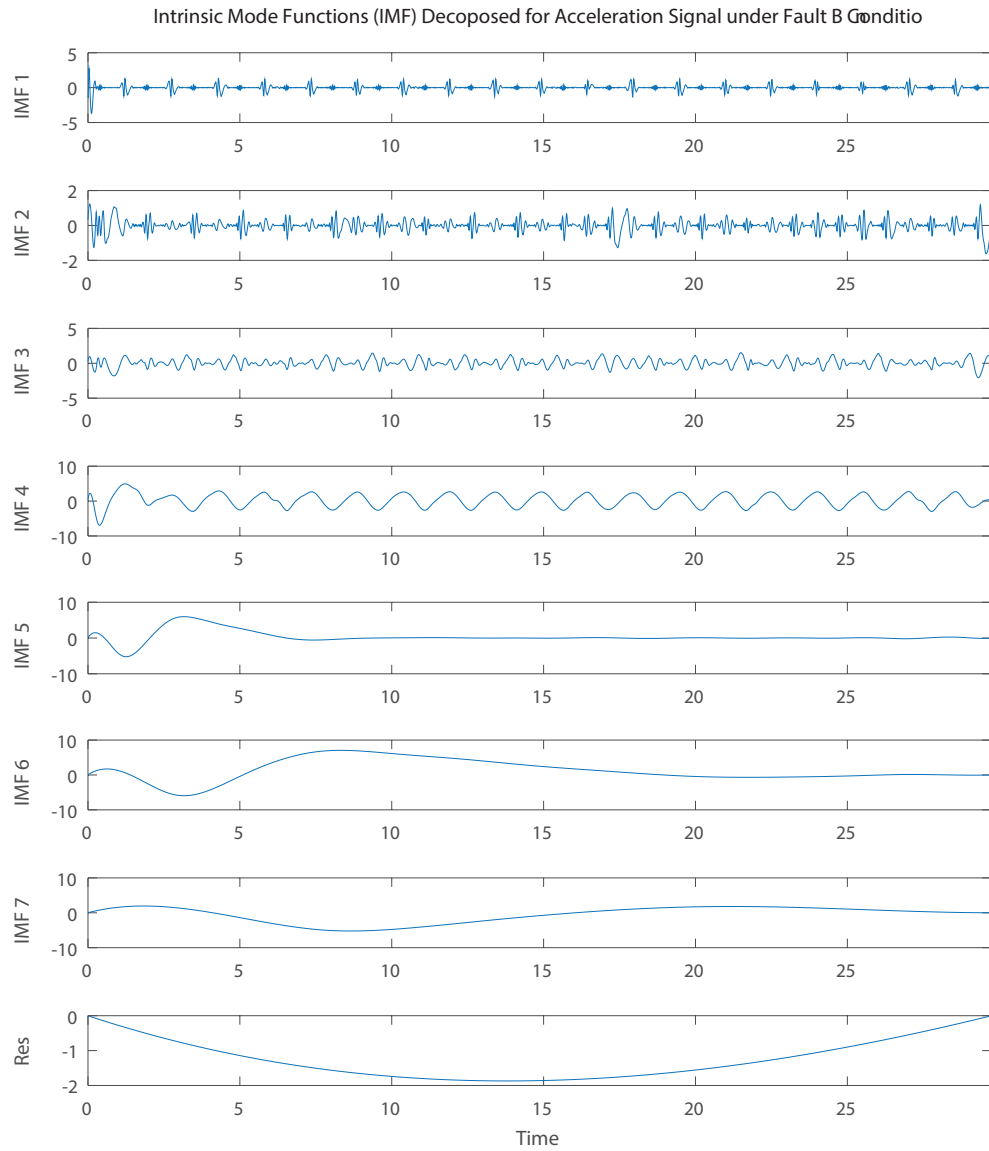


Figure 6.13: EMD Decomposed the Acceleration Signal into seven IMFs for Fault B Condition. The first three IMFs carry signatures of Fault B.

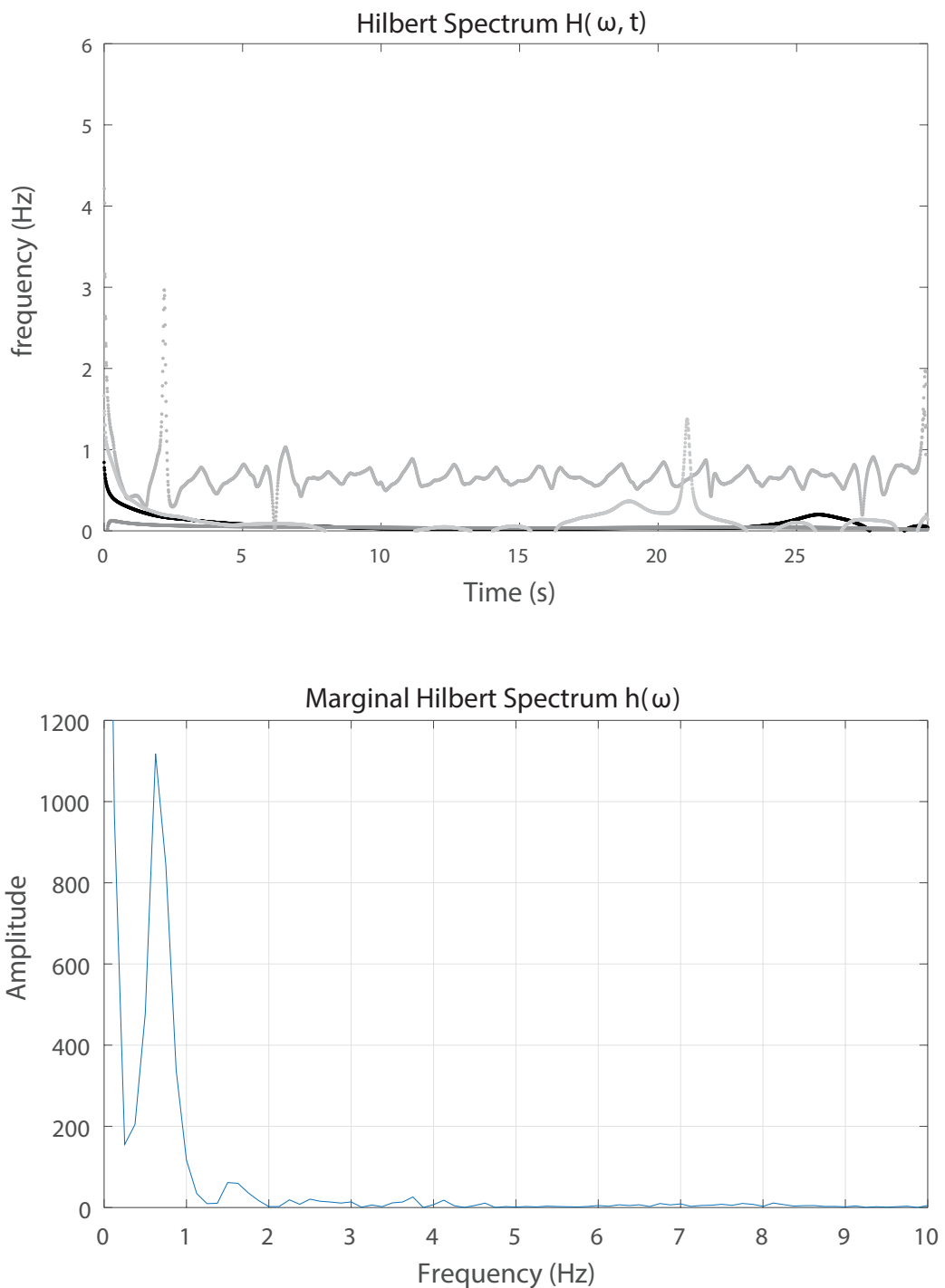


Figure 6.14: HHT analysis of the Acceleration Signal for Fault B Condition (a) Hilbert Spectrum is the instantaneous frequency of each IMF (top), (b) Marginal Spectrum of the entire IMFs (bottom).

d. HHT analysis of the signal under Fault C Condition

Decomposition results of the acceleration signal under Fault C (imbalance/rub) condition is demonstrated in fig. 6.15, which shows nine IMFs and one residue. Along with the normal impulse (at singularity point), IMF1 to IMF3 show two instances of localized and transient disturbance, which can represent impact type force due to rubbing effect.

IMF5 and IMF6 are the $1\times$ and $3\times$ component of the acceleration signal. Figure 6.16a shows the Hilbert spectrum of the signal under Fault C condition. From this figure it can be seen that the instantaneous frequency of the acceleration signal is stable but it is modulated noticeably.

Figure 6.14b shows the main energy peak appears in the frequency 0.5 Hz, followed by a 0.75 Hz sideband. Also a $3\times$ subharmonic is observed at 1.6 Hz. Energy of the spectrum is greatly concentrated at the dominating frequency components for this fault, and shows the highest peak at 1450 (nearly doubled from the normal condition).

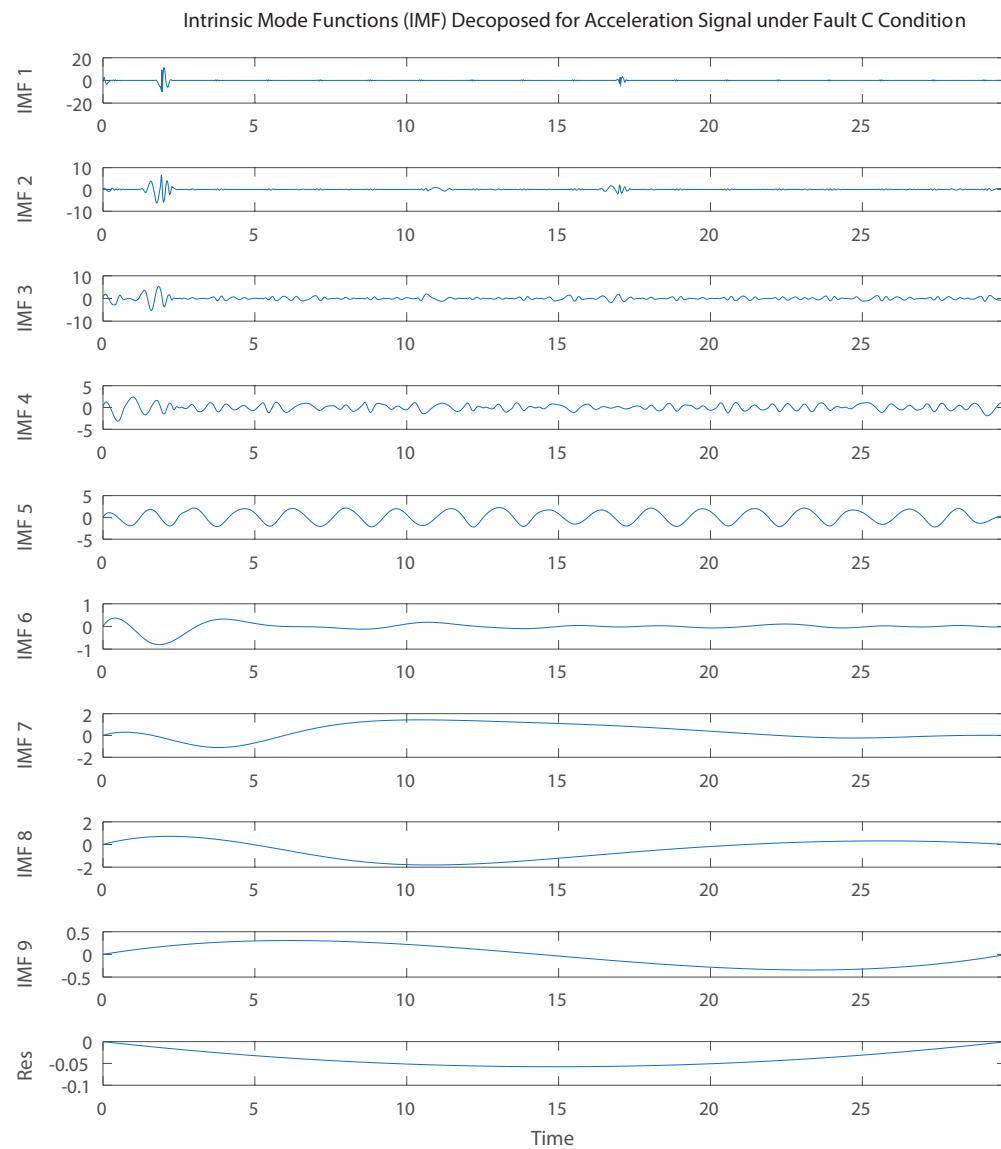


Figure 6.15: EMD Decomposed the Acceleration Signal into nine IMFs for Fault C Condition. The first four IMFs carry signatures of Fault C.

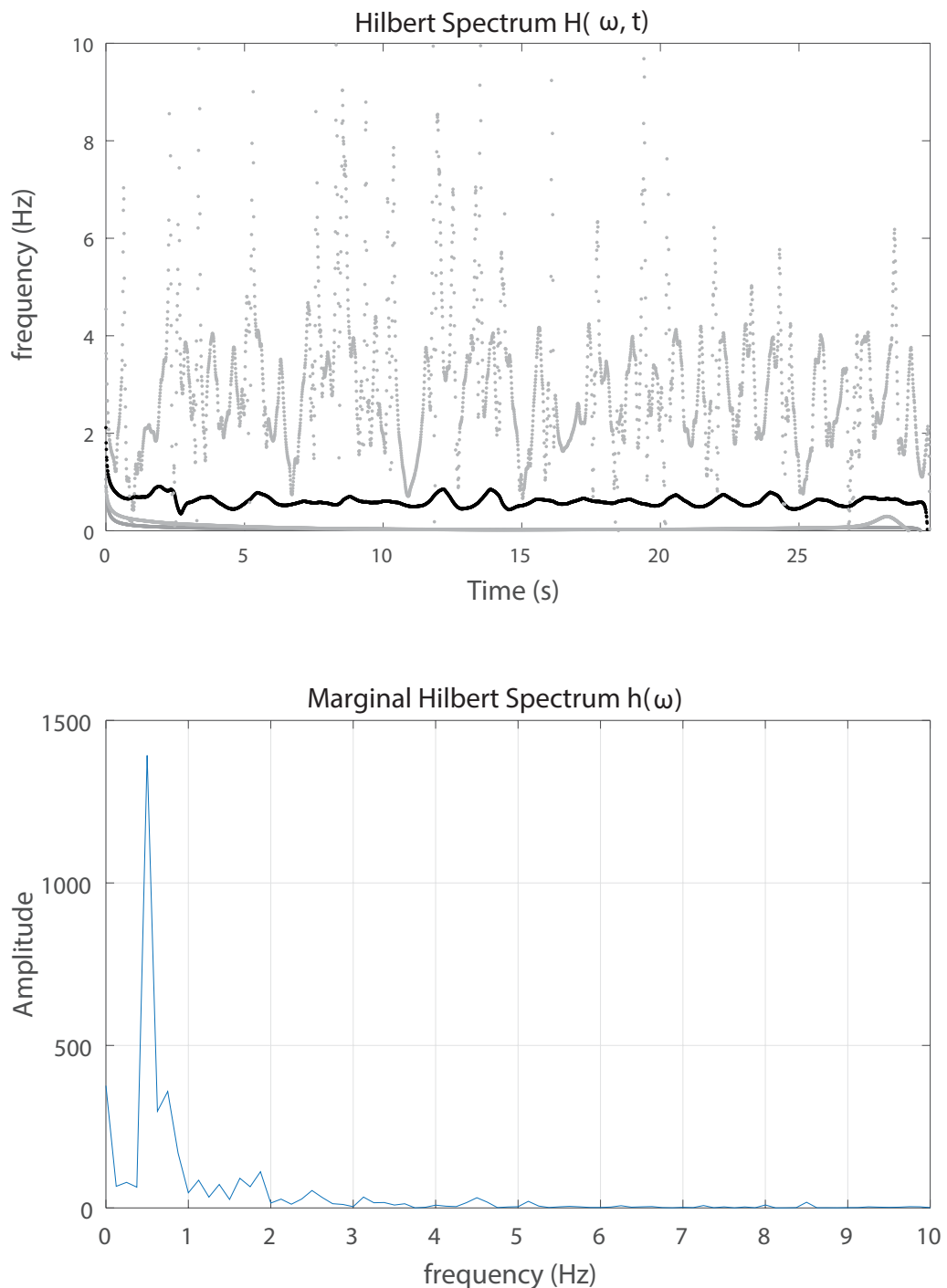


Figure 6.16: HHT analysis of the Acceleration Signal for Fault C Condition (a) Hilbert Spectrum is the instantaneous frequency of each IMF (top), (b) Marginal Spectrum of the entire IMFs (bottom).

d. Study of the IMFs of interest with mhs

When Marginal Hilbert Spectrum mhs is applied on the entire IMFs from each of the four conditions, the frequency content is dominated by the $1\times$ rotational speed. However, by studying the IMFs one can identify the IMFs of interest, the ones that are influenced by the presence of fault. Therefore, applying the marginal spectrum on the select IMFs can provide a greater distinction, compared to mhs of the entire IMFs.

Marginal Spectrum mhs is applied on the select IMFs and the result is shown in fig. 6.17 to fig. 6.20. After applying mhs on the sum of $\{IMF1, IMF2, IMF3\}$ from the Normal condition, it can be observed that the dominating frequency of the select IMFs remains at $1\times$, as expected. This is shown in fig. 6.17.

Similarly, applying mhs on the sum of $\{IMF1, \dots, IMF4\}$ from the Fault A condition, it can be observed that $1\times$ is no longer among the peaks of the spectrum. The largest peak is at $5\times$, with a number of other smaller peaks at $2\times, 3\times, 4\times$

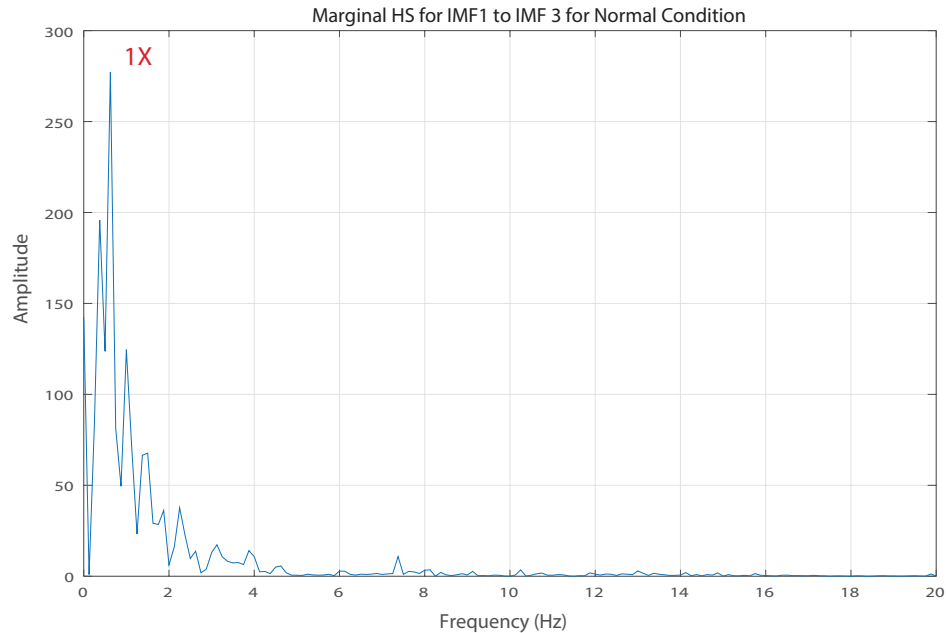


Figure 6.17: Marginal Hilbert Spectrum for the IMFs 1 to 3 for the Acceleration signal for Normal case.

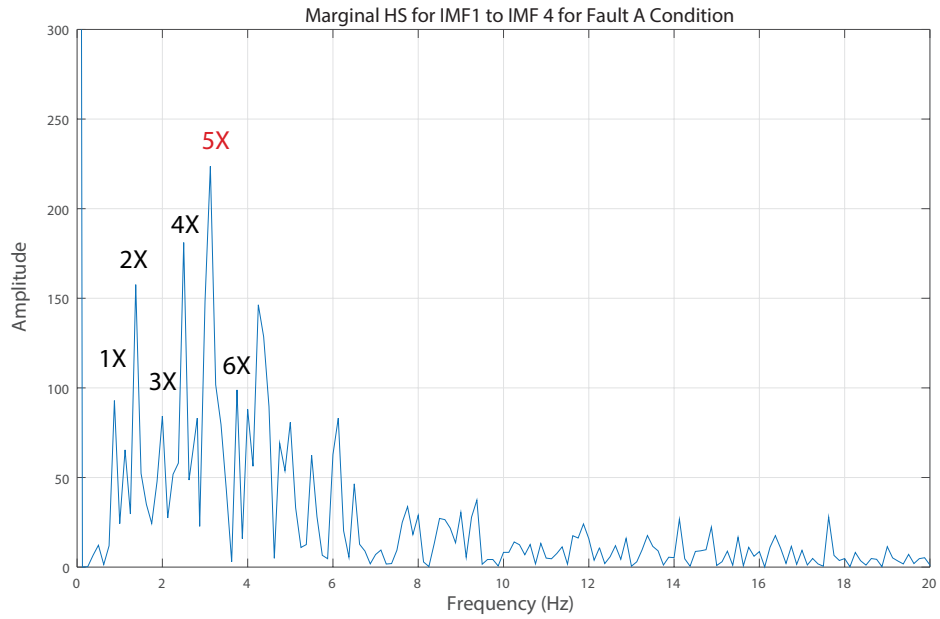


Figure 6.18: Marginal Hilbert Spectrum for the IMFs 1 to 4 for the Acceleration signal for Fault A case.

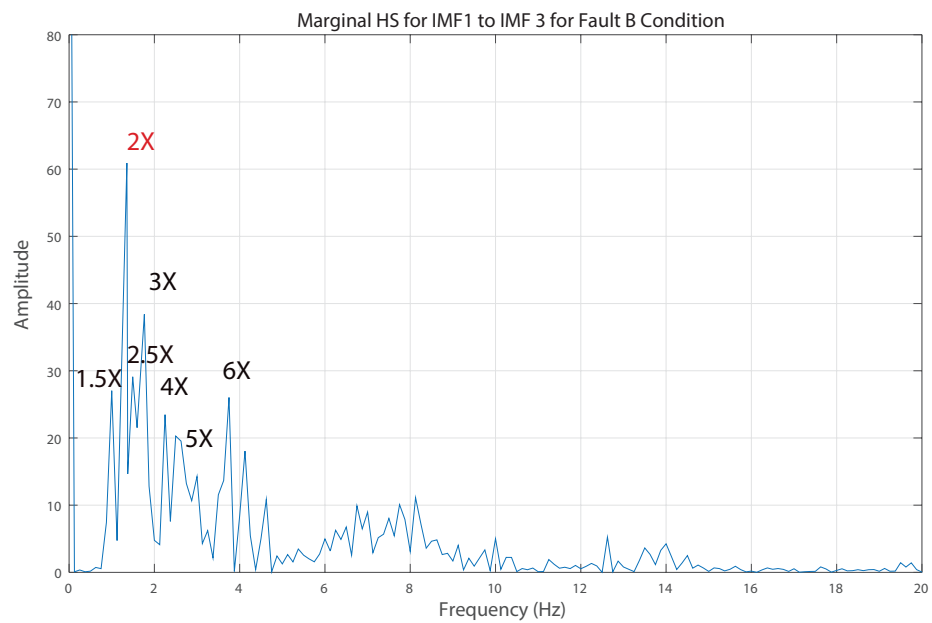


Figure 6.19: Marginal Hilbert Spectrum for the IMFs 1 to 3 for the Acceleration signal for Fault B case.

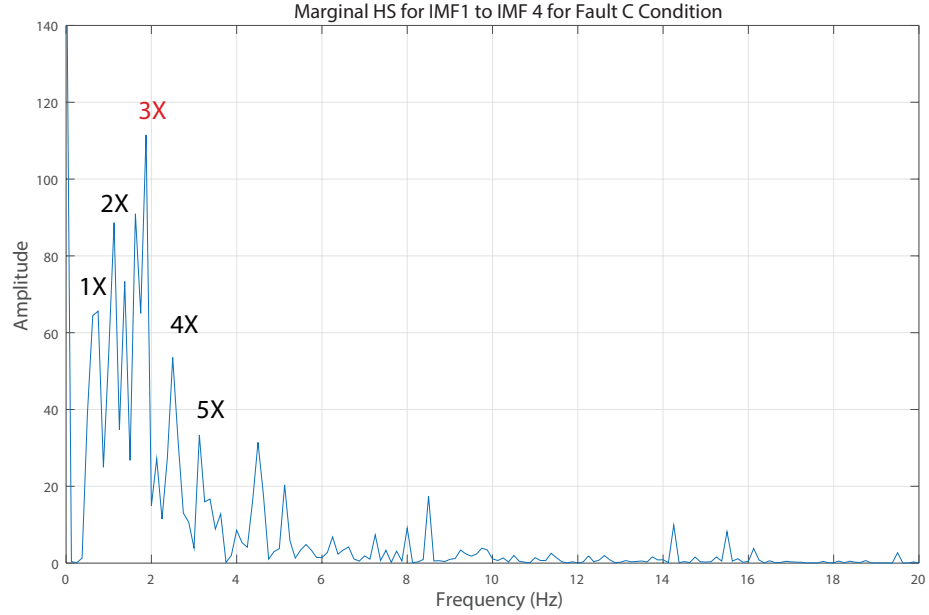


Figure 6.20: Marginal Hilbert Spectrum for the IMFs 1 to 4 for the Acceleration signal for Fault C case.

and $6\times$, as shown in fig. 6.18. This is a significant deviation from the normal behavior (with the largest peak at $1\times$), is similar to the high clearance journal bearing spectral analysis presented in fig. 2.31. Applying mhs on the select IMFs of acceleration signal from Fault B and Fault C also provide a greater insight to the changes of the signal. As noted earlier, IMFs of interest for these two conditions are $\{IMF1, \dots, IMF3\}$ and $\{IMF1, \dots, IMF4\}$, and therefore sum of the IMFs are calculated for each of these conditions. mhs of the summed up IMFs, shows that similar to Fault A, $1\times$ is no longer the dominating frequency. There is a dominating peak at $2\times$ for Fault B, and a dominating peak at $3\times$ for Fault C. Marginal spectrum for Fault B demonstrated side bands at half frequencies, which are signatures of looseness in the assembly. A common feature of all 3 failure modes, is presence of harmonics of $(2\times, 3\times, 4\times, \dots)$.

6.3 Chapter Summary

The main motive for this chapter was the assessment of the potential for monitoring the condition of the equipment through variation in the dynamic parameters of the system. This is in contrast to the conventional monitoring schemes which uses the vibration emitted through equipment housing. This concept is more important when dealing with mobile equipment, and in highly variable environment.

Earlier studies on the failure modes of interest have suggested that presence of these faults can change the dynamics of the system in a way that will affect the acceleration of the slider. In an attempt to monitor the structural integrity through dynamic parameters, it was proposed to investigate the effect of three different failure modes on the acceleration signal of the slider, by adopting the vibration analysis techniques on the data from the non-interactive phase of operation.

The shovel rig is designed based on a crank-slider mechanism, to generate a reciprocal time-varying motion. In section 6.1 the waveform signals obtained from the test rig revealed the non-stationary behavior of the system. Two common monitoring approaches in time-domain and frequency domain were investigated in section 6.2.

Statistical features of the signal were extracted from the acceleration signal in section 6.2.1. Comparison of the extracted features revealed that the failure modes used in this study have an obvious impact on the statistical features of the acceleration signal. A principal component analysis was done to reduce the dimension of the features, and to establish a baseline for normal condition. It was found that for the given training data, the first two principal components can effectively capture the variation in the normal operation. These two ‘pc’s were used to reduce the number of features and mapped them into a two-dimensional coordinate. Then, linear classification was successfully used to separate machines operation with faulty conditions from normal.

Frequency and Time-frequency approaches were investigated in section 6.2.2. The

time-domain analysis is simple and effective, however, it loses frequency information of the signal. Similarly, a frequency-domain analysis one usually look at power spectrum which rejects phase, or oversample to reduce contribution of white noise, and boost signal.

Particularly, for a time-varying system, under conditions of variable loading and speed, a time-frequency approach is more appropriate. To deal with the non-stationary condition of the signal, Short Time Fourier Transform (STFT) was used, which would analyze the signal in small fractions of time; therefore, it can handle the non-stationary signals. However, Fourier transform uses sine and cosine functions to represent the constituent frequency components of the signal. Dealing with signal with modulating frequency, STFT does not offer a very good resolution. An alternative solution, is the application of the Hilbert-Huang transform which can adapt to the changes in the frequency.

Using the Empirical Mode Decomposition (EMD) method, acceleration signal is decomposed into its intrinsic mode function (instantaneous frequencies).

The IMFs extracted for Normal and Fault conditions are found to have a large amount of information about the system behavior. Concentrated and distributed components such as impact and shaking force can be observed through the decomposed signal. Applying the Hilbert Transform (HT) on the decomposed IMFs, Hilbert spectrum of the signal was obtained. In contrast to the STFT, HT demonstrated the frequency modulation very clearly, where changes made to it due to each failure mode can be studied.

Marginal Hilbert Spectrum (mhs) provides a more interpretable data once applied on the Hilbert spectrum. The marginal spectrum of the IMFs of interest, demonstrate that presence of the failure modes impacts both the energy and the frequency of the Hilbert spectrum, and can be quantified to separate the faulty conditions from normal.

Summary of the findings of this chapter is as follows

- Acceleration of the end-effector is used as a monitored signal for fault detection for the first time. Variation in the acceleration signal is a representative of the change in the dynamics of the system, hence effect of a fault can be directly measured. This is a significant improvement over the conventional vibration monitoring, where the vibration signal picked up from the equipment/component housing needs to be propagated through the supporting structure. Furthermore, using the acceleration signal the monitoring system will be unaffected by the environmental disturbance.
- Time-domain analysis demonstrated that this signal (acceleration of the end-effector) can be successfully used to detect presence of fault in the system, and identify all three classes of fault.
- Given the non-stationary behavior of the system, STFT and EMD methods demonstrated that the acceleration signal can be also successfully used in frequency domain for fault detection (presence of fault). Accurate fault classification requires further investigation.

Chapter 7

Conclusions and Recommendations for Future Work

Condition monitoring is an effective tool to protect equipment against unplanned and costly downtime. Conventionally, the monitoring is only focused on the condition of the equipment. However, a number of recent studies pointed out that a complete monitoring approach for mobile equipment (e.g. shovels) should account for both equipment and environment variabilities. Environmental variability of the operating site, such as variable ground condition, can hinder the effectiveness of the condition monitoring efforts, or limit its applicability. Knowledge of the environmental condition, is not only an important factor monitoring the shovel, but it can also offer useful operational information about the payload that can be used to estimate dig capacity, production rate. The scope of the proposed system level monitoring was earlier presented in fig. 1.3 and further explained in fig. 3.2.

Accordingly, internal and external changes can affect the operating envelope, and therefore a formerly safe operating mode becomes unsafe. Change of operating mode might be feasible for some operation, while the others might remain unsafe under the new condition; and this must be detected.

Figure 7.1 demonstrates how the proposed system level monitoring can be implemented to improve the monitoring performance. The process starts by establishing a baseline for the normal condition of the equipment under non-interactive mode (free motion of the end-effector). Immediately after, and during the interactive mode, force measurements can be fed into the estimation scheme to establish the initial

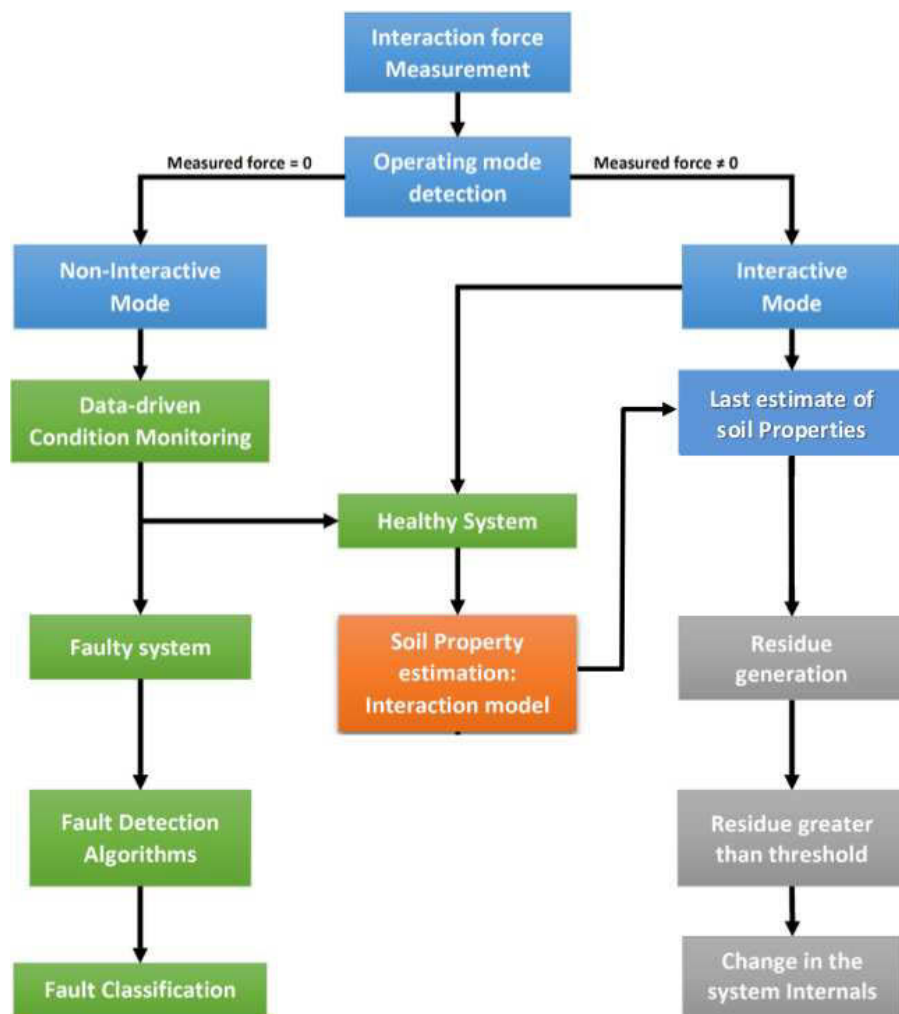


Figure 7.1: Implementation of the System Level Monitoring

soil properties. At this point system level monitoring is completely initiated. Using the updated interaction force, soil properties variation can be tracked and used to identify internal changes in the system. Data collected during the non-interactive mode of operation is also used to detect and classify the failure modes.

7.1 Conclusions

The system level monitoring studied in this work, required a combined approach to monitor the conditions of the environment (soil property estimation) and the equipment (fault detection) through model-based analysis and experimental data. A simplified shovel test rig was designed and fabricated to generate a time-varying motion with significant environmental interaction.

Simulating the cutting and pushing action of a shovel is required for the soil property estimation study. The test rig accounts for all parameters of a soil-tool interaction model, which allows control and adjustment of every parameter of the system, such as angle of attack, depth of penetration, width of the cutting plate, etc. The rig is capable of cutting and dozing through cohesive and noncohesive granular material for a short distance. It is equipped with the instrumentation required for measurement of the cutting force.

The time-varying behavior feature of the rig allowed the study of fault detection under non-stationary conditions. This was accounted by designing the rig based on an off-set crank-slider mechanism, driven by a gearbox system. The modular design of the rig allows seeding of a number of faulty components, replicating certain failure modes.

Significant modifications were made to adapt the design with the requirements for both soil property estimation and fault detection experiments.

Using the shovel test rig, this method was experimentally tested and used to estimated the mechanical property of 3 types of granular material: highly cohesionless

Glass Beads, low cohesion Play Sand, and highly cohesive Oil Sand. The results from estimation algorithm was compared to the directly measured data from standard testing, when available. The algorithm successfully estimated soil properties within 8 – 30%. The estimation accuracy is far greater than the precision required for the force prediction.

The present work proposed and investigated a novel method for monitoring the condition of the equipment through variation in the dynamic parameters of the system. This method, unlike the conventional approach that uses the emitted frame vibration for monitoring, directly uses the acceleration signal of the slider. Hence it is unaffected by the environmental variabilities, and independent of how the vibration propagates through the equipment. The crank-slider mechanism was used as a platform to generate the desired non-stationary signal. Data were collected under normal and faulty condition, and time and frequency domain analysis were applied for fault detection.

Time-domain analysis based on the statistical features of the acceleration signal, proved that the acceleration signal carries important information about the failure modes. Extracted features, were successfully classified using dimension reduction and a linear classifier. The combined technique allowed to identify all four operating condition based on a limited number of data points.

Failure modes not only increased the non-stationary condition of the signal, but in some cases they modulated the frequency of the acceleration signal and this was revealed using the Time-Frequency methods. STFT and HHT methods were used to extract signatures of the failure modes on the acceleration signal. The best results were obtained using the Hilbert-Huang transform, where the influence of each failure mode were observed in the instantaneous frequency of the decomposed acceleration signal. Using HHT, the unique signatures of the failure modes were identified in frequency domain and used toward development of a fault detection algorithm.

Conclusions of this research can be summarized as followings:

- Acceleration signal carries enough information for monitoring the structural integrity of the equipment
- Hilbert-Huang Transform is an effective tool for monitoring the condition of the non-stationary system of interest exposed to structural defects
- Ground-tool interaction force can be used for characterizing the condition of the environment
- System level monitoring studied in this work, presents an opportunity to expand the application of situational awareness

7.2 Recommendations for Future Work

Based on the experience gained from this research, it is highly recommended to further explore the idea of system level monitoring. Although, the wide scope of this research opened up many avenues to explore, but at the same time it limited the extent of our research. It is recommended to develop tools and methods for testing the learning of this research in an industrial setting/application. An examples of an immediate application, is using the soil-tool interaction force measurement - based on the hydraulic pressure of the actuators - for online soil-property estimation. Another example, is using the hoist cable linear displacement/acceleration in cable shovels for monitoring the internal changes in the system.

For soil property estimation study, the Mohr-Coulomb interaction model was used which has some known restrictions (e.g. low predictions at angle of attacks greater than 80°). It is highly recommended to use a soil-tool interaction with higher fidelity. Using a higher fidelity model, requires the use of improved nonlinear solvers, that can handle more parameters. It is a worthwhile effort to use solving methods other than the modified Newton-Raphson method, that are computationally less

expensive and can handle more than two parameters at a time. It is worthwhile to explore methods that can overcome the singularity of the jacobian matrix.

Most of the data used in the fault detection section of this thesis are collected from 20 trials. There were many uncontrolled parameters in the test apparatus due to the evolving procedure of the design, that hampered the quality of data collection. For future work, it is recommended to use high precision manufacturing process or use standard test set ups, which would facilitate larger data collection.

Although the test rig generated the non-stationary condition required for the fault detection study, it is recommended to conduct the test under greater speed and load variability. This would have a more pronounced impact on the stationarity of the signal. Additionally, it is recommended to investigate the monitoring approach, using external loading (i.e. during the interactive phase).

One goal of this thesis has been to evaluate the possibility of condition monitoring and fault detection through system dynamics parameters. This was carried out using the acceleration signal. Acceleration signal was mainly used because the influence of the failure modes on the signal was previously documented. There is opportunity to explore other parameters, e.g. angular velocity and kinetic energy, that may carry the fault signatures as well.

While the fault detection techniques proved that fault signatures are carried over in certain dynamic parameters of the system, it is recommended to use a larger variety of time and frequency method, and evaluate the detection and classification performance on a larger data. It is recommended to use improved decomposition methods such as Ensemble Empirical Mode Decomposition (EEMD), and Winning-EEMD. It is also recommended to use additional features for fault detection. This includes statistical analysis of the time-frequency domain data, and Fusion of the features from both time and time-frequency domain.

References

- Herve Abdi and Lynne J. Williams. Principal component analysis. *Wiley Interdisciplinary Reviews: Computational Statistics*, 2(4):433–459, 2010. ISSN 1939-0068. doi: 10.1002/wics.101. URL <http://dx.doi.org/10.1002/wics.101>.
- J. G. Agar, N. R. Morgenstern, and J. D. Scott. Shear strength and stress-strain behaviour of athabasca oil sand at elevated temperatures and pressures. *Canadian Geotechnical Journal*, 24(1):1–10, 1987.
- T. V. Alekseeva, K.A. Artemev, and A.A. Bromberg. *Machines for earthmoving work: theory and calculations*. Amerind Pub. Co., 1985.
- W.E. Allen and J.N. Sundermeyer. A structural health monitoring system for earthmoving machines. *Electro Information Technology, 2005 IEEE International Conference on*, pages 5 pp.–5, May 2005. doi: 10.1109/EIT.2005.1627011.
- K. Althoefer, C. P. Tan, Y. H. Zweiri, and L. D. Seneviratne. Hybrid soil parameter measurement and estimation scheme for excavation automation. *Instrumentation and Measurement, IEEE Transactions on*, 58(10):3633 –3641, oct. 2009. ISSN 0018-9456.
- M. Amarnath and I.R. Praveen Krishna. Local fault detection in helical gears via vibration and acoustic signals using emd based statistical parameter analysis. *Measurement*, 58(0):154 – 164, 2014. ISSN 0263-2241. doi: <http://dx.doi.org/10.1016/j.measurement.2014.03.011>.

doi.org/10.1016/j.measurement.2014.08.015. URL <http://www.sciencedirect.com/science/article/pii/S0263224114003303>.

A. Anandaraajah. *Computational Methods in Elasticity and Plasticity: Solids and Porous Media*. Springer, 2010.

J.K. Anochie-Botaeng. *Advanced Testing and Characterization of Transportation Soils and Bituminous Sands*. PhD thesis, University of Illinois, 2007.

Vigen Arakelian and Sebastien Briot. Balancing of linkages and robot manipulators. In *Advanced Methods with Illustrative Examples*, volume 27 of *Mechanisms and Machine Science*. Springer International Publishing, 2015. doi: 10.1007/978-3-319-12490-2.

Hirokazu Araya and Masayuki Kagoshima. Semi-automatic control system for hydraulic shovel. *Automation in Construction*, 10(4):477 – 486, 2001. ISSN 0926-5805.

Zvi Asaf. *Determination of Discrete Element Model Parameters Required for Simulation of Soil-Implement Interaction*. PhD thesis, Technion - Israel Institute of Technology, 2006.

K. Awuah-Offei and S. Frimpong. Numerical simulation of cable shovel resistive forces in oil sands excavation. *International Journal of Mining, Reclamation and Environment*, 20(3):223–238, 2006.

Kwame Awuah-Offei. *Dynamic modeling of cable shovel-formation interactions for efficient oil sands excavation*. PhD thesis, University of Missouri-Rolla, 2005.

T. Ramesh Babu, S. Srikanth, and A.S. Sekhar. Hilbert-huang transform for detection and monitoring of crack in a transient rotor. *Mechanical Systems and Signal Processing*, 22(4):905 – 914, 2008. ISSN 0888-3270. doi: <http://dx.doi.org/10.1016/>

j.ymssp.2007.10.010. URL <http://www.sciencedirect.com/science/article/pii/S0888327007002245>. Special Issue: Crack Effects in Rotordynamics.

Nicolo Bachschmid, Paolo Pennacchi, and Ezio Tanzi. Cracks in rotating shafts. In *Cracked Rotors*, pages 1–15. Springer Berlin Heidelberg, 2010. ISBN 978-3-642-01484-0. doi: 10.1007/978-3-642-01485-7_1. URL http://dx.doi.org/10.1007/978-3-642-01485-7_1.

G. Baiden, R. Strom, and C. Preston. Mining automation program. In *98th Annual General Meeting, Canadian Institute of Mining and Metallurgy, Edmonton.*, 1996.

W. Bartelmus and R. Zimroz. A new feature for monitoring the condition of gearboxes in non-stationary operating conditions. *Mechanical Systems and Signal Processing*, 23(5):1528 – 1534, 2009a. ISSN 0888-3270. doi: <http://dx.doi.org/10.1016/j.ymssp.2009.01.014>. URL <http://www.sciencedirect.com/science/article/pii/S0888327009000132>.

W. Bartelmus and R. Zimroz. Vibration condition monitoring of planetary gearbox under varying external load. *Mechanical Systems and Signal Processing*, 23(1):246 – 257, 2009b. ISSN 0888-3270. doi: <http://dx.doi.org/10.1016/j.ymssp.2008.03.016>. URL <http://www.sciencedirect.com/science/article/pii/S0888327008000824>. Special Issue: Non-linear Structural Dynamics.

W. Bartelmus, R. Boustany, R. Zimroz, J. Antoni, and F. Chaari. *Vibration diagnostic method for planetary gearboxes under varying external load with regard to cyclostationary analysis*. Wroclaw University Of Technology Publishing, 2009.

Walter Bartelmus. Object and operation factor oriented diagnostics. In Tahar Fakhfakh, Walter Bartelmus, Fakher Chaari, Radoslaw Zimroz, and Mohamed Haddar, editors, *Condition Monitoring of Machinery in Non-Stationary Operations*, pages 13–23. Springer Berlin Heidelberg, 2012. ISBN 978-3-642-28767-

1. doi: 10.1007/978-3-642-28768-8_2. URL http://dx.doi.org/10.1007/978-3-642-28768-8_2.

Walter Bartelmus and Radoslaw Zimroz. Gearbox condition monitoring procedures. In Giorgio Dalpiaz, Riccardo Rubini, Gianluca D'Elia, Marco Cocconcelli, Fakher Chaari, Radoslaw Zimroz, Walter Bartelmus, and Mohamed Haddar, editors, *Advances in Condition Monitoring of Machinery in Non-Stationary Operations*, Lecture Notes in Mechanical Engineering, pages 249–260. Springer Berlin Heidelberg, 2014. ISBN 978-3-642-39347-1. doi: 10.1007/978-3-642-39348-8_21. URL http://dx.doi.org/10.1007/978-3-642-39348-8_21.

Walter Bartelmus, Fakher Chaari, Radoslaw Zimroz, and Mohamed Haddar. Modelling of gearbox dynamics under time-varying nonstationary load for distributed fault detection and diagnosis. *European Journal of Mechanics - A/Solids*, 29(4): 637 – 646, 2010. ISSN 0997-7538. doi: <http://dx.doi.org/10.1016/j.euromechsol.2010.03.002>. URL <http://www.sciencedirect.com/science/article/pii/S0997753810000422>.

E. Bautista. *Theory of Machines and Mechanisms I*. Nirali, 2009.

Leonhard E. Bernold. Motion and path control for robotic excavation. *Journal of Aerospace Engineering*, 6(1):1–18, 1993.

G.F. Bin, J.J. Gao, X.J. Li, and B.S. Dhillon. Early fault diagnosis of rotating machinery based on wavelet packets - empirical mode decomposition feature extraction and neural network. *Mechanical Systems and Signal Processing*, 27(0): 696 – 711, 2012. ISSN 0888-3270.

Yuri I. Bobrovnikskii. *Handbook of Noise and Vibration Control*, chapter Vibration of Simple Discrete and Continuous Systems, pages 180–204. John Wiley & Sons, Inc., 2007.

David Bock. Large eddy simulation shows limits of downstream wind turbines, 2014. URL <http://www.isgtw.org/visualization/large-eddy-simulation-shows-limits-downstream-wind-turbines>.

Adrian Bonchis, Nick Hillier, Julian Ryde, Elliot Duff, and Cedric Pradalier. Experiments in autonomous earth moving. In *Proceedings of the 18th IFAC World Congress, 2011*, pages 1158–11593, September 2011.

David A. Bradley and Derek W. Seward. The development, control and operation of an autonomous robotic excavator. *Journal of Intelligent and Robotic Systems*, 21:73–97, 1998. ISSN 0921-0296. URL <http://dx.doi.org/10.1023/A:1007932011161>. 10.1023/A:1007932011161.

W. Brookere. Tarsand mechanics and slope evaluation. In *Proceedings of the Tenth Canadian Rock Mechanics Symposium*, volume 1, pages 409–446. Queen’s University, Kingston, Ont., 1975.

D. N. Brown and J. C. Jorgensen. Machine-condition monitoring using vibration analysis. a case study from an iron-ore mine. *Briiel & Kjeer Application Notes*, 1988.

J. H. Burrows. Predictive and preventive maintenance of mobile mining equipment using vibration data. Master’s thesis, McGill University, 1996.

H. Cannon. Extended earthmoving with an autonomous excavator. Master’s thesis, Carnegie Mellon Robotics Institute, 1999.

Howard Cannon and Sanjiv Singh. Models for automated earthmoving. *The Sixth International Symposium on Experimental Robotics VI*, pages 163–172, 2000.

J. Chen and M. Jegen-Kulcsar. The empirical mode decomposition (emd) method in mt data processing. In *Proceedings of the 22nd Colloquium ElectroMagnetic Depth Research*, pages 67–76, 2007.

T.G. Chondros, A.D. Dimarogonas, and J. Yao. Vibration of a beam with a breathing crack. *Journal of Sound and Vibration*, 239(1):57 – 67, 2001. ISSN 0022-460X. doi: <http://dx.doi.org/10.1006/jsvi.2000.3156>. URL <http://www.sciencedirect.com/science/article/pii/S0022460X00931560>.

Olivier Contant, Stephane Lafourche, and Demosthenis Teneketzis. Diagnosis of intermittent faults. *Discrete Event Dynamic Systems*, 14:171–202, 2004. ISSN 0924-6703. URL <http://dx.doi.org/10.1023/B:DISC.0000018570.20941.d2>. 10.1023/B:DISC.0000018570.20941.d2.

R.F. Craig. *Soil Mechanics*. Chapman and Hall, 4th edition, 1990.

I.M. Smith D. Vaughan Griffiths. *Numerical Methods for Engineers*. Chapman and Hall/CRC, 2 edition, 2006.

Zbigniew Dabrowski and Henryk Madej. Diagnostics of internal combustion engine mechanical faults masked by adaptive control systems. In Joseph Mathew, Lin Ma, Andy Tan, Margot Weijnen, and Jay Lee, editors, *Engineering Asset Management and Infrastructure Sustainability*, pages 143–154. Springer London, 2012. ISBN 978-0-85729-301-5. doi: 10.1007/978-0-85729-493-7_13. URL http://dx.doi.org/10.1007/978-0-85729-493-7_13.

Zeng Dechao and Yao Yusu. A dynamic model for soil cutting by blade and tine. *Journal of Terramechanics*, 29(3):317 – 327, 1992. ISSN 0022-4898.

Balbir S. Dhillon. *Mining Equipment Reliability, Maintainability, & Safety*. Springer Series in Reliability Engineering. Springer London, 2008.

B.S. Dhillon. *Engineering Maintenance: A Modern Approach*. CRC Press, 2002.

Simon Peter DiMaio. Position and force trajectory programming within a virtual excavation environment. Master's thesis, The University of British Columbia, 1998.

Stijn Donders. Fault detection and identification for wind turbine systems. Master's thesis, University of Twente, 2002.

E. Douka and L. J. Hadjileontiadis. Time-frequency analysis of the free vibration response of a beam with a breathing crack. *{NDT} & E International*, 38(1):3 – 10, 2005. ISSN 0963-8695. doi: <http://dx.doi.org/10.1016/j.ndteint.2004.05.004>. URL <http://www.sciencedirect.com/science/article/pii/S0963869504000623>.

S. Dubowsky, M. Norris, E. Aloni, and A. Tamir. An analytical and experimental study of the prediction of impacts in planar mechanical systems with clearances. *Journal of Mechanical Design*, 106(4):444–451, 1984.

Jacek Dybala and Adam Galezia. A novel method of gearbox health vibration monitoring using empirical mode decomposition. In Giorgio Dalpiaz, Riccardo Rubini, Gianluca D'Elia, Marco Cocconcelli, Fakher Chaari, Radoslaw Zimroz, Walter Bartelmus, and Mohamed Haddar, editors, *Advances in Condition Monitoring of Machinery in Non-Stationary Operations*, Lecture Notes in Mechanical Engineering, pages 225–234. Springer Berlin Heidelberg, 2014. ISBN 978-3-642-39347-1. doi: 10.1007/978-3-642-39348-8_19. URL http://dx.doi.org/10.1007/978-3-642-39348-8_19.

David J. Edwards, Gary D. Holt, and Frank C. Harris. Predicting downtime costs of tracked hydraulic excavators operating in the uk opencast mining industry. *Construction Management and Economics*, 20(7):581–591, 2002.

Sermin Elevli, Nevin Uzgoren, and Birol Elevli. Correspondence analysis of repair data: a case study for electric cable shovels. *Journal of Applied Statistics*, 35(8): 901–908, 2008. doi: 10.1080/02664760802125627. URL <http://dx.doi.org/10.1080/02664760802125627>.

Selcuk Erkaya and Ibrahim Uzmay. Experimental investigation of joint clearance effects on the dynamics of a slider-crank mechanism. *Multibody System Dynamics*,

24(1):81–102, 2010. ISSN 1384-5640. doi: 10.1007/s11044-010-9192-0. URL <http://dx.doi.org/10.1007/s11044-010-9192-0>.

Zhipeng Feng, Ming Liang, and Fulei Chu. Recent advances in time-frequency analysis methods for machinery fault diagnosis: A review with application examples. *Mechanical Systems and Signal Processing*, 38(1): 165 – 205, 2013. ISSN 0888-3270. doi: <http://dx.doi.org/10.1016/j.ymssp.2013.01.017>. URL <http://www.sciencedirect.com/science/article/pii/S088832701300071X>. jce:title; Condition monitoring of machines in non-stationary operations.jce:title.

F. Geu Flores. Workspace analysis and maximal force calculation of a face-shovel excavator using kinematical transformers. In *International Federation for the Promotion of Mechanism and Machine Science (IFTToMM) World Congress*, 2007.

P. Flores, C.S. Koshy, H.M. Lankarani, J. Ambrosio, and J.C.P. Claro. Numerical and experimental investigation on multibody systems with revolute clearance joints. *Nonlinear Dynamics*, 65(4):383–398, 2011. ISSN 0924-090X. doi: 10.1007/s11071-010-9899-8. URL <http://dx.doi.org/10.1007/s11071-010-9899-8>.

Jacob Fraden. *Handbook of Modern Sensors: Physics, Designs, and Applications*. Springer-Verlag New York, 4 edition, 2010.

Y. Franco, D. Rubinstein, and I. Shmulevich. Prediction of soil-bulldozer blade interaction using discrete element method. *Transactions of the American Society of Agricultural and Biological Engineers (ASABE)*, 50(2):345–353, 2007.

Yaron Franco. Spatial model for performance prediction of bulldozer blade interaction with soil. Master’s thesis, Technion - Israel Institute of Technology, 2005.

S. Frimpong and Y. Hu. Parametric simulation of shovel-oil sands interactions during excavation. *International Journal of Mining, Reclamation and Environment*, 18 (3):205–219, 2004.

S. Frimpong, Y. Li, and K. Awuah-Offei. Cable shovel health and longevity and operator efficiency in oilsand excavation. *International Journal of Mining and Mineral Engineering*, 1:47–61, 2008a.

Samuel Frimpong and Ying Li. Stress loading of the cable shovel boom under in-situ digging conditions. *Engineering Failure Analysis*, 14(4):702 – 715, 2007. ISSN 1350-6307.

Samuel Frimpong, Yafei Hu, and Kwame Awuah-Offei. Mechanics of cable shovel-formation interactions in surface mining excavations. *Journal of Terramechanics*, 42(1):15 – 33, 2005. ISSN 0022-4898. doi: DOI:10.1016/j.jterra.2004.06.002.

Samuel Frimpong, Yafei Hu, and Hilary Inyang. Dynamic modeling of hydraulic shovel excavators for geomaterials. *International Journal of Geomechanics*, 8(1): 20 – 29, 2008b. ISSN 15323641.

Rong-Fong Fung. Dynamic responses of the flexible connecting rod of a slider-crank mechanism with time-dependent boundary effect. *Computers & Structures*, 63(1):79 – 90, 1997. ISSN 0045-7949. doi: [http://dx.doi.org/10.1016/S0045-7949\(96\)00333-1](http://dx.doi.org/10.1016/S0045-7949(96)00333-1). URL <http://www.sciencedirect.com/science/article/pii/S0045794996003331>.

Peng Gao, Shaoze Yan, Liyang Xie, and Jianing Wu. Dynamic reliability analysis of mechanical components based on equivalent strength degradation paths. *Journal of Mechanical Engineering*, 59:387–399, 2013.

George Georgoulas, Theodore Loutas, Chrysostomos D. Stylios, and Vassilis Kostopoulos. Bearing fault detection based on hybrid ensemble detector and empirical mode decomposition. *Mechanical Systems and Signal Processing*, 41(1-2):510 – 525, 2013. ISSN 0888-3270. doi: <http://dx.doi.org/10.1016/j.ymssp.2013.02.020>. URL <http://www.sciencedirect.com/science/article/pii/S088832701300099X>.

Vish Gilat, Amos & Subramaniam. *Numerical Methods for Engineers and Scientists: An Introduction with Applications Using MATLAB*. John Wiley & Sons, Inc., 2 edition, 2010.

William R. Gill and Glen E. Vanden Berg. *Soil Dynamics in Tillage and Traction : Agriculture Handbook No. 316*. U.S. Department of Agriculture, 1967.

Parekh Girdhar. *Practical Machinery Vibration Analysis and Predictive Maintenance*. Newnes, 2004.

R.J. Godwin and M.J. O'Dogherty. Integrated soil tillage force prediction models. *Journal of Terramechanics*, 44(1):3–14, 2007. ISSN 0022-4898.

R.J. Godwin and G. Spoor. Soil failure with narrow tines. *Journal of Agricultural Engineering Research*, 22(3):213 – 228, 1977. ISSN 0021-8634.

Alexander Gummer and Bernd Sauer. Modeling planar slider-crank mechanisms with clearance joints in recurdyn. *Multibody System Dynamics*, 31(2):127–145, 2014. ISSN 1384-5640. doi: 10.1007/s11044-012-9339-2. URL <http://dx.doi.org/10.1007/s11044-012-9339-2>.

Jih-Lian Ha, Rong-Fong Fung, Kun-Yung Chen, and Shao-Chien Hsien. Dynamic modeling and identification of a slider-crank mechanism. *Journal of Sound and Vibration*, 289(4-5):1019 – 1044, 2006. ISSN 0022-460X. doi: <http://dx.doi.org/10.1016/j.jsv.2005.03.011>. URL <http://www.sciencedirect.com/science/article/pii/S0022460X0500218X>.

Q. P. Ha and D. C. Rye. A control architecture for robotic excavation in construction. *Computer-Aided Civil and Infrastructure Engineering*, 19(1):28–41, 2004. ISSN 1467-8667.

R.S Haines. An experimental investigation into the dynamic behaviour of revolute joints with varying degrees of clearance. *Mechanism and Machine Theory*,

ory, 20(3):221 – 231, 1985. ISSN 0094-114X. doi: [http://dx.doi.org/10.1016/0094-114X\(85\)90009-6](http://dx.doi.org/10.1016/0094-114X(85)90009-6). URL <http://www.sciencedirect.com/science/article/pii/0094114X85900096>.

Andrew Hall. Characterizing the operation of a large hydraulic excavator. Master's thesis, The University of Queensland, 2002.

Robert A. Hall and Laeeque K. Daneshmend. Reliability modelling of surface mining equipment: Data gathering and analysis methodologies. *International Journal of Mining, Reclamation and Environment*, 17(3):139–155, 2003. ISSN 1748-0930.

William R. Haycraft. *Yellow Steel: The Story of the Earthmoving Equipment Industry*. University of Illinois Press, 2002.

A Hemami. Robotics and automation in mining: Making things easier in a hostile environment. *IEEE Canadian Review*, pages 11–15, Fall 1993.

A. Hemami. Fundamental analysis of automatic excavation. *Journal of Aerospace Engineering*, 8(4):175–179, 1995.

A. Hemami, S. Goulet, and M. Aubertin. Resistance of particulate media to excavation: Application to bucket loading. *International Journal of Surface Mining, Reclamation and Environment*, 8(3):125–129, 1994. doi: 10.1080/09208119408964772.

Ahmad Hemami. Modelling, analysis and preliminary studies for automatic scooping/loading in a mechanical loader. *International Journal of Surface Mining, Reclamation and Environment*, 6(4):151–159, 1992.

Ahmad Hemami and Ferri Hassani. Simulation of the resistance forces bulk media to bucket in a loading process. In *24th Int. Symp. on Automation and Robotics in Construction (ISARC)*, 2007.

YongHwa Heo and Kwangjoon Kim. Definitions of non-stationary vibration power for time-frequency analysis and computational algorithms based upon harmonic wavelet transform. *Journal of Sound and Vibration*, 336(0):275 – 292, 2015. ISSN 0022-460X. doi: <http://dx.doi.org/10.1016/j.jsv.2014.10.025>. URL <http://www.sciencedirect.com/science/article/pii/S0022460X14008402>.

D.R.P. Hettiaratchi, B.D. Witney, and A.R. Reece. The calculation of passive pressure in two-dimensional soil failure. *Journal of Agricultural Engineering Research*, 11(2):89 – 107, 1966. ISSN 0021-8634. doi: 10.1016/S0021-8634(66)80045-8.

M. Ho and M. Hodkiewicz. Factors that influence failure behaviour and remaining useful life of mining equipment components. *Advances in Mechanical Engineering*, page 9, 2013.

Won Hong. *Modeling, estimation, and control of robot-soil interactions*. PhD thesis, Massachusetts Institute of Technology. Dept. of Mechanical Engineering, 2001.

N. E. Huang, Z. Shen, S. R. Long, M. C. Wu, H. H. Shih, Q. Zheng, N.-C. Yen, C. C. Tung, and H. H. Liu. The empirical mode decomposition and the hilbert spectrum for nonlinear and non-stationary time series analysis. *Royal Society of London Proceedings Series A*, 454(1971):903–995, 1998.

Norden Huang. *The Hilbert-Huang Transform in Engineering*, chapter Introduction to Hilbert-Huang Transform and Some Recent Developments, pages 1–24. CRC Press, 2005.

T. Huntsberger, A. Stroupe, and B. Kennedy. System of systems for space construction. In *Systems, Man and Cybernetics, 2005 IEEE International Conference on*, volume 4, pages 3173–3178 Vol. 4, Oct 2005. doi: 10.1109/ICSMC.2005.1571634.

Yukio Ishida. Cracked rotors: Industrial machine case histories and nonlinear

effects shown by simple jeffcott rotor. *Mechanical Systems and Signal Processing*, 22(4):805 – 817, 2008. ISSN 0888-3270. doi: <http://dx.doi.org/10.1016/j.ymssp.2007.11.005>. URL <http://www.sciencedirect.com/science/article/pii/S0888327007002282>. Special Issue: Crack Effects in Rotordynamics.

Andrew K.S. Jardine, Daming Lin, and Dragan Banjevic. A review on machinery diagnostics and prognostics implementing condition-based maintenance. *Mechanical Systems and Signal Processing*, 20(7):1483 – 1510, 2006. ISSN 0888-3270.

Brian Murphy John M. Vance, Fouad Y. Zeidan. *Machinery Vibration and Rotodynamics*. John Wiley, 2010.

I.T. Jolliffe. *Principal Component Analysis*. Springer Series in Statistics. Springer-Verlag New York, 2 edition, 2002.

T. G. Joseph. Large mobile mining equipment operating on soft ground. In *IMCET*, 2003.

S. Karmakar, S.R. Ashrafizadeh, and R.L. Kushwaha. Experimental validation of computational fluid dynamics modeling for narrow tillage tool draft. *Journal of Terramechanics*, 46(6):277 – 283, 2009. ISSN 0022-4898.

Subrata Karmakar and R. Lal Kushwaha. Dynamic modeling of soil-tool interaction: An overview from a fluid flow perspective. *Journal of Terramechanics*, 43(4):411 – 425, 2006. ISSN 0022-4898.

Masoud Khoshzaban-Zavarehi. *On-line Condition Monitoring and Fault Diagnosis in Hydraulic System Components using Parameter Estimation and Pattern Classification*. PhD thesis, The Univeristy of British Columbia, 1997.

A. J. Koivo. Kinematics of excavators (backhoes) for transferring surface material. *Journal of Aerospace Engineering*, 7(1):17–32, 1994.

A. J. Koivo, M. Thoma, E. Kocaoglan, and J. Andrade-Cetto. Modeling and control of excavator dynamics during digging operation. *Journal of Aerospace Engineering*, 9(1):10–18, 1996.

Ranganath Kothamasu, Samuel Huang, and William VerDuin. System health monitoring and prognostics - a review of current paradigms and practices. *The International Journal of Advanced Manufacturing Technology*, 28:1012–1024, 2006. ISSN 0268-3768.

Joseph Labuz and Arno Zang. Mohr-coulomb failure criterion. *Rock Mechanics and Rock Engineering*, 45:975–979, 2012. doi: 10.1007/s00603-012-0281-7.

M. Lebold, K. McClintic, R. Campbell, C. Byington, and K. Maynard. Review of vibration analysis methods for gearbox diagnostics and prognostics. In *Proceedings of the 54th Meeting of the Society for Machinery Failure Prevention Technology*, pages 623–634, May 2000.

Yaguo Lei, Jing Lin, Zhengjia He, and Ming J. Zuo. A review on empirical mode decomposition in fault diagnosis of rotating machinery. *Mechanical Systems and Signal Processing*, 35(1-2):108 – 126, 2013. ISSN 0888-3270. doi: <http://dx.doi.org/10.1016/j.ymssp.2012.09.015>. URL <http://www.sciencedirect.com/science/article/pii/S0888327012003731>.

P. Lever. Mining automation: The future and the excavation automation example. *Australian Conference on Robotics and Automation*, November 2001.

P. Lever. *SME Mining Engineering Handbook: Automation and Robotics in Mining*. Society for Mining, Metallurgy, and Exploration (SME), 3 edition, 2011.

Paul J. A. Lever and Fei-Yue Wang. Intelligent excavator control system for lunar mining system. *Journal of Aerospace Engineering*, 8(1):16–24, 1995.

Ruoyu Li. *Rotating Machine Fault Diagnostics Using Vibration and Acoustic Emission Sensors*. PhD thesis, University of Illinois at Chicago, 2012.

Yongbo Li, Minqiang Xu, Yu Wei, and Wenhua Huang. An improvement emd method based on the optimized rational hermite interpolation approach and its application to gear fault diagnosis. *Measurement*, 63(0):330 – 345, 2015. ISSN 0263-2241. doi: <http://dx.doi.org/10.1016/j.measurement.2014.12.021>. URL <http://www.sciencedirect.com/science/article/pii/S0263224114006198>.

Y. Liang, D. Hettiaratchi, and O'callaghan J. Mohr-coulomb parameters and soil indentation tests. *International conference on soil dynamics*, 2:307–321, 1985. Structural engineering.

M. G. Lipsett and R. Yousefi. *Modeling Excavator-Soil Interaction*, volume 0 of *Springer Series in Geomechanics and Geoengineering*, pages 347–366. Springer Berlin Heidelberg, 2011. ISBN 978-3-642-18284-6.

Xiaofeng Liu, Lin Bo, and Honglin Luo. Bearing faults diagnostics based on hybrid ls-svm and emd method. *Measurement*, 59(0):145 – 166, 2015. ISSN 0263-2241. doi: <http://dx.doi.org/10.1016/j.measurement.2014.09.037>. URL <http://www.sciencedirect.com/science/article/pii/S0263224114004175>.

Burt G . Look. *Handbook of Geotechnical Investigation and Design Tables*. Taylor & Francis, 2007.

Theodoros Loutas and Vassilis Kostopoulos. *Advances in Wavelet Theory and Their Applications in Engineering, Physics and Technology*, chapter Utilising the Wavelet Transform in Condition-Based Maintenance: A Review with its Applications, pages 273–312. InTech, 2012.

O. Luengo, S. Singh, and H. Cannon. Modeling and identification of soil-tool interaction in automated excavation. *Intelligent Robots and Systems*, 1998.

Proceedings., 1998 IEEE/RSJ International Conference on, 3:1900–1906 vol.3, Oct 1998. doi: 10.1109/IROS.1998.724873.

Guilherme Jorge Maeda. *Learning and Reacting with Inaccurate Prediction: Applications to Autonomous Excavation*. PhD thesis, The University of Sydney, 2013.

S. K. Majumdar. Study on reliability modelling of a hydraulic excavator system. *Quality and Reliability Engineering International*, 11(1):49–63, 1995.

J. Mak, Y. Chen, and M.A. Sadek. Determining parameters of a discrete element model for soil-tool interaction. *Soil and Tillage Research*, 118(0):117 – 122, 2012. ISSN 0167-1987. doi: <http://dx.doi.org/10.1016/j.still.2011.10.019>. URL <http://www.sciencedirect.com/science/article/pii/S0167198711001863>.

Fiorenzo Malaguti. Soil machine interaction in digging and earthmoving automation. In D.A. Chamberlain, editor, *Automation and Robotics in Construction XI*, pages 187–191. Elsevier Science B.V., 1994.

J. Marshal. Toward autonomous excavation of fragmented rock: Experiments, modeling, identification and control. Master’s thesis, Queen’s University, 2001.

J.A. Marshall, P.F. Murphy, and L.K. Daneshmend. Toward autonomous excavation of fragmented rock: Full-scale experiments. *Automation Science and Engineering, IEEE Transactions on*, 5(3):562 –566, july 2008. ISSN 1545-5955. doi: 10.1109/TASE.2007.912709.

P. Martin. A systematic approach to interactive failures. *Symposium on Mechanical Reliability*, 1980.

P. Martin and J. E. J. E. Strutt. Kinkead. A review of mechanical reliability modelling in relation to failure mechanisms. *Reliability Engineering*, 6:13–42, 1983.

Mathworks. About cad translation, 2015. URL <http://www.mathworks.com/help/physmod/smlink/ug/mechanical-export-and-translation.html>.

Jordan McBain. *Condition Monitoring of Machinery Subject to Variable States: Monitoring of Mobile Underground Mining Equipment*. PhD thesis, Laurentian University, 2012.

Jordan McBain and Markus Timusk. Fault detection in variable speed machinery: Statistical parameterization. *Journal of Sound and Vibration*, 327:623 – 646, 2009. ISSN 0022-460X.

P.D. McFadden. A technique for calculating the time domain averages of the vibration of the individual planet gears and the sun gear in an epicyclic gearbox. *Journal of Sound and Vibration*, 144(1):163 – 172, 1991. ISSN 0022-460X. doi: [http://dx.doi.org/10.1016/0022-460X\(91\)90739-7](http://dx.doi.org/10.1016/0022-460X(91)90739-7). URL <http://www.sciencedirect.com/science/article/pii/0022460X91907397>.

E. McKyes and O.S. Ali. The cutting of soil by narrow blades. *Journal of Terramechanics*, 14(2):43 – 58, 1977. ISSN 0022-4898.

Edward McKyes. *Soil cutting and tillage*. Elsevier, 1985.

J. Mecsi. Some problems of the loose soils at geotechnical damages. In *13th International Conference on Civil Engineering and Architecture, Hungarian technical Scientific Soceity of Transylvania*, pages 364–370, 2009.

C. J. Molina Vicuna. Sistema de mantenimiento predictivo avanzado para mquinas crticas de la minera (unpublished). Master's thesis, Universidad de Concepcin, 2006.

Dan Nowe. Online vibration monitoring on electric mining shovels. In *Maintenance World*, volume 2, 2013.

M. Obermayr, C. Vrettos, J. Kleinert, and P Eberhard. A discrete element method for assessing reaction forces in excavation tools. *Congreso de Metodos Numericos en Ingeniera*, 2013.

Martin Obermayr, Klaus Dressler, Christos Vrettos, and Peter Eberhard. Prediction of draft forces in cohesionless soil with the discrete element method. *Journal of Terramechanics*, 48(5):347 – 358, 2011. ISSN 0022-4898. doi: <http://dx.doi.org/10.1016/j.jterra.2011.08.003>. URL <http://www.sciencedirect.com/science/article/pii/S0022489811000589>.

Vrettos C. Obermayr M. Application of the discrete element method for the prediction of draft forces in soil. *Geotechnik*, 36(4):231–242, 2013.

R. Paes and M. Throckmorton. An overview of canadian oil sand mega projects. *Petroleum and Chemical Industry Conference Europe - Electrical and Instrumentation Applications, 2008. PCIC Europe 2008. 5th*, pages 1–9, June 2008. doi: 10.1109/PCICEUROPE.2008.4563541.

Bjorn A. T. Petersson. *Handbook of Noise and Vibration Control*, chapter General Introduction to Vibration, pages 171–179. John Wiley & Sons, Inc., 2007.

Nguyen Hong Quang. *Robust low level control of robotic excavation*. PhD thesis, The University of Sydney, March 2000. URL <http://db.acfr.usyd.edu.au/content.php/292.html?publicationid=166&displaypage=4>.

G. R. Rameshkumar, B. V. A. Rao, , and K. P. Ramachandran. Prediction of coast down time for mechanical faults in rotating machinery using artificial neural networks. *World Academy of Science, Engineering and Technology*, 5:38–44, 2011.

D. Ramirez. Anlisis del comportamiento vibratorio de mquinas rotatorias (unpublished masters thesis). Master's thesis, Universidad de Concepcin, 2003.

Daniel Ramirez. Caring for critical equipment: Monitoring electromechanical shovels in open-pit mining. *Instrumentation and Control*, 25(11):74–75, November 2009.

Daniel Ramirez. Monitoring electromechanical shovels for open-pit mining. Technical report, National Instrument (NI), 2010.

Robert B. Randall. *Noise and Vibration Data Analysis*, pages 549–564. John Wiley & Sons, Inc., 2008. ISBN 9780470209707. doi: 10.1002/9780470209707.ch46. URL <http://dx.doi.org/10.1002/9780470209707.ch46>.

Robert Bond Randall. *Vibration-based Condition Monitoring: Industrial, Aerospace and Automotive Applications*. John Wiley, March 2011. doi: 978-0-470-74785-8.

Muhammad Azeem Raza and Samuel Frimpong. Cable shovel stress & fatigue failure modeling - causes and solution strategies review. *Powder Metallurgy & Mining*, S1:003, 2013.

A. R. Reece. The fundamental equation of earth-moving mechanics. *Proceedings of the Institution of Mechanical Engineers*, 179:16–22, 1964.

Roberto Ricci and Paolo Pennacchi. Diagnostics of gear faults based on emd and automatic selection of intrinsic mode functions. *Mechanical Systems and Signal Processing*, 25(3):821 – 838, 2011. ISSN 0888-3270. doi: <http://dx.doi.org/10.1016/j.ymssp.2010.10.002>. URL <http://www.sciencedirect.com/science/article/pii/S0888327010003201>.

W. Richardson-Little and C.J. Damaren. Position accommodation and compliance control for robotic excavation. In *Control Applications, 2005. CCA 2005. Proceedings of 2005 IEEE Conference on*, pages 1194–1199, Aug 2005. doi: 10.1109/CCA.2005.1507293.

J. Rodriguez, L. Moran, J. Pontt, J. Espinoza, R. Diaz, and E. Silva. Operating experience of shovel drives for mining applications. *Industry Applications, IEEE*

Transactions on, 40(2):664–671, March 2004. ISSN 0093-9994. doi: 10.1109/TIA.2004.824508.

Arthur J. Rutherford. Challenges for the earthmoving industry. *Society of Automotive Engineers*, 1971.

P. Saavedra and E. A. Salamanca. Vibration analysis of mining shovels. *CIM Bulletin*, 95(1065):61–66, 2002.

P. N. Saavedra and J. A. Gonzalez. New revolution-order transform for analysing non-stationary vibrations. *Insight: Non-Destructive Testing & Condition Monitoring*, 47(1):29 – 35, 2005. ISSN 13542575.

P.N. Saavedra and L.A. Cuitino. Crack detection and vibration behavior of cracked beams. *Computers & Structures*, 79(16):1451 – 1459, 2001. ISSN 0045-7949. doi: [http://dx.doi.org/10.1016/S0045-7949\(01\)00049-9](http://dx.doi.org/10.1016/S0045-7949(01)00049-9). URL <http://www.sciencedirect.com/science/article/pii/S0045794901000499>.

P.N. Saavedra and C.J. Molina Vicuna. Online monitoring system for mining shovels focused on vibration analysis. *Canadian Institute of Mining, Metallurgy and Petroleum Magazine*, 2(3):1–9, 2007.

S.E. Salcudean, S. Tafazoli, P.D. Lawrence, and I. Chau. Impedance control of a teleoperated mini excavator. In *Advanced Robotics, 1997. ICAR '97. Proceedings., 8th International Conference on*, pages 19 –25, jul 1997. doi: 10.1109/ICAR.1997.620156.

Paul D. Samuel and Darryll J. Pines. A review of vibration-based techniques for helicopter transmission diagnostics. *Journal of Sound and Vibration*, 282 (1-2):475 – 508, 2005. ISSN 0022-460X. doi: <http://dx.doi.org/10.1016/j.jsv.2004.02.058>. URL <http://www.sciencedirect.com/science/article/pii/S0022460X04003244>.

E. T. Selig. Role of soil mechanics in the future of earthmoving machinery. *Society of Automotive Engineers*, 1966.

Derek Seward, David Bradley, and Robert Bracewell. The development of research models for automatic excavation. In *Proceedings of the 5th ISARC, Tokyo, Japan*, pages 703–708. International Association for Automation and Robotics in Construction (ISARC), 1988.

Hui Shao, Hiroshi Yamamoto, Yuki Sakaida, Takashi Yamaguchi, Yuji Yanagisawa, and Akira Nozue. Automatic excavation planning of hydraulic excavator. In Caihua Xiong, Honghai Liu, Yongan Huang, and Youlun Xiong, editors, *Intelligent Robotics and Applications*, volume 5315 of *Lecture Notes in Computer Science*, pages 1201–1211. Springer Berlin / Heidelberg, 2008. ISBN 978-3-540-88516-0. URL http://dx.doi.org/10.1007/978-3-540-88518-4_128.

R.C. Shekhar and J.M. Maciejowski. Surface excavation with model predictive control. In *Decision and Control (CDC), 2010 49th IEEE Conference on*, pages 5239–5244, 2010.

Jim S. Shiau, Charles E. Augarde, Andrei V. Lyamin, and Scott W. Sloan. Finite element limit analysis of passive earth resistance in cohesionless soils. *Soils and Foundations*, 48(6):843–850, 2008.

Yan-Shin Shih and Chen-Yuan Chung. Vibration analysis of the flexible connecting rod with the breathing crack in a slider-crank mechanism. *Journal of Vibration and Acoustics*, 135(6):061009, 2013. doi: 10.1115/1.4024053.

I. Shmulevich. State of the art modeling of soil-tillage interaction using discrete element method. *Soil and Tillage Research*, 111(1):41 – 53, 2010. ISSN 0167-1987.

I. Shmulevich, Z. Asaf, and D. Rubinstein. Interaction between soil and a wide cutting blade using the discrete element method. *Soil and Tillage Research*, 97 (1):37 – 50, 2007. ISSN 0167-1987.

S. Singh. An operation space approach to robotic excavation. In *Intelligent Control, 1991., Proceedings of the 1991 IEEE International Symposium on*, pages 481–486, 1991. doi: 10.1109/ISIC.1991.187404.

S. Singh. Learning to predict resistive forces during robotic excavation. *Robotics and Automation, 1995. Proceedings., 1995 IEEE International Conference on*, 2: 2102–2107 vol.2, May 1995. ISSN 1050-4729. doi: 10.1109/ROBOT.1995.526025.

S. Singh and H. Cannon. Multi-resolution planning for earthmoving. In *Robotics and Automation, 1998. Proceedings. 1998 IEEE International Conference on*, volume 1, pages 121–126, May 1998. doi: 10.1109/ROBOT.1998.676332.

Sanjiv Singh. The state of the art in automation of earthmoving. *Journal of Aerospace Engineering*, 10(4):179–188, 1997. doi: 10.1061/(ASCE)0893-1321(1997)10:4(179). URL <http://link.aip.org/link/?QAS/10/179/1>.

Sanjiv Singh. State of the art in automation of earthmoving, 2002. *Workshop on Advanced Geomechatronics, Sendai University, Japan*, 2002.

K. Soong and B. S. Thompson. A theoretical and experimental investigation of the dynamic response of a slider-crank mechanism with radial clearance in the gudgeon-pin joint. *Journal of Mechanical Design*, 2(2):183–189, 1990.

Jr. Sottile, J. and L.E. Holloway. An overview of fault monitoring and diagnosis in mining equipment. *Industry Applications, IEEE Transactions on*, 30(5):1326 –1332, sep/oct 1994. ISSN 0093-9994.

Mark W. Spong, Seth Hutchinson, and M. Vidyasagar. *Robot Modeling and Control*. John Wiley & Sons, 1st edition, 2005.

J.V. Stafford and D.W. Tanner. Effect of rate on soil shear strength and soil-metal friction i. shear strength. *Soil and Tillage Research*, 3(3):245 – 260, 1983a.

ISSN 0167-1987. doi: [http://dx.doi.org/10.1016/0167-1987\(83\)90026-0](http://dx.doi.org/10.1016/0167-1987(83)90026-0). URL <http://www.sciencedirect.com/science/article/pii/0167198783900260>.

J.V. Stafford and D.W. Tanner. Effect of rate on soil shear strength and soil-metal friction ii. soil-metal friction. *Soil and Tillage Research*, 3(4):321 – 330, 1983b. ISSN 0167-1987. doi: [http://dx.doi.org/10.1016/0167-1987\(83\)90034-X](http://dx.doi.org/10.1016/0167-1987(83)90034-X). URL <http://www.sciencedirect.com/science/article/pii/016719878390034X>.

Richard J.A.M. Stevens, Dennice F. Gayme, and Charles Meneveau. Effects of turbine spacing on the power output of extended wind-farms. *Wind Energy*, pages n/a–n/a, 2015. ISSN 1099-1824. doi: 10.1002/we.1835. URL <http://dx.doi.org/10.1002/we.1835>.

C.M. Stoiser and S. Audebert. A comprehensive theoretical, numerical and experimental approach for crack detection in power plant rotating machinery. *Mechanical Systems and Signal Processing*, 22(4):818 – 844, 2008. ISSN 0888-3270. doi: <http://dx.doi.org/10.1016/j.ymssp.2007.11.013>. URL <http://www.sciencedirect.com/science/article/pii/S0888327007002294>. Special Issue: Crack Effects in Rotordynamics.

Jian Sun and Guiyun Xu. Deviation analysis and optimization of offset slider-crank mechanism based on the simulation. *Information Technology Journal*, 12: 2390–2397, 2013. doi: 10.3923/itj.2013.2390.2397.

W.C. Swick and J.V. Perumpral. A model for predicting soil-tool interaction. *Journal of Terramechanics*, 25(1):43 – 56, 1988. ISSN 0022-4898.

S. Tafazoli, S.E. Salcudean, K. Hashtrudi-Zaad, and P.D. Lawrence. Impedance control of a teleoperated excavator. *Control Systems Technology, IEEE Transactions on*, 10(3):355–367, 2002. ISSN 1063-6536.

C. Tan, Y.H. Zweiri, K. Althoefer, and L.D. Seneviratne. On-line soil property estimation for autonomous excavator vehicles. *Robotics and Automation, 2003*.

Proceedings. ICRA '03. IEEE International Conference on, 1:121–126 vol.1, Sept. 2003. ISSN 1050-4729.

Choo Par Tan, Y.H. Zweiri, K. Althoefer, and L.D. Seneviratne. Online soil parameter estimation scheme based on newton-raphson method for autonomous excavation. *Mechatronics, IEEE/ASME Transactions on*, 10(2):221–229, April 2005a. ISSN 1083-4435.

ChooPar Tan, Y.H. Zweiri, K. Althoefer, and L.D. Seneviratne. Online soil-bucket interaction identification for autonomous excavation. *Robotics and Automation, 2005. ICRA 2005. Proceedings of the 2005 IEEE International Conference on*, pages 3576–3581, April 2005b.

C.B. Tatum, Michael Vorster, and Mac Klingler. Innovations in earthmoving equipment: New forms and their evolution. *Journal of Construction Engineering and Management*, 132(9):987 – 997, 2006a. ISSN 07339364.

C.B. Tatum, Michael Vorster, Mac G. Klingler, and Boyd C. Paulson Jr. Systems analysis of technical advancement in earthmoving equipment. *Journal of Construction Engineering and Management*, 132(9):976 – 986, 2006b. ISSN 07339364.

Karl Terzaghi. *Theoretical Soil Mechanics*. John Wiley and Sons, 3rd edition, 1943.

Karl Terzaghi, Ralph Peck, and Gholamreza Mesri. *Soil Mechanics in Engineering Practice*. John Wiley and Sons, 3rd edition, 1995.

M. Timusk, M. Lipsett, J. McBain, and C. Mechefske. Automated operating mode classification for online monitoring systems. *Journal of Vibration and Acoustics*, 131:041003–1:10, 2009a.

M Timusk, M Lipsett, J McBain, and CK Mechefske. Automated duty cycle

classification for online monitoring systems. *ASME Journal of Vibrations and Acoustics*, 131(4):041003/1–041003/10, 2009b.

Markus Timusk, Mike Lipsett, and Chris K. Mechefske. Fault detection using transient machine signals. *Mechanical Systems and Signal Processing*, 22(7):1724 – 1749, 2008. ISSN 0888-3270.

Paul D. Tomlingson. *Equipment Management: Key to Equipment Reliability and Productivity in Mining*. Society for Mining, Metallurgy, and Exploration (SME), 2 edition, 2009.

Mate Toth and Surendra Ganeriwala. A comprehensive study of shaft/coupling misalignment signature using vibration analysis. In *MFPT*, 2014.

P. K. Vaha and M. J. Skibniewski. Dynamic model of excavator. *Journal of Aerospace Engineering*, 6(2):148–158, 1993.

P. K. Vaha, A. J. Koivo, and M. J. Skibniewski. Excavator dynamics and effect of soil on digging. In *Proceedings of the 8th ISARC, Stuttgart, Germany*, pages 297–306. International Association for Automation and Robotics in Construction (ISARC), 1991.

S.M. Vahed, H.A. Delaimi, K. Althoefer, and L.D. Seneviratne. On-line energy-based method for soil estimation and classification in autonomous excavation. *Intelligent Robots and Systems, 2007. IROS 2007. IEEE/RSJ International Conference on*, pages 554–559, 29 2007-Nov. 2 2007.

S.M. Vahed, Kaspar Althoefer, Lakmal D Seneviratne, Xiaojing Song, J. S. Dai, and H. K. Lam. Soil estimation based on dissipation energy during autonomous excavation. *Proceedings of the 17th IFAC World Congress*, pages 13821–13826, 2008-Jul. 2008.

Venkat Venkatasubramanian, Raghunathan Rengaswamy, Surya N. Kavuri, and Kewen Yin. A review of process fault detection and diagnosis: Part iii: Process history based methods. *Computers & Chemical Engineering*, 27(3):327 – 346, 2003. ISSN 0098-1354.

Cristian Molina Vicuna. Effects of operating conditions on the acoustic emissions (ae) from planetary gearboxes. *Applied Acoustics*, 77(0):150 – 158, 2014. ISSN 0003-682X. doi: <http://dx.doi.org/10.1016/j.apacoust.2013.04.017>. URL <http://www.sciencedirect.com/science/article/pii/S0003682X13001138>.

Weidong Wang, Lei Zhou, Zhijiang Du, and Lining Sun. Track-terrain interaction analysis for tracked mobile robot. *Advanced Intelligent Mechatronics, 2008. AIM 2008. IEEE/ASME International Conference on*, pages 126–131, July 2008.

W.J. Williams and E.J. Zalubas. Helicopter transmission fault detection via time-frequency scale and spectral methods. *Mechanical Systems and Signal Processing*, 14(4):545 – 559, 2000. ISSN 0888-3270. doi: <http://dx.doi.org/10.1006/mssp.2000.1296>. URL <http://www.sciencedirect.com/science/article/pii/S0888327000912962>.

Ron C. K. Wong. Strength of two structured soils in triaxial compression. *International Journal for Numerical and Analytical Methods in Geomechanics*, 25(2):131–153, 2001. ISSN 1096-9853.

Agnieszka Wylomanska, Jakub Obuchowski, Radoslaw Zimroz, and Harry Hurd. Periodic autoregressive modeling of vibration time series from planetary gearbox used in a bucket wheel excavator. In Fakher Chaari, Jacek Lekow, Antonio Napolitano, and Andrea Sanchez-Ramirez, editors, *Cyclostationarity: Theory and Methods*, Lecture Notes in Mechanical Engineering, pages 171–186. Springer International Publishing, 2014. ISBN 978-3-319-04186-5.

Kaiming Xia. A framework for earthmoving blade/soil model development. *Journal of Terramechanics*, 45(5):147 – 165, 2008. ISSN 0022-4898.

Hongyu Yang, Joseph Mathew, and Lin Ma. Vibration feature extraction techniques for fault diagnosis of rotating machinery: a literature survey. In *Asia-Pacific Vibration Conference*, 2003.

Zhijing Yang, Bingo Wing-Kuen Ling, and Chris Bingham. Trend extraction based on separations of consecutive empirical mode decomposition components in hilbert marginal spectrum. *Measurement*, 46(8):2481 – 2491, 2013. ISSN 0263-2241. doi: <http://dx.doi.org/10.1016/j.measurement.2013.04.071>. URL <http://www.sciencedirect.com/science/article/pii/S0263224113001826>.

Y. Yin, G.Y. Grondin, K.H. Obaia, and A.E. Elwi. Fatigue life prediction of heavy mining equipment. part 1: Fatigue load assessment and crack growth rate tests. *Journal of Constructional Steel Research*, 63(11):1494 – 1505, 2007. ISSN 0143-974X.

R. Yousefi, A. Kotchon, and M. G. Lipsett. Method and apparatus for on-line estimation of soil parameters during excavation. *Journal of Terramechanics*, 49 (3-4):173–181, 2012. ISSN 0022-4898.

A.N. Zelenin, V.I. Balovnev, and I.P. Kerov. *Machines for Moving the Earth: Fundamentals of the Theory of Soil Loosening, Modeling of Working Processes and Forecasting Machine Parameters*. New Delhi: Published for the United States Dept. of Agriculture, and the National Science Foundation, Washington, D.C., by Amerind Pub. Co., 1985.

Xiangwu Zeng, Louis Burnoski, Juan Agui, and Allen Wilkinson. Calculation of excavation force for isru on lunar surface. In *Aerospace Sciences Meetings*, pages –. American Institute of Aeronautics and Astronautics, January 2007. doi: 10.2514/6.2007-1474. URL <http://dx.doi.org/10.2514/6.2007-1474>.

Ji Zhang and R.L. Kushwaha. A modified model to predict soil cutting resistance. *Soil and Tillage Research*, 34(3):157 – 168, 1995. ISSN 0167-1987.

Jinde Zheng, Junsheng Cheng, and Yu Yang. Generalized empirical mode decomposition and its applications to rolling element bearing fault diagnosis. *Mechanical Systems and Signal Processing*, 40(1):136 – 153, 2013. ISSN 0888-3270.

Radoslaw Zimroz and Walter Bartelmus. Gearbox condition estimation using cyclo-stationary properties of vibration signal. *Key Engineering Materials*, 413-414: 471–478, 2009.

Y.H. Zweiri, L. D. Seneviratne, and K. Althoefer. Modelling and control of an unmanned excavator vehicle. *Journal of Systems and Control Engineering*, 217 (4):259–274, 2003.

Appendix A

Mohr-Coulomb Failure Criterion

The Mohr-Coulomb criterion states that the shear stress in a plane at failure is a function of the normal stress in the plane.

$$\tau_{max} = S_0 + \sigma_n \tan \phi \quad (\text{A.1})$$

where S_0 is the inherent shear strength, also known as cohesion c ; and ϕ is the angle of internal friction, with the coefficient of internal friction $\mu = \tan \phi$. The criterion contains two material constants, S_0 and ϕ [Labuz and Zang, 2012]. The representation of eq. (A.1) in the Mohr diagram is a straight line inclined to the σ -axis by the angle ϕ , as shown in fig. A.1.

By constructing a Mohr circle tangent to the line (a stress state associated with failure) and using trigonometric relations, the alternative form of eq. (A.1) in terms of principal stresses is obtained:

$$(\sigma_I - \sigma_{III}) = (\sigma_I + \sigma_{III}) \sin \phi + 2S_0 \cos \phi \quad (\text{A.2})$$

One form of Mohrs failure criterion is:

$$\tau_{max} = f(\sigma_m) \quad (\text{A.3})$$

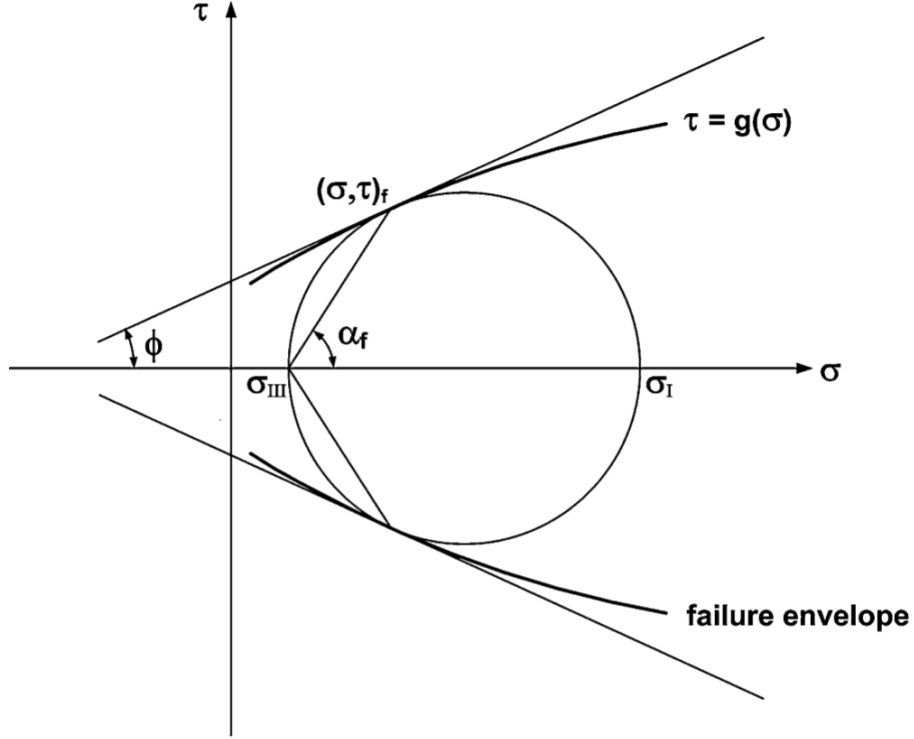


Figure A.1: Mohr Diagram and Failure Envelopes (after [Labuz and Zang, 2012])

where $\tau_{max} = (\sigma_I - \sigma_{III})/2$, and $\sigma_m = (\sigma_I + \sigma_{III})/2$,

Knowing the relationship given by eq. (A.3), the Mohr envelope can be constructed on the τ, σ plane (fig. A.1), and failure occurs if the stress state at failure, the circle of diameter $(\sigma_I - \sigma_{III})$, is tangent to the failure envelope, $\tau = g(\sigma)$. Thus, from eq. (A.2), Coulombs criterion is equivalent to the assumption of a linear Mohr envelope.

Coulombs and Mohrs criteria are notable in that an effect of σ_m , the mean stress in the σ_I, σ_{III} plane, is considered, which is important for materials such as rock and soil; i.e., experiments on geomaterials demonstrate that τ_m at failure increases with σ_m .

Appendix B

Numerical Study of the Crack

Fault

A numerical study was conducted to investigate the impact of the structural defect on machine dynamic behavior. For this purpose a model of the assembly was developed by solid modeling computer-aided design (CAD) software - SOLIDWORKS - and was used as a baseline (healthy condition). The CAD model developed for the assembly is shown in fig. B.1, and is comprised of the crank-slider mechanism and the blade/cutting compartment.

This CAD model is then converted into a MATLAB/SimMechanicsTM model for simulation and analysis, through a process called CAD translation [[Mathworks, 2015](#)]. By translating the CAD assembly into a SimMechanics model, one can combine the benefits of the CAD platform with the strengths of SimMechanics software. Translated CAD model - also known as the XML file - is an ‘import file’ that reflects assembly structure and contains part parameters of the original model. SimMechanics then interprets the import file and generates a new model. During CAD export, the SimMechanics Link utility generates one XML file and a set of

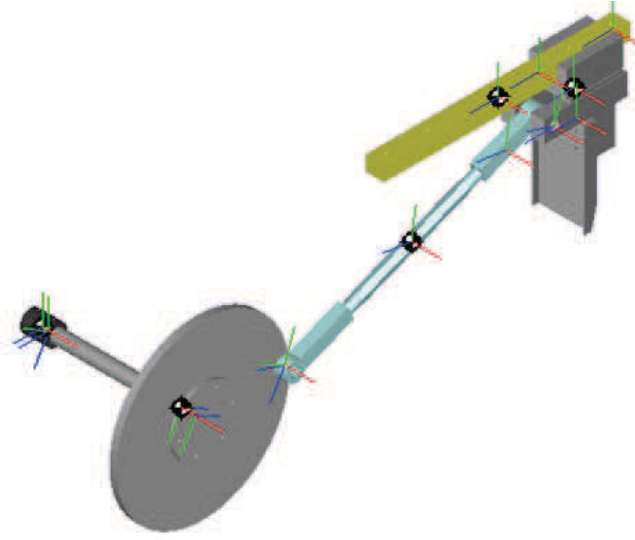


Figure B.1: Original CAD Model Built in SOLIDWORKS

geometry files in STEP or STL format. This process is shown in fig. B.2. Final model structure and part parameters mirror the original CAD assembly. Components of the dynamic behavior of the model, i.e. displacement and velocity, can be monitored and evaluated for different operating conditions. Parameters of interest in our investigation are angular displacement for the crank ϕ_1 and the connecting rod ϕ_2 , angular velocity of the crank $\dot{\phi}_1$, and slider's position x_s and velocity v_s .

The baseline model can be modified and re-translated. For example, one can modify the integrity of the components and produce an artificially fault components, e.g. crack in the connecting rod. By comparing the monitored parameters under healthy and faulty condition a residual can be generated. Therefore, residual signals for all five parameters of interest were generated. Figure B.3 demonstrates the effect of presence of a crack in the residue signals of (R_1, \dots, R_5) .

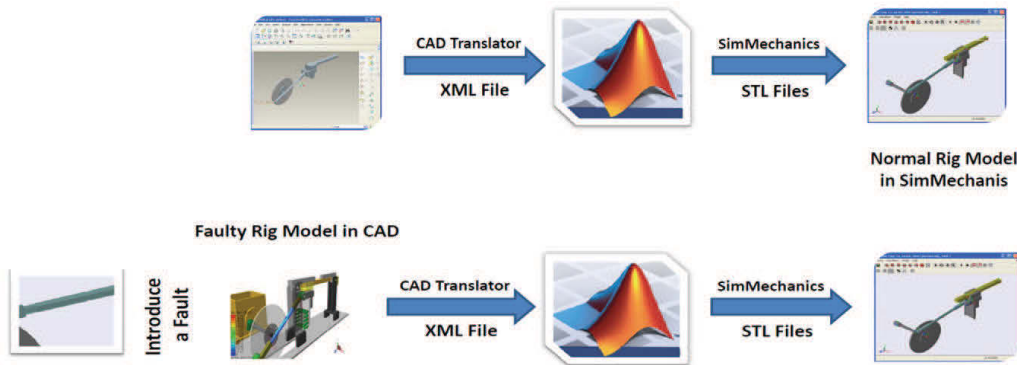


Figure B.2: Numerical Analysis using CAD Translation and SimMechanics: Faulty Condition can be Compared to the Baseline Condition and for Residual Generation.

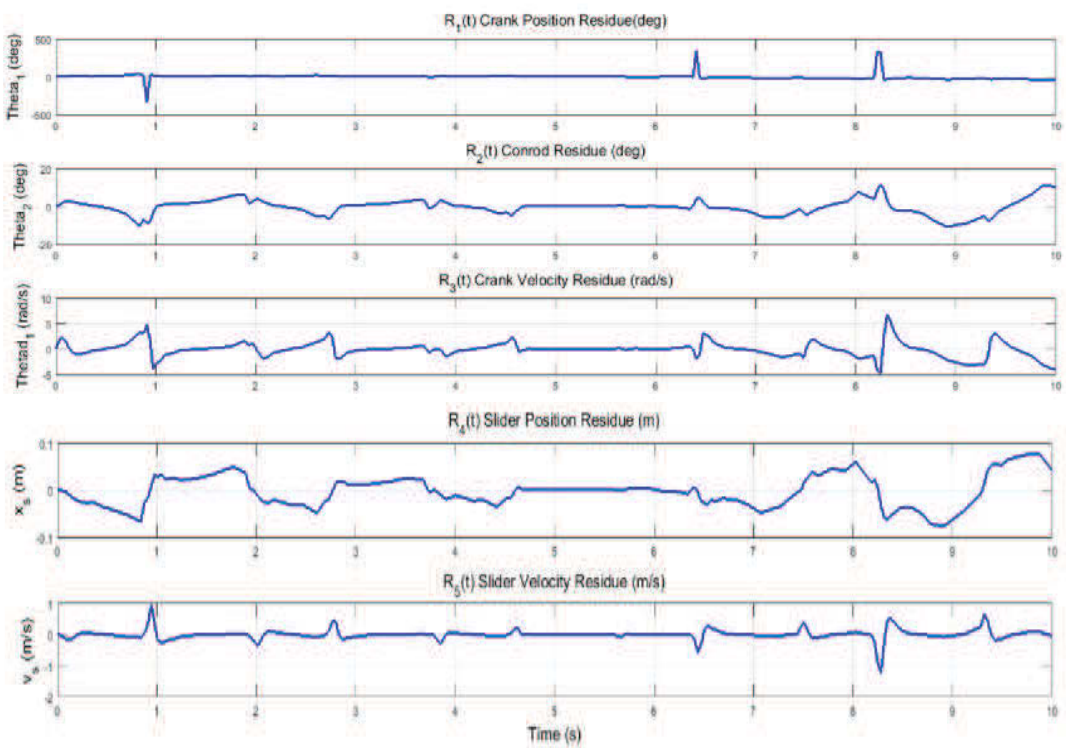


Figure B.3: Impact of the Crack Fault on the Residue Signal

Appendix C

VI Program for Data Collection

All the collected signals are routed to the NI cdaq-9178 chassis, and then forwarded to the LabView VI developed for data collection and pre-processing. This includes slider's displacement and acceleration, motor's speed through tachometer, gearbox output speed through digital encoder, active torque on the crank, and interaction force acting on the blade.

Preliminary signal processing is carried out to convert collected voltage and current signals to the proper parameters of interest. This is shown in the VI screen shot presented in fig. D.1. The digital signal from the encoder is fed into a separate processing box, which first translates the signal into the angular displacement. Time-derivative of This signal is the obtained and converted to the angular velocity in RPM. Both signals are then forwarded to the workspace (the dataset that is logged on the pc).

Remaining four signals are analog and fed to the analog processing box. First and second time derivatives of the slider's displacement signal are obtained and along the displacement are sent to the workspace. Voltage recorded from the strain gauges are converted to torque and force (using the proper relationship), and recorded as well. The acceleration signal acquired through accelerometer is used to calculate

the velocity, and both signals are recorded. Finally, the signal from tachometer is forwarded to the workspace. All ten signals are time stamped and recorded for every experiment.

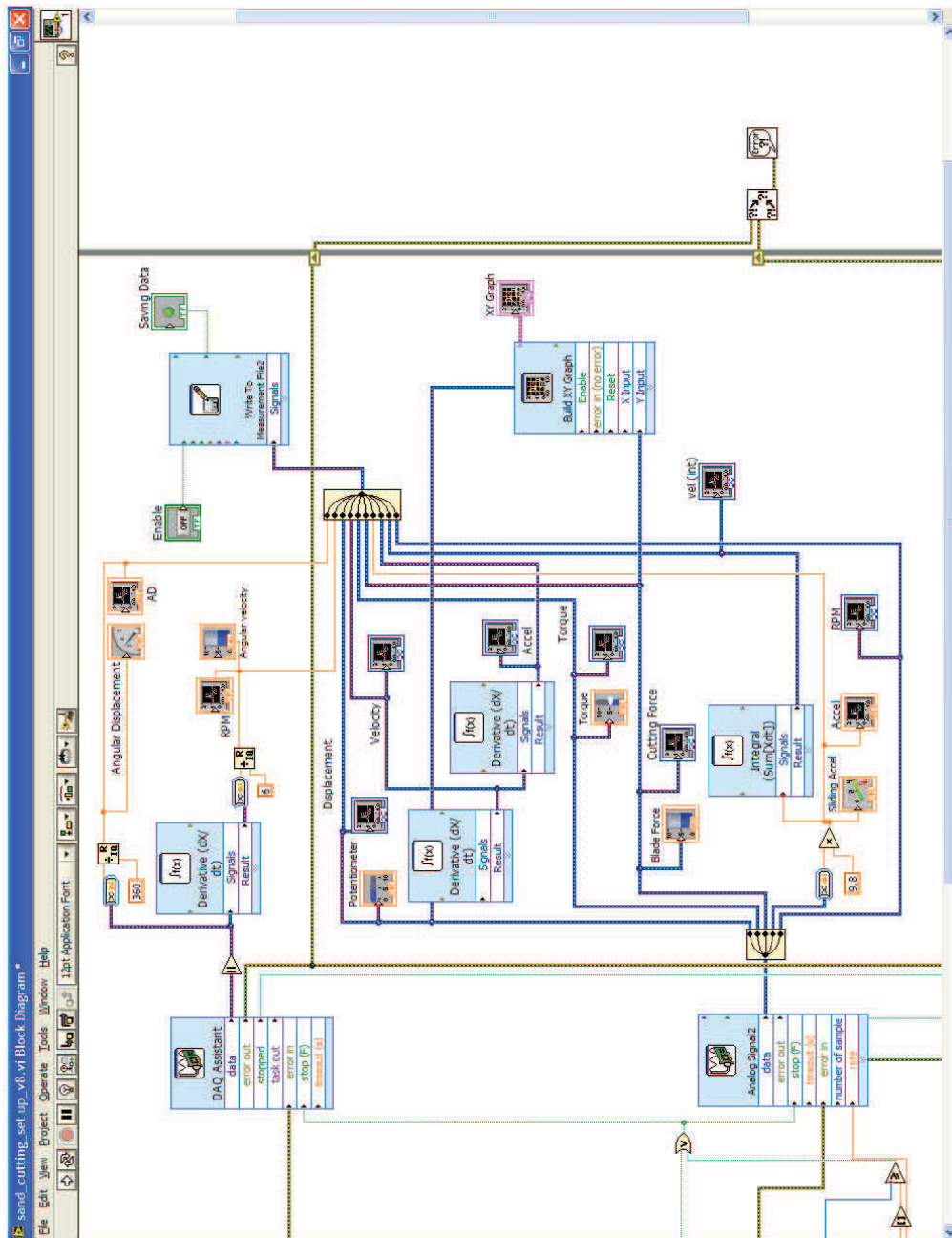


Figure C.1: LabView VI Program for Data Collection

Appendix D

Newton-Raphson Method

For any $f(x)$ as shown in fig. D.1, Newton-Raphson method can be used to find a solution of $x = \hat{x}$ such that

$$f(\hat{x}) = \bar{f} \quad (\text{D.1})$$

where \bar{f} is a constant.

The Newton-Raphson method begins with an estimate for \hat{x} , say x_0 and iteratively refines this estimate until eq. (D.1) is satisfied within a specified tolerance. The algorithm for the iterative process is derived by the Taylor series expansion of the error (or residual) [Anandarajah, 2010]. Let us define the error as:

$$\psi(x) = f(\hat{x}) - \bar{f} \quad (\text{D.2})$$

Denoting the next best estimate by x_1 , let us express the value of $\psi(x_1)$ in Taylor series by expansion about x_0 as

$$\psi(x_1) = \psi(x_0) + \left[\frac{d\psi}{dx} \right]_{x_0} \Delta x + \frac{1}{2} \left[\frac{d^2\psi}{dx^2} \right]_{x_0} \Delta x^2 + \dots \quad (\text{D.3})$$

where

$$\Delta x = x_1 - x_0 \quad (\text{D.4})$$

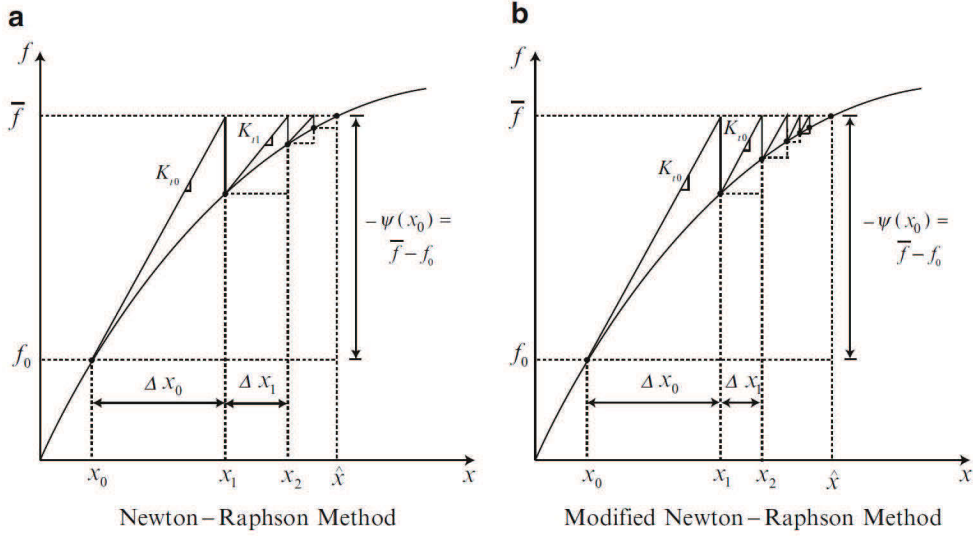


Figure D.1: Newton-Raphson (a) and Modified Newton-Raphson (b) Methods

Truncating the series after the term with the first derivative of ψ , and denoting the derivative at $x = x_0$ by:

$$K_{t0} = \left[\frac{d\psi}{dx} \right]_{x_0} = \left[\frac{df}{dx} \right]_{x_0} \quad (\text{D.5})$$

and setting $\psi(x_1)$ to zero (which is the ultimate desired result), we get

$$\Delta x = \Delta x_0 = -K_{t0}^{-1}\psi(x_0) = K_{t0}^{-1}(\bar{f} - f_0) \quad (\text{D.6})$$

The refined estimate then is (from eq. (D.4))

$$x_1 = x_0 + \Delta x_0 \quad (\text{D.7})$$

Since the Taylor series expansion was truncated after two terms, the estimate x_1 is still an approximation to \hat{x} , but in general x_1 is expected to be a closer to \hat{x} than x_0 is. The geometrical interpretation of the iterative process is shown in fig. D.1(a).

The procedure may be repeated until

$$|\psi(x_n)| < e_{acc} \quad (\text{D.8})$$

where e_{acc} is the acceptable error. Since the slope of the curve is used to guide the iteration, it is seen that the process should quickly converge to the solution of the problem \hat{x} . The rate of convergence is approximately quadratic.

K_{t0} appearing in eq. (D.5) and eq. (D.6) must be evaluated and the full system of equations solved at every iteration. Both of these tasks are highly computationally intensive [Anandarajah, 2010]. In the Modified Newton-Raphson Method however, the tangent K_{t0} is evaluated once at the beginning of the iteration, and kept unchanged throughout the iteration. This process is also depicted in fig. D.1(b). These methods can be easily extended to a non-linear system of equations simply by appropriately treating the scalars as either vectors or matrices.

Appendix E

Interactive Period Monitoring

Acceleration data was also collected and studied during the interactive period, while the tool was engaged with the medium. It is worth mentioning that the data collected during this period has a significantly smaller size (less than a half rotation).

Once the blade starts moving it pushes and compresses the soil in front of it. The amount of accumulated soil - and the reactive force - eventually prevents the shovel assembly to go further.

Therefore, there is a physical limitation for collecting further data. This entire process happens in under 1 second. Study of the non-interactive data showed that collecting enough data from multiple cycles is a necessary step for establishing a proper baseline.

Studying the faulty condition it is observed that external loading becomes the dominating factor when using the STFT and masks other smaller excitations (i.e. contributions from structural defects).

E.1 Short-time Fourier Transform

It can be seen from figs. 5.5 and 5.8 that the interaction under normal condition takes less than a second in most cases. This is not sufficient to establish a steady acceleration signal.

Spectrogram of the acceleration signal for two cases are presented in fig. E.1. It can be seen that the dominating frequency does not look much different from non-interactive operation of the shovel assembly.

This pattern changes once the shovel is used for pushing and cutting the medium under faulty conditions. As can be seen in figs. E.2 and E.4, it takes the assembly a longer time - up to 4 seconds - to complete the half cycle (until the slider stops moving).

Therefore, a larger data set is collected. However, the spectrogram does not offer much valuable data, for detection and identification purpose.

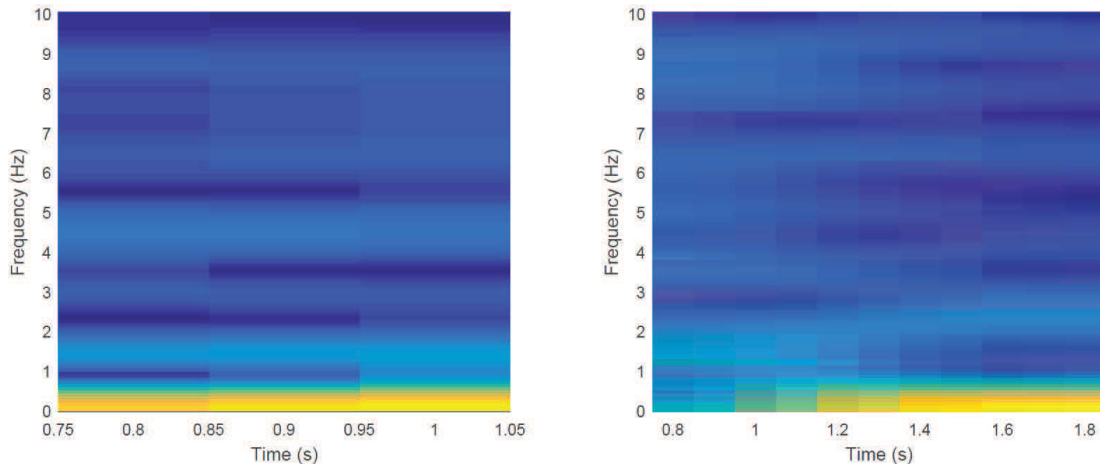


Figure E.1: STFT of the Acceleration During the Soil-Tool Interaction for Normal Condition: Both Trials are Cutting Through Glass Beads

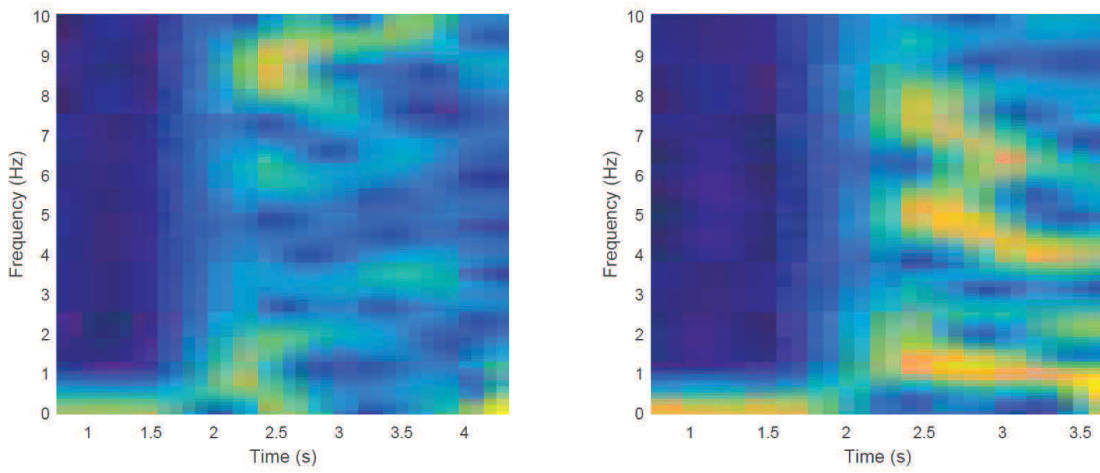


Figure E.2: STFT of the Acceleration During the Soil-Tool Interaction for Fault A
Condition: Glass Beads (left) Play Sand (right)

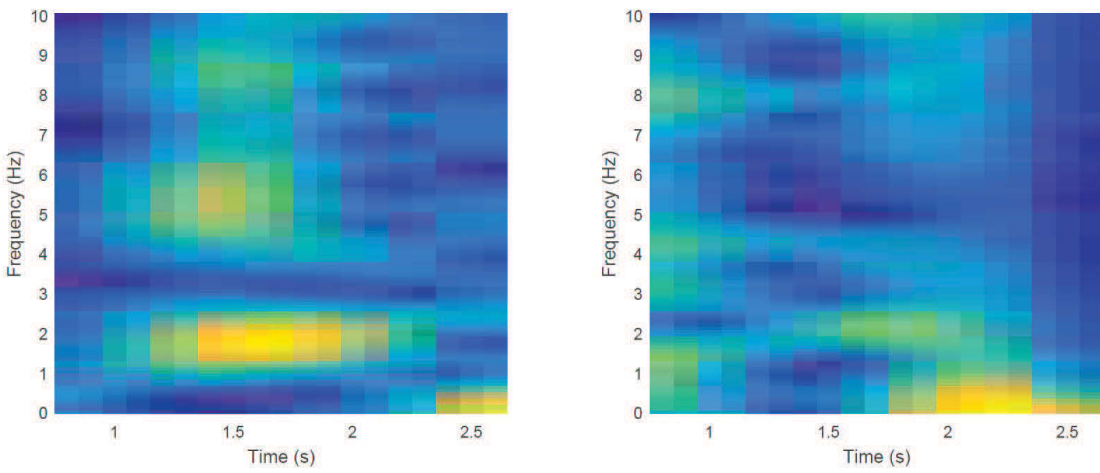


Figure E.3: STFT of the Acceleration During the Soil-Tool Interaction for Fault B
Condition: Glass Beads (left) Play Sand (right)

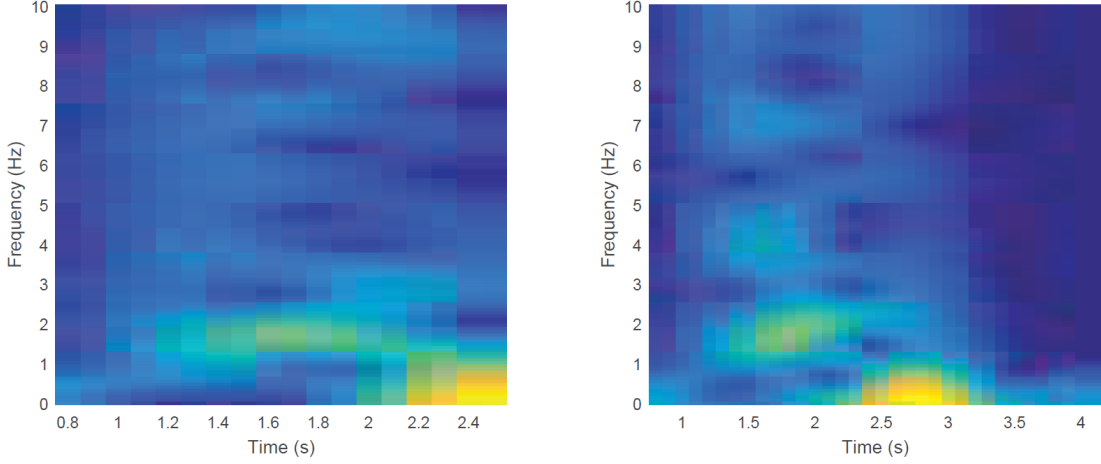


Figure E.4: STFT of the Acceleration During the Soil-Tool Interaction for Fault C Condition: Glass Beads (left) Play Sand (right)

E.2 Hilbert-Huang Transform

Applying Hilbert-Huang transform of the acceleration signal offers a more interesting outlook for how the signal changes in presence of fault. Similar to non-interactive operation, IMFs are extracted using the EMD procedure. Figure E.5 shows that the acceleration signal - during the tool-medium interaction with Play sand - under normal condition is decomposed into 3 IMFs, and it appears to stay close to zero, with no particular sign of impact or disturbance. Marginal spectrum shows a very weak dominating frequency at about $1\times$, and a few harmonics at higher frequencies. Applying the EMD on all 3 faulty conditions, the IMFs can be extracted similarly as depicted in fig. E.7, fig. E.9 and fig. E.11.

In all three cases, it can be seen that IMF1 and IMF2 are affected by presence of fault. Another interesting feature is that unlike the STFT, *mhs* detects a dominating frequency at about $1\times$, and appears to be unaffected by the interaction force, as can be seen in fig. E.8, fig. E.10 and fig. E.12.

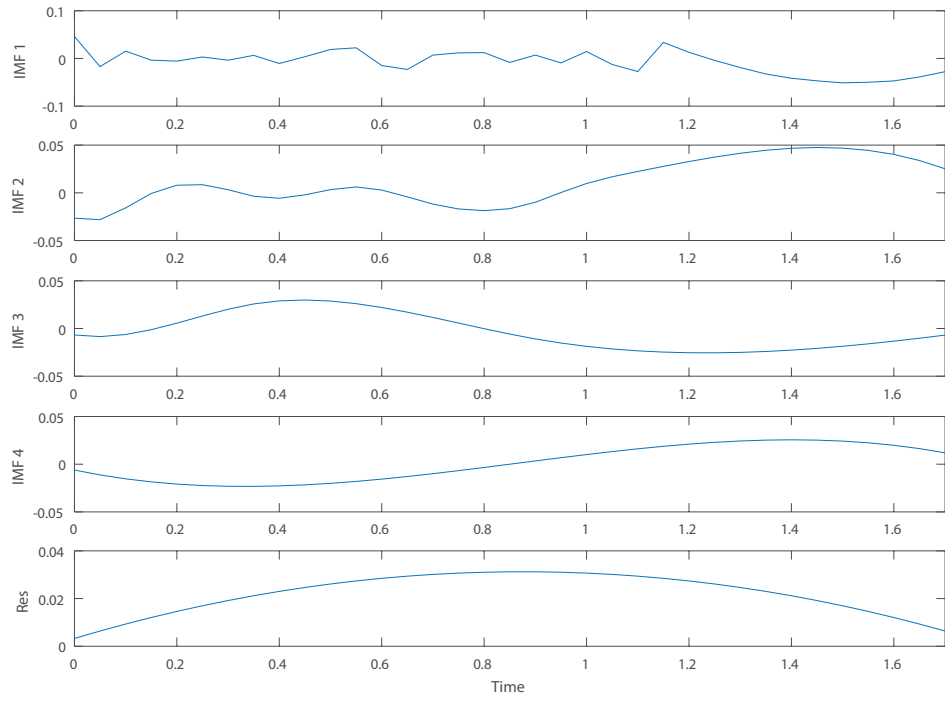


Figure E.5: IMF of the Acceleration During the Soil-Tool Interaction (Play sand) for Normal Condition

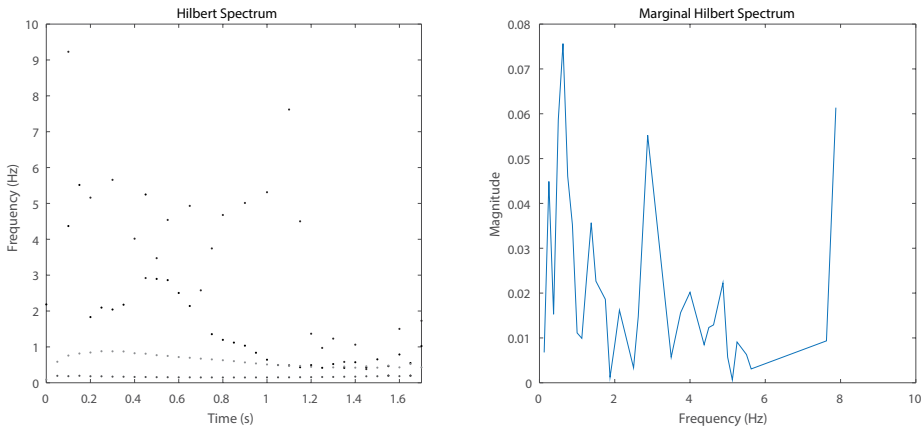


Figure E.6: HHT of the Acceleration During the Soil-Tool Interaction (Play sand) for Normal Condition

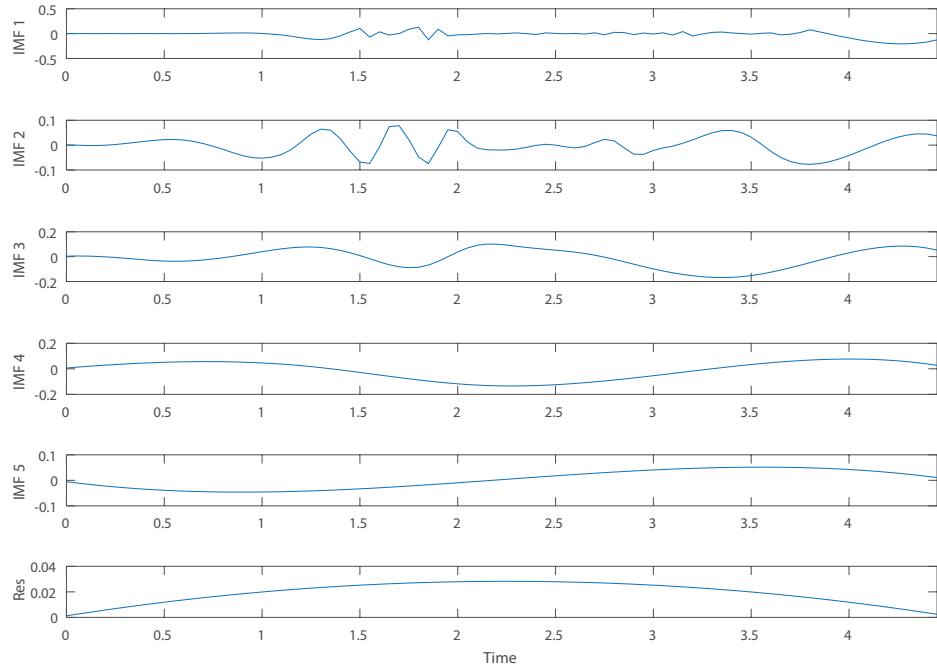


Figure E.7: IMF of the Acceleration During the Soil-Tool Interaction (Play Sand) for Fault A Condition

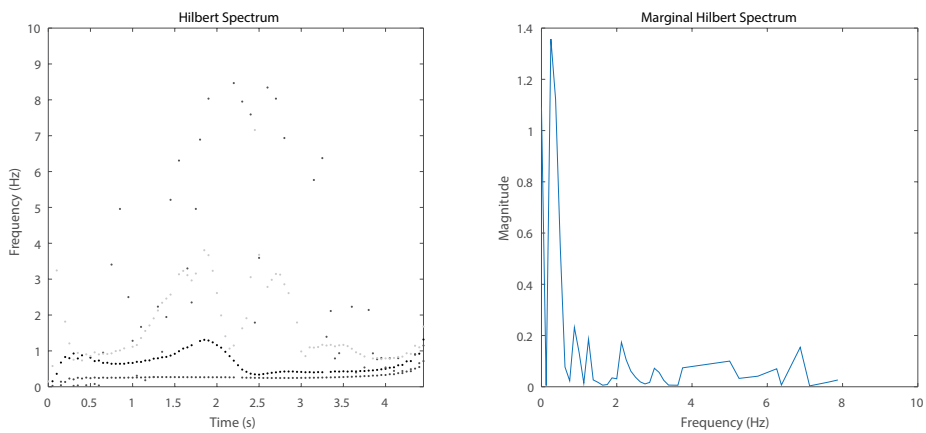


Figure E.8: HHT of the Acceleration During the Soil-Tool Interaction (Play Sand) for Fault A Condition

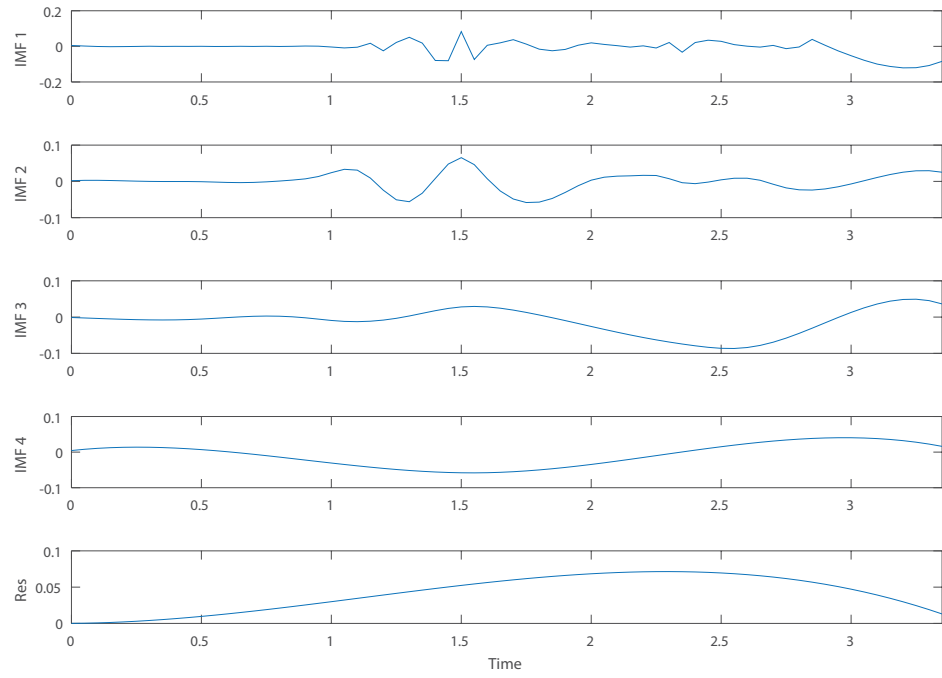


Figure E.9: IMF of the Acceleration During the Soil-Tool Interaction (Play Sand) for Fault B Condition

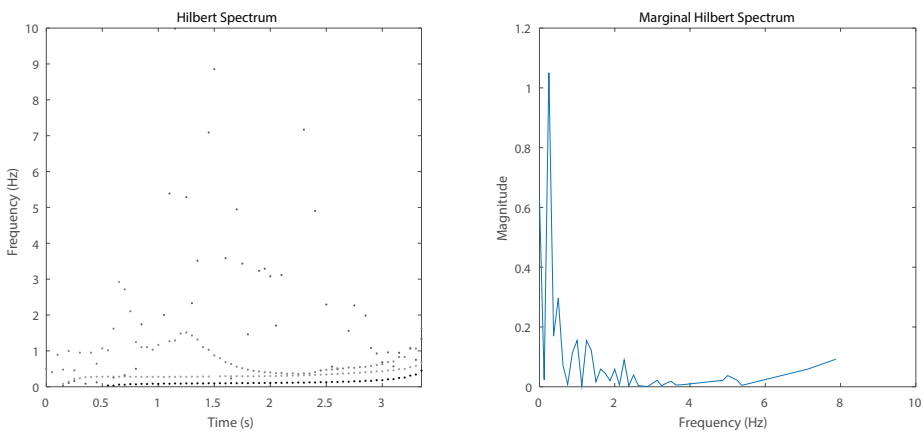


Figure E.10: HHT of the Acceleration During the Soil-Tool Interaction (Play Sand) for Fault B Condition

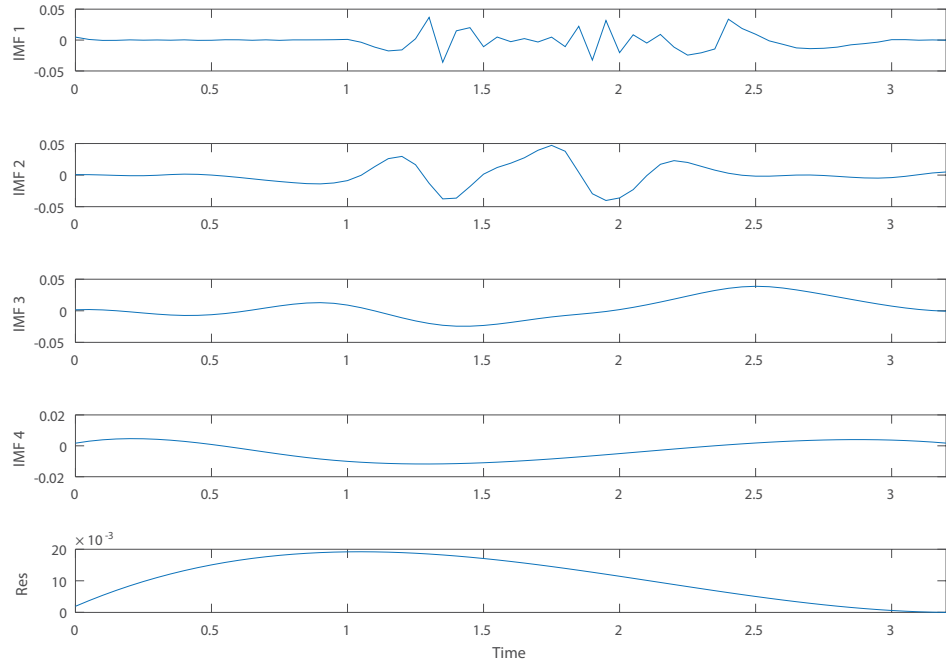


Figure E.11: IMF of the Acceleration During the Soil-Tool Interaction (Play Sand) for Fault C Condition

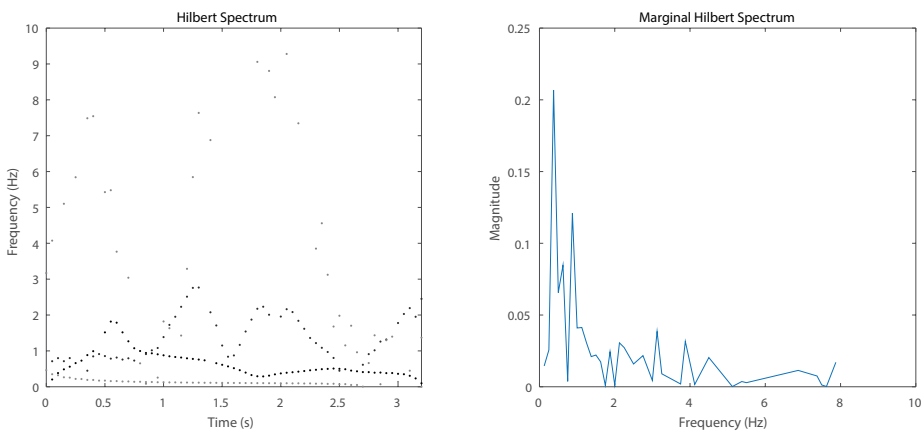


Figure E.12: HHT of the Acceleration During the Soil-Tool Interaction (Play Sand) for Fault C Condition